Innovation Report

Project: Optimisation of Third-Party Technical Evaluation of Stationary Li-Ion Battery Storage

Sponsor: EDF Energy R&D UK centre

Martin Rogall, MSc

Academic Supervisors: David Greenwood, Dr Anup Barai, Dr Patrick Luk, Dr Rohit Bhagat
Industrial Supervisor: Dr Maria Brucoli

Abstract

The work presented in this report documents the development of a Li-Ion battery energy storage system (BESS) multi-physics model based on the limited data available to potential investors in such systems. BESS are essential for the development of a stable and sustainable power grid. Simultaneously they are an asset whose value must be assessed beforehand by a party interested in investing in them. Due to the complex behaviour in both operation and degradation processes of batteries, they are inherently difficult to assess in terms of long-term performance.

For that reason there are many existing models that try to approximate the behaviour of batteries. None of the models investigated displayed sufficient accuracy or flexibility necessary for a reliable simulation of BESS behaviour. Therefore, through a series of short- and long-term testing, extensive literature review and derivation of manufacturer-provided values of the system a new model is generated. This data-restricted multi-physics simulation (DREMUS) is then turned into a tool for industrial application.

The tool developed is capable of modelling through best possible approximation the electrical, thermal behaviour of a battery storage system based only on the data available before making an investment decision. It further was designed easily modifiable so additional data can be added. The tool was used for a case study to assess its long term viability. It was found that under the investigated value streams and current market conditions the system was not viable.

The model and tool can be widespread applied to all carbon-based Li storage applications and allows thus more efficient implementation of BESS throughout the UK power system.

Acknowledgements

I'd like to whole-heartedly thank my family and friends for their loving support throughout the years before and during this project.

This project wouldn't have been possible without my supervisors, in particular Dave Greenwood, Maria Brucoli and Anup Barai who have given me guidance on any topic. I'm also thankful for the help and support I received from my colleagues at the EDF Energy R&D UK centre as well as my peers and the staff at WMG and the University of Warwick, Cranfield and Exeter.

I'm thoroughly thankful to the EDF Energy R&D UK centre, the University of Warwick, the EPSRC and the CDT for Sustainable Materials and Manufacturing for making this project possible and giving me this opportunity which both significantly contributed to my professional and personal development.

Additional research also presented in the report was undertaken with the WMG Centre High Value Manufacturing Catapult (funded by Innovate UK) in collaboration with Jaguar Land Rover.

Declaration

I confirm that the work presented in this report is my own unless otherwise stated. This work has not been previously submitted for any other degree.

Martin Rogall, 15/07/2021

Table of Contents

Abbreviations

AC	Alternating Current
ARB	Arbitrage
ARES	Advanced Rail Energy Storage
BESS	Battery Energy Storage System
BM	Balancing Mechanism
BMS	Battery Management System
BSC	Balancing and Settlement Code
C	Carbon
C-Rate	Current Rate
CAES	Compressed Air Energy Storage
CAL	Calendar
Cap.	Capacity
CC	Constant-Current
CCCV	Constant-Current-Constant-Voltage
CDTF	Capacitance-Diffusion Transitional Frequency
CfD	Contracts for Difference
CHP	Combined Heat and Power
Covid-19	Coronavirus disease 2019
CPE	Constant-Phase-Element
CSV	Comma Separated Values
DC	Direct Current
DNO	Distribution Network Operator
DoD	Depth-of-Discharge
DREMUS	Data-Restricted Multi-Physics Simulation
DV	Differential Voltage
ECM	Equivalent-Circuit-Model
EDF	Électricité de France
EDRP	Energy Demand Research Project
EFR	Enhanced Frequency Response
EIS	Electrochemical Impedance Spectroscopy
EngD	Engineering Doctorate
EOL	End-of-Life
EU	European Union
EV	Electric Vehicle
FCY	Full-Cycling

FEC	Full Equivalent Cycles
FFR	Firm Frequency Response
FIT	Feed-In Tariff
FR	Fast Response
GB	Great Britain
IC	Incremental Capacity
ID	Identification
IRR	Internal Rate of Return
LCO	Lithium-Cobalt-Oxide
LCOE	Levelized Costs of Electricity
LFP	Lithium-Iron-Phosphate
Li-Ion	Lithium-Ion
LMO	Lithium-Manganese-Cobalt
LTO	Lithium-Titan-Oxide
MCY	Micro-Cycling
MFR	Mandatory Frequency Response
N/A	Not applicable
NCA	Nickel-Cobalt-Aluminium
NGESO	National Grid Electricity System Operator
NGET	National Grid Electricity Transmission
NiCd	Nickel-Cadmium
NMC	Nickel-Manganese-Cobalt
NiMH	Nickel-Metal-Hydride
NPV	Net Present Value
NRMSD	Normalised Root-Mean-Square Deviation
MCY	Micro-Cycling
OCV	Open-Circuit-Voltage
PHES	Pumped Hydro Energy Storage
p	parallel
PS	Parallel-Series
PV	Photovoltaic
R&D	Research and Development
RMS	Root-Mean-Square
RO	Renewables Obligation
s	series
SEI	Solid Electrolyte Interface

SMES	Superconducting Magnetic Energy Storage
SP	Series-Parallel
STOR	Short Term Operating Reserve
SO	System Operator
SoC	State of Charge
SoH	State of Health
Temp.	Temperature
TNO	Transmission Network Operator
UK	United Kingdom
WMG	Warwick Manufacturing Group

List of Parameters, Sub- and Superscripts

Constants		Value
F	Faraday Constant	$96\,485\,\frac{sA}{mol}$
R_g	Gas Constant	$8.3145\,\frac{J}{mol*K}$

Parameter		Unit
a	Linear factor	
A	Surface area	m^2
b	Linear offset	
B	Admittance	S
c	C-rate	$\frac{1}{h}$
C	Capacitance	$F \mid \frac{J}{K}$
Deg	Degradation	%
E	Energy	J
f	Conversion factor	%
I, i	Current	A
J	Current density	$\frac{A}{m^2}$
k	Fitting parameter	
m	Cell series count	
n	Cell parallel count	
P, p	Power	W
q	Heating power	W
Q	Coulombic capacity	Ah
R	Resistance	$\Omega \mid \frac{mK}{W}$
SoC	State of Charge	%
SoH	State of Health	%
t	Time	h
T	Temperature	K
V, v	Voltage	V

Sub- and Superscripts	
a	Anode
ac	Activation
abs	Absolute
amb	Ambient
bat	Battery
$BESS$	Battery Energy Storage System
BMS	Battery Management System
c	Cathode
$cell$	Cell
ch	Charge
con	Converter
$conv$	Convection
cor	Corrected
CT	Charge-Transfer
cyc	Cycling
d	Demand
DC	Direct current
DIF	Diffusion
ds	Datasheet
dch	Discharge
e	Exchange current
ent	Entropy
eol	End-of-life
H	Household
ig	Initial guess
in	Input
im	Imbalance

Y	Sensitivity State Variable	
Z	Impedance	Ω
η	Efficiency	$\%$
κ	Heat conductivity	$\frac{W}{mK}$
σ	Standard Deviation / Error	
τ	Time constant	s
ψ	Phase angle	

IR	Irradiance
$joule$	Joule
lin	Linear
max	Maximal
$meas$	Measured
min	Minimal
mod	Module
n	Nominal
oc	Open-circuit
ohm	Ohmic
op	Overpotential
out	Output
p	Provision
PC	Pseudo-Capacitance
PV	Photovoltaic
r	Roundtrip
$reac$	Reaction
ref	Reference
res	Resistive
s	surface
sh	Shortened
$side$	Side
th	Thermal
u	Unidirectional
$\%$	Percent (relative value)

List of Figures

List of Tables

1 Introduction

1.1 EngD Research Focus and Collaborators

The focus of this EngD project was on the long term modelling of battery energy storage systems (BESS) for operation as grid storage system. Pre-requisite for the modelling is the data availability to third-party investors without any knowledge on the detailed functionality of battery storage. This is achieved through an extensive literature review, battery testing and characterisation. The project was executed in collaboration with the EDF Energy R&D UK centre and the WMG.

EDF Energy, partial sponsor to this project, is one of the big six energy suppliers in the UK. Aside from trading energy for both commercial and residential supply they also own nuclear, renewable and gas energy generation assets as well as BESS. Of interest to the EDF Energy R&D UK centre, which is the primary collaborator with this project, is the commercial viability and optimisation of BESS. This is the motivator for this project.

This project has been predominantly conducted on their premises, with the experimental activities being performed at WMG in Warwick University.

1.2 Aim and Objectives

The initial description of this project focussed on the techno-economic feasibility of co-location of battery storage with micro-generation to support the widespread implementation of small-scale renewable energy and the project assessment of EDF. After further assessment of EDF's strategy regarding the implementation and application of battery storage, the specific aim was refined to a universally applicable BESS model which can be applied to this and any further feasibility studies. Therefore the final aim of this project was to develop an industrially applicable battery modelling tool that could be applied without detailed information on the storage system itself.

The objectives of the project were as follows:

1. Identification of the use cases for grid energy storage
2. Identification of the ideal technologies for grid energy storage to fulfil the use cases on a large scale
3. Investigation of physicochemical mechanisms and existing modelling approaches of Li-Ion cells
4. Verification and quantification of these mechanisms though long-term testing
5. Development of a universally adaptable battery storage model and an software tool
6. Tool application to a case study

The portfolio structure as outlined in the following sub-section broadly follows these objectives and will reference them accordingly. This report will follow them as well and is concluded in section 6.

1.3 EngD Portfolio Structure

This sub-section describes the structure of the submitted EngD portfolio along with all the contents of all relevant documents. An overview on the documents is given in Figure 1.

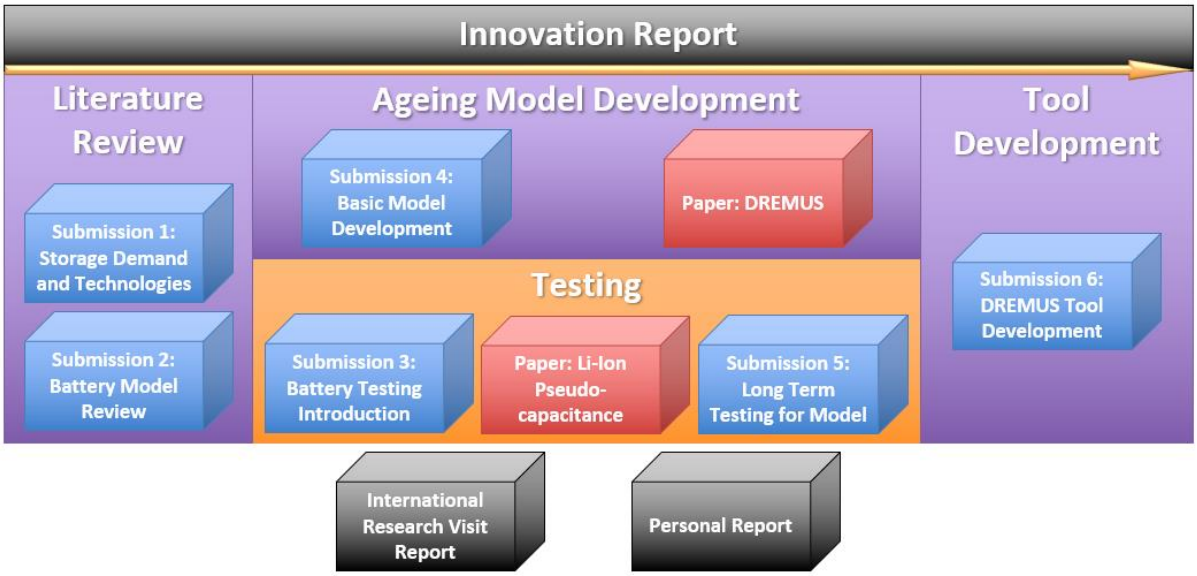

Figure 1: Portfolio Structure

The main project proceeded in three main stages: the literature review, the battery model development encompassing the testing and the tool development for application in EDF. In the following the contents of each correlating document is briefly outlined. They are discussed in the order they should be read and considered.

Submission One: The Reasoning behind Decentralised Energy Storage and the Technologies Available

The first part of this submission addresses the first objective by discussing the motivation for electrical energy storage from a political, grid, consumer and generator perspective. Each of those perspectives have been investigated thoroughly and the individual methods of value generation have been outlined, establishing the need and economic benefit for energy storage systems in Great Britain (GB).

The second part discusses the available energy storage technologies, their readiness and feasibility in the GB market. By their characteristics, an appropriate technology has been chosen to consider the most feasible state-of-the art technologies for the value streams discussed in part one, thus addressing the second objective.

Submission Two: The Current State of Decentralised Battery Storage - Implementation, Analysis and Modelling

This submission delves into the current state and implementation of battery storage in GB, with focus on the legal, commercial and technological barriers for battery storage. After discussing several actions that can be taken to respond to these barriers, battery modelling has been identified as key method for market participants.

Further, Li-Ion battery storage, along with the considerations of ownership and management, technical implementation and chemistry selection are discussed in more detail.

The last section discusses different modelling approaches for the evaluation of battery storage, thus addressing the third objective. The emphasis lies on the detailed investigation of existing electrical, thermal and ageing models for Li-Ion batteries. After a qualitative comparison specifically regarding the various ageing models, the general difficulties and specific issues with the discussed models regarding their application in industrial storage modelling have been identified. From these issues the requirements for a commercially applicable battery storage model have been determined.

Submission Three: Ageing Test Design of Lithium-Ion Stationary Storage Cells and Non-Intrusive Cell Analysis

In preparation for the long-term battery tests to be performed for the development of the battery model and as introduction into the battery characterisation process, this submission focusses on the several approaches to realistic battery long term testing. Taking a use case for a home storage system as reference a small set of cells has been tested. Experimental design, test procedure and ageing analysis tools are discussed along with the critical issues occurring during testing to inform future experiments.

Paper: On the utilisation of the pseudo-capacitive capabilities of Li-ion cells for the provision of frequency response services (1)

This paper, published in the “Journal of Energy Storage”, describes an investigation of the pseudo-capacitance and it’s activation within Li-Ion cells, partially contributing to the third objective. Considering the potential battery health benefits of micro-cycling (2) and its application in frequency response provision, the purpose of this paper was to connect micro-cycling to the pseudo-capacitance of Li-Ion cells. Primarily it was targeted to identify the AC frequency at which the diffusion process of the cell is overtaken by its capacitance. This information was used as reference for ageing tests.

Submission Four: Development of a Multi-Physics BTM Battery Model

The beginning of this submission compares the caveats and benefits of full battery energy storage system (BESS) use case optimisation and the focus on a BESS model before proceeding with the development of the latter. Based on the requirements of the model, electrical, thermal and ageing models are developed based on literature review and pre-collected experimental data, mainly contributing to the fifth objective.

Submission Five: Accelerated Ageing Tests on Li-ion battery modules

This submission discusses the main ageing test performed in this project to validate and improve upon the model developed in submission four and answer any remaining questions to complete it. Electrical, thermal and ageing data is collected and evaluated. The results are combined with the previous data to generate a more generally applicable model, thus addressing both objective four and five.

Paper: DREMUS: A Data-Restricted Multi-Physics Simulation Model for Lithium-Ion Battery Storage (3)

This paper summarises the final model described in submission four and five by describing a full model capable of modelling a BESS based on the data-limitations given. The description takes additionally into consideration a more detailed sourcing of parameters, model limitations and application methodology as well as a sensitivity analysis of the degradation model.

Submission Six: Development of the DREMUS Tool

This submission describes the details of the developed software tool based on the finished DREMUS model, completing objective five. While the individual files, functions and classes are explained in detail, the adjustments and compromises necessary are outlined as well.

The second part applies the tool to a case study, showing the working application and quantifying the financial impact of modelling with this tool. With this the sixth and final objective is completed.

Report on International Research Visit

This report describes the activities and research undertaken during the international research visit at EDF R&D in France. It mainly describes several experiments and data undertaken. While this research is also on the topic of Li-Ion performance and ageing, its results are complementary and are not referenced in this report.

Personal Report

The personal report outlines the personal development achieved in this project. It covers the individual skills and abilities obtained as well as some key experiences. These are also not covered in this report.

1.4 Innovation Report Structure

In contrast to the individual submissions, this report focusses on the main line of reasoning for this project. In the following the structure of the report is outlined as well as the connection between the sections and submissions.

Section 2 can be summarised as literature review. It discusses the UK stakeholders perspective on grid-tied energy storage systems as well as the relevant energy storage technologies – which connect directly to the contents of submission one. The section also discusses the barriers the uptake of BESS in the GB energy market and the existing approaches to battery modelling as possible solution – which connect to the contents of submission two and the introduction to submission four.

Section 3 encompasses the entirety of battery testing undertaken in this project. It thus connects to the contents of submission three, the paper on Li-Ion pseudo-capacitance and the first part of submission five through each sub-section respectively.

Section 4 describes the development of the BESS model. It therefore summarises the contents of submission four and the second part of submission five.

Section 5 summarises the development of the tool based on the BESS model through description of the individual components and their interaction. It further describes briefly the application of the tool to an EDF Energy R&D UK centre case study.

The outcomes and learnings of this project are assessed and concluded in section 6. Further, long term macroscopic impact as well as limitations and opportunities for continued research are outlined.

2 Background and Motivation

This section summarises the literature review for this project. The first sub-section will provide an overview on the functionality of the GB energy grid and market. The second will discuss the motivation and need for energy storage in the UK. The third sub-section will then discuss the energy storage technologies available and why Li-Ion has been chosen as main technology for this project. This is followed by an overview on the economics of battery storage and the necessity of battery modelling. The final sub-section discusses the current state of the art of battery modelling and identifies the main gap in knowledge addressed by this project.

2.1 Basics of Grid Structure and Energy Markets

The Physical Grid and its Operators

The UK power grid is split into the GB and Northern Ireland grid. Due to the physical disconnect they are operated differently by different entities and participate in different market. Of primary interest for this project is the GB market and grid.

The GB electricity grid is a continuous electrical network connecting all generators and consumers operating at an alternating current (AC) frequency of 50 Hz. The general structure is described in Figure 2. The transmission grid operates at very high voltages between 132 kV and 230 kV and connects all distribution grids together. It also connects to large consumers, generators, storage plants and interconnectors to the neighbouring countries (4–6).

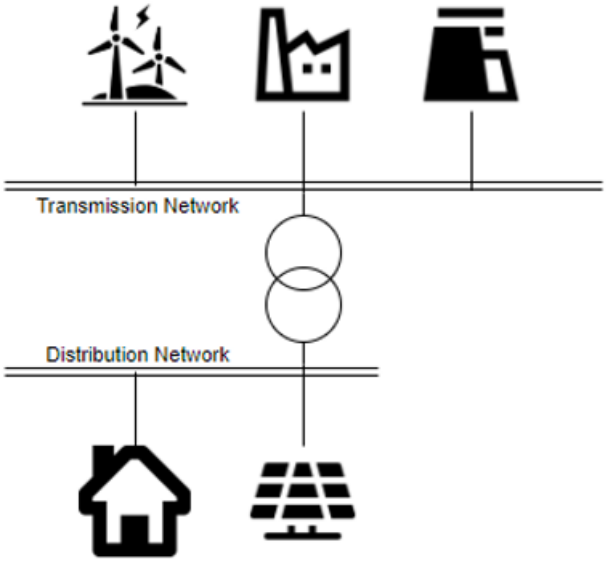

Figure 2: Generalised Grid Structure

The distribution network operates at voltages between 400 V (240 V single-phase) and 132 kV and connects all small-scale consumers and generators. The respective network operators for the distribution and transmission grid sections are displayed in Figure 3.

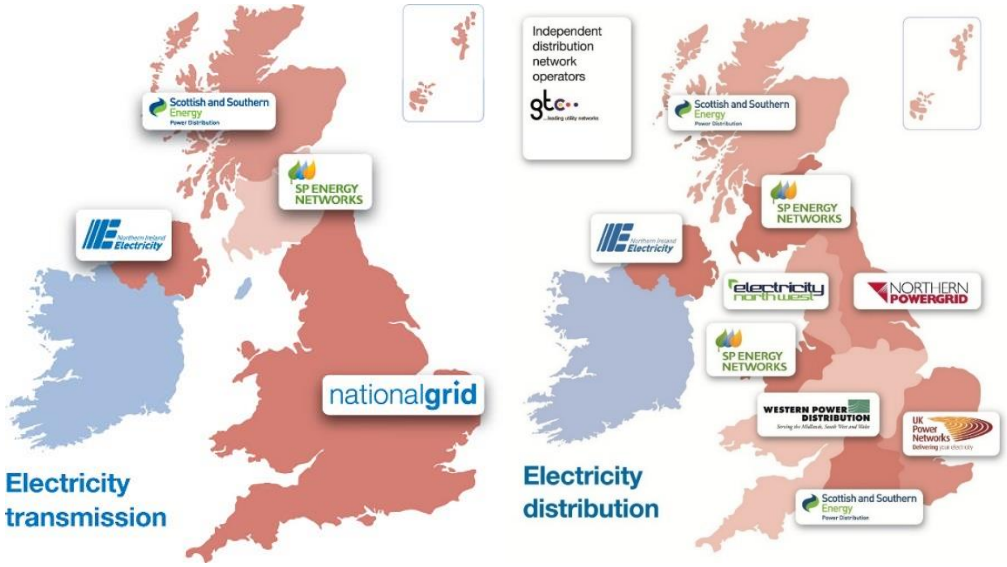

Figure 3: Transmission (left) and distribution (right) network area responsibility (4, 5)

In 2019, National Grid System Operator (NGESO) separated from National Grid Electricity Transmission (NGET) (7). While NGET is responsible for the maintenance and operation of the transmission grid outlined in Figure 3, NGESO is responsible for the net balancing mechanism of energy (matching demanded and generated power) in the entirety of the grid.

The Great British (GB) power grid is connected to the power grids of surrounding countries via interconnectors. As of August 2020, there are four interconnects to France, the Netherlands, Ireland and Northern Ireland with a cumulative capacity of 4 GW. 7.7 GW of additional capacity are currently planned to be implemented by 2022 (8).

The interconnectors trade energy between the markets if there is a sufficient price difference. Thus there is no automatic balancing of the grids. This means that Great Britain has to completely ensure its own dynamic balancing and long term balancing with other countries is limited by the capacity of the interconnectors. This generally incurs a significant need for flexibility and energy storage.

The GB Energy Market and its Participants

The GB Energy Market is physically independent of the location within the grid. Anyone with and without any assets is allowed to participate in any market without regional restrictions or benefits. An overview of the GB energy market is given in Figure 4.

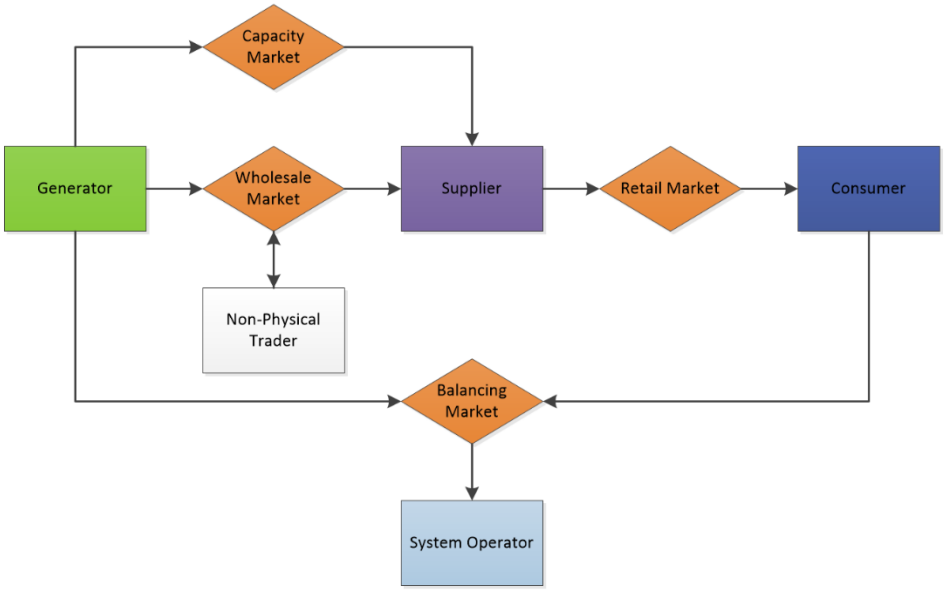

Figure 4: Energy Market Overview

Generators commonly sell the produced energy on the wholesale market in half-hourly periods to the energy suppliers. The suppliers sell the energy then at a long term price agreement to the consumers on the retail market. (9)

The non-physical traders have no assets to consume or generate energy and purely trade with the market with the aim to achieve a net-zero balance. The balancing market will be discussed in 2.2.2, the capacity market will be discussed in 2.2.4. (9)

2.2 The Need for Energy Storage Systems

In the following the need and benefit of energy storage for GB is established from the perspective of four primary stakeholders: the government, the power grid, energy consumers/traders and energy generators. Except for the government, the use cases for energy storage are explained for each of these perspectives.

This sub-section has two purposes:

- Establish the relevance and importance of BESS in the GB energy system and
- Display the multitude of options through which BESS can create monetary value for its operator.

Several aspects of the GB electricity market and grid have changed since the discussion in submission one and are still undergoing changes. This summary should be considered the more up-to-date overview.

2.2.1 Government Perspective

The UK Energy Strategy as outlined in (10) describes an ongoing push towards the achievement of climate goals. In accordance with the Climate Change Act 2008 the CO_2 emissions are supposed to decrease by 80 % compared to 1990 levels. A core strategy to achieve this goal is investment in renewable energy.

As described in (10), the government, together with Innovate UK and the research councils, will have invested approximately £900 million between 2015 and 2021 to reduce the cost of renewables. Further, every two years auctions for contracts for difference (see 2.2.4) are held to support less established technologies such as offshore wind. As of 2019, the current share of renewables in the UK electricity generation is 37.1 % (wind, solar and wave 23.8 %) (11) and as per the Future Energy Scenarios report (12) the wind and solar capacity connected to the grid is projected to double or even triple within the next 10 years.

Renewable energy sources, specifically wind and solar power, introduce two primary difficulties to the UK energy system. They are by nature intermittent and cannot adjust their output to the demand in the grid. Further, in contrast to thermal generators, they don't have a rotating mass attached to them providing inertia (in case of wind energy due to asynchronous operation with the grid and the resulting necessity for frequency converters (13)) to adjust to short term fluctuations in demand. Overall, these decrease the flexibility of the UK energy system, which puts its market and grid stability at risk. It is therefore outlined in (10) how several technologies are promoted to ensure that flexibility including smart grids, interconnection, demand response, aggregation and energy storage.

As per (10), the UK is investing up to £9 million in cost reduction of energy storage in general, up to £600,000 on feasibility studies for a large-scale future energy storage, and further £246 million (now extended to over £300 million (14)) in the Faraday Challenge (15, 16), which aims to promote innovation in electrochemical energy storage.

Aside from the strategy towards achieving climate goals, another problem is the recent global outbreak of Covid-19. Under the given circumstances, any large power plants and particularly nuclear power plants need to adapt severely to make sure that supply is secured without risking the spread of the disease within the facilities (17). Whether this is specifically an issue connected to Covid-19 or a possible future outbreak of a pandemic, automated and distributed power generation can be considered safer to supply the grid during outages. The same can be said about battery storage system in particular to support them.

From this it becomes clear that energy storage in tandem with renewable energy is not only a vital part of the national plan to reduce carbon emissions, but also a necessary asset for a sustainable and secure energy system.

2.2.2 Grid Perspective

This sub-section describes the relevance of energy storage to the GB power grid. First, the GB balancing mechanism and ancillary grid services, meaning options on how private parties can sell the storage services to support the grid, are listed and discussed. Then the major current developments in the grid and the relevance of energy storage for them are considered.

The Balancing Mechanism and Ancillary Services

The balancing mechanism (BM) describes the processes NGESO undertakes to preserve a constant power balance in the grid. Although multiple companies work together to deliver the balancing mechanism, they are in the following collectively referred to as system operator (SO). The power balance is necessary, since the grid is only operational if generation and demand (so the energy going in and out of the grid) are matched at all times.

A measure for this match is the grid frequency, which is constantly held at 50 Hz. Higher generation than demand increases the energy in the grid and hence the frequency. Higher demand than generation incurs a drop in frequency. A certain deviation of frequency is tolerable (limited to 0.5 Hz (18)), but high frequency deviations lead to appliances becoming inoperable and the grid may collapse.

Conventionally large thermal generators operate with rotating masses in sync with the grid. These masses provide inertia that causes them to rotate slightly slower or faster to balance out the frequency deviation. However, this inertia can also be provided by other assets by adjusting their power output.

The balancing mechanism is designed to prevent this imbalance and consists of multiple steps and processes. The first process is to ensure an energy balance, which is shown in Figure 5.

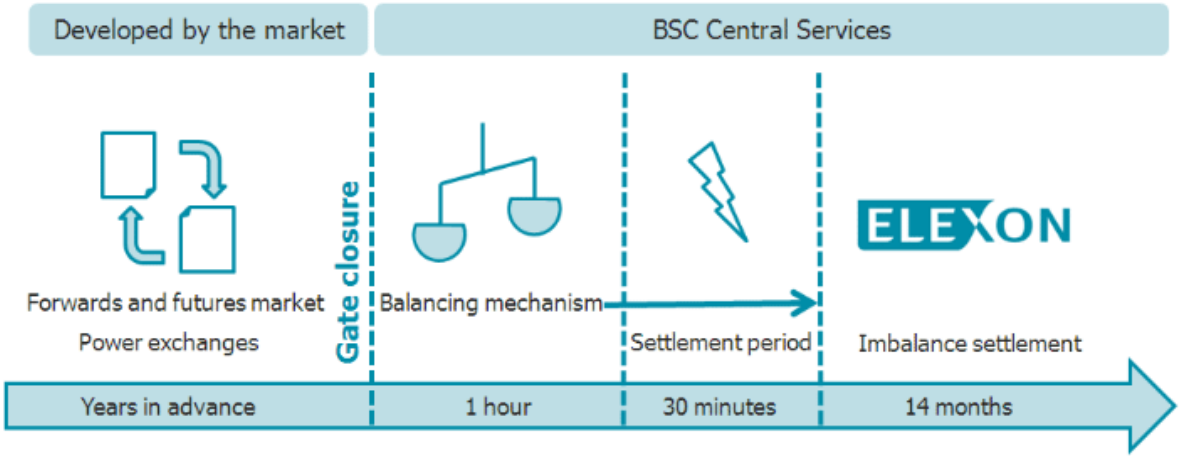

Figure 5: Process of trading, balancing and imbalance settlement for each half hour (19)

Energy is traded as a measure of cumulative energy transferred within a half-hourly (settlement) period. Energy can be traded up to one hour in advance of that period, when the gate is closed. Before gate closure, the BSC (Balancing and Settlement Code) units, meaning all parties involved in the energy market submit their contracted volumes to the SO. Similarly, all large generators (>10 to 50 MW depending on region) and interconnectors submit their planned output. (20–22)

BSC parties may offer to the SO to change their output for a compensation (23) in the balancing market. This process happens within the hour before the settlement period.

Any deviation from the final value by a BSC party is treated as imbalance volume. Depending on whether the imbalance provided by a BSC party is according or opposite of the overall system imbalance, this may result in a penalty or benefit for that party (e.g. providing more energy when the grid did have too much energy results in a penalty). (20)

The second process is to ensure a system balance within the settlement period, since the half-hourly balance only limits the possible mismatch within it. The difference between system and energy balance is displayed through an arbitrary example of two settlement periods in Figure 6.

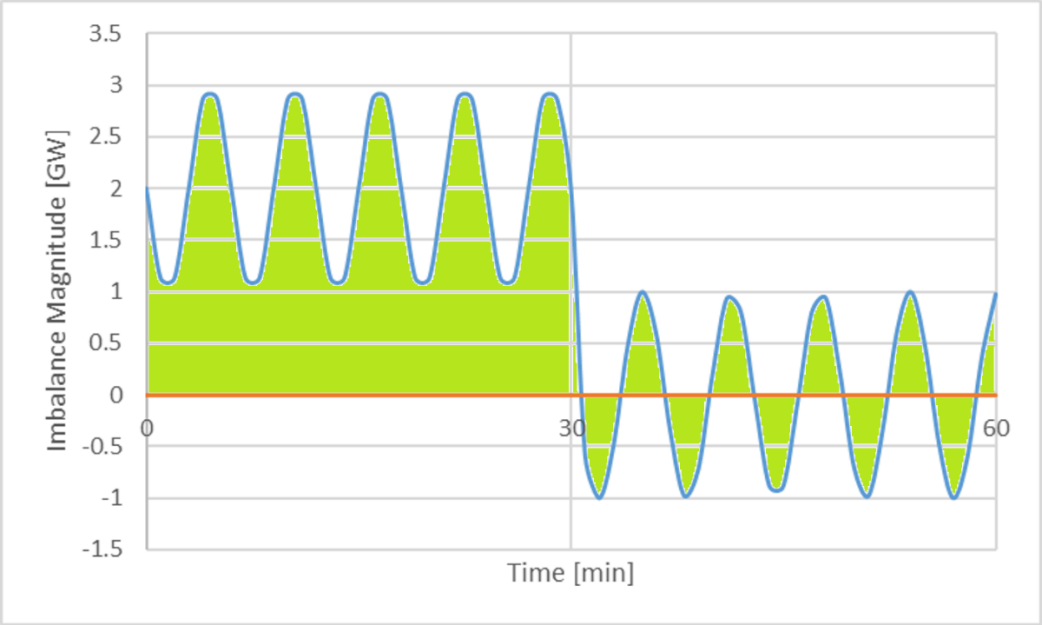

Figure 6: Difference between Energy and System Imbalances

The blue line, representing the system imbalance, describes how the power balance deviates from the equilibrium. The green surface under the curve represents the energy imbalance within the settlement period. In the first settlement period there is an energy imbalance of approximately 1 GWh. While the second period has 0 GWh energy imbalance, there is still a power imbalance of up to 1 GW that must be countered. A wide portfolio of ancillaries services are advertised by the SO to counter the system imbalance.

The most notable service is frequency response. Three main service groups that provide it:

- Mandatory Frequency Response (MFR) is mandatory to be provided by large generators and activates within 10 to 30 s after an imbalance is detected and unidirectional (either ready to increase or decrease generation). (24)
- Firm Frequency Response (FFR) is a voluntary service that has a minimum procurement of 1 MW, activates within 5 to 30 s after imbalance detection and is also unidirectional. (25)
- Enhanced Frequency Response (EFR), is a voluntary service with a minimum procurement of 1 MW, is required to activate within 1 s of detecting an imbalance and must provide its service bi-directional (deliver or absorb power) and is hence specifically targeted to be provided by energy storage with that ability. (26)

Another service group is called reserve services and is meant to increase the active power in the grid in designated time windows. The Short Term Operating Reserve (STOR) is notified four hours in advance to provide its power and the Fast Reserve (FR) has to activate within 2

minutes (27, 28). These services may be satisfied either by delivering power to the grid, or by increasing/shedding load from the grid.

There are a variety of other services that fit in none of these categories (29):

- BM start up, which instructs a normally unavailable BM unit to synchronise with the grid and to be available to provide a bid/offer for the Balancing Market
- Black start, which is procured by power stations to allow to boot up the system after a black out
- Obligatory and enhanced reactive power service, which requires participants to provide or absorb reactive power to stabilise any phase shift in the grid resulting from net inductive or capacitive loads
- Intertrips, which either reduces the output of or disconnects a generator from the grid in case of a fault and
- Super Stable Export Limit, which reduces the output power of synchronous generators below minimum.

The service outlined above are system wide service that can be provided from any location connected to the transmission network and primarily support the stabilisation of grid balance. However, there are also options to support the local grid:

- Transmission Constraint Management is a service provided to the SO where generators adjust their output to reduce constraints in the local transmission network. (29)
- Active Network Management is a service provided to a local DNO where the eligible provider adjusts their output to reduce constraints in the local distribution network. (30)

Instead of frequency, these services allow primarily to relieve local constraints which could otherwise result in extreme voltage deviation or high line currents.

Outside of the ancillary services, another measure to ensure the capability of the generation to match the grid demand is the capacity market, where generators are paid to ensure their power is available. The capacity is auctioned up to 4 years ahead and paid in £/kW of contracted power. The main obligation of participants is to provide the full power when called upon (4 hour notice). (31–33)

With very few exceptions, all of the mentioned services, including the capacity market and the trading of imbalances, can be provided by implementing energy storage provided that they have sufficient scale and, especially regarding the locally bound services, are located in the right areas. Further, the chosen storage system has to fulfil the specific requirements around response time and flexibility.

It should also be noted, that specifically EFR and STOR can be provided through aggregation within a virtual power plant, meaning that the service can be provided cumulatively from different areas of the grid. This would allow even smaller storage installations to participate. (34)

Ongoing Developments

The current ancillary service structure is about to be revamped in the context of the clean energy package (35). Among other changes, the revamp is designed to make the service provision more accessible. This further supports the implementation of storage to provide grid services.

In the electricity ten year statement (36), NGESO outlined several ongoing challenges for the transmission grid. The primary concern is the increasing development of offshore wind, biomass and nuclear power as well as interconnectors at the coast of Great Britain. Coupled with the closure of power plants around the Midlands, the energy stream will go inwards and put high current strain on the network and potentially lead to heavy circuit loading, voltage depressions and stability issues. These are further issues that may be addressed by inserting energy storage strategically to even out the energy transmission and relieve the grid.

It should also be noted, that by gradually replacing conventional energy sources with intermittent energy such as wind and solar power, the grid is losing the inertia of large thermal turbines. Without this inertia, more fast bi-directional frequency response will be required, and thus especially fast-responding energy storage will be in high demand.

2.2.3 Consumer Perspective

This sub-section discusses how energy storage benefits the commercial and private energy consumers of GB. In this context this specifically references all energy market participants without generation assets.

To provide the context of this discussion, the structure of GB wholesale and retail markets (shown in Figure 4) is briefly explained. Then in particular the role of energy storage in these markets is explained.

Wholesale Market

The wholesale market is based on the half-hourly trade of energy between generators and energy suppliers by entering supply contracts (20). While dispatchable generators adjust their output to the amount they sold, intermittent generators try to sell the amount of energy they predict (21). Suppliers try to predict the demand of their customers and buy energy accordingly

(20). Non-physical traders only try to make a profit from buying energy at a cheap price and sell it at a high price.

The latter can be done by any of those parties, but a significant risk with energy trading is the time challenge. At gate closure, all contracts are final, and any deviation from the contract and the consumed/produced value results in an imbalance volume, which is on average more likely to lead to a loss than a profit (see 2.2.2).

Energy storage at scale can support energy trading on all sides by capturing the deviation and neutralising it. Moreover, if a prediction towards the net imbalance volume in the grid can be made, it is possible to create an opposite imbalance flexibly to achieve a profit from the imbalance market.

Generally, energy storage can also be used to perform arbitrage trading by selling energy from a settlement period where the price is low and sell it when the price is high. For this it is necessary to have a storage system with a high roundtrip efficiency. This in particular leads to cheaper energy for the consumer since time restricted surpluses and scarcity are avoided. This also benefits the overall grid efficiency.

Retail Market

Consumers in the retail market receive their energy from energy suppliers at a pre-determined tariff. That tariff contains the costs for the wholesale price, the margin for the supplier and several fees regarding network, operation, environmental and social obligation costs and taxes. (37)

The pricing in the retail market is historically done by either a fixed tariff or a time-of-use tariff that changes the price for separate time periods (peak and off-peak) (38, 39). Since the wide-spread introduction of smart meters in UK households (40), smart tariffs that adjust the price to the current wholesale market price are also possible and applied (41). Irrespective of the tariff, businesses with a nominal connection of 100 kW or greater are required to be half-hourly metered (21).

The primary way of in which both households and businesses can profit from energy storage via the retail market is load-shifting. This is achieved by moving the energy consumption to a low price period. However, there are several other ways they can benefit from it.

Businesses with half-hourly metering pay their transmission network charges through Triads payments. Triads are the three settlement periods of the year with the highest power demand in the grid, which is consequently also the time of maximum strain on the transmission grid. The transmission charges depend upon the measured energy demand of the business within

those settlement periods. By strategically supplying the business through a storage system at those periods or general peak shaving, those charges can be minimised. (42, 43)

Another factor is the connection capacity. Some customers have rare, very high consumption peaks that they would need to account for when requesting a network connection – such as the load required to start-up a plant. Depending on the circumstances, this leads to additional costs to the customer, since the network operator has to provide for that peak at any given time. A storage system can be used to deliver that peak and thus mitigate the required connection capacity and potential grid reinforcement. (44)

In case of a network outage, the consumer can use storage systems to ensure continuity of their supply. This is quantified by the damages avoided and therefore particularly relevant for businesses. (45)

Other, smaller benefits include for instance power quality improvement (45). Consumers can also use storage to provide several of the grid services outlined in 2.2.2.

2.2.4 Generator Perspective

This sub-section describes the generator's perspective on the energy market and the benefits of storage systems. The first section describes the categorisation of generators and the composition of generation in the UK to provide a general representation of different technologies and their relevance. The second section describes the market options and value streams for generators and the last section describes the benefits storage can provide in co-location with generators.

Categorisation and the UK Energy Mix

There are several categorisation approaches for energy sources in the UK. Energy sources are described as:

- "Fossil", if they are based on pre-historic organic material (e.g. oil, gas, coal)
- "Finite" or "Non-renewable", if they rely on a finite source of energy including nuclear
- "Renewable", if they are self-sustainable
- "Intermittent", if their output is not controlled (but potentially limited) by the operators
- "Low-carbon", if they produce significantly less CO_2 than conventional energy sources
- "Thermal", if they are based on the conversion of heat to electricity, primarily through steam and
- "Embedded", if they are connected to the distribution network and have no generation license. (46)

Hence, multiple categorisations can apply to an energy source. The energy mix as of 2019 is displayed in Figure 7.

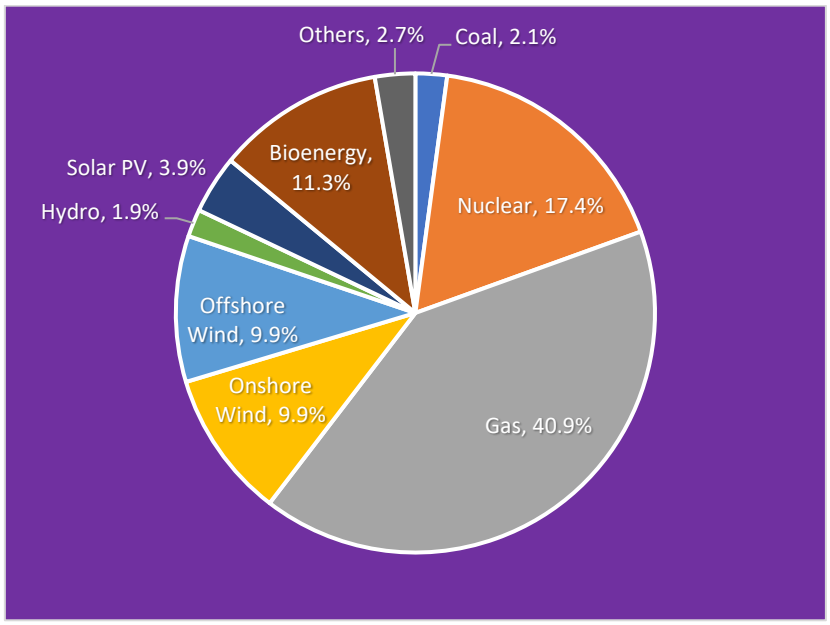

Figure 7: Supplied energy mix 2019 (47)

Not considering the composition of "Others", the vast majority of electrical energy is still provided by thermal (71.7 %) and fossil (60.4 %) power plants. Intermittent energy sources account currently for 23.7 % of the entire electrical energy supplied to the UK.

Markets for Energy Generation

The primary way for generators to earn a profit is to sell their produced energy on the wholesale market. Specifically for renewable energy sources, the renewables obligation (RO) scheme was set up to ensure that suppliers would buy at least a defined minimum of renewable energy from providers.

The RO scheme was closed in 2017 and replaced by the Contracts for Difference (CfD) scheme as part as of the Electricity Market Reform in 2014. This scheme offers operators of renewable generation with a capacity of >5 MW the option to bid for a guaranteed price per MWh. The total amount of supported generation is pre-determined through budgets. If the day-ahead wholesale price is lower than the strike price, the Low Carbon Contracts Company pays the bidder the difference. Should the day-ahead price be higher than the strike price, the bidder pays the difference back. (31, 48)

Any generator, including storage systems, integrated and aggregated generators, with a minimum capacity of 2 MW can participate in the capacity market. Each technology is de-rated based on its reliability, meaning they receive a lower payment for their offered capacity. (31–33)

Small scale operators of photovoltaic (PV), wind, combined head and power (CHP), hydro and anaerobic digestion plants up to 5 MW were able to sign up for a feed-in tariff (FIT) scheme offering them a fixed tariff for the energy generated and for the energy exported to the grid. While the scheme is closed to new entrants since March 2019, the parties signed up before that point are guaranteed the tariff for 20 years from the date of the sign-up. (49)

Embedded generators also have an impact on the overall demand of the supplier or BSC party they are part of by reducing the total amount of energy consumed. This results a reduction in the following charges:

- Assistance for Areas with High Electricity Distribution Costs (50)
- Transmission Loss charges (46, 51)
- Distribution Use of System charges (52)
- Balancing Use of System charges (46)
- Capacity Market Charge (53)

Value of Energy Storage

Since intermittent energy sources on the wholesale market are constrained by environmental conditions, such as clear weather and high winds, it is highly probable that their output will peak within the same settlement periods. Consequently, the competition will be the highest and the achievable price will go down. Having energy storage to sell the energy at higher price periods would therefore be beneficial.

In regards to the CfD, the latest consultation points out that energy storage does not affect the contract, meaning that the generator can claim the full strike price difference (day-ahead price – strike price) for the generated energy and additionally change the time they sell the energy. (54)

Generally, due to the unpredictability of intermittent generators, they are prone to incur some sort of imbalance volume. This volume can potentially be negated entirely through storage systems.

Without the FIT scheme, micro-generation has no viable energy market to participate in. The main incentive for investing in them is hence the reduction in electricity costs through self-consumption. However, the generation of the plant is likely not to match the demand on-site. This is especially true for domestic customers with PV panels, since their average load profiles peak in the morning and evening (55, 56). Home energy storage would allow to increase the self-consumption and minimise the electricity costs. This is also true for existing users of the FIT scheme due to the margin between the FIT export tariff (<5.5 p/kWh (57)) and the import tariff (~14.4 p/kWh (58)).

Generators with an output power of greater than 3.68 kW per phase require a permission by the local DNO to be connected (59). Depending on the location, this can incur high strain (high currents, voltage instabilities) on the network that requires a network extension. Any costs exceeding £200/kW must be paid by the operator unless the DNO offers one of the following alternatives (60–62):

- The plant can be curtailed on demand.
- The plant can be disconnected.
- The connection is reduced to certain time windows.

This limitation can be lifted through the implementation of storage to peak-shave the generation.

Optionally, the storage system can be used to create an island or micro-grid to allow disconnection from the main grid and eliminate any external energy costs and connection charges. (34, 45)

2.2.5 Summary of Value Streams

In Table 1, the primary value streams for BESS in the GB energy system are summarised and categorised by co-location with assets. A storage system has a variety of services that can be accessed as standalone, but through co-location with consumers and/or generators more value streams are unlocked. Hence, all value streams can theoretically be accessed by the same storage system and a co-location is beneficial for the optimisation of the value of a storage asset.

Standalone	Consumer co-location	Generator co-location
Balancing market	Reduction of connection charges	Connection charge / curtailment avoidance
Capacity market	Backup	Increase of self-consumption
Frequency Response	Load-Shifting	Price optimisation
Reserve services	Power quality improvement	
Local grid support	Triad avoidance	
Arbitrage		

Table 1: Summary of energy storage value streams in the GB

There are several considerations that have to be taken into account when planning to utilise energy storage for the provision of these services. Firstly, depending on the technical

capabilities and contractual obligations, some of these services cannot be provided by the same system or at the same time (layered).

Secondly, not all storage sizes can provide all of these services, either due to minimum power/energy requirements or simply due to economic suitability. Domestic applications up to 10 kWh for example would be most suitable for self-consumption or load-shifting. Business scale applications up to 1 MWh can additionally for instance provide local grid support, consider Triad avoidance or reduce their connection charge. Larger storage systems, unless located with large scale factories or wind farms may not be optimal for these applications anymore and instead focus on energy trading and the provision of grid services. To optimise the value generation of the storage system, scalability is therefore highly advantageous.

Lastly, each of these services has a different utilisation profile. Not every storage system is capable of providing every service, but having more available improves its economic viability. Thus, versatility is a desired aspect for them. It should also be noted, that depending on the storage system the use case may affect its performance, which would affect its value.

Hence, the following section will outline the market-available technologies for rechargeable electrical energy storage along with their advantages and disadvantages in respect to the described use cases.

2.3 Electrical Energy Storage Technologies

There are a wide variety of theoretical, experimental and developed electrical energy storage systems. They are commonly categorised by the medium of energy storage as displayed in Figure 8.

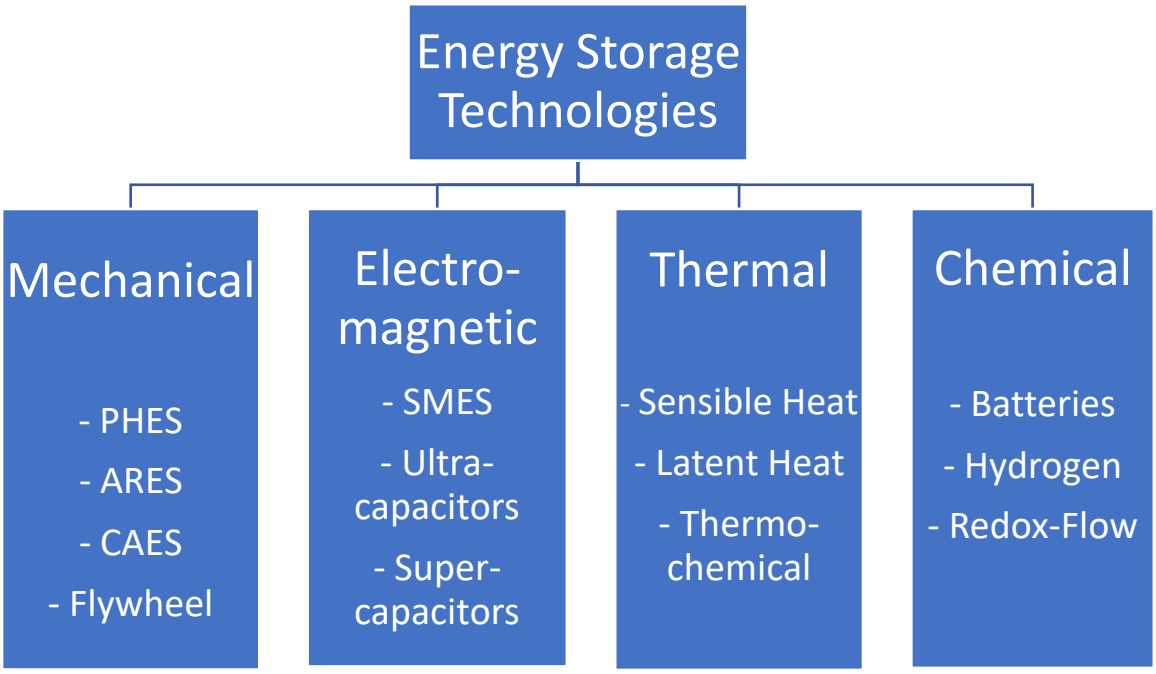

Figure 8: Types of energy storage technologies

The purpose of this sub-section is to discuss the relative merits of the alternative storage systems to provide as many of the services in sub-section 2.2 as possible. In the first part, the storage technologies will be investigated briefly, with focus on their advantages and disadvantages and applicability for the provision of the services. The second part focusses on batteries, exploring the different battery chemistries and judging them by similar standards.

2.3.1 Selection of Storage Technologies

This section investigates several methods of storing electrical energy, with the goal to find the best storage system to fulfil as many roles in the grid as possible. Thus, the following priorities should be set:

- The storage system must be established and market-available.
- The location of the storage system should be flexible.
- The roundtrip efficiency of the storage system should be at least 80 % (approximate based on observations of daily energy price variation) to minimise the loss of energy while optimising the grid.
- The storage system should be capable of high ramp rates to dynamically absorb intermittent demand and generation.

Mechanical Storage

Mechanical energy storage turns electrical in kinetic or potential energy. The prime example is pumped hydro energy storage (PHES). During charge, electrical energy operates pumps to transfer water from a lower to a higher basin. During discharge, the water is led through turbines into the lower basin, which generate electricity again.

Four PHES plants are already in operation in the UK (63). The main advantage is the low levelized costs of electricity (LCOE) of 100 to 230 $/MWh due to their longevity (45). However, while the overall efficiency is over 80 %, the main problem with this technology is the space requirement. Not only does 1 kWh capacity require 367 m^3 of water to be stored at 1 m height difference, to make the system cost effective the environmental conditions need to be already favourable for this application. (9)

Another applied form of potential energy storage is compressed air energy storage (CAES), which also uses pumps and turbines to store air at pressure, commonly inside underground caverns. These also excel through very low LCOE of 120-210 $/kW (45). However, depending on the thermal management of the system, they can only achieve 45 to 70 % efficiency and like PHES they have large space requirements with 1 kWh requiring approximately 50 m^3 of volume (64).

Advanced Rail Energy Storage (ARES) is a novel storage system that utilises the vertical displacement of mass, specifically of railcars, by using electricity to drive them up mountains. While still being an immature technology, ARES displays high ramp rates, low self-discharge and great longevity. However, it shares similar issues with PHES regarding the space and environmental requirements as well as efficiency (~80 %). (9)

In contrast to the previous technologies, flywheels store kinetic energy. Through a motor a large mass is put into rotation in a near friction-less environment, returning the energy through the same motor. Even small flywheels can store large amounts of energy if operated at high rotational speeds - only limited by the material strength of the rotor. The advantages of this technology lie in the extremely high ramp rates and lifetime. While the efficiency is comparable to the afore-mentioned technologies (70-80 %), its self-discharge is significantly larger at high speeds and is therefore only feasible for short-term storage. (9)

Mechanical storage overall has the benefits of long-life and low costs. Potential and kinetic energy storage have a trade-off of self-discharge and spatial requirements. Overall, they are only suitable on medium to large scale where the low efficiencies have less impact.

Thermal Energy Storage

Thermal energy storage turns electrical energy into either heat or cold and regains that energy by utilising the natural dissipation to the ambient environment. How the heat is stored is divided into three categories (9):

- Sensible: stores heat only as a change in temperature of the medium.
- Latent: stores heat by changing the physical state of the medium.
- Thermochemical: stores heat by causing a chemical reaction in the medium.

The most common medium for sensible heat storage is water, which offers a high thermal capacity (4.2 J/kg) (9). A common factor for this variety of storage is size, where smaller sizes have a high surface-to-volume ratio, meaning they lose their heat a lot faster than large systems.

Latent heat storage changes the phase of a material from, for instance, solid to liquid and thus stores fusion enthalpy. The reverse state change releases the heat. Although partially a mechanical (by applying pressure to allow for the phase-change) and sensible heat storage system, liquid-air storage is a practically applied example of this technology. It provides a very high energy density, but due to the required temperature difference also works best at scale. (9)

Thermochemical storage uses sorption or reaction process to store energy in a material for instance through salt hydration. (9)

An inherent consequence of thermal energy storage is the extremely low efficiency achieved near ambient temperature. The Carnot Efficiency, derived from the second thermodynamic law, is the upper limit and dependent upon the temperature difference between the storage medium and the ambient temperature. Higher temperature difference leads to higher efficiency, but also to higher self-discharge through dissipation. Even liquid air, which theoretically has a chance to reach near 100 % efficiency only accomplishes practically 50-60 %. This makes thermal storage unfavourable for our intended application spectrum. (9)

Electromagnetic Energy Storage

These systems utilise electromagnetic effects to store large amounts of energy. Like mechanical storage, they can be divided into categories - potential (capacitive) and kinetic (inductive) energy storage.

Capacitors store energy by using the electric field effects between a positively and negatively charged surface. They have the advantage of high ramp rates and efficiency. Advanced designs include double-layer and supercapacitors, which outperform conventional capacitors as they appear in electronics with higher energy and power density. However a big disadvantage of capacitors is their high self-discharge rate, which limits its applicability to time windows of a few minutes. (65)

Inductive energy storage utilises the property of the magnetic field of a coil to sustain the current that is incurring it. It can be led in a loop and would thus stay uninterrupted until required. Under normal circumstances, high currents lead to high losses within the conductor. Superconducting Magnetic Energy Storage (SMES) counters this problem by cooling the conductor to cryogenic temperatures, where it loses its resistance and eliminates losses. (66)

SMES has the advantage of very high efficiency for the charge discharge process (95 % to 97 %). The main issue, however, is the necessary cooling for the operation, which must be sustained constantly, leading to constant secondary losses. They also have a very low energy density of ~3.5 Wh/kg. (66)

Overall, electro-magnetic energy storage requires very specific circumstances and applications to be feasible as commercial system.

Electrochemical Energy Storage

Electrochemical storage systems are the most common form of electrical energy storage, with batteries being the most established technology. They commonly consist of anode, cathode

and electrolyte and store energy by electrically forcing a reversible chemical reaction which holds the energy until the circuit is closed. Only rechargeable batteries (secondary elements) are used for grid supply.

Common cell chemistries include lead-acid, alkaline, nickel-cadmium, nickel-metal-hydride, lithium-sulphur and lithium-ion. While the detailed performance of battery cells varies by chemistry, they generally excel through high efficiency (>90 %), high energy and power density, almost instantaneous ramp rates, scalability and environmental independency. Specifically compared to mechanical storage systems, they cannot compare in longevity and LCOE, but some chemistries have nonetheless impressive cycle life and reasonable costs. (9, 67, 68)

High-temperature batteries are a sub-category, that requires the system to be kept at temperatures around 300 °C. The most mature technology of this category is Sodium-sulfur, which has similar longevity to Li-Ion batteries, but has the advantage of low costs. The disadvantage is, aside from the average efficiency of 74 to 86 %, the requirement of providing constant heating. This makes this technology on small scale infeasible. (44, 45)

Redox-flow batteries are another sub-category, that makes use of the chemical reaction storing energy in the electrolyte and storing that electrolyte in a tank detached from anode and cathode. Common chemistries in practice and development include Vanadium, Polysulfide, Iron-Chromium and Hydrogen-bromine. (9)

The costs and performance can vary between chemistries, but there are several common factors. The ability to store energy in a separate tank allow for a very flexible design and separate scaling of power and capacity. However, this also incurs additional losses through the requirement to operate pumps transporting the electrolyte. Further, the power of aqueous electrolyte cells is limited by the threshold of electrolysis at high voltages, requiring more cells to create good power supply and incurring high power costs. Lastly, current efficiency values peak at around 90 %. (9)

A different version of chemical energy storage is hydrogen. Through electrolysis water can be split into hydrogen and oxygen. The hydrogen can be stored via several methodologies (e.g. compression, liquification, sorption) and turned back into electricity through fuel cells. The space requirements of the hydrogen storage trade off with costs and energy requirements. But while the technology is overall relatively cheap and renewable, the efficiency of hydrogen energy storage caps out at just above 50 %. (9)

Summary

An overview on the advantages and disadvantages of the discussed storage technologies is given in Table 2. Efficiency considers self-discharge and operating losses as well.

	Power Cost	Energy Cost	Efficiency	Ramp Rate	Space
PHES	>1000 $/kW	<1000 $/kWh	<90%	>1min	Large
CAES	<1000 $/kW	<1000 $/kWh	<80%	>1min	Large
Flywheel	<1000 $/kW	>1000 $/kWh	<90%	<1min	Medium
Thermal	<1000 $/kW	>1000 $/kWh	<80%	>1min	Large
Capacitor	<1000 $/kW	>1000 $/kWh	<90%	<1min	Small
SMES	<1000 $/kW	>1000 $/kWh	<90%	<1min	Small
Battery	>1000 $/kW	<1000 $/kWh	>90%	<1min	Small
High-temp battery	<1000 $/kW	<1000 $/kWh	<90%	<1min	Medium
Redox-Flow	>1000 $/kW	<1000 $/kWh	<90%	<1min	Medium
Hydrogen	<1000 $/kW	<1000 $/kWh	<80%	<1min	Medium

Table 2: Overview on storage technologies performance (derived from (69, 70))

Most of the given storage technologies have niche applications and could potentially fulfil some of the given services mentioned in 2.2.5. In the current energy storage market, however, only batteries are flexible and efficient enough to provide almost all of those services reliably. The most important factor is that battery storage is scalable from home to large-scale grid storage and flexible in location. The closest competitor is redox-flow, which may be able to compete on small scale and power capabilities in near future.

2.3.2 Selection of Battery Technologies

There are many battery technologies theoretically capable of grid support. This sub-section will provide a quick overview on the current commercial options and inform the focus of this project. Ideally, a technology should be found that has good techno-economic performance, is long lasting and market-established. The main technologies are summarised in Table 3.

Technology	Lead-Acid	NiCd	NiMH	Li-Ion
Cycles	200-3000	300-3000	300-1400	500-15000
Calendar life (years)	3-20	5-20	5-10	5-20
Efficiency	60-90	60-90	65-75	75-95
Capacity costs ($/kWh)	60-640	800-1500	430-640	210-2130
Power costs ($/kW)	2070-3300	400-2470	1420-2470	1030-4550
Self-discharge (%/month)	1-10	0.5-20	1-30	0.04-10

Table 3: Comparison of different selected battery technologies, based on data presented by Matthias Vetter in "Energy storage – renewable energy's key 'blade' for grid integration" on the Canada Energy Storage Summit and in "Decentralised PV battery storage systems – system design, integration and optimization" at the Intersolar Conference North America 2014 (9) *and other sources* (9, 44, 77–83, 45, 68, 71–76)

Lead-acid is the most mature rechargeable chemistry on the market. Established through car batteries, they also have found application on grid scale. The chemical reaction is based on the formation of lead-sulfate from lead and lead-dioxide electrodes and sulfuric acid. Compared to other battery chemistries they are cheap, easy to recycle and robust to environmental conditions. Among the disadvantages are the production of hydrogen, which must be vented, the requirement of maintenance, and the performance limitations by low voltage and degradation susceptibility to large cycle depths. (45, 84)

Nickel-based batteries are also very mature. Formerly made with cadmium, they are largely replaced by Nickel-Metal-Hydride cells, which have competitive energy density and cycle life, but are susceptible to deep cycles, like lead-acid (85). They predominantly used for consumer electronics.

Lithium-Ion batteries cover a large group of chemistries that are based on the transfer and intercalation of lithium-ions between anode and cathode as charge/discharge process. An overview on the chemistries is given in Table 4.

Cathode	NMC	LFP	LMO	NCA	LCO
Electrolyte	Organic Liquid Solution				
Anode	C (+Si)		LTO		

Table 4: Commercially common Li-Ion cell materials (86, 87)

While many cathode chemistries offer similar capabilities, the major categorisation within them is by anode chemistry. The two most commonly applied ones are Carbon and Lithium-Titanate. (9, 84)

Carbon (typically graphite) anodes make Li-Ion batteries cheaper and are fairly stable. Two common downsides of this anode is the expansion during charge, which can lead to cracking and damages to the active material/electrode of the cell, and the requirement of a passivating layer to protect the anode from reacting with the electrolyte (88). There are varieties of carbon anodes containing up to 5 % silicon, which offers even higher capacity, but also a reduction in cycle-life since the Silicon particles suffer from extreme expansion during charge (89, 90).

Lithium-Titanate anodes are considerably more resilient than Carbon. They have none of its disadvantages, higher safety, higher discharge rates and incredibly long cycle life. However, they also have a low cell voltage, which results in lower energy density and additional required cell management due to higher cell count in series for the same output voltage. This is amplified by the high cost of titanium, which often outweighs its advantages. (91)

An overview on the different chemistries and some of their capabilities is given Figure 9. The cathode chemistries refer to their performance with a carbon anode while LTO is using NMC or LMO as cathode. Generally different cathode/anode chemistries have very different performance limits, which emphasis the need to consider their differences and to not focus on a single combination.

	Cell level specific energy (Wh/kg)	Cell level energy density (Wh/l)	Typical power (C-rate)	Approx. safety thermal runaway onset	Typical nominal potential (V)	Typical temp. range (ambient)	Year of introduction into market
LCO	175-240	400-640	~1C	150°C	3.6	-20 to 60°C	1991
NCA (EV)	130-240	490-670	2-3C	150°C	3.6	-20 to 60°C	1999
LFP (EV/PHEV)	90-150	190-300	5C cont 10C pulse	270°C	3.2	-20 to 60°C	1996
LFP (HEV)	70-110	100-170	30C cont 40C pulse	270°C	3.2	-30 to 60°C	1996
NCM (EV/PHEV)	100-200	260-400	3C cont 6C pulse	210°C	3.7	-20 to 60°C	2008
NCM (HEV)	70-100	150-200	10C cont 40C pulse	210°C	3.7	-20 to 60°C	2008
LTO	90-130	170-230	10C cont 60C pulse	Not susceptible	2.4	-30 to 75°C	2008
LMO (EV/PHEV)	150-240	240-360	3-10C	250°C	3.8	-20 to 60°C	1996

Figure 9: Li-Ion chemistries and performance aspects

Generally, Li-Ion is considered more expensive than other chemistries but excels through long cycle life and high energy and power density. Using chemical differences they can also be optimised for energy- (e.g. arbitrage) and power- (e.g. frequency response) oriented applications, which is why they are found in a wide variety of use cases ranging from consumer electronics over electric vehicles to stationary storage system.

Lithium-Sulfur batteries, are a promising chemistry that provides a significantly amplified energy and power density at much lower costs. A key problem with this chemistry is the cycle-life which is still very limited. (92)

While Li-Ion covers all of the given chemistries, even on the lower end of the cycle count it outperforms the other chemistries. Regarding efficiency it is the better choice as well. Expectedly, Li-Ion is on the higher end of the cost spectrum, but the technical advantages and its continued improvement and innovation – driven by its existing dominance in the grid storage and electric vehicle market – make it the most favourable technology to investigate for grid storage.

Based on this investigation, Li-Ion battery storage appears best suited for a widespread application as grid storage. Although it still faces challenges regarding recycling, its

performance is both powerful and flexible for a wide variety of applications. Further, it has a long life that requires infrequent replacement and constant improvements in the manufacturing process and ongoing and funded research ensure consistent optimisation of crucial cost and sustainability factors.

Although the technical advantages of Lithium-titanate are of interest to the grid storage market, it is chemically very different and shows significant cost challenges. Therefore this anode chemistry will be excluded from this investigation.

2.4 Barriers of BESS

Widespread implementation of BESS may be attractive, but is not without issues which disincentivise the investment in them. The barriers of BESS can be identified on three main levels: regulatory, commercial and technological. Each of these will be explained here.

Regulatory Barriers

As of the current version of the grid code, energy storage has now a definition as a subset of generation assets and is deemed exempt of several EU regulations (93). However, as a generation asset, it is still subject to unbundling conditions which deny TNOs and DNOs ownership or operation of energy storage (94). This means that energy storage cannot actively be deployed for grid support by the grid operators.

An issue that has been consistent throughout the implementation of storage in the grid is the double-charging of energy storage. For both import and export of energy storage systems are and will continue to be charged locational Distribution/Transmission Use of System charges. It should be mentioned that several other charges like residual Use of System charges are planned to be reduced for storage systems (95).

Another problem is the changing landscape around energy storage and balancing service value streams (96, 97). Especially that the ongoing changes on the grid service structure and regulation mentioned in 2.2.2 make it difficult to estimate the potential value generation.

Although the grid and regulations around battery storage continuously adapt to the ongoing changes in supply of power and inertia, they are still developing and hence pose a risk of unpredictability for investors.

Commercial Barriers

Commercial barriers mainly relate to the inability to fully profit from the different value streams of BESS. This may be a financial, contractual or access disadvantage. In the following it is referred to the value stream discussed in 2.2.5.

While currently under development, the present grid services have very high minimum power thresholds for participation, discouraging the small scale application of storage for grid support. While in some cases aggregation is possible, this requires a sub-contract under the said aggregator (9).

There is an argument to be made, that small scale operators would not be able to compete in the service tenders with larger providers. This however should not disqualify them from provision since there is an opportunity for them to stack value streams from different services.

This leads into another issue with grid services, which is that many of them prohibit the provision of other grid services in parallel, even if that is a technical possibility, would provide additional revenue to the owners and penalty systems are in place (9). One example is the capacity market, which prohibits participation in reserve services (32).

Regarding the retail energy market, price control measures lead to a flattening of the energy price curve (9, 98). While this is beneficial to consumers, this also reduces the ability for energy storage to be a profitable and market supportive asset. Further, the increasing participation of energy storage along with the addition of interconnectors to other countries will flatten the wholesale prices as well.

A minor but potentially very damaging factor for domestic customers is that they have to pay higher value-added-tax rate on energy they import to charge batteries. (99–101)

The ongoing support for renewable energy, especially under the consideration of the CfD scheme, guarantees a profit for their operators. This, however, has the downside of missing incentives to put any control measures on their output, reducing both power and energy stability. While battery storage as a counter measure is not incentivised, it can potentially greatly support their stability.

Technological Barriers

As a long term investment asset, Li-Ion BESS should provide competitive pricing. However, not only is the dominance of this technology in the long term not guaranteed, Li-Ion itself is subject to a constant fall in prices, which went from about $1100/kWh in 2010 to $137/kWh in 2020 (102, 103). While this makes a steadily replaced system attractive, one-off investments are discouraged.

While distributed application of energy storage is beneficial to local grids and allows for more widespread implementation, many technical factors of BESS, such as space, battery management and power conversion, become cheaper with scale. Larger BESS on the other

hand have to compete with existing storage systems (e.g. PHES) and there are fewer businesses and generators available for co-location.

Response to Barriers

As existing and potential providers of BESS, there are limited options to respond to these barriers and make sure their investment remains profitable. EDF Energy as one of the “Big Six” energy suppliers and owner of several both dispatchable and intermittent generation plants has the potential to capitalise on BESS alone or in collaboration with small- and large scale customers. While being able to participate in regulation consultations regarding the UK market and grid operations, as a business they have to ensure through good management and prediction that BESS they invest in are profitable. The best way to accomplish this is modelling.

2.5 Battery Storage Modelling

This sub-section discusses the modelling of BESS. The first part describes the structure of typical BESS for a more detailed analysis and to establish the terminology. There are two general approaches to be taken for battery modelling, which are discussed in detail in the second part.

The sub-sections 2.5.3 to 2.5.6 discuss existing battery models for application. They will be reviewed to whether they can be applied to the targeted use case and advantages and disadvantages will be discussed. It is aimed to find battery models usable for investors with a third-party (disconnected from manufacturing, trade or modelling of batteries) perspective and identify the gap in knowledge in the last section.

Between submission two and the writing of this report some new models have been identified and included in this review.

2.5.1 Structure of BESS

To construct a full BESS model, the structure must be described and identified. Figure 10 displays an example for a setup of a BESS AC co-located with a consumer and a DC generator. While, depending on the generator, a DC co-location (connects generator and battery over the same DC line and only requires one AC/DC converter) is possible this setup allows for a focus on the components of a standalone BESS as well.

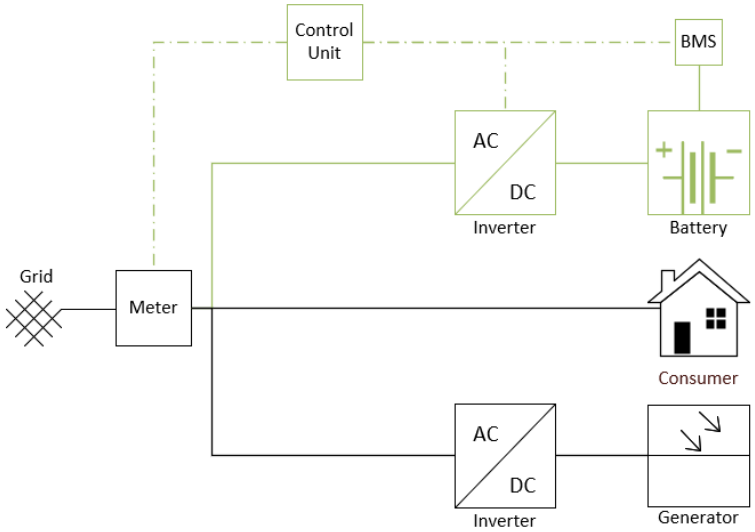

Figure 10: Example of a AC-co-located BESS setup

The BESS elements are shown in green. The UK power grid operates at AC voltage, while batteries require a DC voltage for charge and discharge. Hence, a con-/inverter is required to convert AC to DC current between them. This converter directly controls the charge and discharge processes.

It is important to note that converters are additional elements that require operating power, have a limited power and conversion losses. They also incur additional costs that need to be considered for use cases.

Further, a control unit is required telling the converter to charge/discharge depending on the circumstances. This can, as in this example, happen by connecting it to the meter and have the battery minimise the grid interaction. For frequency response provision it is also necessary to measure the grid frequency or interface with the grid operator.

The battery management system (BMS), which is often part of the converter and mainly relevant to Li-Ion batteries, ensures the safety of the battery through balancing of the cells at high voltages. It also should monitor the battery voltage and prevent over-heating.

The battery itself consists of a matrix of battery cells, which are connected in series and parallel. An overview on the different configuration options is given in Figure 11. Cells are commonly bundled into modules. A string of modules can be described as a pack or rack. The racks are connected in parallel to form the full battery.

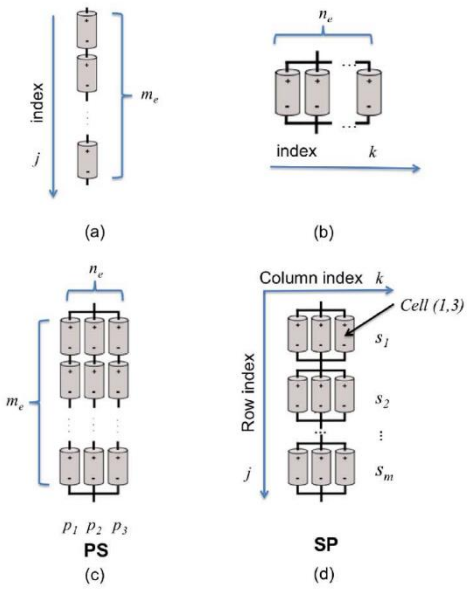

Figure 11: Battery series (a), parallel (b), parallel string (c) and series of parallel pack (d) configuration (104)

The battery cells can have different architectures as well. Common architectures are hard-cased prismatic or cylindrical cells and laminated polymer pouch cells. The latter are usually constrained in modules to provide physical support.

Ideally, all components of the BESS are considered in the model, both regarding their functionality and their cost impact. The main focus, however, should be on the battery itself.

2.5.2 General Modelling Approaches and Priorities

Outputs and Inputs

Modelling of BESS can take a variety of different approaches with different objectives. Ideally, it optimises for maximum net present value or internal rate of return (IRR) and outputs the best choice of storage system, the best value streams and best sizing.

The inputs for the model are subject to severe limitations. Data on the battery services is largely dependent on the use case and historical data. Guidelines and requirements can either be given as per NGESO or be derived from technical values such as peak power of local equipment and generators. A forecast is necessary for the detailed load profile which may be very different from the actual utilisation.

Data on the battery storage systems is also limited, especially before investment. The potential customers, who are usually third-parties (not actively involved in the manufacturing trading or operation of BESS), are commonly provided in advance with datasheets, manuals, warranty conditions and a quote. These describe at high level the technical information on the system, but provide nearly no information on the structure, electrical or thermal behaviour or the ageing.

Wholistic and Focussed Modelling

Wholistic modelling as shown in Figure 12 aims to achieve all of the above, optimising every aspect of the storage system by extrapolating the limited data given in advance. Wholistic modelling needs to consider the financial aspects, the scheduling of the services and the response of the battery to these options (electrical response, degradation etc.).

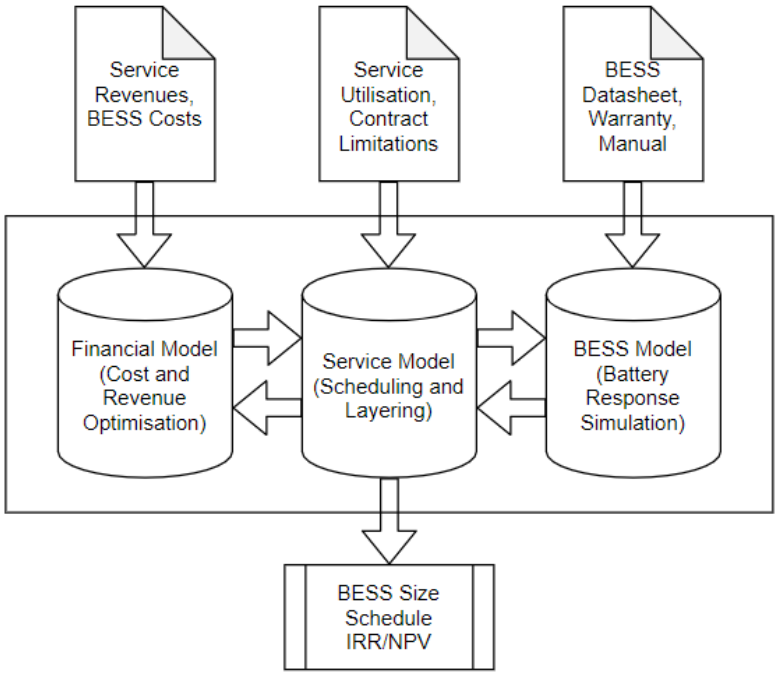

Figure 12: Wholistic BESS Project Modelling

The main advantage of this model is that it requires very little effort from the user aside from the acquisition of the data. After the data is provided, the wholistic model will process everything standalone and provide all the data required.

The main problem with this model is its complexity. The battery model would ideally contain a detailed model of electrical, thermal and ageing behaviour that can be applied for any time period. The service model would need to call this model for every single combination and series of services possible within the maximum contract duration, and then need to compare the revenue of each. Considering the variety of services and layering opportunities this would quickly become too complex to be computationally processed within reasonable time periods.

Another problem is the inflexibility. Considering how quickly the data on services can change, having to regularly update and re-run it would take a lot of effort. Sensitivities would be hard to identify and the outputs are only the ones pre-determined. Also, even small changes to the model would be very difficult to implement.

Focussed Modelling takes a different approach by focussing on a specific part of the BESS project modelling, specifically one of the sub-models of the wholistic modelling. The sub-model with the most benefit to the EDF Energy R&D UK centre would be a BESS model (especially as they already have a number of optimisation algorithms available). This model does not consider the service composition, nor the financial impact of the service and instead purely focusses on impact any utilisation has on the system.

Examples for this kind of model are given in (105, 106) and the basic structure can be described as in Figure 13. It consists of an electrical, thermal and ageing model that work dynamically together. Inputs are the initial and environmental conditions of the system and utilisation (i.e. cycling) of the use case. As output, the final response of any of these models can be selected depending on the chosen purpose.

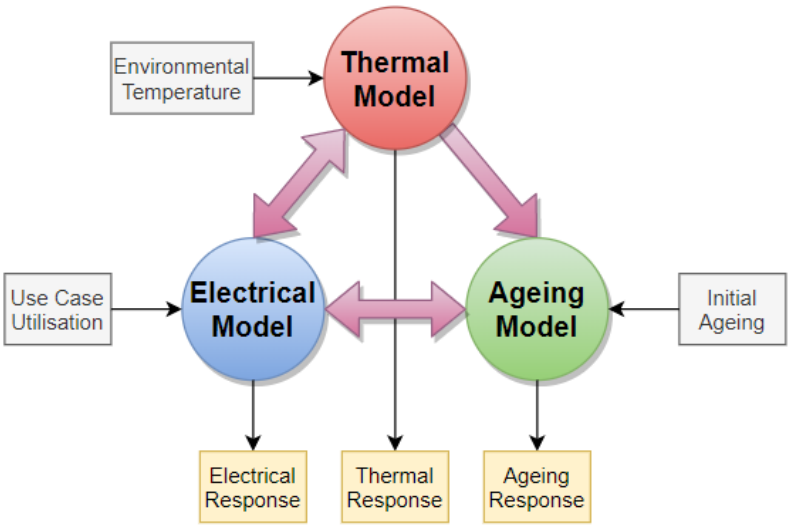

Figure 13: BESS Focussed Modelling

This modelling approach offers great levels of flexibility:

- Outputs: Not only can it be used to extract the degradation of the model, any aspect of interest like power capability and heating can be extracted as well.
- Modification: Each of the models can easily be modified without interfering with the operation of the overall model.
- Time: The model can be used for any time period.
- Integration: The model can be directly integrated in other tools/models or used as pre-calculation for different types of services.
- Enhancement: Additional information on the storage system can easily be added to the model.

Since it only focusses on the simulation of the three core models, it can also be expected to be computationally fast to process. It can be easily optimised to provide better accuracy or speed.

The disadvantage of this model is that users have to have more understanding of how the BESS works in connection with the grid. But detailed knowledge on the functionality, while beneficial, is not required. The overall use case comparison also has to be done by the user or a shell tool.

Whilst initially the wholistic modelling was the more desirable approach, based on the mentioned pros and cons, a focussed tool has been found to be of greater benefit to the EDF Energy R&D UK centre.

2.5.3 Full Modelling

Full models are existing models and tools that consider electrical, thermal and ageing aspects and can directly be applied to a use case. The authors of (105) provide such a model as a focussed modelling approach for EV applications. The model is shown to simulate the interactive behaviour of many cells in a pack configuration of arbitrary size. The model is based on experimental data on cylindrical LMO cells and allows for a detailed evaluation of capacity loss and voltage responses for power limitations and the differentiation between the impact of different utilisation profiles.

It also provides an indication for the calculation time for multiple cells in parallel and series as shown in Figure 14.This graph shows that a combination of parallel and series cells can quickly lead to multiple minutes of calculation for a single cycle, which is very impractical considering long term modelling.

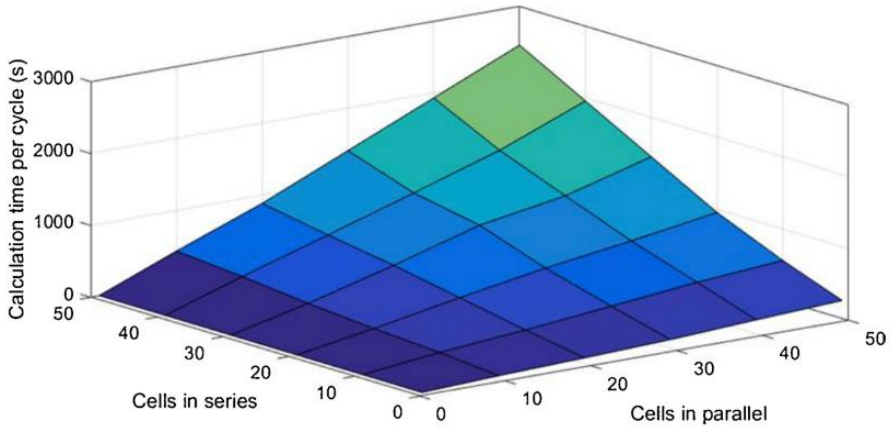

Figure 14: Calculation time per cycle as function of cells in series and parallel (105)

Further, while the detailed modelling process is given, their approach does not contain the numerical data necessary to fully replicate it. It can also be considered inflexible to changes in the replicating system (for instance change of cell size, chemistry).

The Battery Lifetime Analysis and Simulation Tool by the National Renewables Energy Laboratory is a free wholistic modelling tool that allows for the financial analysis of BESS. This model is also using a combination of electrical, thermal and degradation models based on data of NCA cells. The tool is fully automated and requires as input some basic information on the storage system and price and cost information. The full simulation of energy trading aims to optimise for the IRR of the system. (106)

The advantage of this tool is the accessibility for unexperienced potential investors in energy storage. It allows for an easy approximation of the behaviour of the BESS and a use case optimisation. As a wholistic model, the main drawbacks compare to the ones mentioned in 2.5.1. The tool is not applicable to any other use case than energy arbitrage and any other storage system. (106)

Similar problems occur with the model of (107). While this modelling approach investigates the full application and feasibility for a photovoltaic storage system and includes an in-depth investigation in ageing mechanisms, it is also very specific for that use case and not easily translatable to other problems.

Several other wholistic models and tools have been developed to specifically investigate the viability of energy arbitrage and grid applications of BESS in several energy markets. These models, however, heavily abstract the electrical and rarely consider thermal behaviour of BESS and utilise simplified references for battery degradation. They also focus on very specific applications (such as optimisation of arbitrage trading), making the models inapplicable to other use cases without severe modification. (108–111)

In conclusion, while there are existing models and tools available, they are either very detailed and extremely difficult to replicate ((105–107)) or fully or partially replicable and heavily abstracted ((108–111)). In all cases, the models are only applicable to specific use cases and/or chemistries. Considering the requirements of adaptability and the inability of current full models to fulfil them, a new model should be constructed.

2.5.4 Electrical Modelling

The electrical model of a BESS contains three main steps:

- The translation from the AC to DC voltage via the converter
- The split of the power across the interconnected cells of the battery and
- The internal processing of the power by the cell.

Models for the converter response are mostly unnecessary, since values such as self-consumption, power rating and efficiency are commonly given in the datasheet. Thus the focus will be on the latter two steps.

Battery Pack

Battery packs are mostly subject to the normal circuit rules of series and parallel connection of batteries. This applies to both the stacking of voltages and the addition of battery resistances. However, there are several considerations to be taken regarding the capacity management of cells in series.

Li-Ion cells are commonly operated around 3-4 V, subject to the choice of cathode. Each type has upper and lower voltage limits that should not be exceeded during operation, since otherwise the cell can experience severe damage. This means that when approaching the upper and lower SoC of the storage system, the battery pack will have power limitations that need to be considered in the model.

Even when considering the battery pack voltage limits, depending on the state of charge (SoC; charge of cell relative to total capacity) and the degraded capacity of cells in series, it is possible to exceed the voltage limit for individual cells. An example is shown in Figure 15.

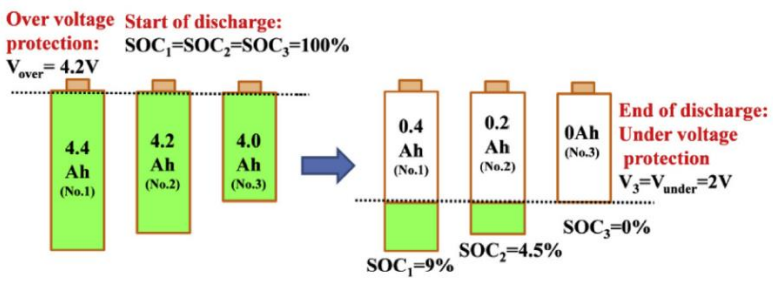

Figure 15: Impact of charge imbalance on voltage limit (112)

The authors of (113) summarised all methods of active and passive methods of cell balancing. They describe that initially cells in modules are matched to minimise the variability and thus the possible imbalance, which is confirmed in (114).

Generally, balancing methods are categorised differently depending on the author so the following categorisation is based on the structure outlined in (113). Passive methods of balancing requires no monitoring or action from a BMS. For lead-acid and other chemistries it is possible to have the cells overcharge, turning remaining energy into heat but consequently also leading to hydrogen release and premature ageing. Since that is not possible for Li-Ion batteries, the only passive option is to have the batteries be connected to resistance that

discharge the cells once the maximum allowed voltage is achieved. This leads to high additional losses. (113)

There are a multitude of active balancing methods involving bypassing or charge-redistribution. The best bypassing technique is shunt resistor bypassing, which connects a resistor in series when an overcharge is detected. This method is very cheap and easy to implement. The best way for charge re-distribution is using switched capacitors which move energy overheads from cell to cell. This increases the efficiency but also the pricing of the BMS. (113)

Since active methods of balancing has major advantages it can be expected to be implemented in all modern Li-Ion BESS. The method of implementation is likely to be shunt resistors due to the price factor.

Cell Equivalent Circuit Model

The electrical behaviour of battery cells can be regarded from various perspectives. Since technically a battery is not a simple circuit element, methods of abstraction are necessary. Circuits representing the battery cell behaviour are therefore called equivalent circuit models (ECM).

The model by (115) describes each of the chemical process as a series and parallel combination of various resistors and capacitances. Many existing ECMs use simplified, phenomenological versions of this model that aim to summarise the processes. An overview of the commonly used ECMs is given in Figure 16.

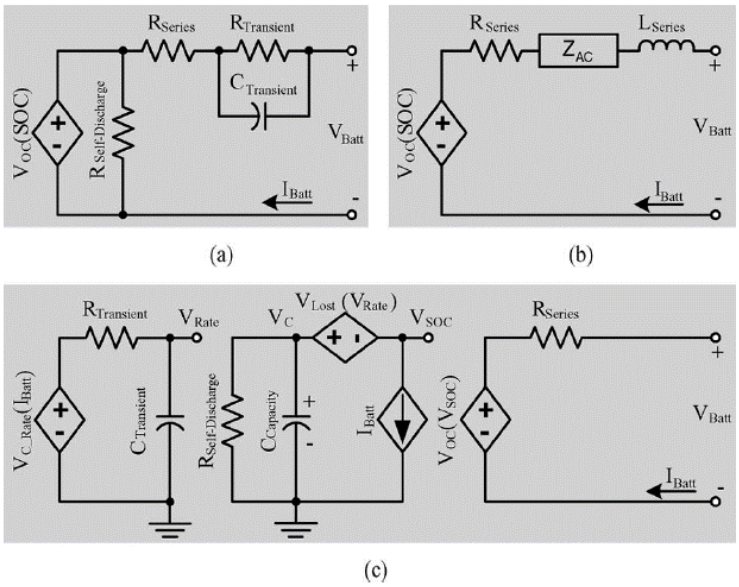

Figure 16: Common Li-Ion ECM a) Thevenin-model, b) Impedance-based model, c) Runtime-based model (116)

The Thevenin model is the most referenced approach for ECMs. This model replicates the transient behaviour of battery cells through one or more RC elements with the series resistance providing the initial voltage jump of the cell. There are many modifications to this model that mostly involve the number of RC elements and different implementations of the self-discharge. (107, 116–123)

The impedance based model is one of many AC generated ECM. It considers aside from the series resistance an inductance (commonly active at very high frequencies) incurred mostly through cable connections (124), and a Z element, representing a cross-connection of many RC elements. (116, 122)

An extended version of this model is displayed in Figure 17. This version contains instead of one Z element a combination of constant-phase-elements (CPE; themselves a combination of capacitors and resistance incurring a constant phase shift) and resistors. One particular CPE in this circuit is the Warburg element, which reflects the diffusion process of charge and discharge. This model is commonly parameterised through electrochemical impedance spectroscopy (EIS) at high frequencies and provides the impedance spectrum shown. (124)

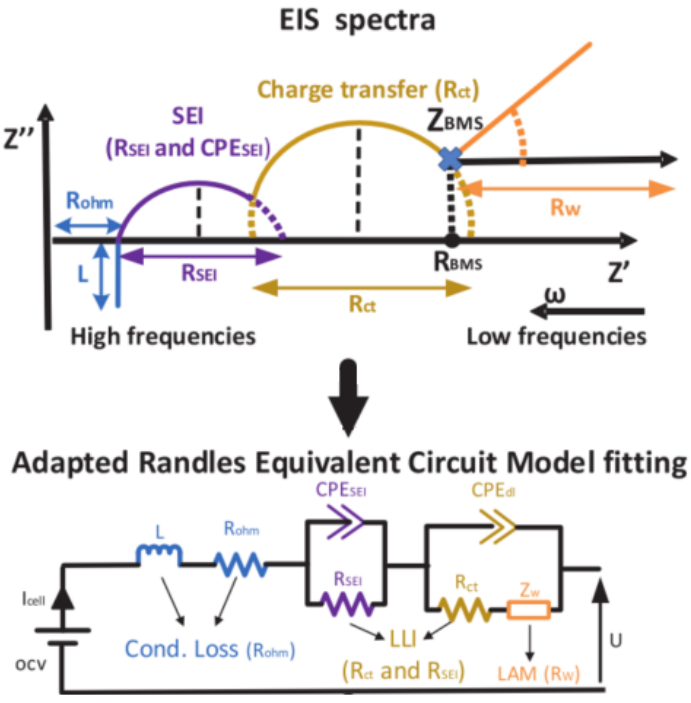

Figure 17: Typical EIS spectrum of Lithium-Ion batteries and ECM adaption (124)

This ECM works well with AC utilisation of batteries, but fails to properly project transient or DC behaviour. It is therefore mostly used for diagnostic purposes.

The last ECM displayed in Figure 16c is the runtime-based model. This model splits the various electrical characteristics of a battery cell into multiple sub-circuits, namely a surface circuit with the series resistance, a transient circuit modelling the transient voltage response as in the Thevenin model and a state-of-charge (SoC) circuit with a capacitor representing the charge of the cell.

The SoC is expressed as percentage of the maximum coulombic charge of the battery:

$$SoC = SoC_0 + \frac{\int Idt}{Q} \quad (1)$$

This relationship can be electrically expressed through a capacitor charged with the cell current I. The cell capacity Q serves as capacitance and the SoC is the voltage over that capacitor. The voltage of the SoC circuit and the transient circuit control the voltage source of the surface circuit. (116)

This ECM is again more a phenomenological approach and tries in particular to capture the change in open-circuit voltage (OCV) depending on the SoC of the cell. The OCV itself is subject to many existing modelling approaches. Commonly it is recorded from experiments by charging/discharging the cell and then having it rest. Some sources, such as (125) attempt to describe the OCV curve through an equation.

While experimental data can provide the OCV curve for different chemistries, there three additional impacts on the OCV curve to consider:

- Two different cells with the same chemistry from different manufacturers may have different curves, for instance due to differences in electrode composition, charge priming or initial SoH. However, the voltage windows don't commonly change.
- The OCV curve may change over time depending on the ageing mechanisms. (125, 126).
- The OCV is impacted by temperature. (127)

It should be noted that the OCV is subject to a small hysteresis. After a charge or discharge, the OCV is subjected to a small voltage offset (positive after charge, negative after discharge). This hysteresis has been identified in (128, 129) and is small enough to be commonly ignored for modelling (120, 130–132).

While the self-discharge is in Figure 16 represented as a resistance, representing it as dependent upon either open circuit voltage or SoC, other sources also describe it as a current (133). Generally it can vary between 0.1 and 5 % SoC loss per month depending on the cells and conditions (134–138). Dependencies upon SoC and temperature are inconsistent across

these sources and seem to generally not exceed that boundary under nominal conditions. This rate is extremely small.

Overall, while many ECMs already exist and can be replicated, they are only applicable to the cells investigated. Even ECMs that adapt to changing SoC, state of health (SoH) or temperature such as (117, 122, 139, 140) can only be applied to that specific cell type. The relationship between OCV and SoC is generally similar within chemistries, but unknown dependencies should be acknowledged. To make a usable model it is important to be able to adapt the electrical characteristics of the ECM to the given system.

2.5.5 Thermal Modelling

Thermal models describe the temperature (T) development based on heat generation and transfer. There are again multiple perspectives to be taken on each. Cell heating is described in (141) as a summary of joule heating, enthalpy of reaction, enthalpy of mixing and phase change. Several authors consider the latter two factors to be negligible (127, 142) although this can be very dependent on use case. Overall this relationship can be described as follows:

$$q_{th} = q_{joule} + q_{ent} \tag{2}$$

$$q_{th} = I * (V_{cell} - V_{OC}) + I * T * \frac{dV_{OC}}{dT} \tag{3}$$

It should be noted that the joule heating q_{joule} contains two processes: The purely ohmic resistance of the cell and the overpotential (cell voltage V_{cell} minus open-circuit voltage V_{OC}) incurred by the diffusion processes. Phenomenologically, they correspond in sum to the resistances of the electrical ECM. Thus, Joule heating can be calculated from the ECM currents through the resistances.

The enthalpy of reaction q_{ent} is also often referred to in literature as entropic heat, and is a reversible heat generation incurred by the chemical reaction. During charge/discharge, the heating/cooling is reversed. The value for entropy $\frac{dV_{OC}}{dT}$ is dependent on the SoC and this curve also changes depending on the cathode chemistry, manufacturer and can also be different from cell to cell. (127, 143, 144)

Heat transfer requires a model that encompasses all elements that may have a reasonable impact on the battery cell temperature. The most basic approach is to only consider the cell as a lumped model with a heat capacity, conduction and convection. Those can be expressed through an ECM as shown in Figure 18.

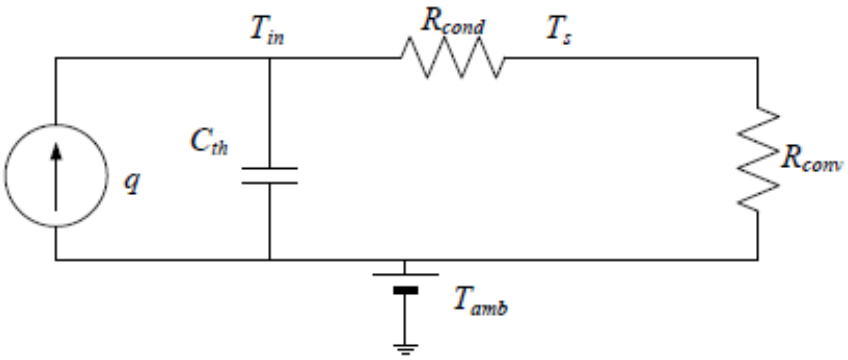

Figure 18: Simplified thermal model of a single Li-Ion cell (127)

q represents in this figure the heat generation as a current source, T_{in} the cell core temperature, T_s the surface temperature, T_{amb} the ambient temperature, R_{conv} the convection resistance, R_{cond} the conduction resistance and C_{th} the heat capacity. In order to keep the consistency with the electrical ECM and to avoid confusion with the cell capacity, the heat capacity will be referred to as heat capacitance from here on.

This ECM only encompasses the battery cell, which is a reasonable approach considering it is both the only unavoidable heat resistance and the only referenceable part of a full BESS, since depending on the assembly of the module and or rack the cooling methodology and efficiency can change significantly.

On a more macroscopic level, the models in (145, 146) explore the cell to cell relationships of heat transfer, while the authors of (106) consider the thermal model a lumped model of the entire storage system. In the other direction, there are models that try to increase the precision of heating and distribution within the cell body, such as (146–148). But these models only apply to the cases investigated and are not necessarily universally applicable.

While the heat generation can be approximated through the electrical characteristics of the cell, the heat dissipation is much more difficult to determine, since it is highly dependent upon cell structure, material and cooling system. It is therefore recommended to use a reference cell or module. However, in that case the heat generation must be scaled to the parameters of the cell in the dissipation model.

2.5.6 Ageing Modelling

Degradation Measures and Mechanisms

Battery degradation or ageing models attempt to identify two things: a measure for the degradation of the battery and the factors impacting said degradation. In reality there are a

multitude of ageing mechanisms that can lead to a variety of failure modes. An overview on these mechanisms is given in Figure 19.

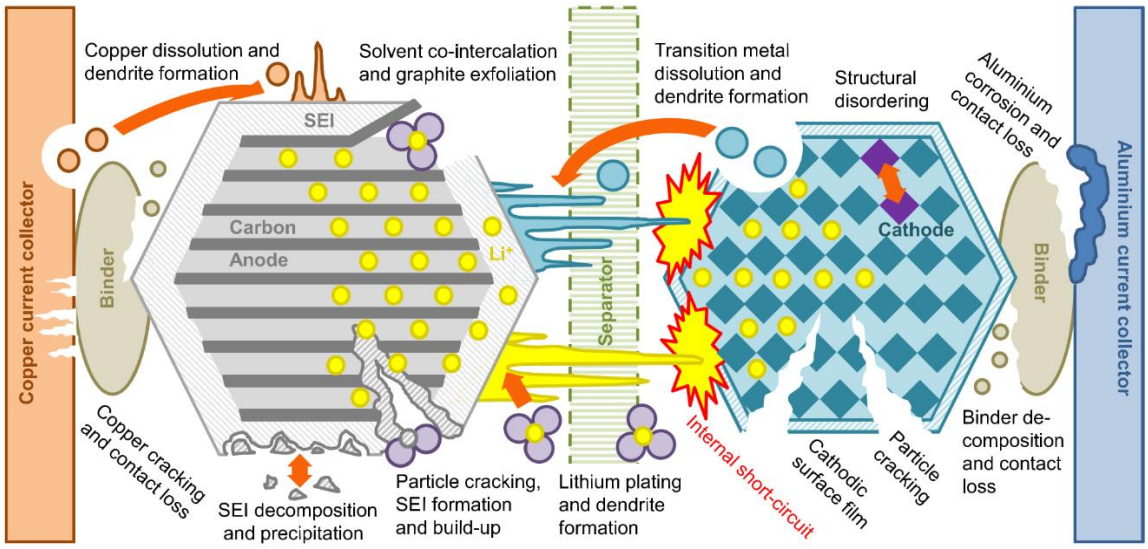

Figure 19: Degradation Mechanisms in Li-Ion Cells (126)

Effectively, battery cell degradation can have three main consequences: the loss of coulombic capacity, the increase of internal resistance and possible the immediate death of the cell through internal short-circuits. Since the latter is extremely unlikely in modern Li-Ion batteries and commonly a result of abuse or extreme conditions outside of manufacturer recommendations (including fast and/or low temperature charge) it will be disregarded as possible consequence.

Nearly every process within the cell can affect the cell resistance, since any damage on the transmitting materials blocks the movements of electrons and/or ions through the cell. Capacity loss on the other hand is connected to three values: the capacity of the anode, the capacity of the cathode and the lithium inventory. The overall capacity is representative of the minimum of these three values. (126)

Figure 20 provides an overview of how operation of the battery affects the different degradation mechanisms and consequently capacity and resistance. These are specifically focussed on the processes reducing capacity.

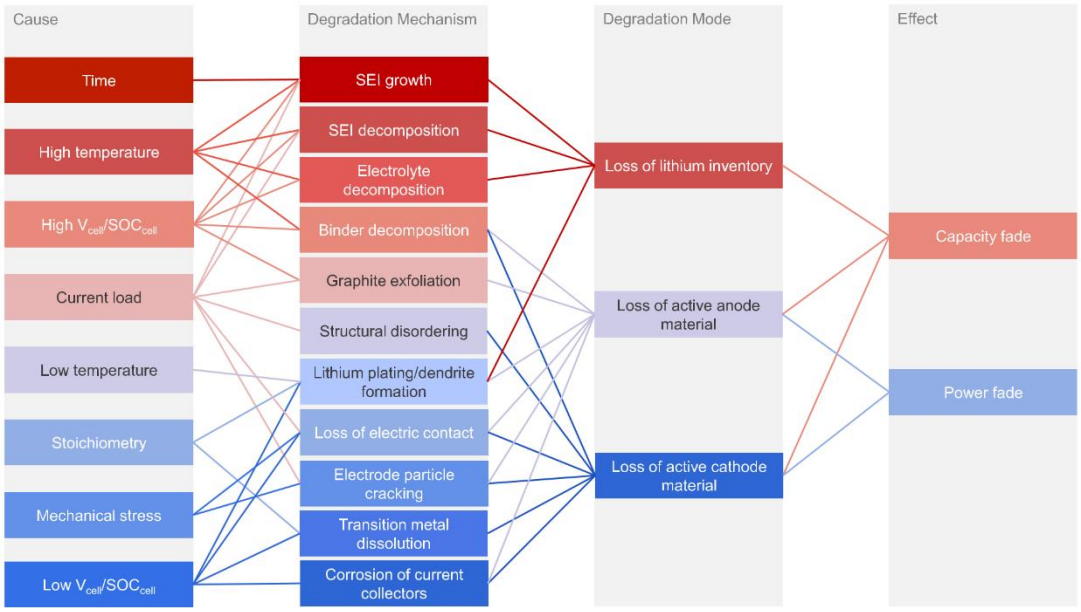

Figure 20: Cause and effect of degradation mechanisms (126)

In practical battery modelling, it is impossible to forecast the detailed development of each of these processes. Therefore most authors either reduce degradation modelling to the most common and impactful process or approach degradation modelling empirically.

The coulombic cell capacity is commonly used as main indicator for ageing. The most common shape for cell degradation over time and/or charge/discharge cycles is given in Figure 21. Essentially the capacity loss starts very rapidly and decreases over time until reaching a certain threshold. At this threshold, called the knee-point, the cell loses capacity rapidly. For this reason it is commonly defined as the end-of-life (EOL) (149, 150)

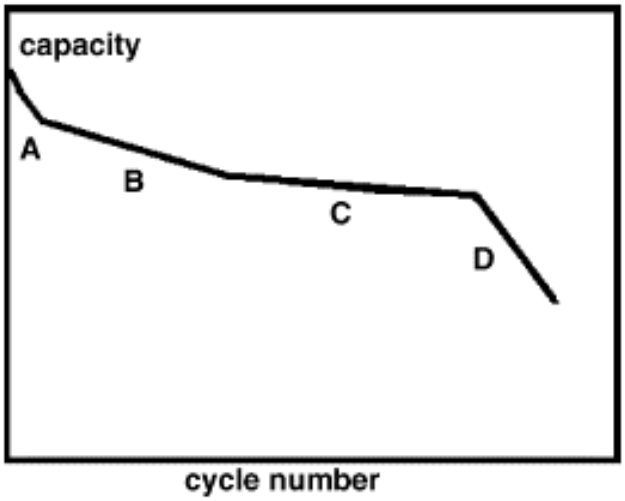

Figure 21: General shape for capacity versus cycle number plots (149)

The zones A-C are the main usable life of a battery cell. They are therefore the most commonly modelled zones. Most authors identify these zones primarily as a result of the growth of the solid electrolyte interface layer (SEI), which reduces lithium inventory (151–153). The knee point is described as the onset of lithium plating when the SEI layer is too thick to allow for intercalation into the anode (88, 154, 155).

The threshold between C and D is commonly identified by the remaining cell capacity. In the automotive industry it is usually placed at 80 % to ensure performance (although cell resistance is there a more dominating factor), but for stationary systems it can be 70 % or less. Generally, 80 % can be seen as minimum value up to which the cell will not reach the knee point.

The ageing of the internal resistance (specifically the DC resistance) is sometimes used as indicator for the power fade of the battery, wherein the overpotential of the battery increases with rising resistance R_{ch} and thus limits the maximum charge (P_{max}) and discharge (P_{min}) power near the voltage limits V_{max}, V_{min} (156):

$$P_{max} = V_{max} * \frac{V_{max} - V_{OC}}{R_{ch}} \tag{4}$$

$$P_{min} = V_{min} * \frac{V_{min} - V_{OC}}{R_{dc}} \tag{5}$$

Resistance constantly increases as the cell ages, which is incurred by the increase in SEI thickness and damages to the individual parts of the cell (124). While some sources ((118, 157–160)) developed models specifically to forecast resistance ageing, others recognise the similarity to the capacity decrease and instead state a linear correlation (154, 161). The authors of (162) recognise the end-of-life of the cell as the point when the cell resistance is twice its original value.

Overall, the capacity is the more dominating factor, since it is a more reliable and the industrially accepted degradation indicator. It is also more relevant to this project since many grid services are energy oriented. Therefore, the SoH at a time t is here expressed as a measure of relative capacity loss:

$$SoH_t = \frac{Q_t}{Q_0} \tag{6}$$

Modelling Approaches

Knowing the principal measure of ageing as well as the dominating processes, it is now necessary to find a suitable model. Models for capacity ageing can be roughly divided into three sub-categories:

- Datasheet: Based on data obtained from the manufacturers' datasheet.
- Chemical: Based on the chemical relationships within the battery cells.
- Empirical: Based on the phenomenological data obtained from testing.
- Mechanical: Scaled by data from testing the model is derived from mechanical strain relationships.

There are several models which mix these approaches as well. It should be noted that in the following the focus will be on capacity degradation models.

Datasheet modelling is the most straightforward modelling approach, since it only takes data as input that is available to the customer. The authors of (163) utilises a cycle count to depth-of-discharge (DoD) curve to derive an adaptive cyclic ageing model. Also part of this group are bucket models that consider purely the throughput as a measure of degradation such as described in (110).

The advantage lies in the accessibility and adaptability of the model. It can be applied to any storage system and is close to the data available to the manufacturer. However, specifically the given models consider only the smallest amount of information on the system. Further, they are not flexible towards different utilisation approaches and are likely to be false when deviating from the utilisation the manufacturer tested.

The most common ageing models are empirical, such as the approaches of (157, 158, 170–173, 159, 160, 164–169). These model establish connections between the calendric and cyclic utilisation and capacity loss based on approximate mathematical descriptions. Some of the inputs are derivations or summaries of the parameters in Figure 20, such as full equivalent cycles (FEC) or DoD.

These models achieve very high accuracy for the data and cells they are based on. Consequently some of them are just refitted version to other sets of data. This means that to apply them to other cells they would need to be refitted to data on those cells again. Further, since the models are based on very specific utilisation and partially derived parameters, they are unlikely to fit slightly altered conditions.

Mechanical models, such as (110, 151, 174, 175), utilise mechanical analogies of material strain and treat batteries as if they were subject to it in the same way. These relationships are fitted to the experimental data. They often involve rainflow-counting to evaluate charge/discharge cycles. The advantage of these models is their linearity, allowing the user to compare linear health loss to the benefit of its utilisation.

The disadvantage is the obvious implication that batteries behave like homogenous materials. They are subject to several non-linearities, of which the capacity curve in Figure 21 is a good example. This makes them less accurate than purely empirical models.

Chemical modelling as shown in (153, 176, 177) is not based on experimental data but rather the actual chemical first principles leading to degradation. The models shown are based on a single particle model, meaning that all of the cells relationships are averaged onto a single particle. The parameters are mostly determined from data on the materials and dimensions, although some parameters can only be obtained from experimental data.

Assuming that all relevant processes are captured, chemical modelling can be considered the most robust and accurate. Compromises taken upon the considered mechanisms, the single-particle approach and differences between individual cells may impact its accuracy. Further, being the most specific approach, this model cannot be applied to any other cell chemistry, type or even given manufacturer and may require and in-depth cell autopsy to recreate.

Semi empirical models as shown in (133, 161, 166, 178) are a mix of chemical and empirical modelling. They adapt chemical dependencies confirmed through experimental data, such as the Arrhenius equation for temperature, and fit them to the experimental data. This makes them inherently more robust to changing circumstances. However, the equations shown are only partially adapted from chemical relationships.

All of these modelling approaches have individual advantages and disadvantages, but none of them are suitable for accurate third-party modelling of BESS. Datasheet modelling is the only one possible, but less accurate than the other models.

The ideal model is a combination of all of the mentioned models:

- It should only rely on data obtainable from BESS documentation since that is the only data available.
- It should be based on chemical relationships to be robust towards use modification.
- It should be fitted to experimental data to confirm factual sensitivities to parameters.
- It should contain a linearity that allows the direct comparison between value and impact of use.

It should be noted that generally battery degradation modelling is extremely difficult for the following reason:

- Li-Ion cells age over a very long time span with very little change in the most reliable indicator (capacity).

- Li-Ion cells are subject to many degradation processes which are difficult to identify and which may excite each other.
- Capacity measurement methods vary with the use of constant-current (CC) vs constant-current-constant-voltage (CCCV) and different cut-off currents and environmental temperatures.
- Every cell is different as a result of manufacturing differences, both between manufacturer and from cell to cell.

All of these factors make a fully accurate forecast impossible. It should therefore be aimed to construct an ageing model that just provides the best possible accuracy in regards to chemical relationships, experimental data and available manufacturer data.

Model Dependency Analysis

This sub-section briefly discusses the dependencies upon different impact factors identified from the (semi-) empirical models (110, 133, 166–169, 171–175, 179, 151, 157–159, 161, 163–165). A detailed description of the methodology for this comparison has been outlined in submission two, and the full graphs including keys to sources and chemistries are given in Appendix A. Generally, the following graphs are based on the reference conditions in Table 5, with all but the investigated factor held constant. Further, the graphs have been normalised to achieve EOL under reference conditions.

Parameter	*Value*
Temperature	40 °C
DoD	50 %
Cycles at 80 % DoD until EOL	8500
Average SoC	50 %
Charge/Discharge Current	1 C
Nominal Calendar Life	8 years

DoD to Cycle life

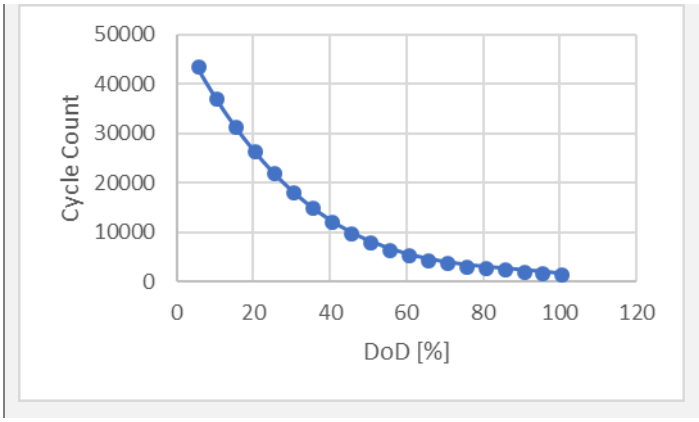

Table 5: Reference Case Conditions (180)

The first two graphs shown in Figure 22 display the degradation dependency of both time and throughput (measured in FEC). They essential display calendric and cyclic ageing separately. While some models are linear or even display a steadily increasing capacity loss, most models show slowing capacity loss over time, replicating a $\sqrt{t}$ dependency. This discrepancy is likely due to the modelling approach chosen by authors, wherein linear models provide advantages in the evaluation and/or are seen as sufficiently accurate approximation. Since time and throughput share these relationships, it can be expected that cyclic utilisation affects the calendric ageing process linearly.

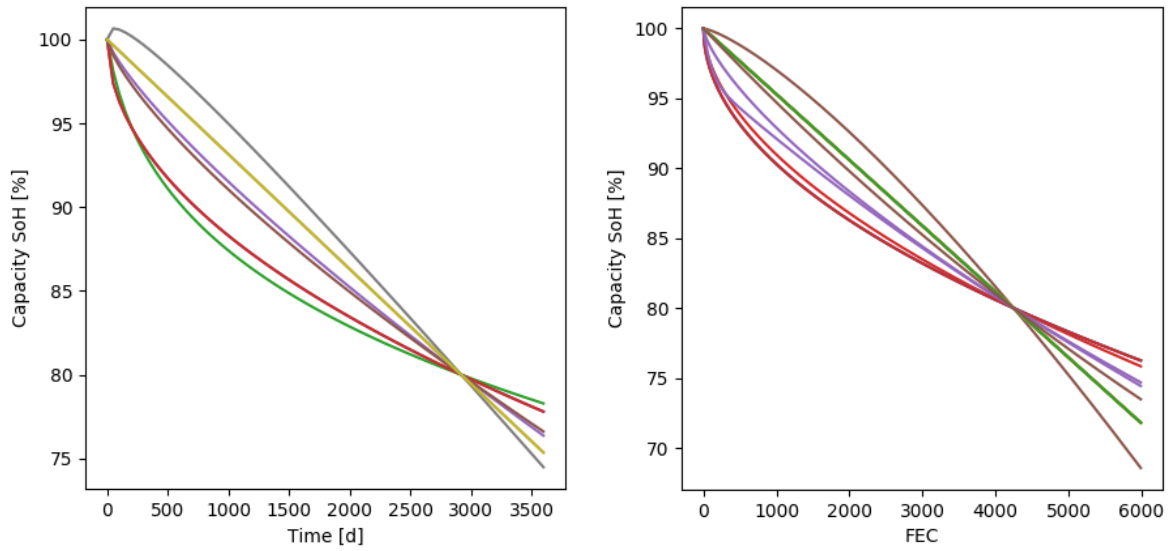

Figure 22: Time and FEC dependency of each investigated ageing model

Figure 23 displays the temperature dependency of the ageing models. Almost all models confirm that higher temperature leads to a higher degradation. The semi-empirical models utilise an Arrhenius (reaction rate) dependency $e^{-\frac{1}{T}}$, which lead to a steady increase in degradation with rising temperature and also matches some of the fully empirical equations obtained from experimental data.

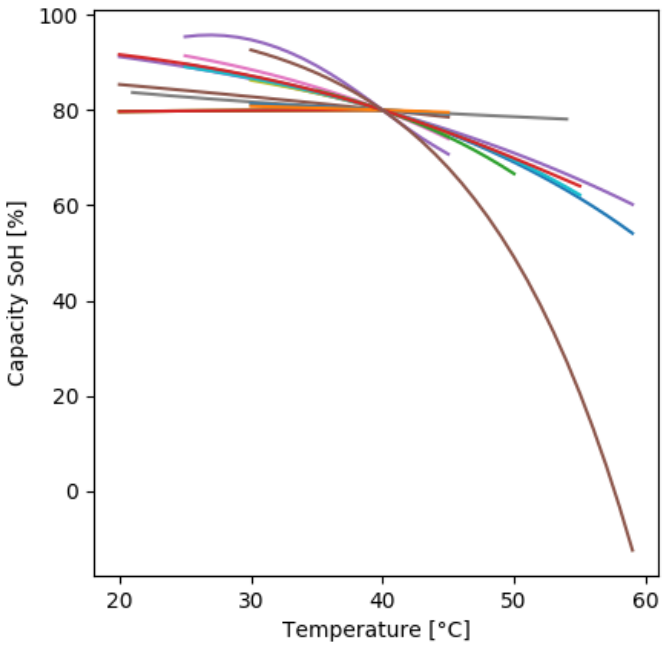

Figure 23: Temperature dependency of each investigated ageing model

Figure 24 shows the current dependency (measured as C-Rate) displayed by the models. They do not distinguish between charge and discharge currents. Generally, all models agree that higher current leads to higher degradation. However, there are a few exceptions. The model in (170) displays a higher degradation at low current due to a supposed regenerating effect of storage time. The results of (166) primarily regard discharge currents, which are shown to slow ageing. While high currents can be expected to increase ageing, it is worth considering a differentiation between charge and discharge current, since some chemical models such as (176) for instance show that charge currents have a much higher impact on SEI formation.

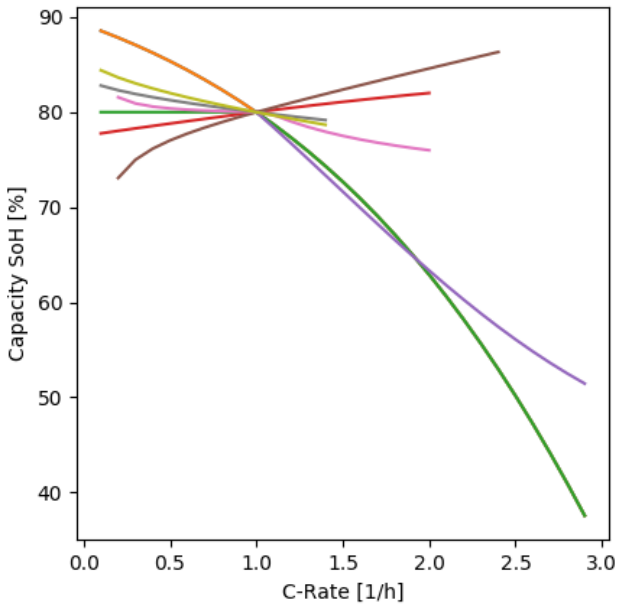

Figure 24: C-Rate dependency of each investigated ageing model

Figure 25 shows the SoC and DoD dependency of the degradation. With the exception of few almost all models confirm that higher SoC results in a higher degradation. The same is true for the DoD. Those cases vastly outnumber the exceptions and can therefore be expected to be correct for most cases. While the discrepancy between those perspectives is likely incurred by differences in experimental data, no definitive connection to chemistries or architecture was identified.

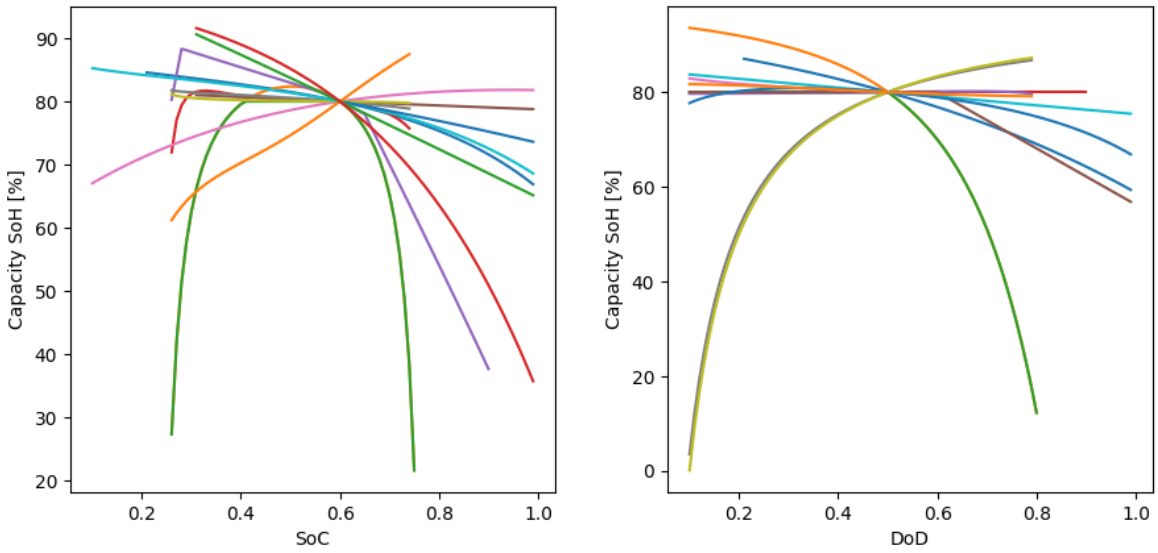

Figure 25: SoC and DoD dependency of each investigated ageing model

The shown dependencies of experimentally confirmed models provide an overview on how batteries are expected to behave under different conditions. This information influenced the selection of the ageing model in 4.4. Considering the conflicts between the literature models, experimental data is absolutely necessary to develop and confirm a new degradation model.

2.5.7 Issues and Gaps in Existing Modelling

For the analysis of BESS for potential investors, it is important to have a reliable adaptable model that can forecast performance as best as possible based on the information given. To achieve this, it should fulfil two key forms of adaptability:

- Adaptability to battery documentation: All sub-models need to adapt to the data given on the storage system. Unknown data must therefore be either extrapolated from given data or relatively referenced from experiments or literature.
- Adaptability to utilisation: The model should be able to compute any kind of utilisation and reflect the battery behaviour, including the power and energy limits, accordingly.

Further, to be accessible and usable, a tool is necessary that allows for an easy evaluation of storage systems and utilisation profiles. It is important that that tool is guided by the complete model but also achieves a full evaluation within a reasonable time period.

If reference degradation values are met, the model would accurately replicate the behaviour outlined by the manufacturer. If it also follows electro-chemical principles, experimental fit is considered necessary but secondary to other factors such as computational speed and reduction of necessary assumptions. A fit of the individual models of maximum 10 % NRMSD is considered acceptable.

A tool that fulfils these requirements would significantly support the commercial assessment of investors by providing crucial information on degradation and performance. That information can either be used directly in financial assessment or in conjunction with other tools and models that aim to optimise use cases.

3 Battery Testing

In 2.5.7, the importance of high quality experimental data has been pointed out to develop a reliable BESS model. This section therefore describes all three primary experiments undertaken in this project to provide data and references for such a model.

The first experiment focussed on the optimisation of the long-term testing of Li-Ion battery cells in general. The second testing series aimed to identify the extent and value of pseudo-capacitive properties of Li-Ion cells and how that may affect the degradation process. In the last testing series, 20 cells have been subjected to long-term degradation tests under a variety of utilisation profiles, which provided data for the development of the BESS model.

3.1 Testing Series One: Degradation Testing Analysis

3.1.1 Purpose

Battery degradation testing is extremely beneficial to model development, but poses several difficulties. Since the capacity fade in particular is very gradual, these have to be long-term tests and must be very consistent and efficient. Any change in methodology may invalidate the results of the entire test. Therefore, it is advisable to optimise the testing process in advance.

This short-term test was primarily designed to optimise the design and analysis process of ageing testing for the long-term experiment undertaken in 3.3. To achieve this, this testing series focusses on:

- Review of testing approaches
- Organisation and practical implementation of the testing process
- Safety considerations
- Non-intrusive battery characterisation methodologies
- Data analysis tools and reliability
- Assurance of testing consistency and error handling

The test is also based on a realistic use case, specifically the use case of home solar energy storage. Hence the methodology of developing an appropriate charge/discharge profile will be outlined as well. Using the testing data several methods of data evaluation have been reviewed.

3.1.2 Experimental Design

Test Orientation Choice

Two different approaches for battery ageing tests have been identified: parameter and utilisation oriented testing. The advantages and disadvantages of each approach is shown in Table 6.

	Advantages	Disadvantages
Parameter-Oriented Testing	• Isolation of ageing factor • Identification of favourable and unfavourable conditions	• Limited investigation • Factor interconnection
Utilisation-Oriented Testing	• Reflection of realistic battery behaviour • Possibility of direct comparison between utilisation strategies	• Limited factor impact derivation • Non-repetitive profile • Long testing time

Table 6: Advantages and disadvantages of the two testing approaches

Parameter oriented testing is the most commonly practiced approach for battery testing by focussing on specific parameters to test their impact on the battery degradation. For instance, in literature, cells have been tested against the impact of time (161, 181, 182), coulombic throughput (166, 183, 184), charge and discharge current amplitude (107, 185, 186), DoD (163, 183, 187), SoC (126, 164, 188), cell temperature (128, 185, 189) and mechanical pressure (190, 191). Parameter-oriented tests are either cyclic, which means they are cycled through identical repetitive charge and discharge, or calendric, meaning they are not cycled and only stored.

Parameter-oriented testing attempts to isolate the impacting factors, which is better for the empirical development of an ageing model. However, this isolation is difficult for many factors, if not impossible, meaning that you cannot change one parameter without affecting the others.

Utilisation-oriented testing means that tests are based on utilisation profiles of actual battery applications, such as in (151, 192). Charge-discharge profiles are either recorded or generated for specific applications to simulate realistic circumstances.

Utilisation-oriented testing is beneficial for the evaluation of one specific service but fails to predict the batteries behaviour beyond that. Varied profiles and a thorough data processing is necessary to use this data for battery modelling. Further, these tests tend to be longer when pause periods are replicated as well.

In this test, the utilisation-oriented test has been chosen with the intent of arriving at a degradation statement for a specific use case. This is advisable since there were only four cells readily available.

Cell Details

The data on the battery cells provided is given in Table 7. The cells originated from a module disassembly. Said module was previously part of an EV and has thus been subjected to degradation already. No additional data on that utilisation or the current state of health has been provided.

CHARACTERISTIC	VALUE
CELL TYPE	Pouch
COUNT	4
CAPACITY	55 Wh (15 Ah)
VOLTAGE LIMITS	2.8 – 4.15 V
CATHODE CHEMISTRY	LMO-NMC

Table 7: Tested cell details

Cycle Profile Generation

The use case chosen is a self-consumption profile for a UK household. An arbitrary household profile P_H from the EDRP database (193, 194) with the Acorn (see (195)) category description "Established home owning workers" in Warwickshire has been selected. The consumption data is half-hourly, which has been taken as time reference. The mean yearly energy consumption of this profile is 2504 kWh.

Using solar irradiance data E_{IR} from Warwickshire provided by the Environmental Change Network (196), a matching PV profile can be generated. Several measures have been taken to match both profiles on the time scale as best as possible (outlined in detail in submission two).

The theoretical system is based on the data from several PV panels ((197–199)) and converters ((200–202)):

- Panel size $\mathrm{A} = 1.64 m^2$
- Panel efficiency: $\eta_{PV} = 16\,\%$
- Converter Efficiency: $\eta_{con} = 96\,\%$

From the global radiation reference of 1000 $\frac{W}{m^2}$ a single panel would have the nominal power rating of 262 W. The panel count n was chosen so that the battery would be fully utilised at least once, which resulted in $n = 4$. The PV power output is then calculated as follows:

$$P_{PV} = n * E_{IR} * A * \eta_{PV} * \eta_{con} \quad (7)$$

The battery system chosen as reference is a small scale system of 3.3 kWh (203), since the cells originate from the same manufacturer as those tested here. The charging strategy is to

charge all generated energy not already consumed by the household and then supply the household with that energy for as long as possible, minimising grid interaction as soon as possible. A sample of this profile is given in Figure 26.

$$P_{BESS} = P_H - P_{PV} \quad (8)$$

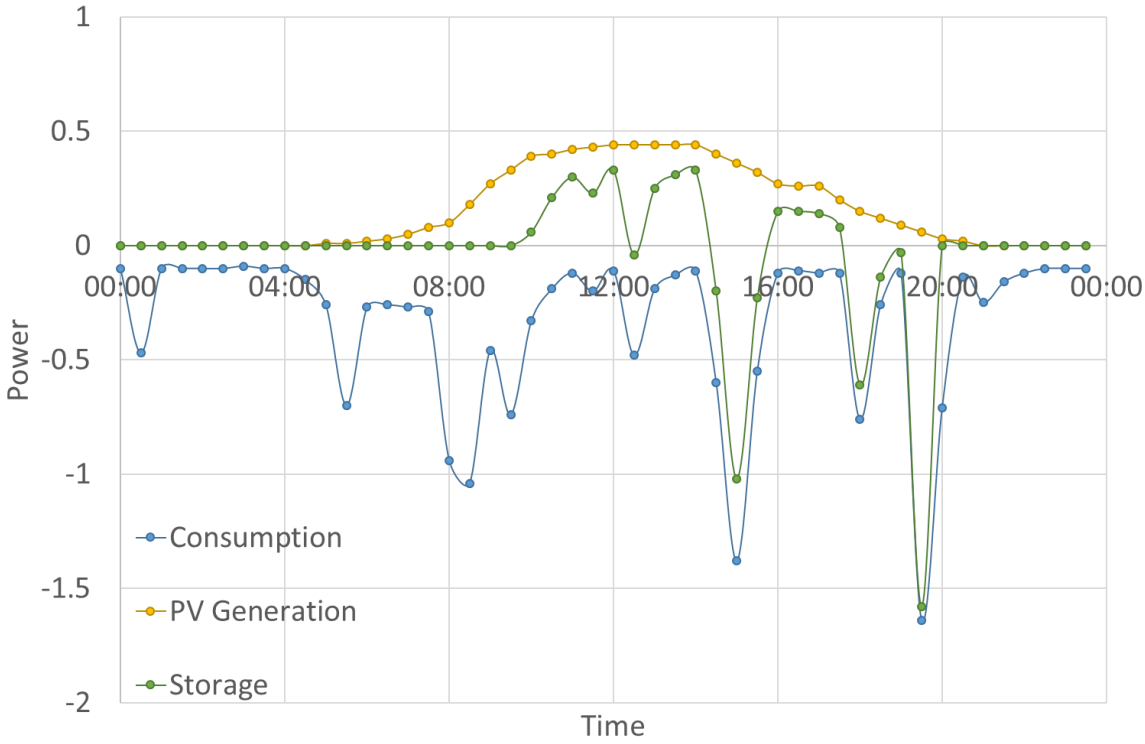

Figure 26: Power curves for a sample day

It should be noted that since the profile is half-hourly, some extremes in charge and discharge that would occur in a realistic profile are not reflected.

To avoid self-discharge below 0, the lower SoC limit has been set to 5 %. Further the current has been limited to 1 C (15 A) for battery health benefit. Finally, the profile must be scaled down to the capacity of the tested cells (55 Wh):

$$P_{cell} = P_{BESS} * \frac{E_{cell}}{E_{BESS}} \quad (9)$$

Due to the issues mentioned regarding the length of utilisation-oriented tests, the profile has been accelerated to achieve degradation results within a reasonable time period. This was achieved by reducing the time periods during which the storage system would be inactive to 30-minutes of rest, reducing the profile time by 50 %. The downside of this is that the calendric periods of the actual application and their impacts are not covered in the profile, which are targeted to be captured separately.

Experimental Design Matrix and Test Strategy

The experimental design matrix is displayed in Table 8. Three cells have been subjected to the cycling profile, while one cell was chosen as dedicated reference cell for calendric ageing. This was done so the incurred cyclic impact could be isolated from the calendric ageing.

	ID	Count	Cycling time (hours)	Chamber-Temp.	Compression	Temp.-Sensors	Intermittent Tests
Cells	“Cyclic”	3	2542.5	25 °C	0.5 bar, flexible	2	weekly
	“Calendar”	1	0	25 °C	No	2	weekly

Table 8: Experimental design matrix for Testing Series One

The environmental temperature has been set to 25 °C to replicate environmental conditions of indoor home storage. To replicate the module conditions, the cyclic cells have been pressurised flexibly at 0.5 bar, which is stated in (190, 191) as ideal pressurisation for prolonged battery life.

The detailed test procedure is shown in Figure 27. The cells were prepared through an initial characterisation using a capacity and EIS test. After being subjected to their respective utilisation for a week, they are characterised again. In the final procedure, the cells were stored at 100 % for a week to replicate the conditions of a storage system left unattended and automated in case the inhabitants are on vacation.

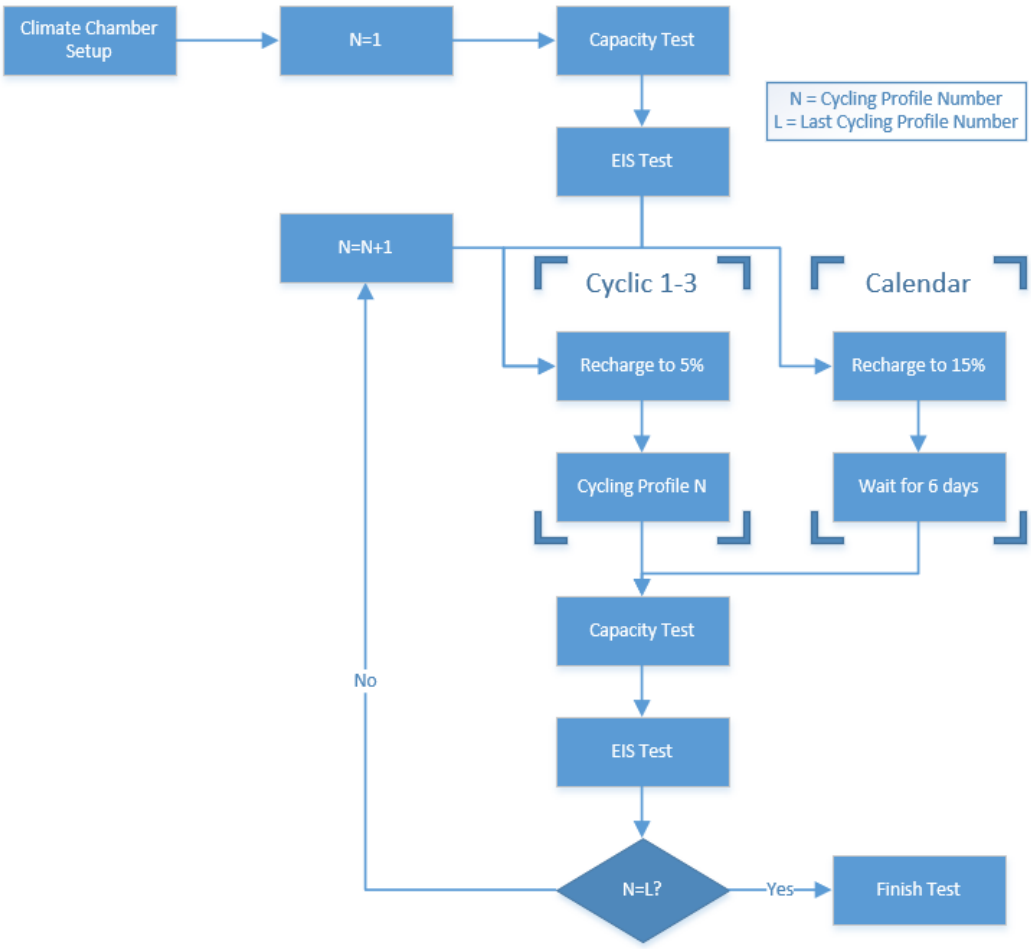

Figure 27: Testing Procedure

The capacity tests were performed with a CCCV charge and full discharge at C/2 with C/20 cut-off current as per lab recommendations. The EIS was done at 0 % SoC for a range of 5 kHz to 20 mHz with 300 mA and as lab recommended safety precaution without pressurisation.

3.1.3 Equipment and Setup

The battery cells have been cycled in a Vötsch environmental chamber with a Bitrode Battery Cell Tester. The EIS was primarily performed with a Solartron potentiostat. The overall setup is displayed in Figure 28.

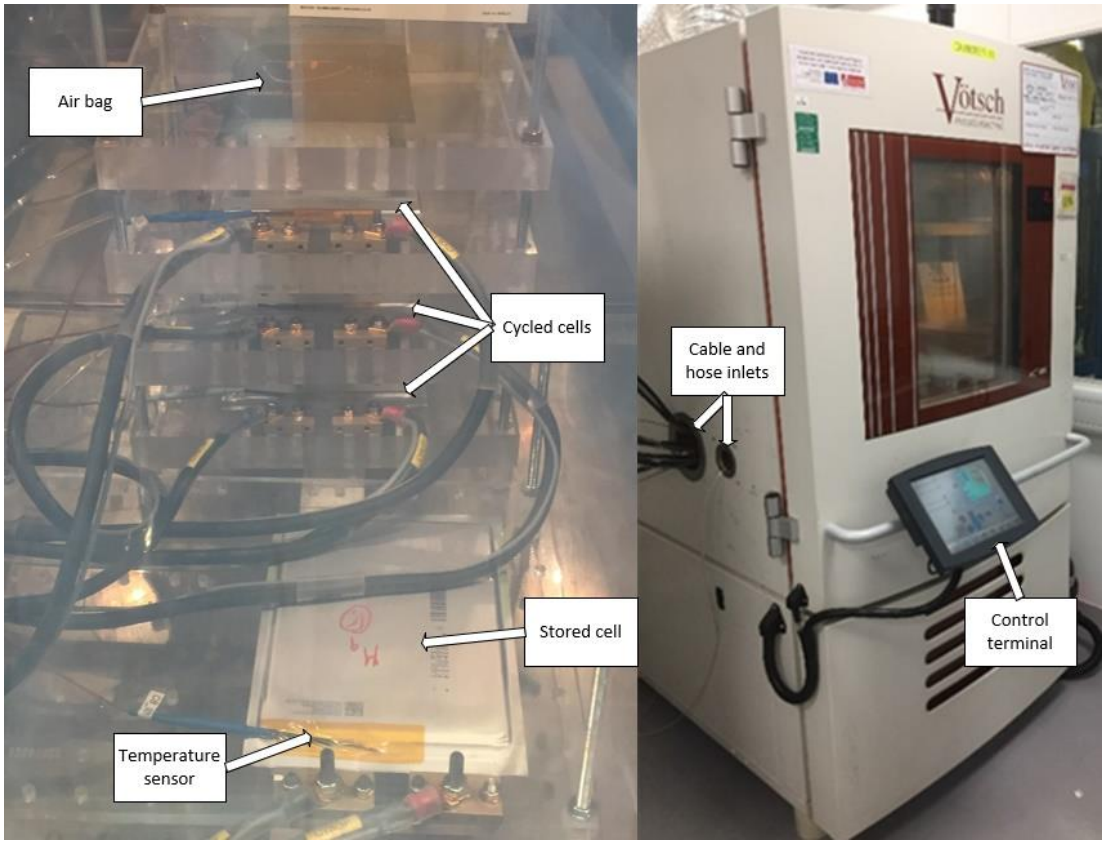

Figure 28: Experimental setup inside (left) and outside (right) the climate chamber

The cyclic cells were fixed on a jig with polymer blocks and the inflated air bag in-between the layers to exert the pressurisation. Since the temperature sensor could not be placed on top of the cell in case of potential piercing from the pressure, it was placed near the tabs on all cells.

Several additional safety measures have been taken to ensure safe operation as well as disassembly and movement of the jig:

- Safe distance between brass blocks
- Handling only by qualified personal
- Use of insulated tools
- Attachment and detachment under isolated conditions
- Connection of temperature sensor to failsafe condition in the battery cycler

The full risk assessment has been added in Appendix C.

3.1.4 Results and Conclusions

This sub-section discusses the analysis and results of the testing, as well as the issues that occurred during testing and the determined methods for improvement.

Cycling Analysis

In order to understand the degradation the “Cyclic” cells were subjected to, the individual parameters impacting ageing outlined in 2.5.6 were summarised. The tests stopped after 3 months during which the “Cyclic” cells underwent 88.8 FECs and the “Calendar” underwent 17.5 FECs (capacity tests only). Therefore the capacity tests alone yielded almost a fifth of the total utilisation, which is comparatively high.

Figure 29 shows the C-Rate histogram of the “Cyclic” cells. Positive values denote charging, negative discharging. The histogram does not include 0 C.

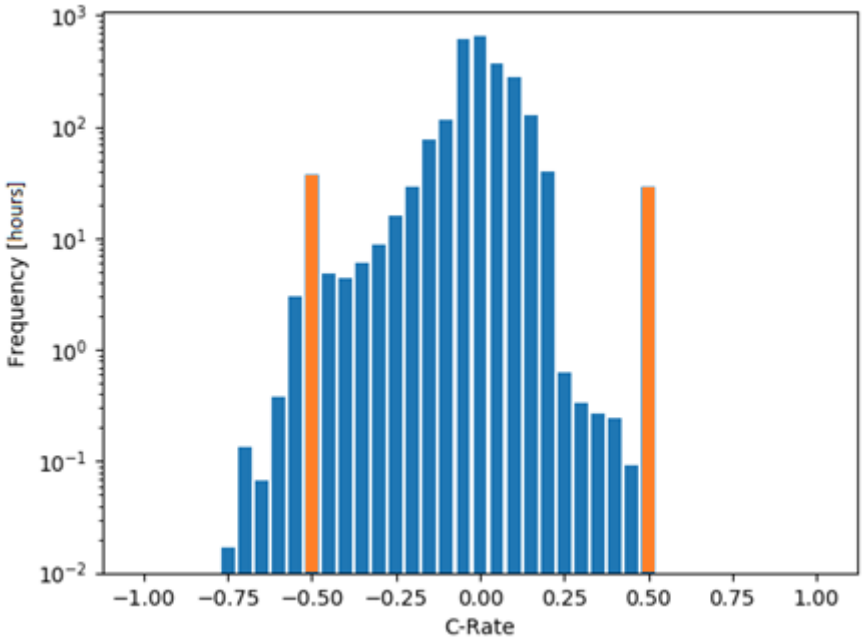

Figure 29: C-Rate histogram of “Cyclic”

From the profile it is apparent that the cells were charged at lower rates than discharged, and generally the C-rates were below C/2, which was the rate at which the capacity tests were performed (hence the spikes at C/2). Therefore the current stress was very low.

The SoC distribution is shown in Figure 30. Overall the cells spent most of the time below 50 % SoC. Since the BESS returns to 5 % every time, this distribution is reasonable. The peak at 100 % can be explained partially through the chosen profile where the BESS gets sometimes full charged and is not able to release that charge until the PV generation is below household consumption. However, most of it is likely connected to the rest introduced during the capacity tests.

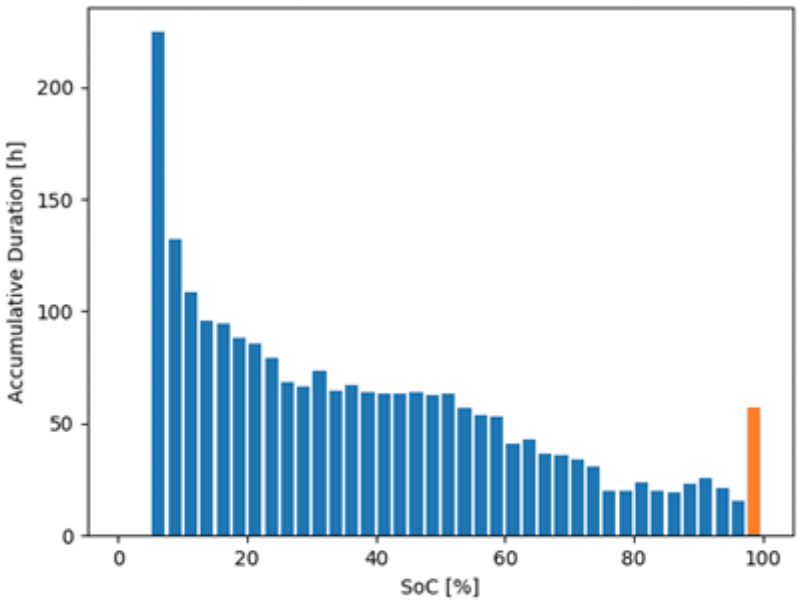

Figure 30: SoC histogram of "Cyclic"

The DoD distribution is given in Figure 31. The vast majority of cycles was very shallow, but deeper cycles of 5 to 70 % seem to be somewhat equally distributed. This correlates to the SoC histogram.

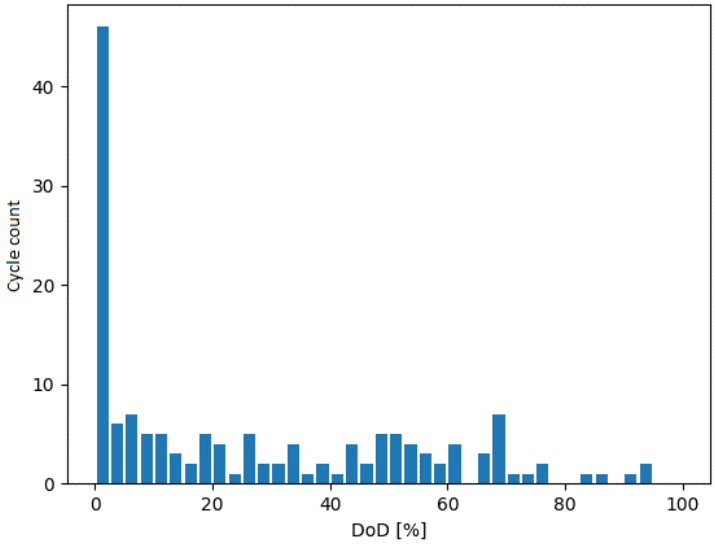

Figure 31: DoD histogram of "Cyclic"

The temperature data did not differ by more than 2 K from the environmentally set temperature and did not have a high enough resolution to be considered reliable.

Degradation Analysis Methods

The first value to analyse is cell capacity. The development of the cell capacity compared to throughput is shown in Figure 32. The graph contains also error margins σ_Q calculated using

the propagation of the current error σ_I (obtained from equipment parameters) and sample step time Δt:

$$\sigma_Q = \sqrt{\sum_{n=0}^{t} \left(\frac{\sigma_I}{\sqrt{2}}\right)^2 * {\Delta t_n}^2} \tag{10}$$

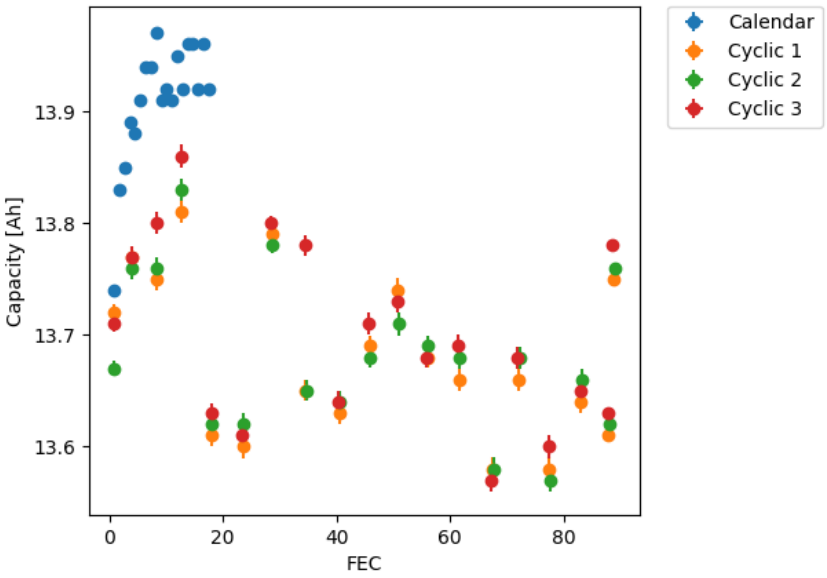

Figure 32: Cell capacity development

While the error propagation displays high confidence in the accuracy of the capacity tests, the actual values show no definitive trend. The cyclic battery capacity went down until the week-long storage period, after which it almost completely recovered. The only consistent result has been shown by the “Calendar” cell which showed an increase in capacity and then fluctuated at 13.95 Ah.

Next, the DC resistance was investigated. The value for DC resistance was derived using the pseudo-OCV curve shown in Figure 33. This curve was obtained by combining the charge and discharge signal for each SoC on the basis that the resistance is symmetrical in both directions:

$$R_{ch} = \frac{V_{ch} - V_{oc}}{I_{ch}} \tag{11}$$

$$R_{dch} = \frac{V_{dch} - V_{oc}}{I_{dch}} \tag{12}$$

$$V_{oc} = \frac{I_{dch}V_{ch} - I_{ch}V_{dch}}{I_{dch} - I_{ch}} \tag{13}$$

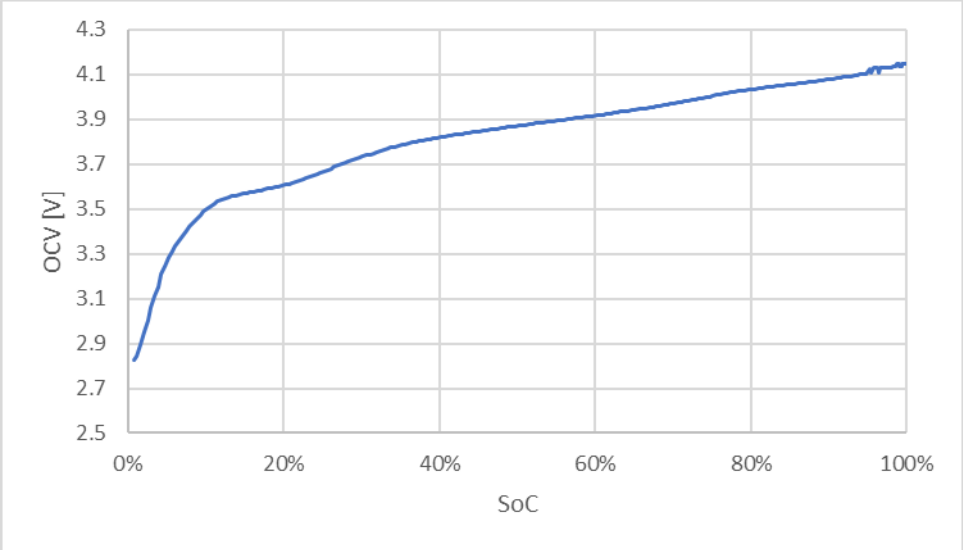

Figure 33: Pseudo-OCV curve of investigated cells

Using equation (12) the discharge resistance at 50 % SoC has been determined from each capacity test. The results are given in Figure 34 and contain the resistance error margins as calculated via the voltage and current errors:

$$\sigma_R = R * \sqrt{2} * \sqrt{\left(\frac{\sigma_V}{V_{ch} - V_{dch}}\right)^2 + \left(\frac{\sigma_I}{I_{ch} - I_{dch}}\right)^2} \quad (14)$$

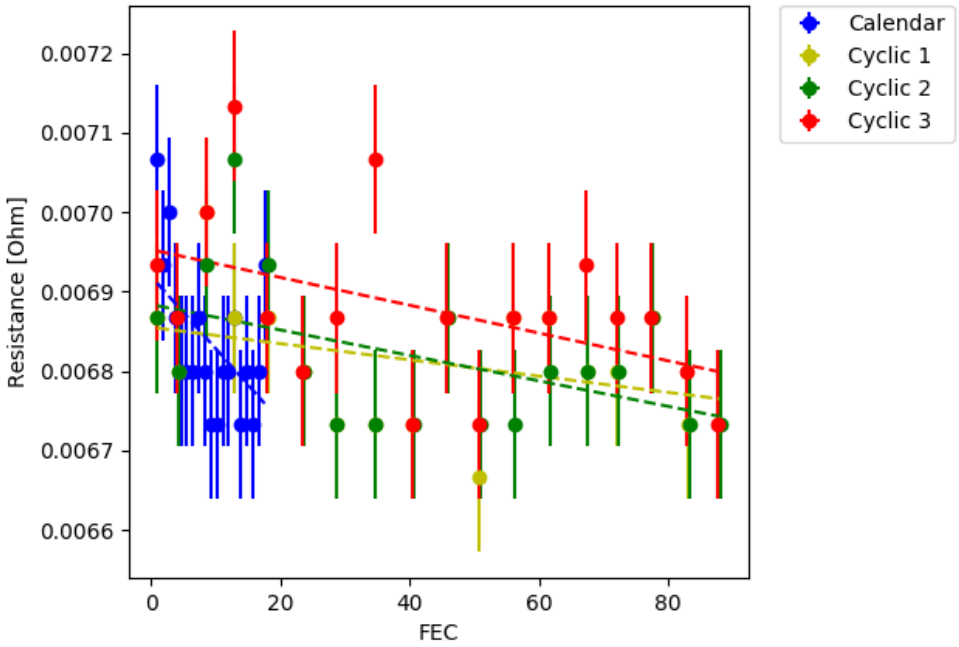

Figure 34: Charge-discharge resistance development from capacity tests

The given data shows a tendency in declining resistance. However, considering the equipment error and the selection of a single data point, the error margin for all data points is quite high.

The calendar cell show almost identical decline over time although it has not been cycled as often.

Another measure to identify the degradation of the battery is the analysis of the incremental capacity (IC, $\frac{\partial Q}{\partial V}$) and differential voltage (DV, $\frac{\partial V}{\partial Q}$) curve. Those curves are generated by deriving the change in capacity by the change in voltage and vice-versa. Due to the data resolution these curves have been generated through weighted moving average and are displayed in Figure 35.

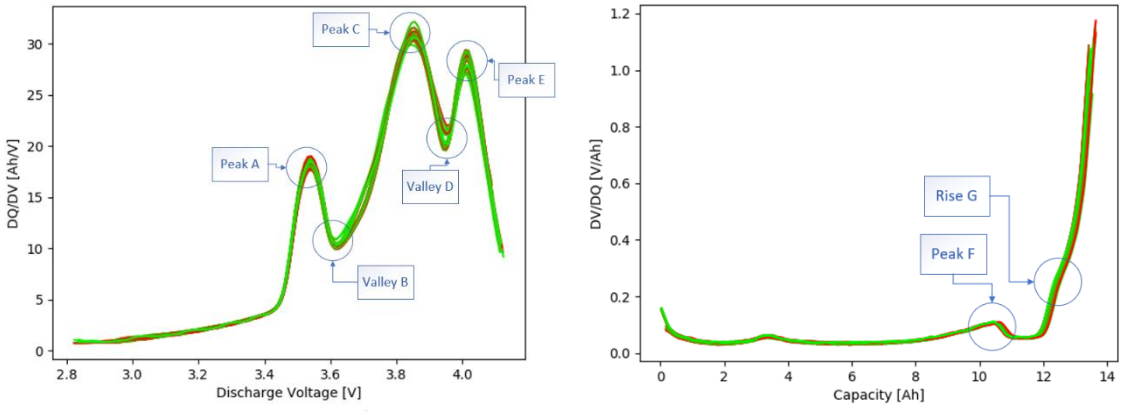

Figure 35: IC (left) and DV (right) overlaid over all capacity tests

The identified points of interest underwent the most fluctuation and indicate according to (132, 162, 204) a change in the active material. While there were trends, such as a decline in A, B and D, the fluctuations were too large to make a definite statement.

Lastly, the EIS signal was analysed. The Nyquist plot of the overlaid measurements are displayed in Figure 36. Overall, the EIS signal was difficult to analyse, since hardly any change appeared during the project. The main difference between the “Calendar” and “Cyclic” cells is an offset in DC resistance that would overlay the curves almost perfectly.

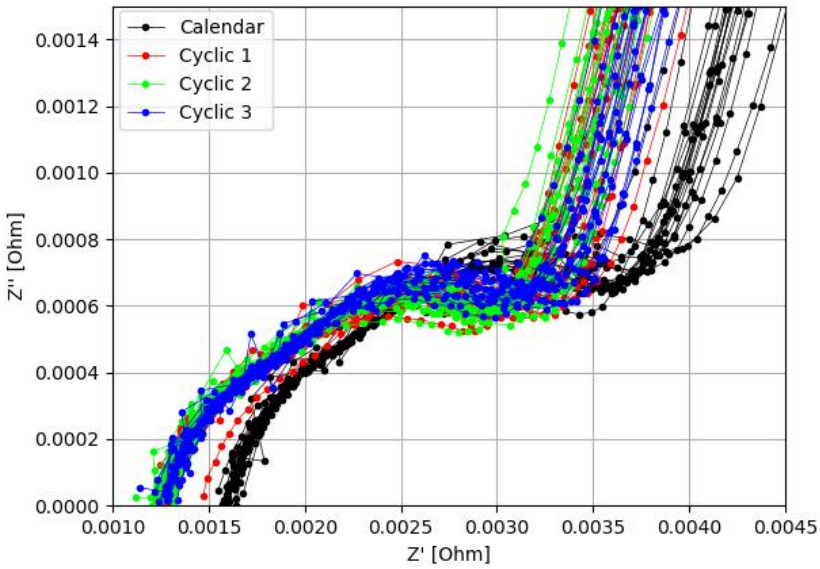

Figure 36: Overlaid EIS measurements over all cells

An additional problem is that different equipment was used during the test, affecting the clarity of the measurements and leading to an erratic Nyquist plot. Fitting software was not able to create a circuit solution for all curves.

Overall, the degradation values were very inconsistent. None of the degradation values identified provided consistent results that were in agreement with the findings from literature (see 2.5.6).

Further, while there are many degradation analysis tools available, they should be selected and analysed with the target of the testing in mind.

Improvements for Reliable Testing

In the following, several issues that occurred during testing and how to mitigate them for future testing are discussed:

- Details on the previous utilisation of the cells was not provided to this project. The cells may have been subject to significant degradation before the first test, explaining the already below nominal capacity. Therefore cells should be sourced to be as new as possible and not subjected to any environmental stresses.
- While the utilisation profile has been accelerated, there was little to no impact on the overall performance of the cell. To achieve reliable degradation data within a reasonable time period, further acceleration measures should be taken.
- The pressurisation attempted to replicate the conditions of a battery module. However, it can be further improved by actually testing the cells while subjected to module

conditions. This further would allow to perform all tests under the same conditions without safety concerns.

- Intermittent capacity test may, depending on the utilisation profile, have a significant impact on the degradation themselves, falsifying the conclusions on said profile. Also, since they had to be performed manually, they took additional hours away from the cycling profile. Therefore, these tests should be taken less frequently.
- The temperature sensor position close to the tabs was necessary from a safety standpoint, but provided no reliable data and no additional benefit beyond being a safety measure. A safe sensor solution close to the centre of the cell and ideally with high resolution should therefore be used instead.
- Generally, identical testing equipment (and specifically in this case EIS equipment) should be used for all tests to ensure minimum variance in the results.
- The testing equipment required many manual steps, that frequently lead to small variations and errors. The amount of manual steps should therefore be minimised.

These conclusions allowed for an optimisation and improvement of the long-term test design in 3.3.

3.2 Testing Series Two: Capacitive Property Investigation

3.2.1 Purpose

This testing series was performed to investigate the pseudo-capacitive properties of Lithium-Ion cells. There are three main premises motivating this investigation:

- Li-Ion battery cells store most of their energy through chemical reaction, but some energy in the capacitive properties of the cell design. In accordance with the description of the EIS circuit in (124), the diffusion process is only triggered at low frequencies, meaning that high frequencies utilise on the capacitive properties of the cell. (129, 205–207)
- The (bi-directional) provision of frequency response to the grid is partially utilising BESS at high frequencies. For the provision of dynamic frequency response, the provider is required to change the output dynamically with the grid frequency (outside of the tolerable frequency window known as deadband). (18, 24–26, 208–210)
- Micro-cycling, meaning the cycling of batteries with small DoD, has been shown to have minimal impact on battery cell degradation compared to cycling the battery at the same throughput with large DoD. (2)

Two questions arise from these premises. Firstly - is the threshold between capacitive and chemical utilisation of a Li-Ion cell relevant for the provision of frequency response? Secondly

– does the capacitive utilisation of Li-Ion batteries incur less degradation than chemical cycling? This testing series attempts to answer the first question, the second is targeted in 3.3.

It should be mentioned that similar investigations have been performed by other on the impact of ripple current originating from attached electronics on battery cells. The authors of (211–213), who applied different frequencies (1Hz - 15kHz) both alone and superimposed with a DC signal, found varying but overall very mild impact on cell degradation, which was partially attributed to additional heat. Citing capacitor equalizers as origin, the authors of (214) found more significant deterioration below 10 Hz. Overall, the specific thresholds and conditions for the impact of AC cycling haven't been precisely identified.

3.2.2 Experimental Design

Galvanostatic EIS has been shown to be a reliable method to identify the electrical properties within the cell (124, 206, 215–217). Thus it has been chosen as primary method in this experiment. An overview on the tested cells and conditions is given in Table 9.

ID	A	B	C	D
Count	3	4	1	1
Chemistry	NMC-LMO/C	NMC-LMO/C	LFP/C	NMC/C
New	No	Yes	Yes	Yes
Form	Pouch	Pouch	Pouch	Cylindrical
Capacity	15 Ah	33 Ah	19.5 Ah	3.1 Ah
SoC	25 %, 50 %, 75 %	50 %	50 %	50 %
RMS-Current	C/20, C/10, C/5, C/2, 1C	C/16, C/3, 2/5C	C/10, C/2, 2/3C	C/10, C/2, 1C
Temperature	22 °C	22 °C	22 °C	22 °C

Table 9: Experimental design matrix for Testing Series Two

To ensure a reliable statement about the capacitance of Li-Ion cells, four different cells with three different chemistries and two architectures and different states of degradation have been selected. Since the SoC affects the physiochemical structure of the cell, cell type A has been tested at different SoC as well.

Due to the Butler-Volmer equation, current amplitude may have a significant impact on the pseudo-capacitive response of the cells (206, 216). Therefore, the EIS tests are performed on different current amplitudes up to an RMS value of 1 C. Consecutive tests have been performed at increasing current rate.

The chosen frequency band for the EIS was 5 kHz to 20 mHz.

3.2.3 Equipment and Setup

Primary testing equipment was a Solartron potentiostat coupled with a 20 A booster used to perform the EIS (218). Cells were tested separately at room temperature. The test setup with the cell type A is displayed in Figure 37.

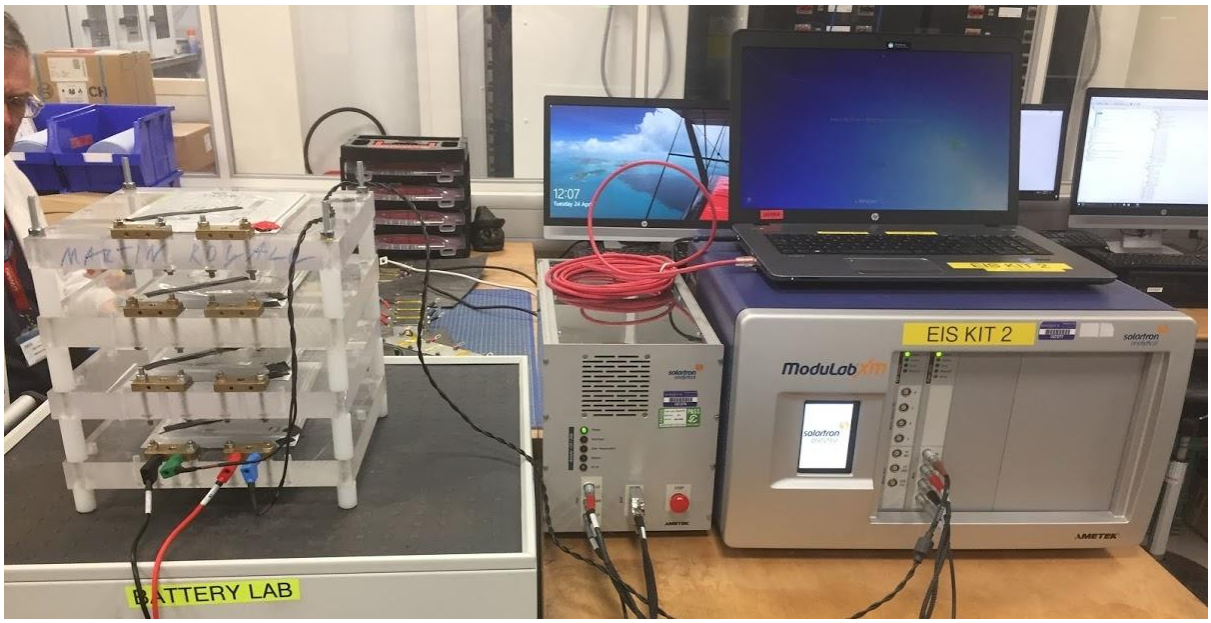

Figure 37: Experimental Setup for Testing Series Two

3.2.4 Results and Conclusions

Initial Evaluation

The Nyquist plots of the EIS tests are given in Figure 38. The high frequency reactances have been neglected, since they likely induced by cable connections and bear no additional information on targeted analysis. Further, an analysis of the Lissajous data on a separate cell has shown very low reliability in data obtained above 10 Hz (see Appendix B) Some low frequency data points have been cut as well since they displayed a significant change in behaviour reminiscent of a Warburg element.

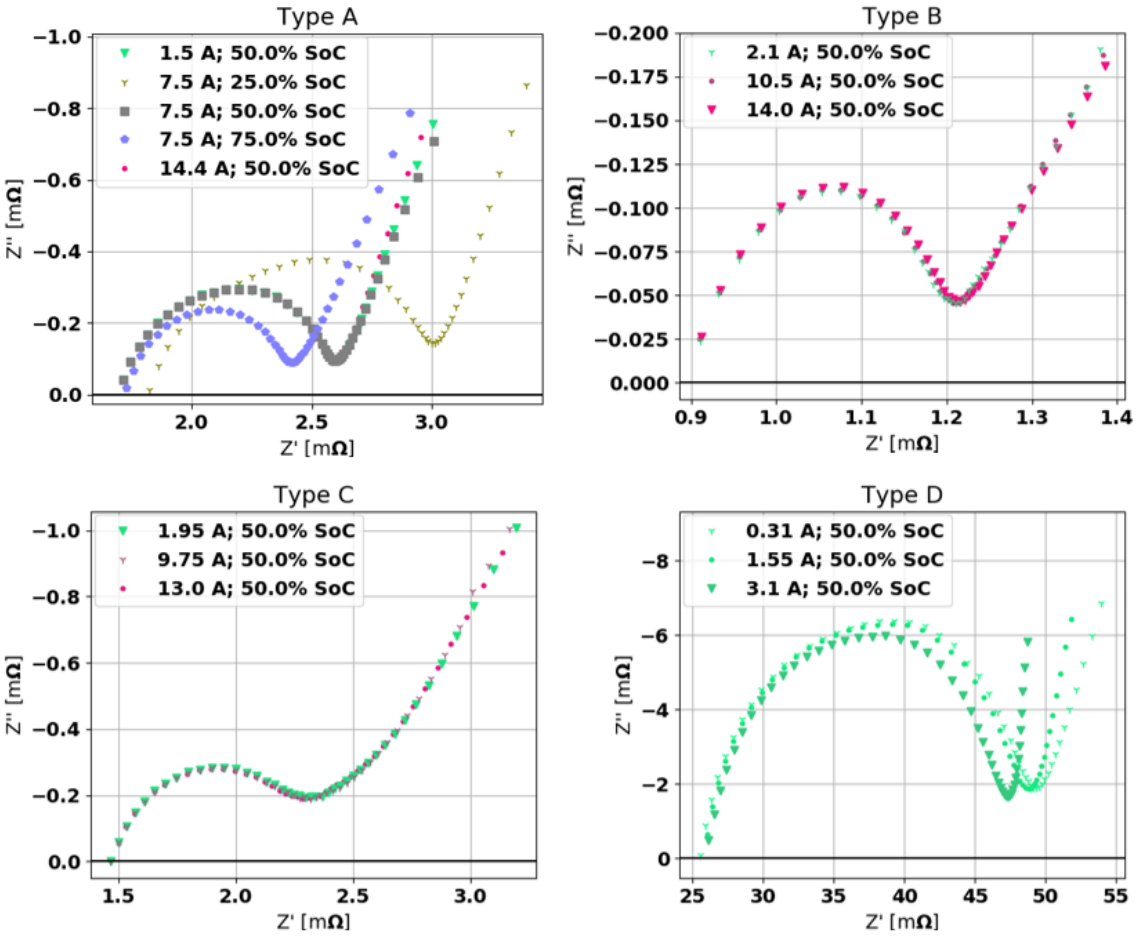

Figure 38: Nyquist-Plots of the different cell types at different currents

The current amplitude did not seem to have a significant impact upon the EIS response within the investigated spectrum, with the exception of cell type D (which is the only cylindrical cell). The change in SoC in cell type A, however, changed the response significantly.

Data Processing

In order to identify the threshold between the pseudo-capacitive and diffusion processes, their impedance will be used as reference. After consideration of various ECMs for EIS responses ((124, 129, 205, 207)), the one displayed in Figure 39 was selected as being most accurate. Through parallel and series combination, they can be summarised in the three impedances Z_0 (series resistance), Z_{PC} (pseudo-capacitance) and Z_{DIF} (diffusion).

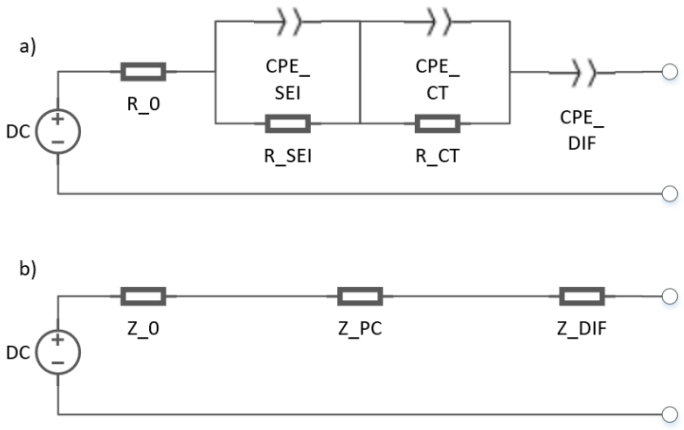

Figure 39: Chosen Equivalent Circuit Model (a) and complex simplification (b)

The governing equations of this circuit are the following:

$$Z = Z_0 + Z_{PC} + Z_{DIF} \tag{15}$$

$$Z_0 = R_0 \tag{16}$$

$$Z_{PC} = \frac{R_{SEI}}{1 + B_{SEI} * (j\omega)^{\psi_{SEI}}} + \frac{R_{CT}}{1 + B_{CT} * (j\omega)^{\psi_{CT}}} \tag{17}$$

$$Z_{DIF} = \frac{1}{B_{DIF} * (j\omega)^{\psi_{DIF}}} \tag{18}$$

B refers here to the admittance of constant-phase elements. B, Resistance $R$and phase angle ψ are unknown parameters of the signal, and the angular frequency ω is the dependency. Since, as discussed in 3.1.4, automated fitting software does not always provide a circuit and further a complete fit is not necessary to arrive at the relevant information for this experiment, a manual fitting approach has been chosen instead.

Only two of the three impedances must be identified correctly to separate them. R_0 can be found through linear interpolation where the impedance would have no imaginary component.

Z_{DIF} is the only active component at low frequencies. Therefore it can be fitted from low frequency data. Since the real component Z' of the measured impedance is cumulative towards low frequencies, only the imaginary signal Z'' can be used to fit only the diffusion. An example is shown in Figure 40.

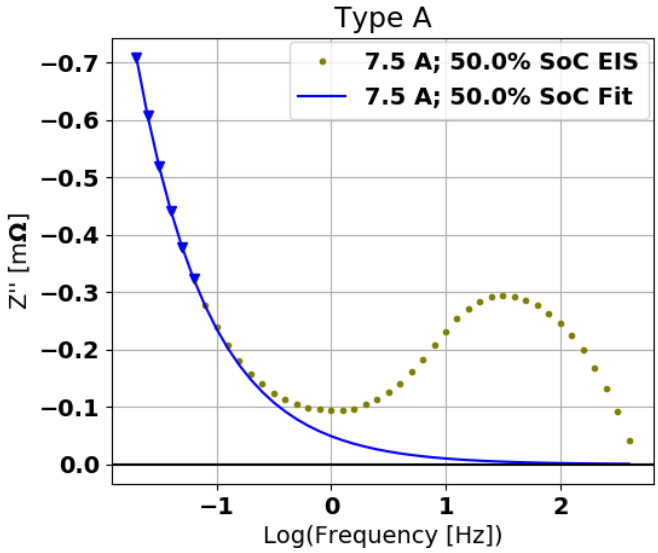

Figure 40: EIS-measured reactance and fitted Z''_{DIF} function (Type A)

The datapoints have been selected as to provide the best fit for the curve of equation (18), with a minimum of three. The fitting results for B_{DIF} and ψ_{DIF} are given in Table 10.

Type	SoC [%]	Current [A]	B_{DIF} [S]	ψ_{DIF} [°]	RMSE [%]
A	25	0.75	4543.80	40.85	3.85E-04
		1.5	4549.26	40.92	4.70E-04
		3	4677.51	41.29	3.81E-04
		7.5	4556.11	40.97	4.01E-04
		14.4	4694.82	41.04	3.63E-04
	50	0.75	5060.27	39.81	9.53E-03
		1.5	5188.33	40.23	8.90E-03
		3	5264.31	39.92	8.59E-03
		7.5	5075.32	39.26	8.40E-03
		14.4	4906.42	38.09	7.87E-03
	75	0.75	4154.34	39.04	3.08E-03
		1.5	4147.85	38.64	2.90E-03
		3	4215.73	39.24	2.36E-03

		7.5	4104.11	38.17	2.30E-03
		14.4	4107.67	37.93	3.58E-03
B	50	2.1	4953.25	23.68	2.83E-03
		10.5	4882.84	23.71	2.77E-03
		14	4895.66	23.57	2.77E-03
C	50	1.95	2459.65	32.12	4.69E-04
		9.75	2001.07	28.77	3.49E-03
		13	2208.62	29.18	3.49E-03
D	50	0.31	405.43	34.16	8.48E-04
		1.55	389.84	32.43	8.47E-05
		3.1	446.78	33.04	1.11E-03

Table 10: Diffusion element parameters and RMSE

The overall fit was deemed accurate and able to approximate the diffusion element sufficiently. After deducting Z_{DIF} and Z_0 from Z, the remaining signal represents Z_{PC}. It is displayed in Figure 41.

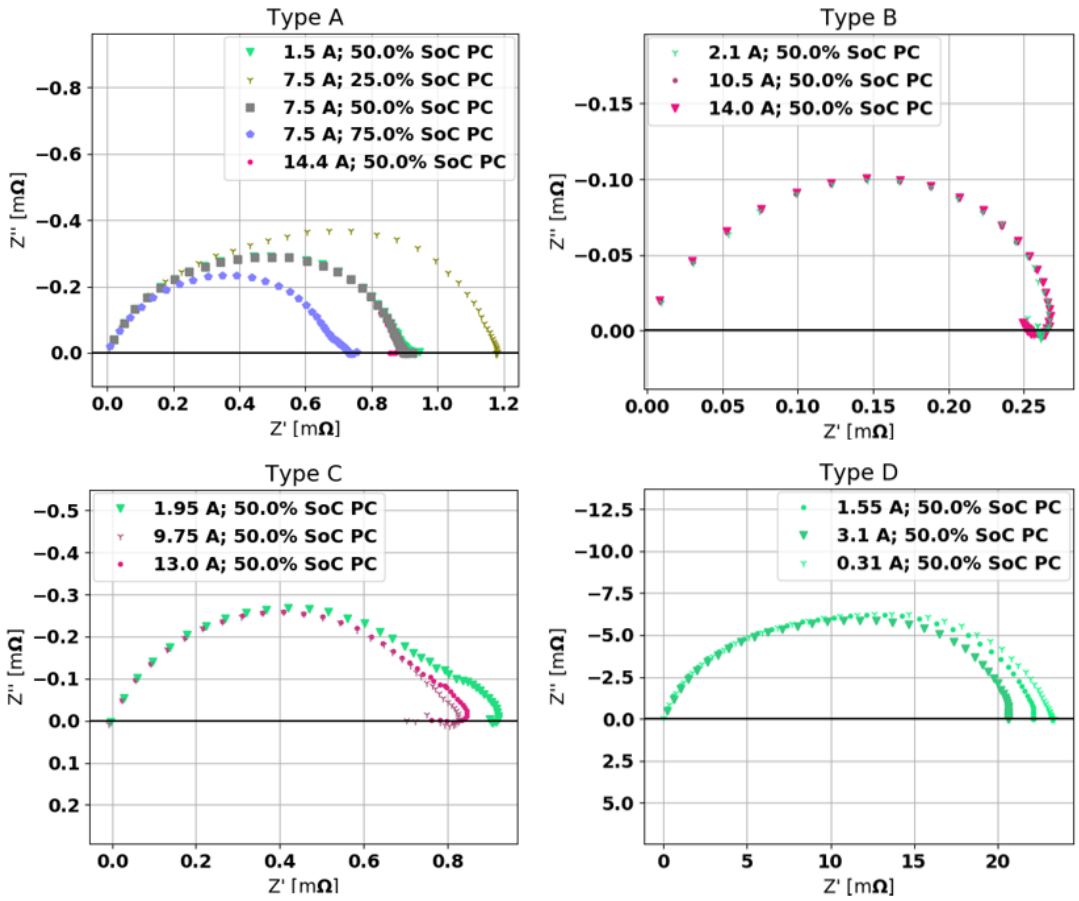

Figure 41: Isolated Pseudo-Capacitance from EIS data

Towards low frequencies, the signal displays several deviations from the expected semi-circle. Whether they originate from a fourth, un-determined component or simply an error in measurement or fitting could not be established. To smooth the response towards a purely pseudo-capacitive signal, all datapoints with a decreasing real component and positive imaginary components have been ignored.

In the last step, the impedances of all three components are compared in a Bode graph as shown in Figure 42. This graph displays how the overpotential is split between them.

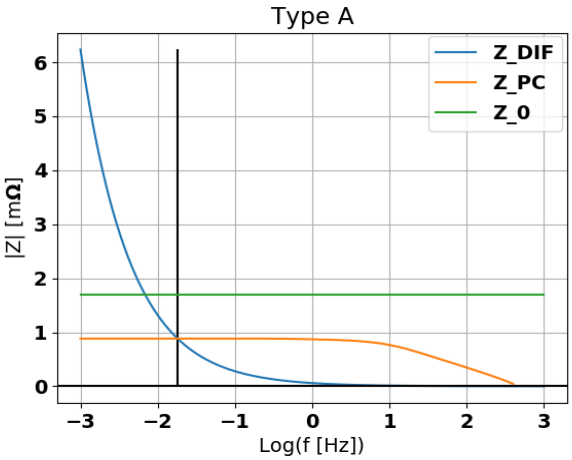

Figure 42: Bode Plot for type A at 14.4 A and 50 % SoC

At very high frequencies, the battery cell behaves like an ideal voltage source with a series resistance. There is effectively no interaction between the cell and the environment. At medium frequencies, the capacitance becomes involved and serves as short-term energy storage. At low frequencies the diffusion becomes gradually more involved until being the dominant process.

Of particular interest for the comparison of pseudo-capacitive and diffusion utilisation is the point at which the latter is greater. This frequency (marked by a black vertical line), which has not been identified in existing literature, has been dubbed capacitance-diffusion-transition-frequency (CDTF). While at this point the diffusion process is already active, it can be described as the threshold at which it becomes the dominant process.

It should be noted, that in all cases the CDTF was below the tested frequency and the terminal value of Z_{PC} as well as the model for Z_{DIF} had to be taken for all frequencies below measurement. Due to the high accuracy of the fit for Z_{DIF} and the Z_{DIF} already reaching its terminal value this does not affect the confidence in the results.

CDTF Analysis

The CDTF for all cells is displayed in Figure 43. From this data it is apparent that the CDTF is not dependent upon the current rate. However, the CDTF does rise with SoC. Out of all cells, the cylindrical cell had a much lower CDTF by a factor of 10 compared to the other cell types.

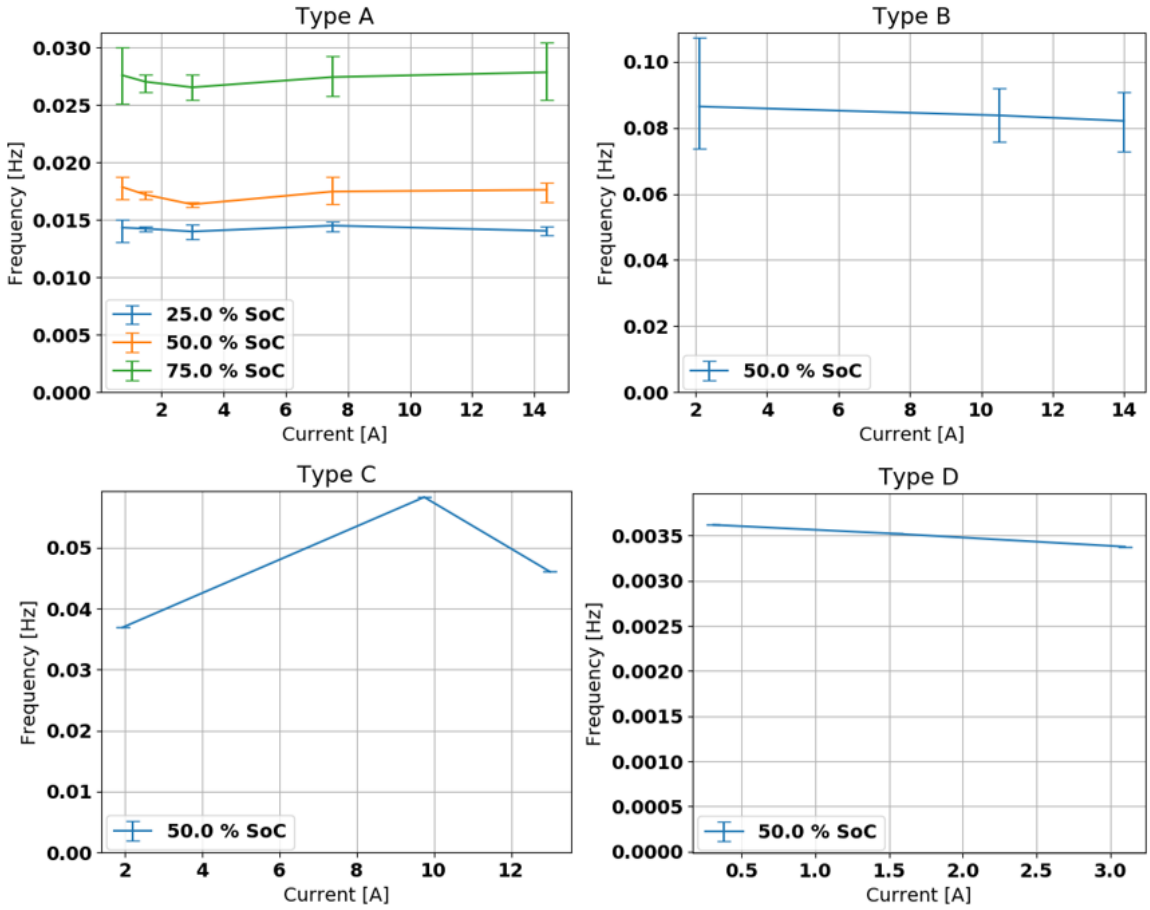

Figure 43: CDTF for changing currents and varying states of charge for all types

The CDTF overall varied between 3.5 mHz and 0.1 Hz. According to the rules of Fourier transformation, a pulse signal can be disassembled into a combination of sinusoidal signals with the lowest frequency being the inverse of the total pulse time. If all higher frequencies are captured by the capacitance as well, it is the dominant mechanism for symmetric charge-discharge pulse with a maximum length between 10 seconds and 4.7 minutes.

In accordance with the documentation of EFR, the provider of frequency response is mandated to sample the grid frequency every 100 ms (26). Thus, depending on the fluctuation of the grid frequency it is entirely possible that not only charge-discharge pulses happen within that time period, but also that the initial response to a change in direction of at least 10 s is provided almost entirely by the pseudo-capacitance.

To provide a rough estimate, an arbitrary month (June 2016) of data was chosen from the frequency data provided by National Grid (219). This data was converted to the throughput a storage system would experience to fulfil the minimum provision necessary (as reference see Figure 45). Using the pulse time windows, the EFR throughput that would be buffered by the pseudo-capacitance was determined. The buffered throughput amounted to almost 0 % (for 10 seconds) to 5.5 % (for 4.7 minutes) of the overall throughput. These numbers do not reflect

potential charge strategies to restore neutral SoC or even to target pseudo-capacitance draining using the flexibility of the deadband, which may increase even further the process relevance.

Therefore considerations regarding the impact of capacitive utilisation of Li-Ion cells are absolutely relevant. Potentially, Li-Ion cells can provide frequency response service with much lower impact on degradation than expected purely by using their pseudo-capacitive properties. However, this needs to be further investigated through ageing tests.

3.3 Testing Series Three: Module Long-Term Cycling

3.3.1 Purpose

The purpose of this testing is to provide additional experimental data for the development of the electrical, thermal and ageing model. Other available experimental data is outlined in 4.1.

It is targeted in this series to test cells in modular configuration, which should represent similar conditions to an actual BESS. This would be especially useful for the determination of the thermal model.

Ageing model data is obtained to answer several questions. Primarily, how is the degradation of batteries affected by service load profiles compared to conventional cycling? Also, how do completely different service profiles compare to each other?

Also, for this study, it is targeted to identify whether high frequency cycling of battery cells have a different ageing impact on the cells based on the results in 3.2.4. In (2), cells have been cycled for 200,000 cycles with a 40 second charge/discharge pulse, which appeared to have no significant impact on the cell degradation.

Electrical data will be obtained in the process of battery degradation, which will further support the development of the electrical model.

3.3.2 Experimental Design

Cells

The battery cells used in this experiment are 33 Ah NMC-LMO pouch cells with a voltage window of 2.8 to 4.2 V. The cells were still in a 2p-2s configuration in an metal case module. An X-Ray scan of the cells was performed to analyse the mechanical structure and is shown in Figure 44.

Figure 44: X-Ray of the battery module

The cells are placed on top of each other, glued together and connected via copper bars. The aluminium casing is exerting a bracing effect on the cells, preventing them from expansion. The module has three terminals for the negative, positive and centre connection respectively. The centre terminal is intended for voltage measurement and control rather than high current and is a little smaller, but the bridge is physically identical to the other ports and can thus carry similar currents. This allows the cycling of both levels individually.

Prior to this experiment the modules have been characterised through a full module capacity and EIS test. After that they have been in storage for approximately one year at 10 °C. The modules have then been subjected to five full cycles, during which they displayed no detectable capacity or even charge loss.

Cycling Profiles

Five battery modules with each four cells have been provided. To ensure confidence in the results, each module has been cycled with one profile. Each profile has been assigned an arbitrary label and is described in the following.

The “CAL” profile does not contain any cycling and similarly to the test in 3.1 serves as reference for calendric ageing.

The “EFR” profile emulates the provision of EFR by following the provision requirements as shown in Figure 45 for a sample of recorded GB grid frequency from 2016 (provided by the EDF Energy R&D UK centre). It is expected that the battery can provide 2 C (100%), since it

must only sustain that extreme up to 30 min (18). Further, the battery will utilise the deadband, where output is limited but not required, to re-establish the starting SoC of 50 % whenever possible. This will prevent an over- or complete discharge of the battery.

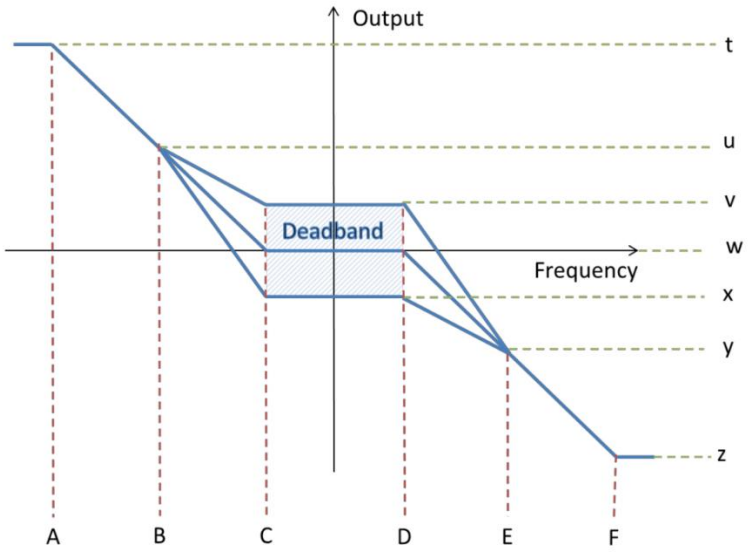

Reference Point	Service 2 (Hz)
A	49.5
B	49.75
C	49.985
D	50.015
E	50.25
F	50.5

Reference Point	Service 2 (%Capacity)
t	100%
u	48.45361%
v	9%
w	0%
x	-9%
y	-48.45361%
z	-100%

Figure 45: EFR Service 2 Provision Requirements (18)

Since the targeted testing time of six months would not cover (if present) the spectrum of seasonal differences, the profile has been resampled to sets of 28 days, where each day contains the response profiles of one weekday of each season. The average throughput of this 28 day profile is approximately 1 FEC per day.

The “ARB” profile emulates the provision of arbitrage trading in the UK intraday wholesale market. This profile has also been provided by the EDF Energy R&D UK centre. The profile has been resampled similarly to EFR and the average throughput of this profile is 1.9 FEC per day.

The “FCY” profile replicates a conventional full cycling of battery cells as close as possible. To be comparable to the above-mentioned profiles, the throughput has been limited to 2 FEC per day, performing two full CCCV cycles each day at C/2. Rest-SoC is 50 %.

The “MCY” profile consists of repeated charge-discharge pulses at C/2. In accordance to the results in 3.2.4 the duration of the full pulse has been set to 2 seconds, which is equivalent to 0.5 Hz and well above all measured CDTFs. Similarly to FCY, the throughput has been adjusted to 2 FEC (8 hours of pulsing) per day.

An overview on the resulting cycling profiles for one day is given in Figure 46. MCY and FCY progress through their assigned cycling and then stop. EFR follows the frequency response

profile which consists of fluctuating charge and discharge pulses and ARB focuses on energy trading and pre-defined settlement periods. CAL does not cycle until the capacity test. Overall, these profiles display great variability.

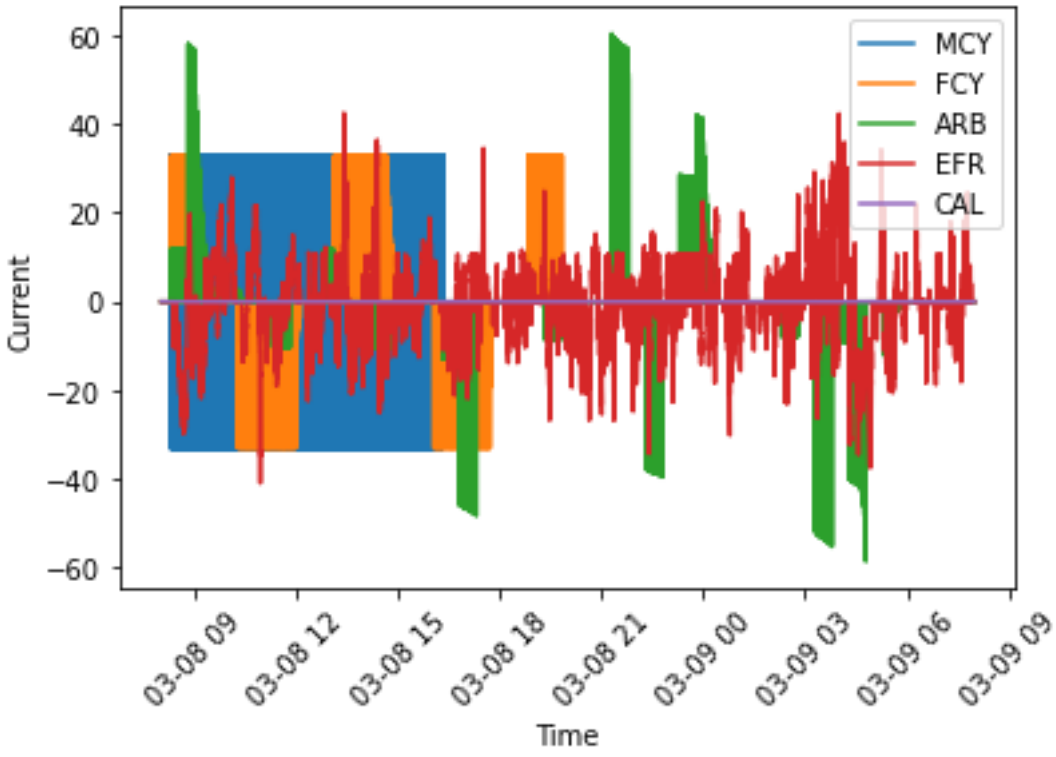

Figure 46: Cycling profile sample for one day

Test Acceleration

As found in 3.1.4, the test may not incur a significant degradation within the targeted time period. Therefore, additional measures should be taken to ensure this. Commonly, cell degradation is accelerated through high environmental temperature (118, 160, 220).

The limitation for this is the recommendation set by the manufacturer to prevent thermal runaway. Although higher temperature reduces the cell resistance and consequent self-heating, there should still be a buffer allowed to account for it. The environmental temperature has therefore been set to 50 °C. This will have an impact on the overall degradation, which will have to be considered for the ageing model development, but this effect is well understood and without this there is a risk that insufficient degradation may occur for analysis.

Intermittent Tests

The main intermittent test performed is the capacity test. It has been performed at CCCV charge and discharge at C/2 and C/20 cut-off current. Since in 3.1 the frequency of capacity tests was deemed too high due to their relative throughput, they have been performed every

28 days in this test. For the cycled cells the relative throughput of the capacity tests therefore varied between 1.8 % and 3.4 %.

EIS allows to identify the CDTF of the modules before and after cell testing and provides a way to ensure cell-to-cell consistency after the test, but intermittent testing has been found unnecessary for the development of the degradation model. Further, skipping EIS characterisation means maintaining 50 °C and possibly full automation of the test. It has been consistently performed at C/20 from 5 kHz to 20 mHz at 50 % SoC and 20 °C.

Full Experimental Design

The full experimental design matrix is shown in Table 11. In contrast to 3.1 all modules are subjected to the identical environmental conditions throughout the test.

ID	1	2	3	4	5
PROFILE	CAL	EFR	ARB	FCY	MCY
CELLS	2x2	2x2	2x2	2x2	2x2
TEMPERATURE	50 °C				
PRESSURISATION	Module Bracing				
PROFILE FEC/DAY	0	1	1.9	2	2

Table 11: Experimental design matrix for Testing Series Three

The testing process is outlined in Figure 47. The modules are first subjected to an initial characterisation at 20 °C, including an EIS at 50 % SoC and capacity test. Then each of the modules is subjected to their individual profile. All profiles have been set to a duration of 28 days after which they are subjected to a capacity test. Ideally, this process can be fully automated, but for the purpose of better control the monthly procedure has been initiated manually. The detailed cycling profiles for one 28 day period are shown in Appendix D.

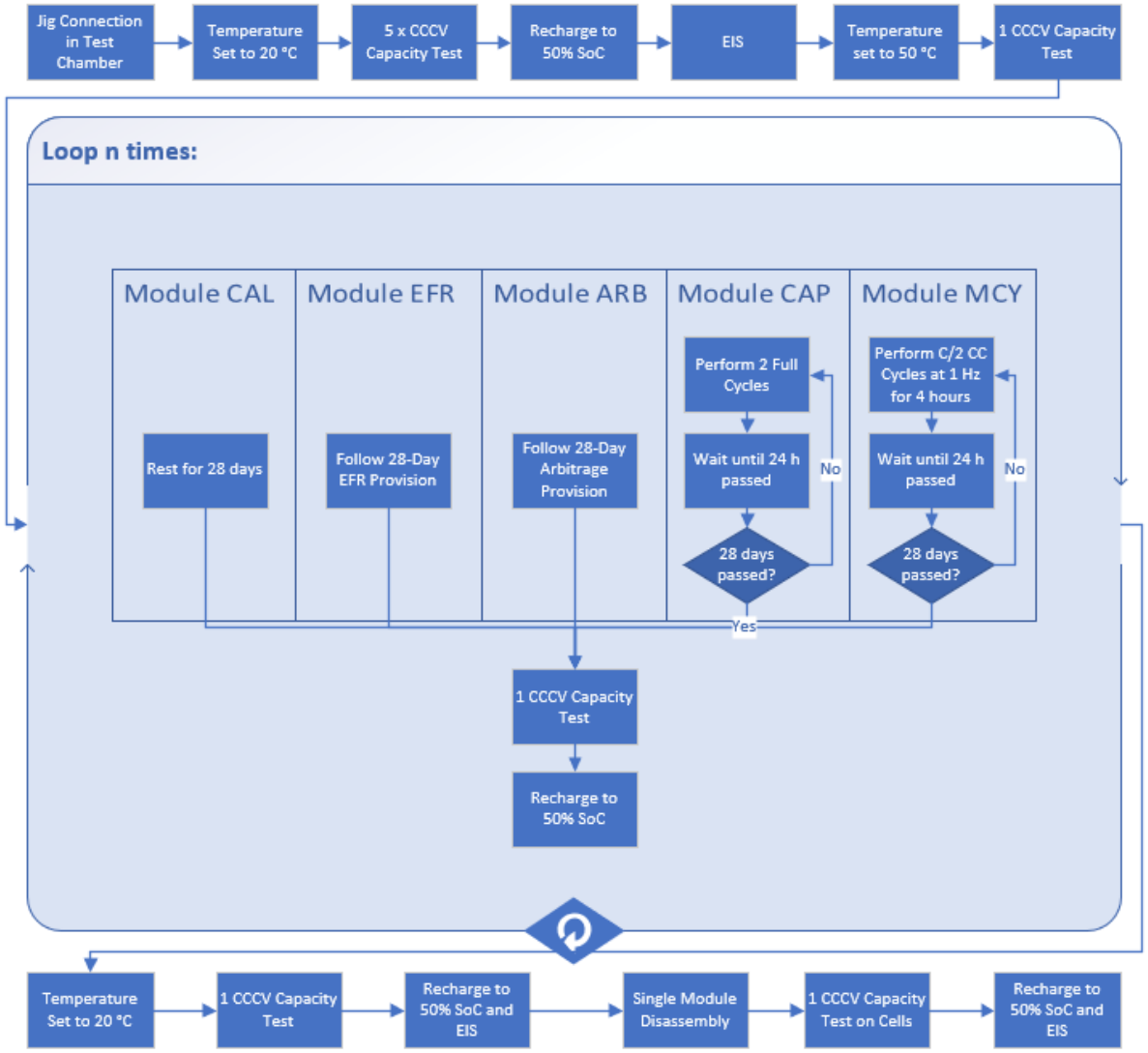

Figure 47: Testing procedure overview

After the test, the modules are characterised at 20 °C once again. One module has then been disassembled into individual cells to identify the cell-to-cell variation between the cells in parallel.

3.3.3 Equipment and Setup

The equipment used for this experiment were a Vötsch environmental chamber, a Digatron battery cycler, Picolog 1216 loggers with thermistors for the collection of temperature data and a Solartron ModuLab potentiostat for EIS. The same equipment was used consistently throughout the test.

Images of the jig used for module testing are shown in Figure 48. The modules were fixed onto jig plates and connected via wire bridges to the brass blocks. This design allowed for the simultaneous connection of cycler and EIS equipment. The cycler channels were connected

between the positive and neutral and negative and neutral terminals, each cycling two cells in parallel.

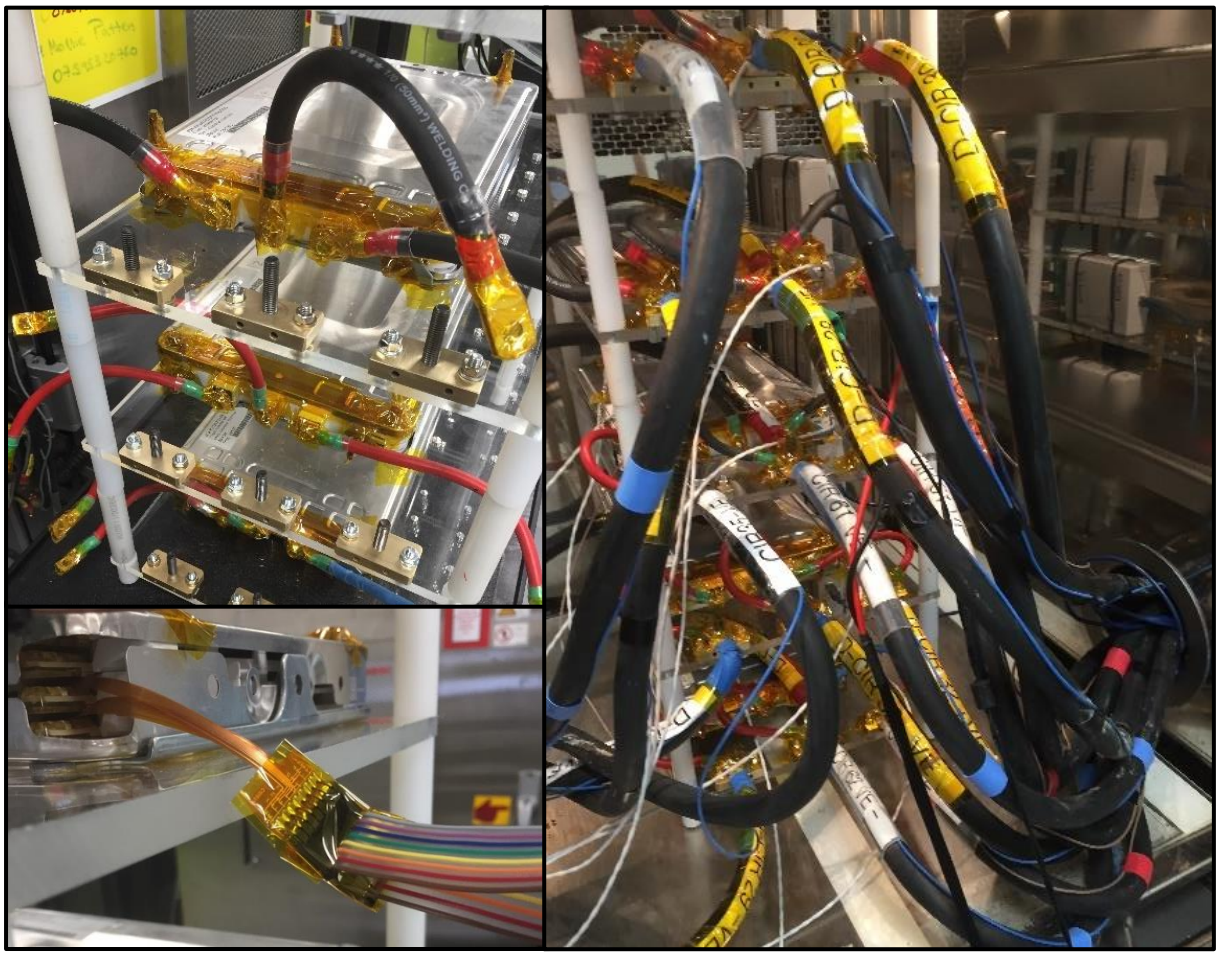

Figure 48: Jig construction steps

The Pico loggers are fixed on the jig and connected via USB to an external laptop recording the temperature data. The sensors have been inserted as displayed in-between three cells to record internal module temperature. Due to the flat design of the thermistors they posed no danger to the cells. Further, the Digatron thermocouples have been placed on top of the modules.

It should be noted that the experiment experienced several unexpected interruptions due to unforeseeable errors and faults in the cycler software. Also there was a 2 week testing pause due to lab shutdown.

3.3.4 Results and Conclusions

Data Processing

In the first step after the testing the collected data must be adjusted to be suitable for evaluation. Firstly, the thermistor data (which is given in voltage) needed to be translated via

the Steinhart-Hart equation into temperature. This equation was given and linearly corrected via collected datapoints at 10, 20 and 50 °C:

$$T = a * \left(\frac{1}{\frac{\ln\left(\frac{V}{2.5 - V}\right)}{4251} + 0.00335402} \right) + b \tag{19}$$

The linear correction factors a and b were determined for each sensor separately and were approximately 1.109 and -35.86 K respectively. The data from three sensor points for each strip was averaged to arrive at the module temperature.

Further, the continuous SoC had to be determined. For this, the current has been integrated over time to determine the cumulative charge, two samples of which are shown in Figure 49.

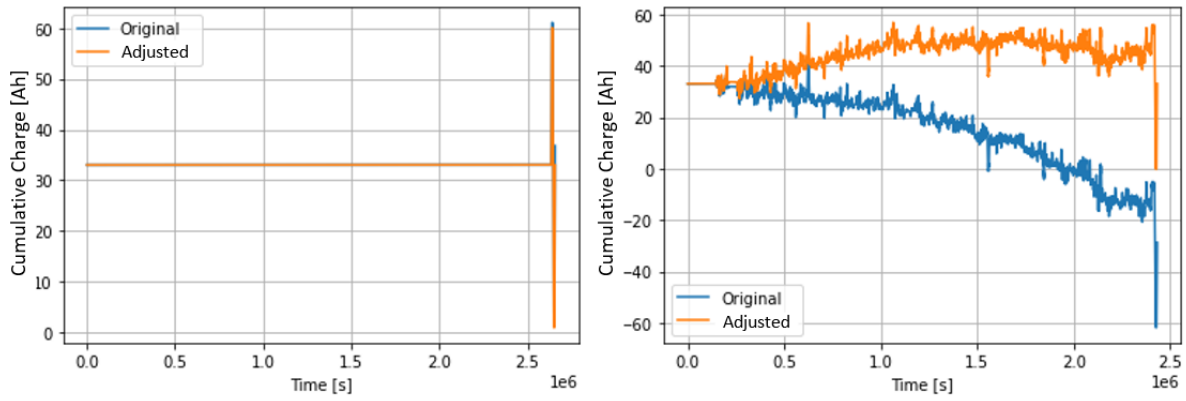

Figure 49: Measured and adjusted cumulative charge of one set of CAL (left) and EFR (right) data

The cumulative charge originally displayed a shift resulting in SoC values that were negative or greater than 100 %, although the cell stayed within voltage limits throughout. Since this effect was mostly observed in profiles with high throughput, it was attributed to an inaccuracy in the current measurement. Thus, the currents have been adjusted as follows:

- The cumulative charge at the lowest point during the capacity test should be 0 Ah. Hence the measured cumulative charge at that point is identical to the imbalance Q_{imb}:

$$Q_{imb} = \min\left(Q_{CT}(t)\right) \tag{20}$$

- The imbalance is then spread over the cycling time t_{cyc} and applied to the measured current I_{meas}:

$$I_{adj} = I_{meas} - \frac{Q_{imb}}{t_{cyc}} \tag{21}$$

The adjusted current is more likely to represent the actual applied current, since the resulting SoC stays within 0-100 % throughout in accordance with the measured voltages between 2.8

and 4.2 V. The SoC is determined for an assumed linear loss of capacity between measurements.

The DC resistance was determined based on the pseudo-OCV curve determined for the cells and the capacity test discharge between 45 % and 55 % SoC:

$$R_{DC} = \frac{\int_{0.45}^{0.55} \left(\frac{V_{oc}(SoC) - V_{DC}(SoC)}{I_{DC}} \right) dSoC}{0.1} \tag{22}$$

Since this takes the average of multiple measurements (approx. 720), there is higher confidence in these values than with a single measurement as in 3.1.4.

Cell-to-Cell Consistency

Since through each of the channels two cells were cycled at once, proof must be provided that the cells displayed identical ageing. To that effect, the module FCY, which experienced the most cycling throughout the test, has been disassembled after the test. Both capacity tests and EIS have been performed on the combined and separated cells.

The results of the capacity test are shown in Table 12. The capacity of the individual cells was found to be 0.27 and 0.52 Ah higher than the capacity of the combined cells. The residual voltage windows (measured 30 minutes after charge and discharge) were more narrow in the combined state, which means results in a smaller ΔOCV and thus in a lower capacity. This was likely incurred by the resistance of the copper bridges connecting the cells, which added to the cell resistance and meant that the same cut-off current incurred a higher overpotential.

	Level			Cell		
Module Level	Cap. [Ah]	Upper and lower residual voltage		Cap. [Ah]	Upper and lower residual voltage	
A	49.04	4.113	2.958	24.83	4.115	2.938
				24.48	4.116	2.969
B	48.95	4.115	2.965	24.69	4.116	2.949
				24.78	4.117	2.95

Table 12: Capacity comparison of module level vs cell

The overall difference between the cells was 0.35 and 0.09 Ah, which is extremely small considering that the overall SoH of the cell has already fallen below 75 %.

Additionally the EIS measurements have been compared as shown in Figure 50. As in 3.2.4, the inductive response has been eliminated. Further, the series resistance has been cut out to eliminate the impact of the afore-mentioned copper bridges.

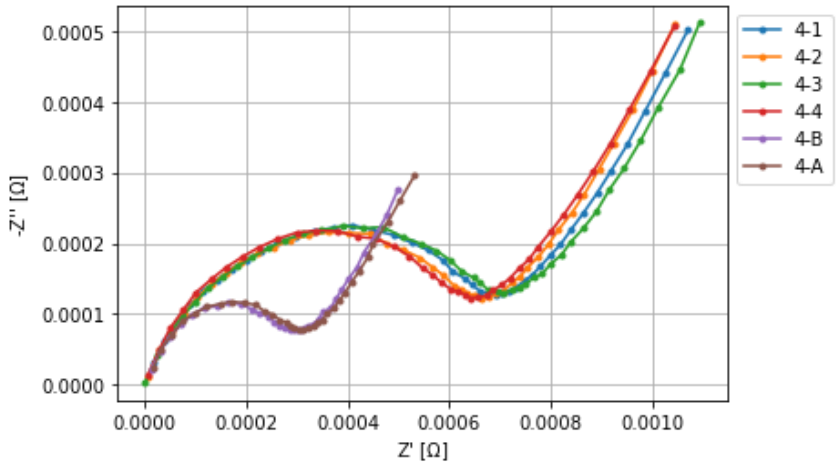

Figure 50: EIS impedance of module level vs cell (corrected by series resistance)

Although there a slight differences between the cell signal, they are much smaller than expected from cells that experienced 25 % degradation. Also the combined EIS signals represent almost exactly half the response of the individual cells, which matches the parallel combination of both impedances.

Based on these results the two cells connected in parallel in the module levels are treated as identically aged.

CDTF Analysis

The CDTF has been determined four times: Before going into storage for the entire module, before testing for each level, after testing for each level and after testing for the individual cells of module 4. The results are displayed in Table 13.

				Time			
	CDTF [Hz]			First	Start	End	
				2p2s	2p1s	2p1s	1p1s
Module/Cell	1	A		0.0603	0.1302	0.034	
		B			0.0614	0.0283	
	2	A		0.0479	0.1486	0.0317	
		B			0.3664	0.0362	
	3	A		0.0576	0.4411	0.0361	
		B			0.551	0.0405	
	4	A	1	0.0521	0.2253	0.0323	0.0177
			2				0.0181
		B	3		0.6225	0.0264	0.0173
			4				0.0189

	5	A		0.0413	0.3226	0.036	
		B			0.2545	0.0242	

Table 13: CDTF of all EIS measurements on the battery modules

The first conclusion to be taken from this data is that the chosen frequency for the MCY profile was above most and in particular the CDTF of the MCY levels. Secondly, the CDTF decreases when cells are put in series and increases for cells in parallel. Thirdly, the degradation decreased the CDTF in all cells, meaning that the pseudo-capacitance became significantly more relevant.

Capacity Development

The development of the double-cell capacities over time is shown in Figure 51. It should be noted that the mentioned disruptions in the testing of EFR and ARB led to a significant decline in throughput over the time period, making them more difficult to compare.

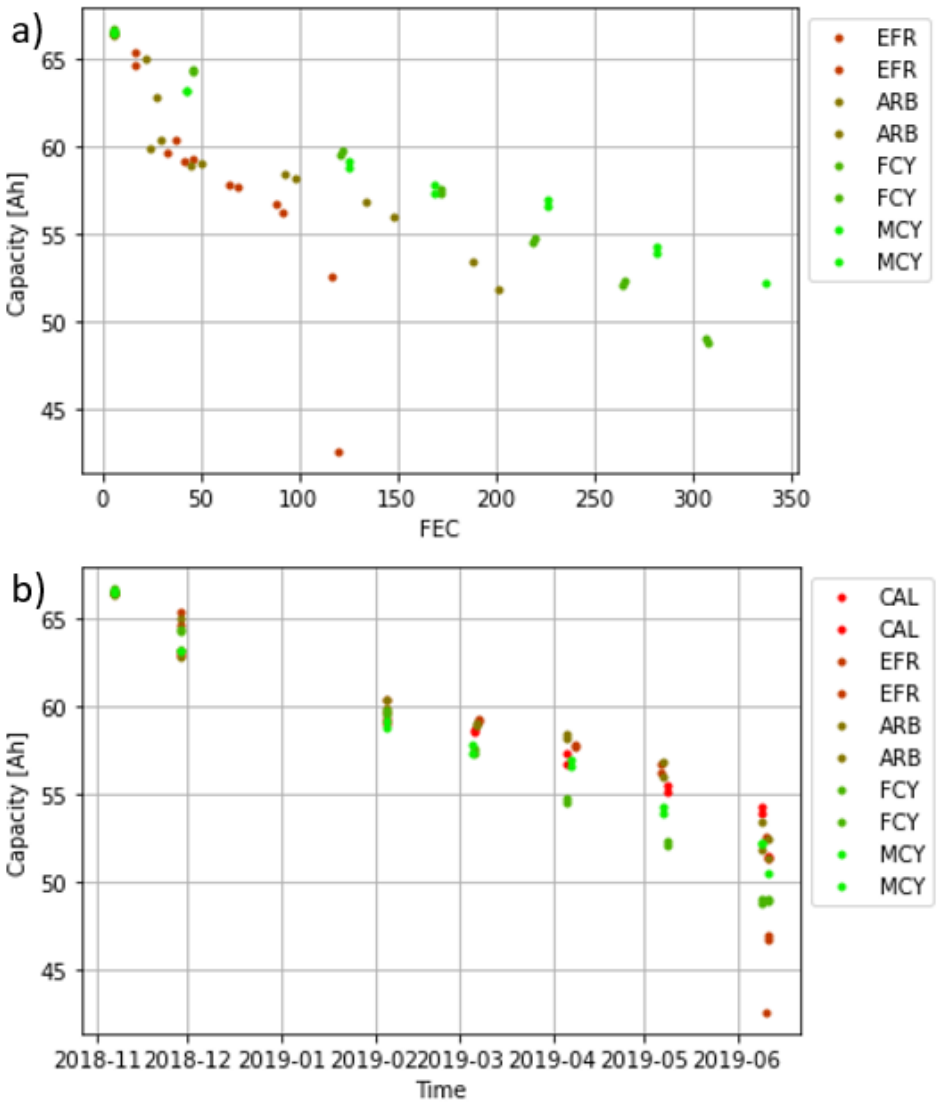

Figure 51: Capacity development over throughput (a) and time (b)

Compared to throughput, the MCY module experienced the lowest amount of degradation compared to its throughput while also having the highest overall throughput. The module with the second highest measured throughput FCY experienced the highest degradation over time with the exception of a few outlying data points at the end.

Overall it is apparent that the storage at 50 °C had the most impact on the degradation. While an acceleration was expected, these conditions likely triggered unwanted side-reactions within the cell that may go beyond conventional SEI formation.

This means that from the experimental data, no definite statement towards the comparative impact of the cycling profiles can be made. While MCY did experience the least degradation per throughput, it is invalidated by the time comparison and thus is not considered sufficient evidence to support a statement about the impact of high frequency cycling.

Conclusion

Over multiple months the tested cells were subjected to a variety of cycling profiles and heavily degraded, likely due to thermal acceleration of calendric processes. While this provided a significant amount of data for use in model development, it may not provide reliable ageing data. The homogeneity of degradation between parallelly connected cells has been proven. Further, the new information on the behaviour of the CDTF has been collected, and the capacitive cycling of the MCY cells has been confirmed.

3.4 Conclusion on all Testing Series

Testing series one and two provided the foundation for the investigation of the electrical, thermal and ageing behaviour of battery modules in testing series three. That series in particular provided data that will be used in the development of the DREMUS model in section 4. While a lot of data on the cells has been collected, the severely accelerated calendric degradation may potentially disqualify it from being used in a universally applicable ageing model, since 50 °C are extremely unlikely environmental conditions.

4 DREMUS Model Development

In this section a BESS model is developed fulfilling the requirements outlined in 2.5.7. The main challenge is to construct a full multi-physics model based on the very limited amount of data available to third-parties. The modelling approach is therefore dubbed Data-REstricted MUlti-physics Simulation or DREMUS.

The approach outlined prioritises the data available on the system where possible and substitutes unknown parameters or relationships with data and relationships from experiments and literature scaled to the use case. This section describes an ideal modelling approach with few considerations about computational capabilities.

The first part discusses the available resources for the development of the model. Afterwards, each of the sub-models are outlined in detail. The final section describes the interconnection and application strategy of DREMUS.

4.1 Resources

Datasheet and warranty data should take priority for the development of the model. Generally manufacturers provide different sets of information for their storage systems, making benchmarking between them difficult. However, in addition to costs, the following technical information on the BESS should always be made available:

- Converter: power rating $P_{con,n}$, minimum power, converter type, maximum roundtrip efficiency $\eta_{con,r}^{max}$ and DC voltage, no-load and standby consumption
- Battery: nominal energy capacity $E_{bat,n}$, nominal DC voltage $V_{bat,n}$, roundtrip efficiency $\eta_{bat,r}$, temperature and charge/discharge current limits, nominal temperature T_n, cathode chemistry, end-of-life (EOL) capacity $SoH_{abs,eol}$, EOL reference conditions

The EOL reference conditions outline the conditions under which (according to the manufacturer) the battery should reach its EOL capacity, for instance if the manufacturer provides a determined throughput per day and a lifetime.

It should be noted that this data is the bare minimum to be expected from the manufacturer/retailer. If additional data is available that may improve the modelling approach, such as the OCV curve and details on the BMS, that data should be considered as well.

As experimental data, two primary sets are available. Type A describes a pre-collected dataset of 18650 NMC cells which has been made available to this project by WMG Centre High Value Manufacturing Catapult (funded by Innovate UK) in collaboration with Jaguar Land Rover. The project was undertaken to develop a degradation model to be applied in EV. However, the data is generic enough to be used for this project as well.

The cells were tested using a Bitrode battery cycler. For temperature control they were suspended in a liquid cooling bath. An overview on the experimental data used for this project is given in Table 14.

	Cell Count	Temperature	SoC	Current	DoD	Intermittent Tests
Calendric	30	10, 25, 45 °C	20, 50, 90 %	N/A	N/A	every 2 months
	3	60 °C				every month
Cyclic	6	25 °C	N/A	0.3/0.4 C, 0.3/0.8 C, 0.3/1.2 C	80	every 100 cycles
	12				30	every 300 cycles

Table 14: Type A experimental design matrix

Each individual storage and cycling condition was confirmed through three cells. Intermittent tests contained pulse power characterisation for the determination of the ECM and capacity tests and were performed at 25 °C.

Type B describes the data obtained from the experiment in 3.3. The two cell types are compared in as outlined in Table 15.

	TYPE A	TYPE B
CELL CAPACITY	3 Ah	33 Ah
DC RESISTANCE	0.0413	0.0030
CHEMISTRY	NMC	NMC-LMO
ARCHITECTURE	Cylindrical	Pouch
CONFIGURATION	1s1p	2p2s
BRACING	No	Yes
CELL COUNT	51	20

Table 15: Experimental cell data for modelling

The remaining data and relationships are derived from existing modelling approaches in literature.

4.2 Electrical Model

The electrical behaviour of the BESS contains three main levels: the converter, the battery structure and the intra-cell ECM. This structure is shown in Figure 52.

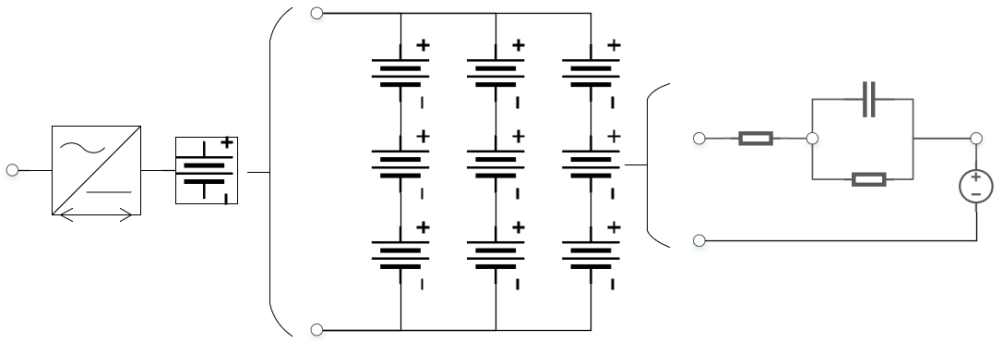

Figure 52: Component structure of the electrical model

The converter takes in the AC demand profile and turns it into a DC response, where voltage and current must be balanced to meet the power demand. The power is then split across all battery cells, where the individual cell responses affect each other. The cell responses themselves must be emulated with an appropriate ECM. Each of these models are discussed in the following.

4.2.1 Converter

The battery converter takes the AC power P_{con} as input. Then, this power needs to be adjusted according to the roundtrip efficiency $\eta_{con,r}$ of the converter:

$$\eta_{con,u} = \sqrt{\eta_{con,r}} \tag{23}$$

$$P_{bat} = \begin{cases} P_{con} * \eta_{con,u} \; for \; P_{con} > 0 \\ \dfrac{P_{con}}{\eta_{con,u}} for \; P_{con} < 0 \end{cases} \tag{24}$$

$\eta_{con,u}$ is the unidirectional converter efficiency. P_{bat} is the power transmitted to the battery. According to the authors of (221), the converter efficiency is dependent upon the output power. That dependency in turn is dependent upon the type of the converter, meaning whether it is contains a transformer for the voltage step-up.

While the authors of (221) did provide a dependency curve for each type, they must be adjusted to the efficiency given in the datasheet. The unidirectional efficiency is then determined as follows:

$$\eta_{con,u}^{max} = \sqrt{\eta_{con,r}^{max}} \tag{25}$$

$$P_{con,\%} = \frac{P_{con}}{P_{con,n}} \tag{26}$$

$$\eta_{con,u}(P_{con}) = \eta_{con,u}^{max}\left(\frac{16.470}{P_{con,\%} + 16.162} - \frac{2.657 * 10^{-4}}{{P_{con,\%}}^2}\right) \tag{27}$$

$$\eta_{con,u}(P_{con}) = \eta_{con,u}^{max}\left(\frac{1.283}{P_{con,\%} + 0.076} - 0.230 * P_{con,\%}\right) \quad (28)$$

(26) refers to a transformer-less and (27) refers to a transformer-based converter. The differences occur due to the overlaid efficiency behaviour of transformers, which declines more rapidly at lower power. It should be noted, that at very low powers (<5 %) the converter efficiency is in all cases extremely low and the power cannot be provided anymore.

For more theoretical estimations, detailed converter data may not be given. For that case the data of converters of varying sizes from six manufacturers (222, 223, 232, 233, 224–231) has been analysed. Logarithmic trends between the nominal power and values such as efficiency, no-load and standby consumption have been determined:

$$\eta_{con,r}^{max} = 0.0031 * log\left(P_{con,n}\right) + 0.9449 \quad (29)$$

$$P_{con,standby} = (-2e-4 * log\left(P_{con,n}\right) + 0.0036) * P_{con,n} \quad (30)$$

$$P_{con,no-load} = (-6e-4 * log\left(P_{con,n}\right) + 0.0112) * P_{con,n} \quad (31)$$

Standby and no-load consumption are considered to be drawn from the grid and hence an overhead on the normal charge/discharge profile with no implications for the BESS itself. To determine the current I_{bat} for the DC cycling, the battery voltage V_{bat} must be permanently measured:

$$I_{bat} = \frac{P_{bat}}{V_{bat}} \quad (32)$$

Optionally, the implementation of no-load and standby consumption of the converter can be considered in the model. These can be added on top of the provided response or deducted from the demand profile.

4.2.2 Battery Circuit

In the next step the current must be distributed across the cells. For this the structure of the battery must be assumed. Taking the battery module of type B as reference, each battery string would be made up of 2p2s modules. The amount of modules in series m can be determined from the nominal voltage of the cathode chemistry $U_{cell,n}$ and the nominal battery voltage $U_{bat,n}$:

$$m = \frac{V_{bat,n}}{2 * V_{cell,n}} \quad (33)$$

This equation applies to the type B modules, but by eliminating the factor 2 can also be applied to the cell count. The number of strings in parallel is sometimes given, but can also be derived by taking the capacity of the module as reference for an approximate:

$$Q_{bat} = \frac{E_{bat,n}}{V_{bat,n}} \tag{34}$$

$$n = \left\lceil \frac{Q_{bat}}{66\ Ah} \right\rceil \tag{35}$$

Using this configuration data the cell ECMs can be connected accordingly. The actual module capacity is then determined as follows:

$$Q_{mod} = \frac{Q_{bat}}{n} \tag{36}$$

The DC resistance of the battery R_{bat} is unknown, but can be approximated under the following premises:

- The charge and discharge resistance are identical.
- The temperature is identical for charge and discharge.
- The DC resistance is consistent throughout all SoC.
- The roundtrip efficiency does not consider coulombic or connection losses.

Using the roundtrip efficiency $\eta_{bat,r}$ and it's representation of output energy E_{out} divided by input energy E_{in} as well as the nominal battery voltage $V_{bat,n}$, nominal current I_n and charge/discharge time t, the relationship can then be derived as follows:

$$\eta_{bat,r} = \frac{E_{out}}{E_{in}} \tag{37}$$

$$E_{out} = E_{in} - |I_n|^2 R_{bat} t_{ch} - |I_n|^2 R_{bat} t_{dch} \tag{38}$$

$$E_{in} = |I_n| V_{bat,n} t_{ch} + |I_n|^2 R_{bat} t_{ch} \tag{39}$$

$$t_{ch} = t_{dch} \tag{40}$$

$$\eta_{bat,r} = 1 - \frac{2|I_n| R_{bat}}{V_{bat,n} + |I_n| R_{bat}} \tag{41}$$

$$\frac{(1 - \eta_{bat,r}) V_{bat,n}}{(1 + \eta_{bat,r})|I_n|} = R_{bat} \tag{42}$$

The average module and cell DC resistance can then be determined from the configuration:

$$R_{mod} = \frac{n * R_{bat}}{m} \tag{43}$$

$$R_{cell,DC} = \frac{2 * R_{bat}}{2} = R_{bat} \tag{44}$$

The final part of the battery section is the BMS. The most straightforward solution is the resistive balancing to prevent overcharge of the battery cells (113). The resistor must activate when the cell steps over the maximum cell voltage V_{max} and be able to take on the entire current surplus. Thus, using the maximum expected imbalance current $I_{i,max}$ the balancing resistance can be determined as follows:

$$R_{BMS} = \frac{V_{max}}{I_{im,max}} \tag{45}$$

The imbalance current depends on the expected cell imbalance between cells. For heavy imbalances the maximum allowed battery charge current (per string) can be used. An appropriate voltage hysteresis should be considered when implementing this condition since it may otherwise lead to instabilities.

4.2.3 Cell Equivalent Circuit

DC Resistance

With the average (over SoC and charge/discharge) DC resistance obtained from the battery circuit, several dependencies should be considered. Firstly, the DC resistance is generally non-linear and the current follows the Butler-Volmer equation (67, 234–237):

$$I = I_e \left(e^{\frac{\alpha_a F V_{op}}{R_g T_{cell}}} - e^{\frac{\alpha_c F V_{op}}{R_g T_{cell}}} \right) \tag{46}$$

I_e represents the exchange current, α_a and α_c the anodic and cathodic transfer coefficients, V_{op} the reaction overpotential and I the resulting current. However, it has been shown in (1), that currents up to 1 C, which is the most common spectrum for battery operation, do not display non-linearities.

Another relationship derivable from the Butler-Volmer equation is the temperature dependency, which can be expressed as Arrhenius equation (238, 239):

$$R_{DC}(T) = R_{DC,n} * e^{\frac{-E_{ac}}{R_g} * \left(\frac{1}{T_n} - \frac{1}{T_{cell}}\right)} \tag{47}$$

R_n is the reference resistance at nominal temperature T_n and R_g is the Boltzmann constant. E_{ac} is the activation energy and the only unknown parameter. Many values have been found in literature for the activation energy ranging from 14 and 29 kJ/mol with no consistent dependency upon chemistry or cell architecture (238–242). The experimental data obtained from type B (DC resistance at 20 and 50 °C as determined in equation (22)) was used to determine E_{ac} through equation (47):

$$E_{ac} = \frac{-R_g * \ln\left(\frac{R_{DC,50}}{R_{DC,20}}\right)}{\left(\frac{1}{293.15} - \frac{1}{323.15}\right)} \tag{48}$$

This showed a value for E_{ac} of approximately 15 kJ/mol and declining to 9 kJ/mol over its lifetime. Considering that the battery module is the closest given approximation to the BESS and the decline in activation energy of the lifetime, 14 kJ/mol is considered a good static approximation.

Multiple sources confirm that the DC resistance increases at very low SoC (106, 239, 241, 243–246). However, the rates and for this dependency vary strongly. Further, including this dependency would contradict the assumptions made for the determination of the average DC resistance. A constant value over the SoC spectrum is considered sufficiently accurate and minimises the amount of assumptions made on the system. The consequent impact the temperature and DC power limit is neglected.

The last dependency of the DC resistance is upon the SoH of the cells. As stated in 2.5.4 the authors of (154, 161) recognised a linear connection between the SoH and the DC resistance. The experimental data on the development of the DC resistance in type A and B is shown in Figure 53.

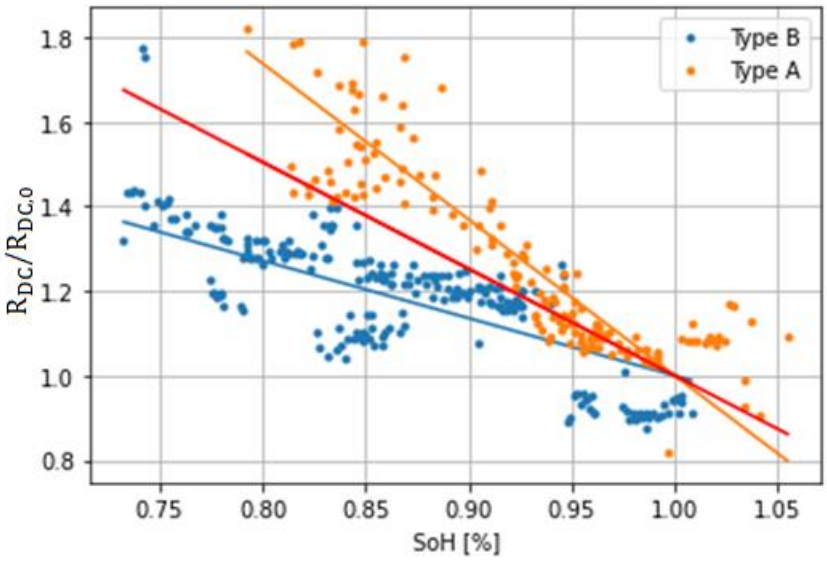

Figure 53: DC Resistance in dependency of the SoH

Based on the displayed correlation of both types a linear fit between the DC resistance and the absolute SoH provided the best results. However, they slightly vary between cell types. To provide a representative connection between the parameters, the average dependency (red line on Figure 53) is chosen:

$$R_{DC}(SoH_{abs}) = R_{DC,n}(-2.525 * (SoH_{abs} - 1) + 1)\ \mathrm{R_{DC}/R_{DC,0}} \qquad (49)$$

This determination can potentially be improved through additional data on more cell types and differentiation between the ageing modes, but under the given circumstances is not possible. To quantify the impact of this estimation, the full model has been used with the case study in 5.4 using the upper and lower resistance increase curves. The ageing rate changed by 0.1-0.2 % for reference conditions, which is considered negligible.

Thus, the overall DC resistance dependency can be expressed as follows:

$$R_{DC} = R_{DC,n}(-2.525 * (SoH_{abs} - 1) + 1) * e^{\frac{-14\frac{kJ}{mol}}{R_g} * \left(\frac{1}{T_n} - \frac{1}{T_{cell}}\right)} \quad (50)$$

Equivalent Circuit Model

In the next step, the full ECM must be derived. For this project, a combination of the Thevenin and runtime-based model from Figure 16 has been chosen and is displayed in Figure 54. This model covers the transient response as well as the SoC and self-discharge component.

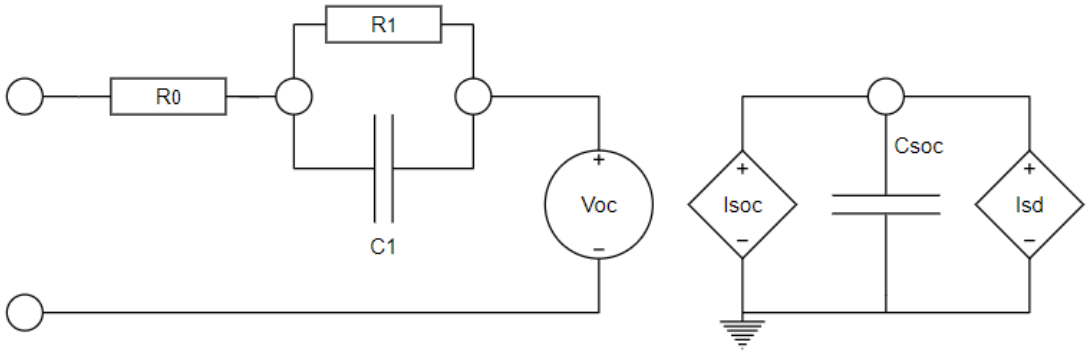

Figure 54: Electrical ECM for DREMUS

The transient circuit was chosen to have only one RC couple for multiple reasons. Firstly, the experimental data of type A was provided with single RC circuit data for all tests. Secondly, the circuit was found to fit well the C/2 charging pulses at 50 % SoC of type B (0.49% NRMSD). Lastly, this further minimises the amount of assumptions necessary on the circuit to replicate an accurate response.

The resistances R_1 and R_0 form in sum the DC resistance R_{DC}. However, more data is necessary to derive the components from R_{DC}. Relative parameters that scale with the size of the cell are ideal for this determination, in particular $\frac{R_1}{R_0}$ and the RC time constant $\tau = \mathrm{R}_1 C_1$. The experimental data on the SoH dependency of these parameters is displayed in Figure 55.

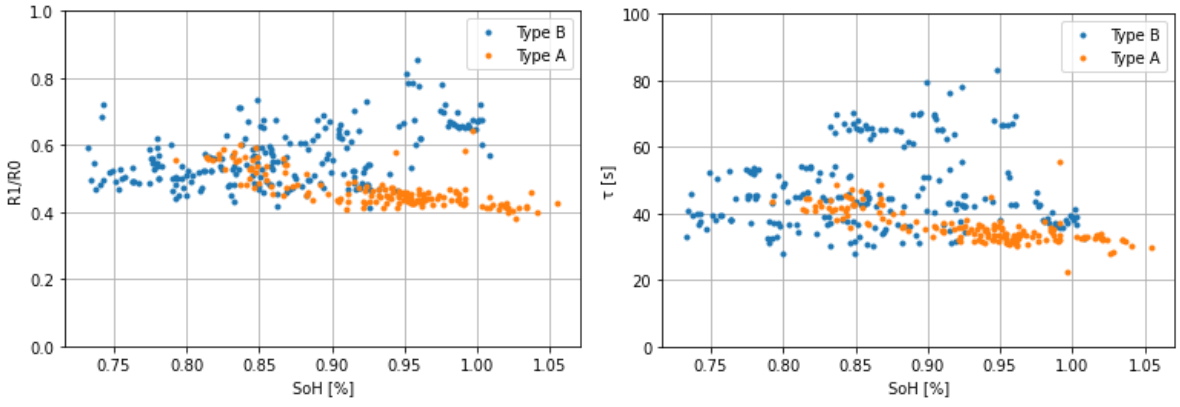

Figure 55: $\frac{R_1}{R_0}$ and τ over different SoH

This data provides several useful statements. Firstly, the SoH did not seem to have a notable impact on the values for $\frac{R_1}{R_0}$ or τ. Secondly, even though the capacity of both cell types differed by the factor of 10 and they were based on different chemistries and cell architecture, the values for $\frac{R_1}{R_0}$ and τ were consistently in the same range. The transient voltage measurements from pulse characterisations in literature displayed very similar behaviour as well (247, 248). Therefore, the values of 0.52 and 41.91 s for $\frac{R_1}{R_0}$ and τ are taken as reference for the average cell behaviour.

Using those values, the elements of the transient ECM can be determined as follows:

$$R_0 = \frac{R_{DC}}{\frac{R_1}{R_0} + 1} \tag{51}$$

$$R_1 = R_{DC} - R_0 \tag{52}$$

$$C_1 = \frac{\tau}{R_1} \tag{53}$$

Open Circuit Voltage

The OCV is, as described in 2.5.4, primarily dependent upon the chemistry, the SoC, the SoH and the cell temperature. Curves for the SoC dependency for the different chemistries can be found in literature for all relevant chemistries (125, 181, 249, 250). They are displayed in Figure 56.

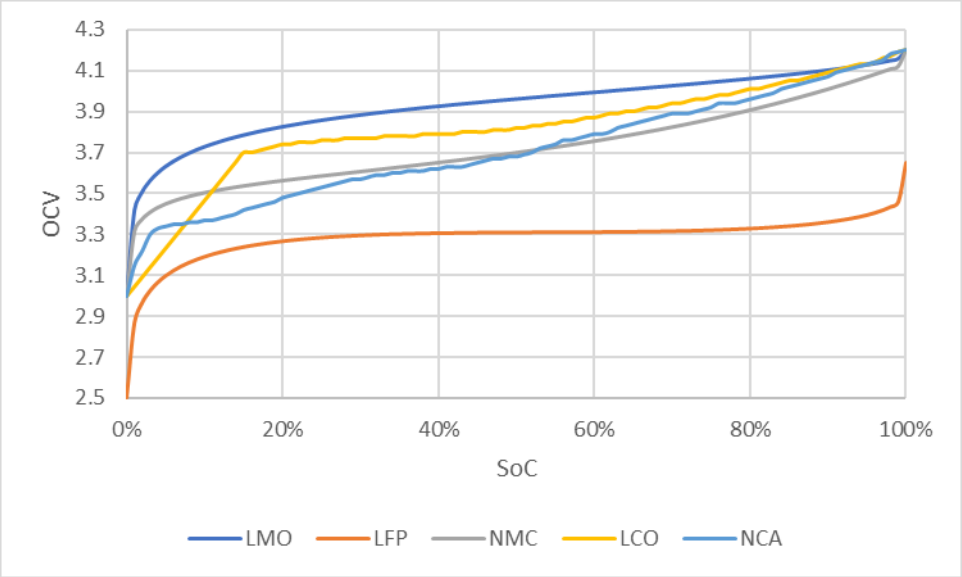

Figure 56: OCV curves

The dependency upon the SoH is very minimal compared to the overall spectrum of the OCV as shown in (125) and is considered negligible. Therefore only the temperature dependency

remains. This dependency can be obtained from the entropy curves provided in (127, 143, 144, 240, 251), which describe simultaneously the dependency of the change in OCV upon the change in temperature (127). The entropy curves are given in Figure 57.

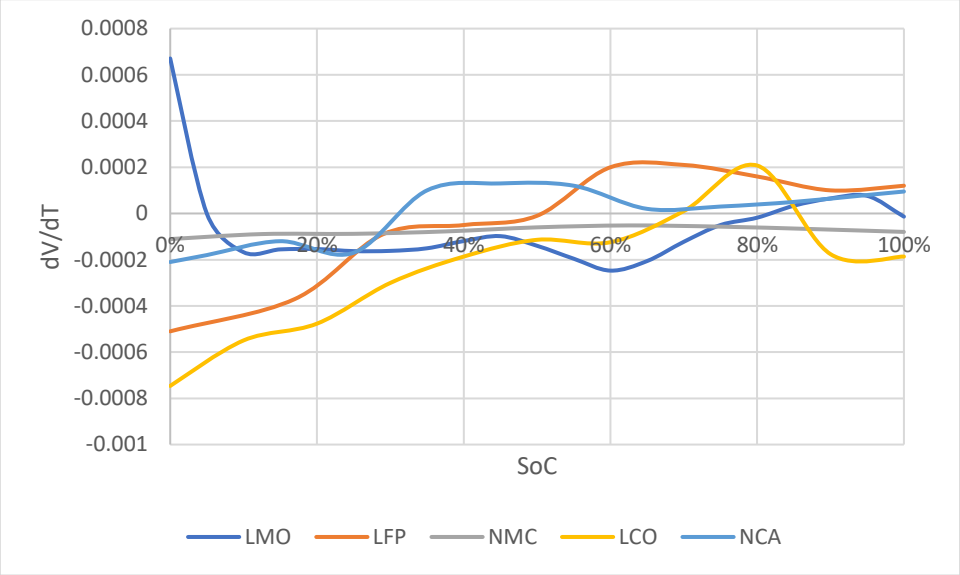

Figure 57: Entropy curves

Combining the dependencies, the OCV can be expressed as follows (127):

$$V_{oc} = V_{oc,n}(SoC) + \frac{\partial V_{oc}}{\partial T}(SoC) * (T_{cell} - T_n) \tag{54}$$

SoC Circuit

The SoC circuit on the right of Figure 54 follows the principle of (116) and consists of three main elements. The current source I_{SoC} copies the current going into V_{OC}. The capacitor has the capacitance identical to the current cell capacity, which is dynamically calculated as follows:

$$Q = Q_n * SoH_{abs} \tag{55}$$

Another impact factor on the capacity is the environmental temperature. For this, the capacity measurements of type B before and after testing at 20 and 50 °C have been collected and are displayed in Figure 58.

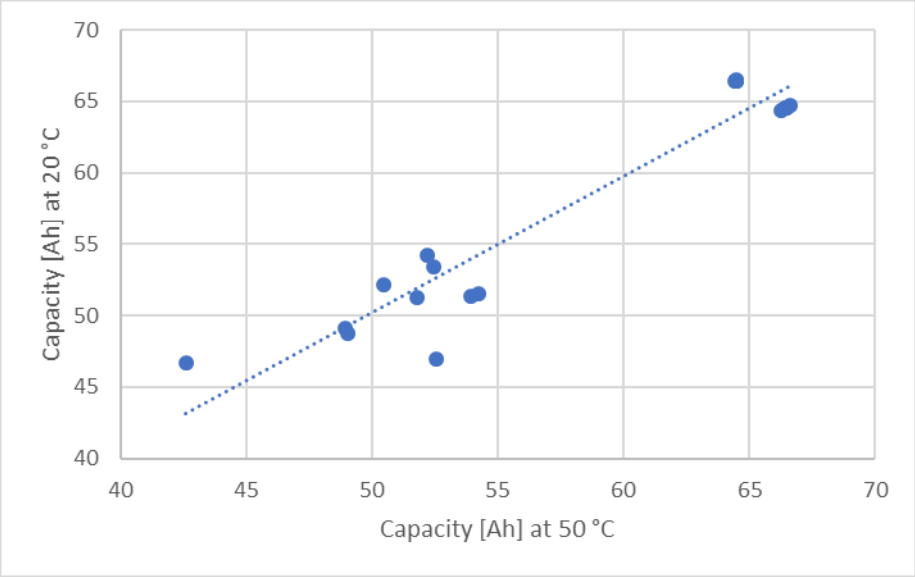

Figure 58: Capacity of the modules at different SoH at 20 and 50 °C

The trendline represents the average translation curve between capacities at 20 and 50 °C. Some cells displayed an increase, others a decrease in capacity under higher temperature. On average, they did not display any changes. This is in agreement with (246), which predominantly only measured a capacity variation at high currents where lower temperature incurred higher resistance and cut off the CC step, and at temperatures below 10 °C. Since this is the approximate temperature range expected from a realistic use case, temperature dependency of the cell capacity has been neglected.

The last element of this circuit is the self-discharge. Since as described in 2.5.4 there is no consistent connection between SoC, temperature and self-discharge and the range is generally between 0.1 and 5 % per month, a value of 1 % per month for a constant leakage current has been chosen as sufficiently representative. If a value is given by the manufacturer, it should be used instead.

Cell-to-Cell Variability

Imbalances between cells are incurred by small differences in the electrical, thermal and ageing behaviour which propagate over time. They are primarily of interest for the modelling of the battery pack relationships. While cell-to-cell variability has been briefly investigated in this project, it was primarily not considered for the final tool development for the reasons outlined in 0 and therefore not included in the model development either.

4.3 Thermal Model

The thermal model is split into heat dissipation and heat generation, as discussed in 0. The heat dissipation model is based on a reference, which consequently impacts how the heat generation must be scaled, and will therefore be discussed first.

Heat Dissipation

As in chapter 4.2.3, the heat dissipation model can be expressed through another equivalent circuit. The difficulty with dissipation models is that every battery is structured differently with changing cooling strategies and data is not commonly provided. Hence, the best approximation can be made using the experimental data.

The module of type B provides the closest reference to a BESS storage module. The module structure and its corresponding thermal ECM is displayed in Figure 59.

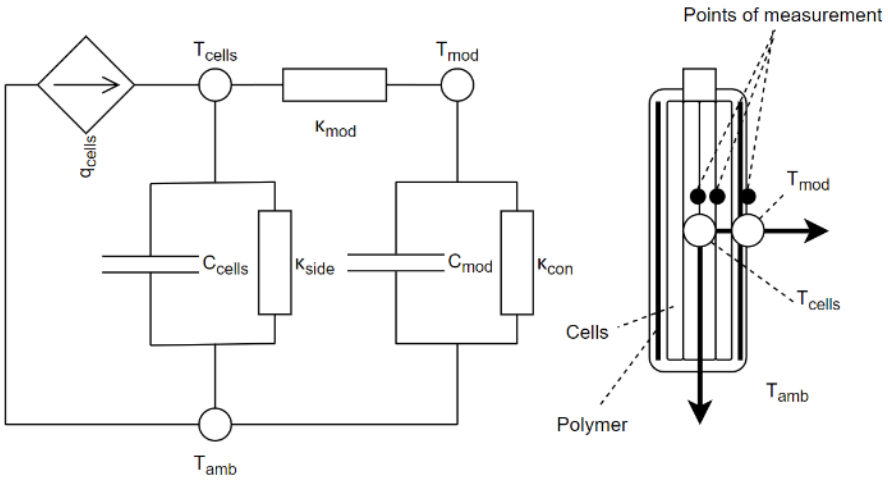

Figure 59: Type B module bulk thermal ECM and module structure

C_{cells} describes the cumulative cell heat capacitance and C_{mod} the heat capacitance of the module casing. κ_{side} is the total heat loss of the open surfaces on the side of the module, κ_{mod} is module heat conductivity and κ_{con} is the surface convection. Although two points of measurements were applied to the module, this ECM was found to provide the best fit to the data.

Passive cooling after a full discharge has been used to fit the ECM. The parameters are outlined in Figure 59 and resulted in a NRMSD of 1.07 %.

PARAMETER	VALUE	UNIT
C_{cell}	3.512e+03	J/K
C_{mod}	2.653e+02	J/K
κ_{side}	8.878e-01	W/K

κ_{mod}	4.891e-03	W/K
κ_{conv}	1.313e-01	W/K

Table 16: Parameters of the module thermal ECM based on Type B

If the manufacturer states that the temperature of the cells is actively controlled, the ECM provided for the cell type A, displayed in Figure 60 can be chosen instead. It only contains the ECM of a single cell and thus assumes that ambient temperature around the cell is held constant.

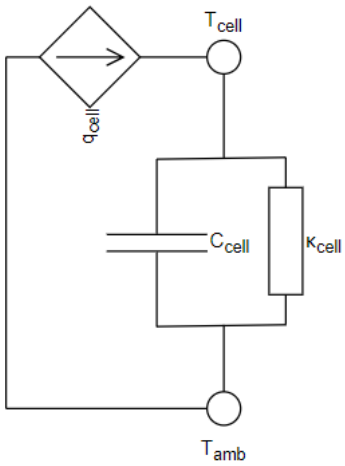

PARAMETER	VALUE	UNIT
C_{cell}	83.3704	W/K
κ_{cell}	0.1605	W/K

Figure 60: Type A cell bulk thermal model

Thermal radiation has been excluded from both models due to the increase of assumptions on the environment necessary, the difficulty of including this non-linear process into the ECM and the possible absorption of the radiation by other cells.

Cell Heating

The bulk heat generation model from equation (3) has been chosen to reduce the necessary assumptions. However, since an electrical ECM is given, the resistance heating is used instead of the total overpotential:

$$q_{th} = q_{joule} + q_{ent} = {I_{R_0}}^2 R_0 + {I_{R_1}}^2 R_1 + I * T_{cell} * \frac{dV_{oc}}{dT} \tag{56}$$

The values for entropy $\frac{dV_{oc}}{dT}$ are the same as in Figure 57.

Since the cell size can vary strongly from that of the reference thermal circuit, the heat generation must be adjusted accordingly. Joule heating must be scaled by both the nominal resistance $R_{n,ref}$ and capacity $Q_{n,ref}$ of the chosen ECM cell. Since temperature and entropy are relative, entropy must only be scaled by the cell capacity:

$$q_{joule,ref} = \left({I_{R0}}^2 R_0 + {I_{R1}}^2 R_1\right) * \frac{R_{DC,ref}}{R_{DC}} \left(\frac{Q_{n,ref}}{Q_n}\right)^2 \quad (57)$$

$$q_{ent,ref} = \left(I * T_{cell} * \frac{dV_{oc}}{dT}\right) * \frac{Q_{n,ref}}{Q_n} \quad (58)$$

$$q_{th,ref} = q_{joule,ref} + q_{ent,ref} \quad (59)$$

4.4 Ageing Model

The development of the ageing model follows the approach displayed in Figure 61. It consists of two main parts:

- Universal cell behaviour: Applicable to all carbon-anode based Li-Ion cells based on chemical principles and empiric sensitivities.
- Cell-specific behaviour: Applicable only to a specific cell and consisting of the cathode specific behaviour and manufacturer data.

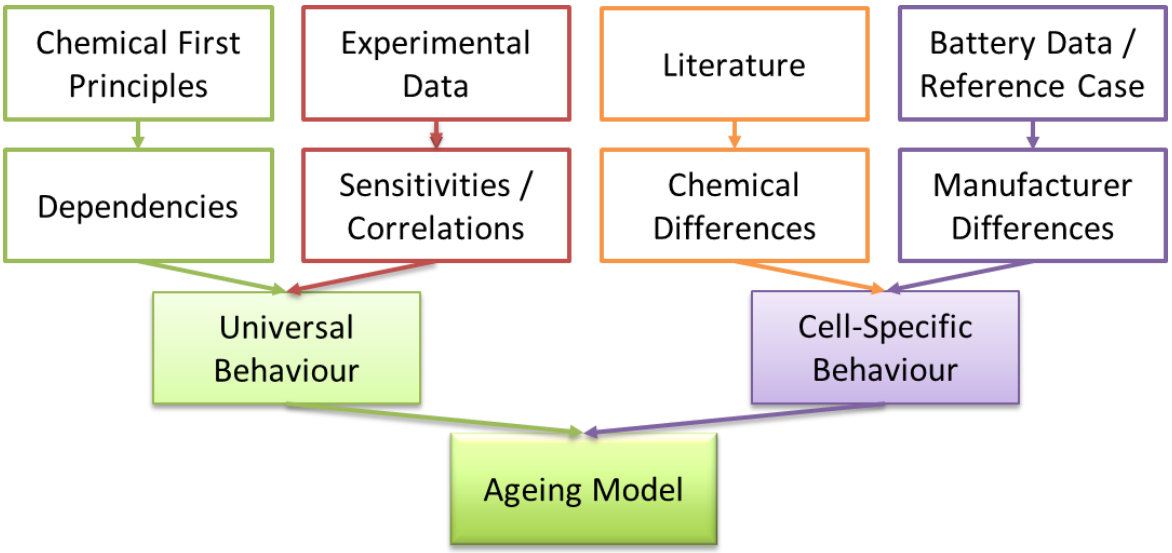

Figure 61: Ageing model development process

Firstly, the relevant ageing processes are investigated and narrowed down. Then, a chemical model for that process is chosen, which is adjusted to the experimental data and requirements of the model. Then to implement the cell-specific behaviour the model is modified to applicability to the BESS.

Ageing Process Identification

According to the authors of (161, 252, 253), the most common capacity degradation processes in Li-Ion cells are SEI formation, Lithium Plating, loss of active anode material from cracking during expansion and loss of active cathode material from severe de-lithiation. As described in 2.5.6 the cell capacity is the minimum of three capacities: anode, lithium inventory and cathode. Out of the four degradation processes mentioned, cathode de-lithiation is the only

process that doesn't affect lithium inventory (only cathode capacity). It is therefore reasonable to assume that loss of lithium inventory is the primary mechanism of capacity loss and to eliminate cathode de-lithiation as relevant ageing process.

Lithium plating is primarily caused by operation at extreme conditions outside of manufacturer recommendations, such as charging above 100 % SoC, temperatures below 0 °C or charging currents above 1 C (88, 126, 152, 254, 255). Since these conditions should be avoided (as they also often break warranty conditions) it should be considered to have minor impact.

Anode expansion occurs during charge. Bracing, as it is found in battery modules and particularly the one of type B, can mitigate the expansion and has been shown in (190, 256) to reduce ageing effects. Further, only the lithiated part of the anode cracking will actually affect the lithium inventory.

Hence, while neither lithium plating, nor anode cracking will be completely absent, SEI formation will be considered the primary ageing process for the development of the ageing model.

Chemical Reference Model

There are multiple approaches to SEI modelling. The most preferred approach is the single-particle modelling following the Arrhenius principle (149, 153, 176, 257). Initially, the model by (153) has been chosen as reference for this project. Since this model did not consider the difference between charge and discharge current and (176) provided a better connection to the experimental data, that one has been used instead:

$$J_{SEI}(t_1) = i_{os} \exp\left(-\frac{\alpha_c F}{R_g T}\left(U_n - U_{ref,s} - J\left(R_{SEI} - \frac{M_{SEI}}{\kappa_P F \rho_{SEI}} * \int_0^{t_1} J_{SEI} dt\right)\right)\right) \quad (60)$$

It should be noted that the parameters and subscripts in model, as outlined in Table 17, only apply to this formula and do not connect to the remaining parameters in this report.

	Value	Unit	Meaning
Local Constants	i_{0s}	$\frac{A}{m^2}$	Side reaction exchange current density
	α_c		Anode charge transfer coefficient
	$U_{ref,s}$	V	Side reaction equilibrium potential
	R_{SEI}	$\frac{\Omega}{m^2}$	SEI resistance
	M_{SEI}	$\frac{kg}{Mol}$	SEI molecular weight

	κ_P	$\frac{S}{m}$	Anode activation energy
	ρ_{SEI}	$\frac{kg}{m^3}$	SEI density
Global Constants	F	$\frac{As}{mol}$	Faraday constant
	R_g	$\frac{J}{Kmol}$	Boltzmann constant
Independent Variables	J_{SEI}	$\frac{A}{m^2}$	Side-reaction current density
	T	K	Temperature
	U_a	V	Anode potential
	J	$\frac{A}{m^2}$	Current density
	t	h	Time

Table 17: Constants and variables of the SEI degradation equation (176)

The model displays the chemically reasonable variable dependency. However, in this state the model is not recommended for use in practical applications due to several factors:

- Time dependency: the model describes a time dependency wherein the side-reaction current increases over time due to increase in SEI thickness. The in 2.5.6 discussed $\sqrt{t}$ dependence of the cell capacity, however, displays a decrease in degradation over time (until reaching EOL).
- Current density: The use of current density requires knowledge of the electrode surface area.
- Chemical reference values: the model requires detailed knowledge on the local constants of the cell and are only relevant for that cell.

Hence, this model must be modified. Since this model is based on the carbon anode only, chemical differences do not need to be considered for its development. They are considered to be implemented by the differences in OCV and entropy curves.

Adjustments and Fitting

To address the issues of this model, several measures are taken. Firstly it is assumed that the SEI resistance increases minimally over the lifetime of the cell (which is in accordance with the assumptions made in another SEI-based chemical model (153)):

$$J_{SEI} = i_{os} \exp\left(-\frac{\alpha_c F}{R_g T}\left(U_a - U_{ref,s} - J R_{SEI}\right)\right) \tag{61}$$

Secondly, since the primary point of interest of this model is the variable dependency, the constants are replaced by parameters and J_{SEI} by a linear measure of linear degradation Deg_{lin} affecting a measure of linear state of health SoH_{lin}:

$$Deg_{lin} = \int k_1 \exp\left(-\frac{k_2}{T}(U_a - k_3 - k_4 J)\right) dt \tag{62}$$

$$SoH_{lin,1} = SoH_{lin,0} - Deg_{lin,1} \tag{63}$$

Under the assumption that anode surface area A_a increases proportionally to the nominal capacity Q_n, the current density J can be expressed as a multiple of the C-rate c:

$$J = \frac{I_{cell}}{A_a} \tag{64}$$

$$c = \frac{I_{cell}}{Q_n} \tag{65}$$

$$Q_n = k_s * A_a \tag{66}$$

$$J = k_s * c \tag{67}$$

Since the factor k_s is unknown it can be regarded as part of the factor k_4:

$$Deg_{lin} = \int k_1 \exp\left(-\frac{k_2}{T}(U_a - k_3 - k_4 c)\right) dt \tag{68}$$

To implement the $\sqrt{t}$ dependency the absolute SoH, representing the capacity loss, is set up accordingly:

$$SoH_{abs} = \frac{Q_t}{Q_0} \tag{69}$$

$$SoH_{abs} = 1 - \left(1 - SoH_{abs,eol}\right) * \sqrt{1 - SoH_{lin}} \tag{70}$$

$SoH_{abs,eol}$ denotes the terminal cell capacity. For the purpose of referencing identical conditions 80 % has been used as value since it is most commonly referred to as EOL capacity (258).

Now the only unknown variable is the anode potential U_a, which is dependent upon the SoC. The typical potential curve for carbon anodes is given in Figure 62.

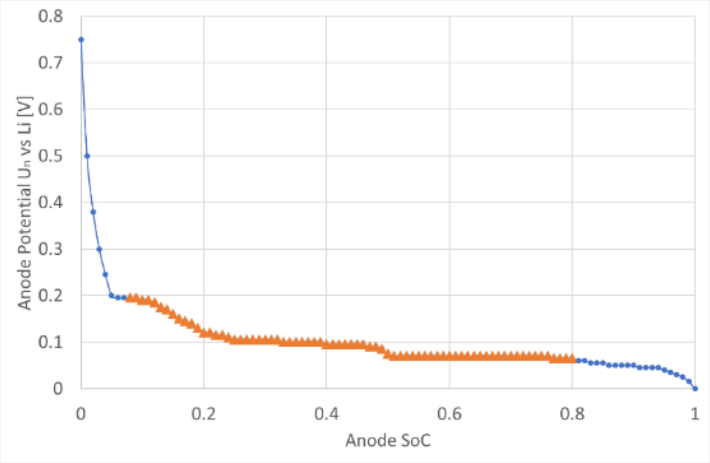

Figure 62: Anode Potential Curve (259)

The anode SoC is different from the full cell SoC. To avoid effects from over-/undercharging the cell, the spectrum is only partially utilised with an overhead serving as buffer. Therefore another dependency needs to be introduced:

$$SoC_a = SoC_{cell} * k_5 + k_6 \tag{71}$$

In the last step, all parameters have been fitted to the ageing data of type A. The parameters, along with the applied boundary conditions are listed in Table 18. The ability of the overall model to forecast the next ageing state had an overall NRMSD of 7.2 %, which was considered sufficient considering the detected spread in data.

Parameter	Bounds		Value	Unit
k_1	0	+∞	1.441e-08	s^{-1}
k_2	0	+∞	3.352e+03	KV^{-1}
k_3	0	+∞	1.230e-02	V
k_4	0	+∞	8.046e-01	Vh
k_5	0.5	1	8.028e-01	
k_6	-0.2	0.2	5.859e-02	

Table 18: Ageing Model Fitting Parameters based on type A

Separately, the fit has been compared to the datasheet degradation profile provided for cell type A. The fitting result is shown in Figure 63. Differences between the model and the datasheet (maximum 0.1 Ah) can potentially be explained by the difference in initial capacity stated or an over-estimation by the manufacturer to account for outliers. Overall the fit is considered sufficiently accurate.

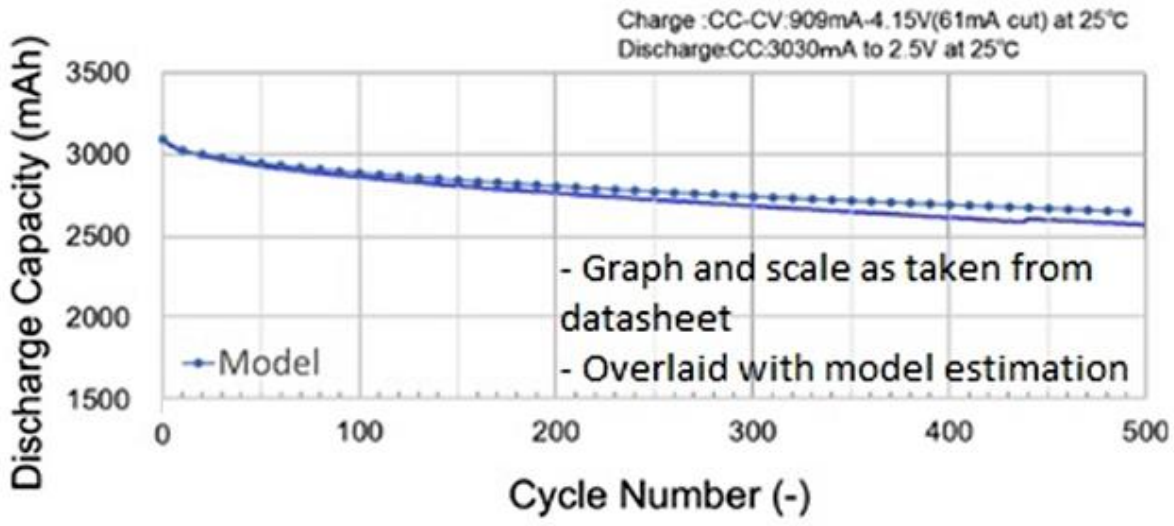

Figure 63: Model overlaid on cell datasheet

Regarding high temperature dependency, the model did not align with the data of cell type B or the calendric cell data at 60 °C of type A. No parameter modification was capable of capturing the excessive degradation acceleration these cells experienced. Therefore, the model should not be applied to cells subjected to environmental temperatures over 40 °C.

Sensitivity Analysis

A comparative sensitivity analysis of the degradation model towards the three core input parameters has been performed: C-rate, temperature and SoC. Since all of the parameters are contained within the exponent of the linear degradation formula, the output has been determined on the logarithmic scale:

$$\log\left(\frac{dDeg_{lin}}{dt}\right) = Y = log(k_1) + \left(-\frac{k_2}{T}(U_n - k_3 - k_4 c)\right) \quad (72)$$

Y represents here the sensitivity output and state variable, which logarithmically affects the degradation speed. The reference conditions for this investigation are 50 % SoC, 20 °C and 0 C. The boundaries for the sensitivity analysis are 0 to 100 % SoC, 0 to 40 °C and +2 to -2 C.

To quantify the impact of the parameters, the value Y has been derived by each of them within the boundaries, averaged, and multiplied by the boundary range to normalise the sensitivity against the other parameters. The sensitivity values are given in Table 19.

$\frac{dY}{dSoC}\left(SoC^{max} - SoC^{min}\right)$	0.540968
$\frac{dY}{dT}\left(T^{max} - T^{min}\right)$	0.0314
$\frac{dY}{dc}\left(c^{max} - c^{min}\right)$	11.94867

Table 19: Average normalised sensitivities of the ageing model

From these values it is apparent that Y, and consequently the overall degradation speed, is most sensitive towards the C-rate. Due to the comparatively small changes on the Kelvin scale, the temperature was found to have the least impact, making the SoC the predominant ageing factor during storage.

Adaptability to BESS

The model has now been adjusted for the experimental cells of type A, but is no longer applicable to other battery cells. To allow for that, another parameter k_{DS} is introduced in the linear equation. This parameter represents faster or slower degradation depending on the investigated storage system:

$$Deg_{lin} = k_{DS} \int k_1 \exp\left(-\frac{k_2}{T}(U_a - k_3 - k_4 c)\right) dt \tag{73}$$

For type A the value is 1. To determine the factor k_{DS} for a specific storage system, the EOL reference conditions must be taken into account. Using the electrical and thermal model, those conditions can be used to determine the degradation stresses type A would have experienced. Further, since under these conditions the targeted battery would have reached EOL, Deg_{lin} can be set to 1. k_{DS} can then be calculated as follows:

$$k_{DS} = \frac{1}{\int_{t_0}^{t_{eol}} k_1 \exp\left(-\frac{k_2}{T}(U_a - k_3 - k_4 c)\right) dt} \tag{74}$$

An overview on this process is also given in 4.5. Using the same reference conditions again with the applied k_{DS}, the model results in 100 % degradation.

4.5 Model Interconnection and Application

The three models are interconnected as displayed in Figure 64. The electrical model, which primarily interacts with the utilisation of the battery, provides the SoC, currents and voltages necessary to the thermal and ageing model. The thermal model updates the temperature influencing electrical and ageing model. The ageing model determines from the circumstance the current SoH and updates the electrical behaviour regarding both capacity and resistance.

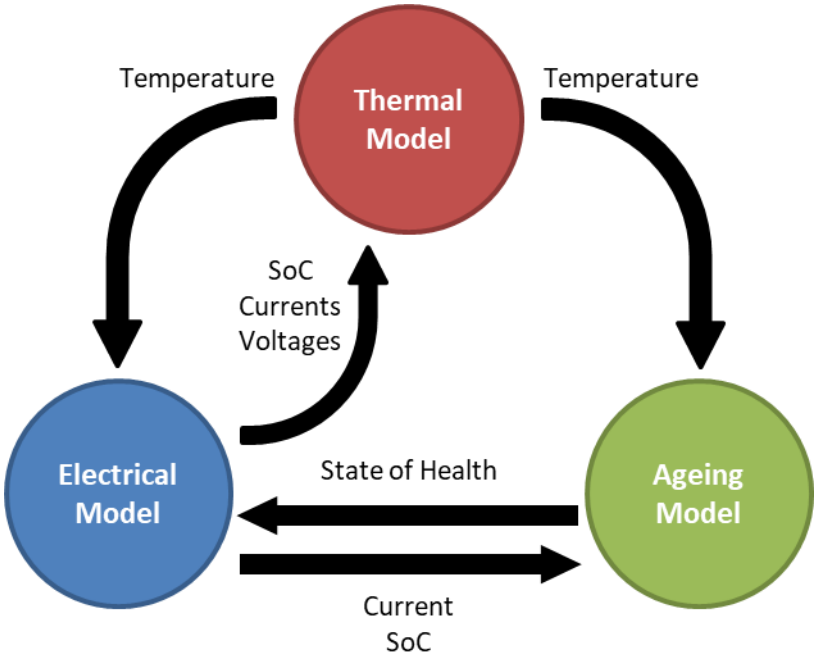

Figure 64: DREMUS interconnections

This model can be developed in a variety of ways, both with discrete approaches and dynamic interconnections. The latter offers more accuracy and allows for a more precise estimation of the BESS capabilities to provide power and energy capacity.

The application method of the model is displayed in Figure 65. In the first step the available BESS documentation is used to scale and determine the electrical and thermal model. Using then the EOL degradation reference with k_{DS} set to 1, the k_{DS} for the BESS can be determined.

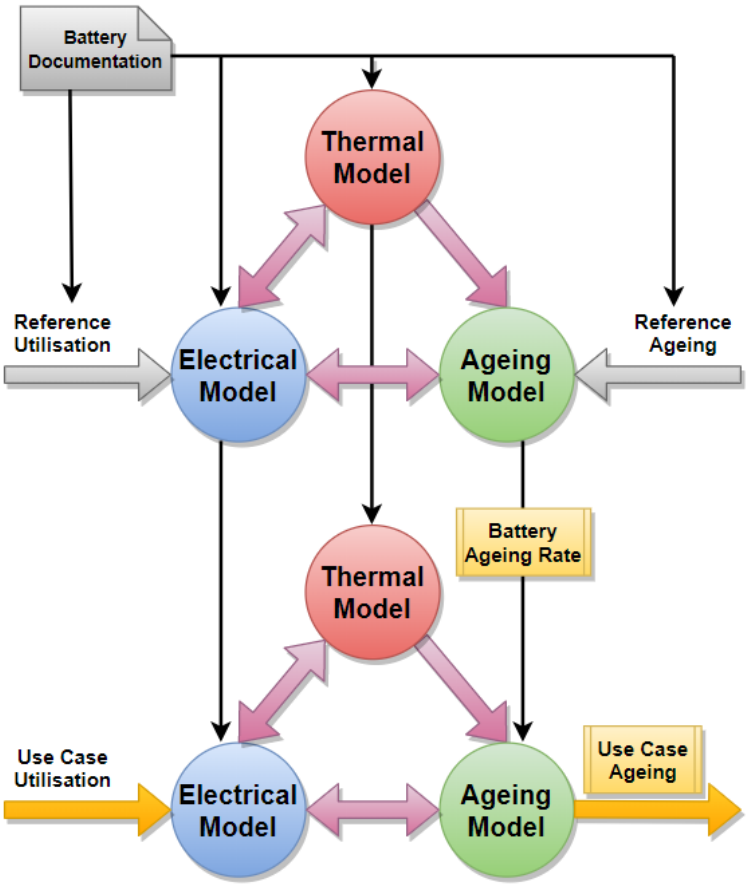

Figure 65: DREMUS model structure

With the full model completed, it is possible to apply any utilisation profile to it. Aside from identifying from that the degradation that the utilisation would incur, it is also possible to provide an estimate on the behaviour of any parameter included in the model (e.g. temperature, SoC) and receive feedback on the potential inability of the BESS to provide the required power or energy.

Using the information obtained from this model the long term BESS value generation can be determined. The model itself does not contain such an assessment to make it more flexible in application.

While this modelling approach is based on carbon anode Li-Ion, it can be applied to other chemistries as well. All models would have to be adapted accordingly, especially the degradation formula. To achieve the same level comparability it also needs to contain a linear degradation component.

5 Software Development

In the next step the model developed in section 4 is implemented into an applicable software tool. The tool is to be used primarily by the EDF Energy R&D UK centre and hence is constructed to their requirements.

First, the available and utilised software tools are discussed. Then the individual documents and functions involved are described. The last part outlines the adjustments made in these functions to fulfil the practical requirements of both stability and computability.

5.1 Utilised Software and Tools

Due to the preference of the EDF Energy R&D UK centre, Python was the primary coding language used to develop the DREMUS tool. This also allows for an implementation of the tool into the existing EDF Energy R&D UK centre tools and applications. The majority of the tool has therefore been implemented into a library.

Since both the electrical and thermal model are represented through a circuit model, a circuit simulator was chosen as primary method of computation. Circuit simulation also allows for a dynamic adjustment and interaction of all parameters.

The circuit simulator chosen was Ngspice, an open-source tool that can be connected to python code via the library PySpice. The circuit is developed in Python, allowing for the implementation of all known parameters. From the circuit a simulator is constructed that is then processed in Ngspice, carrying out the majority of the computation. An example is displayed in Figure 66.

```
circuit=Circuit("Example")
circuit.R(1,circuit.gnd,"N1",1)
circuit.C(1,circuit.gnd,"N1",1)
circuit.I(1,circuit.gnd,"N1",1)
circuit.raw_spice=(".ic v(N1)=0")
simulator=circuit.simulator()
print(simulator)
analysis=simulator.transient(end_time=10@u_s,
                             step_time=1@u_s)
plot(analysis["N1"],".-")
```

```
.title Example
.ic v(N1)=0
R1 0 N1 1
C1 0 N1 1
I1 0 N1 1
.options TEMP = 27C
.options TNOM = 27C
.ic
.end
```

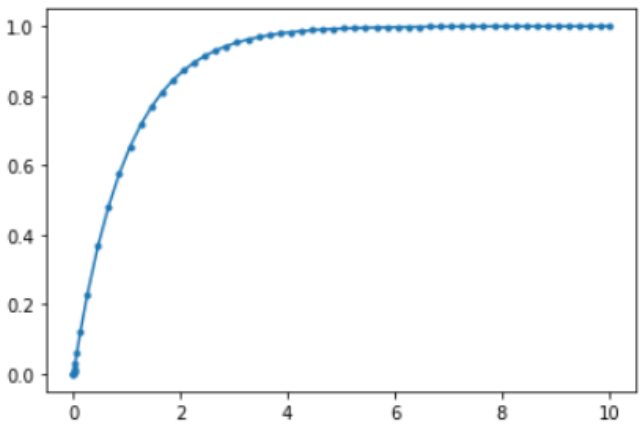

Figure 66: Example circuit build in PySpice and processed in Ngspice

The graph displays the voltage at node N1 versus time in seconds. A particular advantage of Ngspice is that, although the step time has been set to 1 s, the simulation automatically increased the default resolution to accurately capture the circuit behaviour.

Other libraries utilised for pre-calculation and data processing include math, numpy and pandas. Input files were pre-developed in Excel as csv and xlsx files and forms.

5.2 Tool Structure

The structure of the DREMUS tool is outlined in Figure 67. The arrows indicate the process of application as well as the transfer of data between the documents, functions and classes.

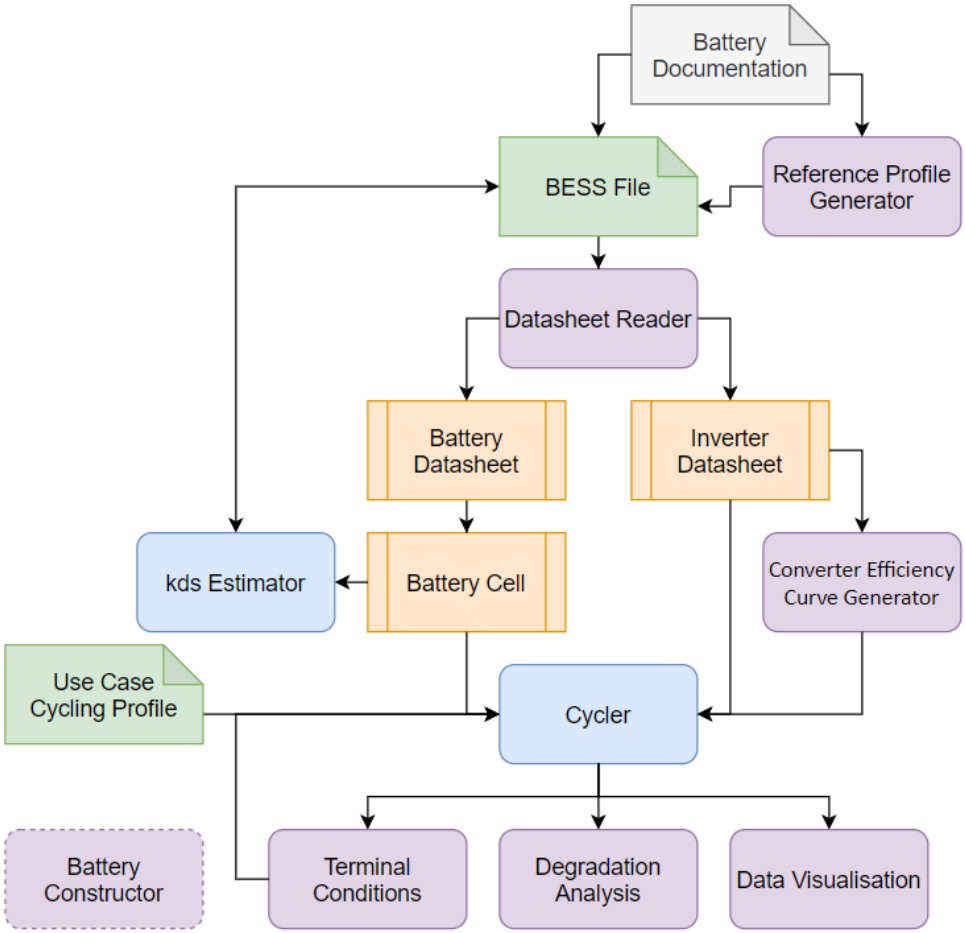

Figure 67: DREMUS Tool Structure (green: Excel input files; orange: classes/objects; blue: core functions; purple: supporting functions)

BESS Documentation Processing

The first element is the Excel BESS File. This file serves as input for all available data on the battery and converter. Of particular interest are the parameters outlined in 4.1. An initial estimate for k_{DS} can be added as well, the default value is 1. A screenshot of that input file is shown in Figure 18.

	A	B	C	D
1			Value	If unknown:
2	Converter	Name		Only for identification
3		Count		Number of inverters splitting the power demand
4		Nominal Power [W]		
5		Max. Roundtrip Efficiency		leave empty
6		Transformer-based?		FALSE
7		Standby consumption [W]		leave empty
8		No-load consumption [W]		leave empty
9		Cut-off		leave empty
10				
11	Battery	Name		Only for identification
12		String count		Number of batteries in parallel or leave empty
13		Capacity [Wh]		
14		Nominal Voltage [V]		51.8
15		Maximum Current [A]		Maximum power divided by minimum voltage
16		Roundtrip Efficiency		97%
17		Self-discharge [1/day]		0.033%
18		End-of-Life Capacity		80%
19		Nominal Ambient Temperature [C]		25
20		Active Cooling		FALSE, TRUE will take cell thermal equivalent circuit
21		Chemistry		NMC
22		kds		Fill in remaining information and "Reference Utilisation" and run "kds Estimator".

Figure 68: Screenshot of Datasheet tab in Input Excel File

Column D provides the user with default values to use if values are unknown. Battery capacity and converter nominal power are the only necessary values, although this will reduce the precision of the model.

For the converter many values are automatically approximated using the equations given in chapter 4.2.1 if not provided. This may under/overestimate the strain on the battery to provide the power necessary and affect the overall system efficiency significantly.

For the battery the impact of the input factors are as follows:

- String count and nominal voltage are in the current state not impactful since the power is equally split across all cells (see chapter 5.3 for details).
- Maximum current is a safety measure given by the manufacturer, but if it is not given will still be limited by voltage and internal resistance, as well as converter limits.
- Efficiency will affect the resistance and thus the power capability and heating of the battery and should therefore be given as accurately as possible.
- Self-discharge will likely be too small to have a significant impact on the long term performance, save for backup focussed services.
- End-of-life capacity will significantly affect the degradation curve. It will affect both capacity and resistance/power and should therefore always be taken by the manufacturer.
- Nominal temperature for Li-Ion is expected to always be around room temperature.
- The chemistry will determine the OCV curve, which affects the power capability, and the entropy, which affects the heat generation. The first one is most significant for LFP,

since the permissible voltage window is much smaller. The latter becomes more important at low power utilisation.

In addition to the general battery data, the degradation reference is needed to determine k_{DS}. The reference is added on a separate table in the Excel file as shown in Figure 69. The profile consists of current steps in A and covers the expected lifetime of the battery.

	A	B
1	timestep	current
2	3659.642	52
3	3659.642	-52
4	3659.642	52
5	3659.642	-52
6	71761.43	0
7	3659.642	52
8	3659.642	-52
9	3659.642	52
10	3659.642	-52
11	71761.43	0
12	3659.642	52
13	3659.642	-52
14	3659.642	52
15	3659.642	-52

Figure 69: Screenshot of Reference Profile tab in Input Excel File

The reference profile can either be generated manually or using the “Reference Profile Generator”. This function uses some basic assumptions around the maximum throughput, maximum calendric life and nominal conditions to create a repetitive cycling profile. It is separate and easily modifiable depending on the given parameters. It is imperative to provide this profile along with the EOL for the tool to provide reasonable value to its user.

Using the function “Datasheet Reader”, datasheet objects for both the battery and the converter are generated. Its task is to derive most of the unknown parameters from the known parameters and thus complete the necessary information for the simulation.

The battery datasheet contains the given battery data and upon generation, imports the relevant OCV and entropy profiles from prepared CSV files. Further, the structure of the BESS is derived along with the individual cell capacity and average cell resistance in accordance with the methodology in 4.2.2,

The converter datasheet contains the given converter data. Upon generation it also calls the function “Converter Efficiency Curve Generator”, which determines the efficiency data based on the approach in 4.2.1. In effect this results in a conversion curve f_η with an efficiency value for each percentage of applied power $P_{\%}$ as displayed in Figure 70. The converter count

involved in the BESS is considered as well, wherein in case of reaching the lower power limit fewer converters participate.

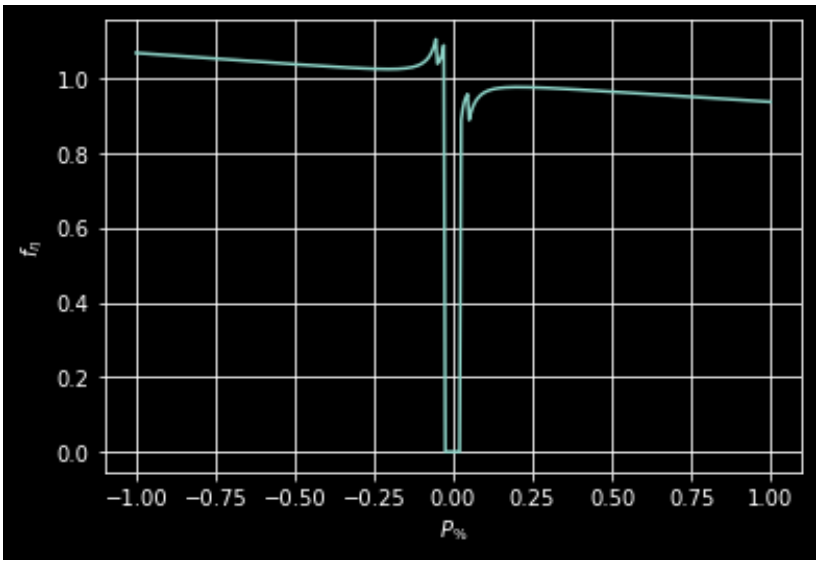

Figure 70: f_η in dependency of the fractional power $P_\%$ utilisation of 2 converters

Battery Cell Circuit

From the battery datasheet, a “Battery Cell” object containing the circuit of a single cell can be created. This circuit is displayed in Figure 71 with the active cooling circuit. Although separated into three sub-circuits, each element is interconnected according to its dependency and calculated simultaneously.

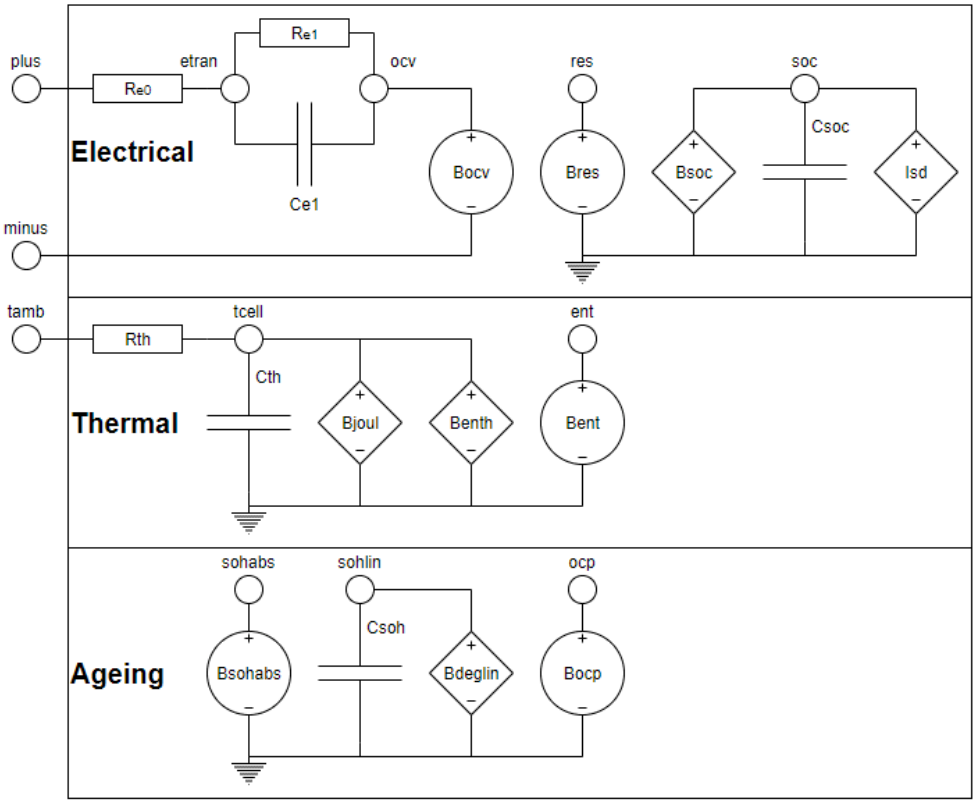

Figure 71: Battery cell sub-circuit (active cooling)

Elements denoted as B are non-linear current and voltage sources. Some source nodes have been added for the pre-calculation of intermediate values such as the DC resistance in Bres, the entropy in Bent and the open-circuit potential Bocp. The corresponding node voltage serve as input for other elements and provide additional data for subsequent analysis.

The electrical and thermal circuits follow the ECMs discussed in 4.2.3 and 4.3. The linear ageing circuit is represented through a capacitor Csoh with an initial charge of 1 V (100% SoH_{lin}) and a current source Bdeglin (Deg_{lin}) that constantly discharges it and thus ages the battery. The node Bsohabs calculates from the present voltage at node sohlin the absolute SoH.

Determination of k_{DS}

In the "k_{DS} Estimator", the cell circuit is subjected to the reference current profile to determine the specific ageing factor for the BESS using the methodology in 4.4. Two factors are determined through the estimation: k_{DS}, which is the ageing factor of the BESS for the given SoH_{eol}, and k_{DS80}, which is the ageing factor for 80 % SoH_{eol}. The latter is calculated as follows:

$$Deg_{lin80} = \left(\frac{1 - 0.8}{1 - SoH_{abs,eol}}\right)^2 \quad (75)$$

$$k_{DS80} = \frac{k_{DS}}{Deg_{lin80}} \quad (76)$$

k_{DS80} is useful for performance comparison between two different BESS as further detailed in 5.5. It is also relevant for applications where less than 80 % capacity are not useful. Either value can be applied to the BESS file (or directly the datasheet object), only affecting the consideration of the EOL.

It has been found that the determination of kds should undergo at least three iterations to increase confidence in its accuracy. This is partially due to the possibility of overestimating the degradation speed and thus the cell not being able to fully process the reference profile.

It should be noted that the kds evaluation also provides a data frame with the development of all node voltages. This data can be used for debugging and (if necessary) adjustment of the degradation reference profile.

BESS Cycling and Evaluation

With the datasheets completed the BESS model can now be generated and cycled. First, the "Use Case Cycling Profile" must be provided. The profile draft contains three columns for each the power, the environmental temperature and the duration as time step.

The "Cycler" function imports the cycling profile, and then creates the full circuit, scaling and interconnecting the converter with a single-cell model abstracting the BESS (details in 5.3). It also takes initial conditions as input, allowing to consider the results of existing systems or previous calculations. The use case profile is applied to the circuit under consideration of all power, current and voltage limits. The output of this function is a data frame containing recordings of all nodes.

Aside from manual evaluation, three prepared tools can be applied to output. The "Data Visualisation" function outputs the graphs displayed in Figure 72. They provide an overview on the key points of interest of the operation: demanded vs provided power, cell temperature, SoC and linear and absolute SoH.

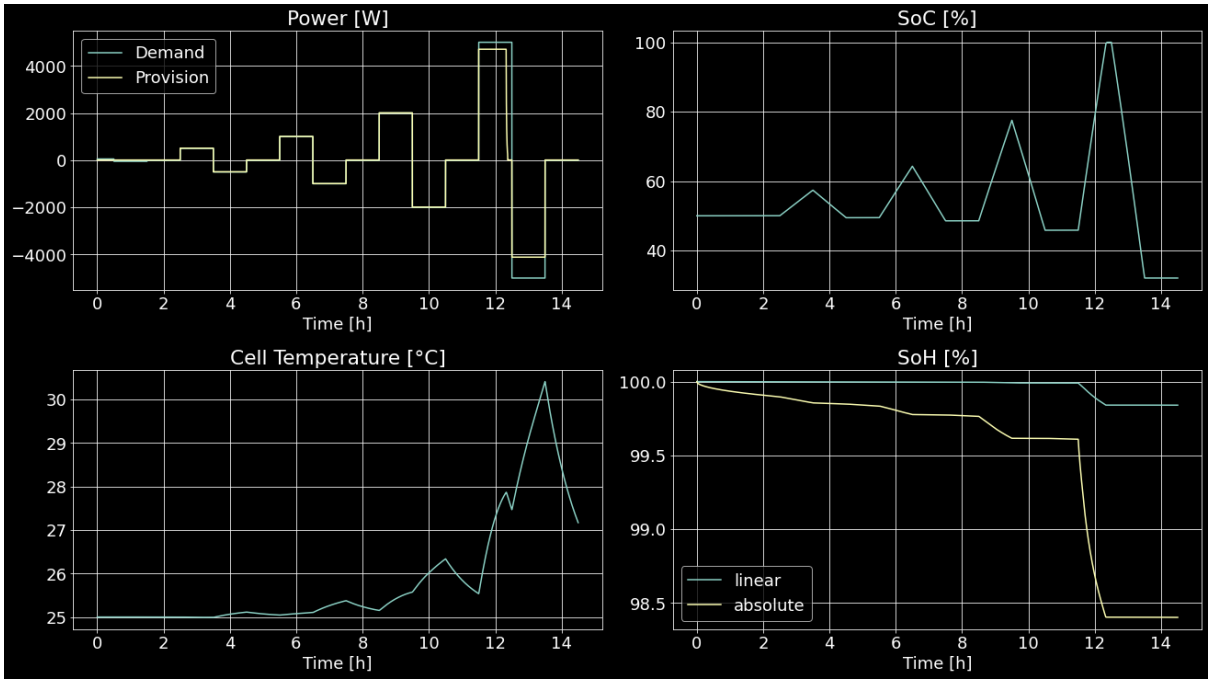

Figure 72: Data visualisation for an arbitrary use case

“Terminal Conditions” extracts the terminal conditions of the simulations, which can be directly applied as input for the next simulation. “Degradation Analysis” is a custom tool providing the daily and total incurred linear degradation. The total degradation in particular is useful for the application outlined in 5.5.

Battery Constructor

In its present state, the tool does not support the simulation of multiple cells for the reasons outlined in 5.3. However, in case of a future application, a function called battery constructor has been added that generates and interconnects individual cell models.

5.3 Model Adjustments for DREMUS Tool

While the DREMUS tool follows as best as possible the model outlined in section 4, several measures had to be taken to allow for an efficient and fast computation. These are outlined in the following.

Single-Cell Modelling

The tool described follows a single-cell modelling approach. There were two practical reasons for this:

- Instability: Simulations with two or more cells frequently led to instabilities and consequent interruptions in simulations.
- Computation Speed: Successful simulations with two or more cells lead to an according increase in computation time. A full simulation of a BESS would, with the current method, provide results in unfeasible time periods. For a 48 V single string system, a simulation of 30 days operation with a simple degradation reference would jump from 50 s (single cell) to at least 20 minutes computation time.

There were also several realistic justifications for this method. First of all, battery cells are commonly matched by capacity and/or resistance (113). This matching process significantly reduces not just the immediate but also long-term imbalances as found in (114) and the evaluation in 3.3.4.

Secondly, cells and strings in parallel balance each other automatically. A difference in SoC results in a difference in OCV and thus not only in an automatic current redirection into the cells with lower SoC but also an auto-redistribution of energy during the rest period (current flow from higher OCV to lower OCV).

Thirdly, cells in series are controlled via a BMS. The BMS assumed for this model (see 4.2.2) allows for a utilisation of the full capacity of all cells while ensuring the adherence to upper voltage limits. The cells are just equalised at higher voltage minimising the additional losses incurred through the resistors. These additional losses, as well as the possible over-discharge of individual cells and the thermal disparity between cells are the only impacts not covered through a single-cell perspective.

There are aspects that are, however, not covered through this this method. Generally speaking those are the effects do not linearly scale with size and that are configuration specific. One example is the additional cycling introduced from cell balancing both through parallel configuration and active BMS. Another is the increase in losses incurred from cell balancing especially for resistive equalisation.

Overall, since the cell is based on the data provided by the manufacturer it will behave as described by the manufacturer. Adjustments for over- or underestimation by the manufacturer can be implemented but should be based on reasonable assumptions and, if non-specific, be applied to all compared systems.

Charge/Discharge Conversion and Filtering

The current and power profiles applied in the k_{DS} estimation and cycling function have been taken as input of power and timestep. They have been implemented into the circuit as a piece-wise linear element. Since these elements operate through linear interpolation of the input it must be converted into a rectangular profile by determining start and stop of each step.

Many limitations and modifications apply to the power profile that must be considered for the battery profile. The procedure chosen for filtering the "Cycler" demanded power profile p_d is as follows:

1. Scale power to cell capacity (division by cell count):

$$p_1 = \frac{p_d}{m * n} \tag{77}$$

2. Apply efficiency and power limit curve f_n:

$$p_2 = p_1 * f_\eta \left(\frac{p_1}{P_{con,n}} * m * n \right) \tag{78}$$

3. Convert power to current using cell voltage v_{cell}:

$$i_1 = \frac{p_2}{v_{cell}} \tag{79}$$

4. Take the minimum of demanded current, maximum current i_{max}, current incurring maximum voltage v_{max} and current incurring nominal converter power $P_{con,n}$:

$$i_2 = \min \left(i_1, i_{max}, \frac{v_{max} - v_{oc}}{R_{DC}}, \frac{P_{con,n}}{m * n * v_{cell}} \right) \tag{80}$$

5. Take the maximum of demanded current, minimum current i_{min}, current incurring minimum voltage v_{min} and current incurring nominal converter power $P_{con,n}$:

$$i_3 = \max \left(i_2, i_{min}, \frac{v_{min} - v_{oc}}{R_{dc}}, \frac{-P_{con,n}}{m * n * v_{cell}} \right) \tag{81}$$

6. Check if power is still above minimum converter power $P_{con,min}$:

$$i_4 = \begin{cases} 0 \; for \; |i_3 * v_{cell}| < \frac{P_{con,min}}{m * n} \\ i_3 \; for \; |i_3 * v_{cell}| > \frac{P_{con,min}}{m * n} \end{cases} \tag{82}$$

When determining the provided power p_p, the function f_n is applied in reverse:

$$p_p = \frac{i_4 * v_{cell}}{f_\eta\left(\frac{i_4 * v_{cell}}{P_{con,n}} * m * n\right)} \tag{83}$$

For the k_{ds} estimation, only the voltage and current limitations apply.

Acceleration of k_{DS} Estimation

In its default state the k_{DS} estimation would need to calculate 10-15 years of utilisation. Since this time frame would take a significant calculation time (>1 hour), a method to speed up this process has been chosen.

Since the degradation factor k_{DS} is a linear acceleration of degradation speed and the profile for the k_{DS} estimation is generally repeating, the time period can be shortened by accordingly increasing k_{DS}:

$$k_{DS,sh} = k_{DS,ig} * \frac{t_{eol}}{t_{sh}} \tag{84}$$

$k_{DS,ig}$ is the initial guess for k_{ds}, t_{eol} is the normal profile length, t_{sh} is the shortened profile length and $k_{DS,ac}$ is the accelerated k_{DS}. After the estimation, k_{DS} is then determined as follows:

$$k_{DS} = k_{DS,sh} * \frac{1}{1 - SoH_{lin}} * \frac{t_{sh}}{t_{eol}} \tag{85}$$

The results for k_{DS} for an arbitrary storage system for various time periods has been determined in Table 20. Overall the acceleration method has, as expected, very little impact on the overall results, but loses precision below t_{sh} of 1 month.

Time (months)	k_{DS}
12	0.1448
6	0.1449
3	0.1442
1	0.1428

Table 20: k_{ds} for different simulation times

Stability Measures

Several measures had to be taken to ensure a reliable simulation. The impact of each measure has been assessed as well:

- Several 1 TΩ resistances have been inserted to avoid errors incurred by isolated capacitors. At the given voltages up to maximum 5 V this would incur error currents of 5 pA which is regarded as neglectable.
- The minimum SoC had to be set to 0 %. The potential impact is only applicable to cases where the storage system is fully discharged (which due to the converter's minimum power cannot happen solely through operation) for a prolonged time period. Considering the size of the discharge current this has also been considered negligible.
- Some exponents were limited due to initial estimation of voltages as 0. This only affected pre-calculation and not the actual results.
- Gear was set as integration method. In tests results did not change between default trapezoidal and Gear integration.

Without these measures the simulation would run into errors before finishing.

5.4 Example Case Study

To provide an example on how to use and apply the tool to a case study, the data for an arbitrary residential storage system (260–262) has been collected and inserted into the Excel file. Most of the general information is directly provided within the datasheet and product book as shown in Figure 73.

Electrical Characteristics	
Total Energy Capacity	6.5 kWh
Usable Energy Capacity[1)]	5.9 kWh
Battery Capacity	126 Ah
Voltage Range	42.0 to 58.8 V_{DC}
Nominal Voltage	51.8 V_{DC}
Max. Charge/Discharge Current	100A
Peak Current[2)]	109.5A for 3 sec.
Max. Charge/Discharge Power[3)]	4.2kW
Peak Power[2)]	4.6kW for 3 sec.
Battery Pack Round-Trip Efficiency	>95% (under specific condition)
Communication Interface	CAN 2.0B
DC Disconnect	Circuit Breaker, Contactor, Fuse

Operating Conditions	
Installation Location	Indoor / Outdoor (Stand / Wall-Mounted)
Operating Temperature	-10 to 50°C
Operating Temperature (Recommended)	15 to 30°C
Storage Temperature	-30 to 60°C : ~7 days -20 to 45°C : ~ 6 months
Humidity	5% to 95%
Altitude	Max. 2,000m
Cooling Strategy	Natural Convection

	Sunny Island 4.4M
Maximum efficiency	95.3 %
European weighted efficiency	94.0 %
Standby consumption	6.8 W
Consumption in no-load operation and in discharge mode	18.0 W

Figure 73: Datasheet data on RESU 6.5 and Sunny Island 4.4M

As battery capacity the full capacity is used as reference. Since the efficiency is quoted as >95% it likely considers degradation effects and 97% has been chosen as estimate for a starting value. As maximum current the continuous value is used. As nominal temperature the room temperature has been chosen. "Natural convection" implies no active cooling system.

The reference profile is generated based on the warranted throughput of 20 MWh and the 10 year lifespan. Although the rated current is 100 A, the datasheet explicitly states that 2.2 kW should be used for maximum battery life. This is in this case considered more realistic than applying the maximum warranted stress conditions, since those are unlikely for real world applications. The throughput is equally distributed across all days using that power.

Figure 74 displays the data implemented as well as a 48h cut of the reference profile detailed on the respective page. Using the k_{DS} estimator, three iterations determined 0.269 as approximate value.

	A	B	C
1			Value
2	Converter	Name	Sunny Island 4.4M
3		Count	1
4		Nominal Power [W]	4,400.00
5		Max. Roundtrip Efficiency	95%
6		Transformer-based?	FALSE
7		Standby consumption [W]	6.8
8		No-load consumption [W]	18
9		Cut-off	5%
10			
11	Battery	Name	LG Chem RESU 6.5
12		String count	
13		Capacity [Wh]	6,500.00
14		Nominal Voltage [V]	51.8
15		Maximum Current [A]	100
16		Roundtrip Efficiency	97%
17		Self-discharge [1/day]	0.033%
18		End-of-Life Capacity	60%
19		Nominal Ambient Temperature [C]	25
20		Active Cooling	FALSE
21		Chemistry	NMC
22		kds	

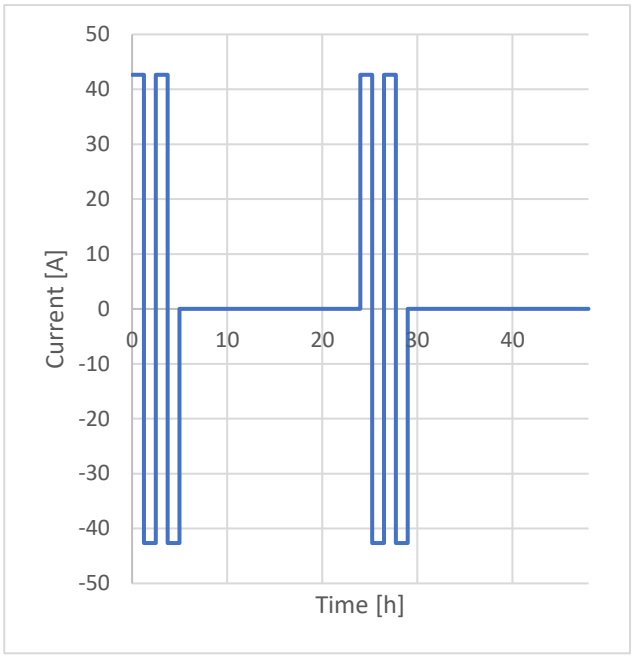

Figure 74: Residential storage system data and reference profile

Having determined the value for k_{DS} the base battery data is complete. As a simple example application, the self-consumption profile from testing series one for one year (see 3.1.2) has been scaled to the size of the storage system. Since the profile starts in winter with no use, the initial SoC has been offset to 20% to prevent self-discharge below 0. The general data for year one is shown in Figure 75.

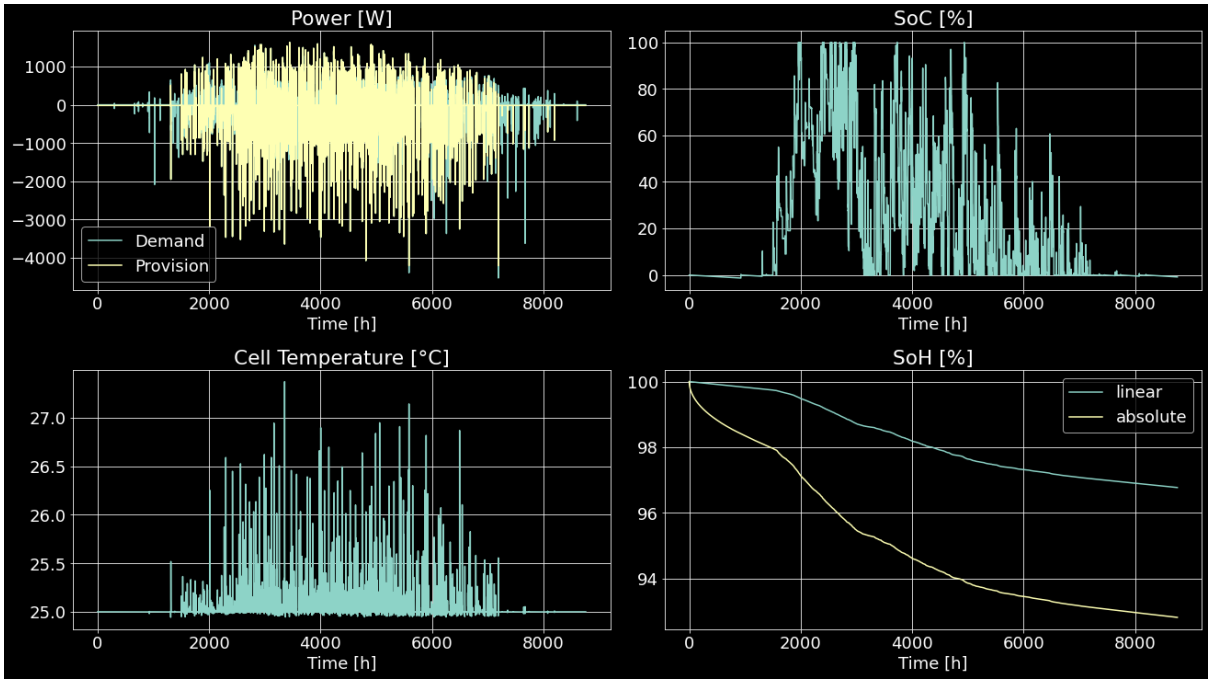

Figure 75: Example case study technical data for year one

It is apparent that the storage system is barely used during the winter months. Based on the expiration of the feed-in tariff scheme, the value generation is entirely based on electricity costs. The saved energy is the provided power integrated over time. All relevant cost/revenue data is given in Table 21.

ELEMENT	PRICE	REFERENCE
LG CHEM RESU 6.5	£3,448.23	(263)
SMA SUNNY ISLAND 4.4M	£2,198.57	(264)
ELECTRICITY	£0.172 per kWh	(265)
DISCOUNT RATE	1.5 %	(266)

Table 21: Example case study cost data

Ten years are chosen as scope for this example since it is the warranty limit. The cashflow is given in Table 22.

Year	*Energy [kWh]*	*Cashflow*	SoH_{lin}
0		-£5,646.80	100%
1	418.3993	£71.96	97%
2	417.276	£71.77	94%
3	416.3847	£71.62	90%
4	415.7196	£71.50	87%
5	414.7693	£71.34	84%
6	413.9472	£71.20	81%
7	413.141	£71.06	78%
8	412.3694	£70.93	74%

9	411.5776	£70.79	71%
10	410.8738	£70.67	68%

Table 22: Energy and Cashflow for 10-year period

The Net Present Value (NPV) for this application is -£4,989.24, resulting in an Internal Rate of Return (IRR) of -27 %. The battery degraded linearly by 32 %, while only returning 12 % of the initial investment. Thus, even if the timespan was extended the BESS would never be able to amortise.

A similar assessment has been performed on a case study for EDF Energy in submission six. The objectives of the case study were:

- Forecast of value generation
- Determination of approximate lifetime
- Determination of the amortisation period
- Determination of system weak points for amortisation and amortisation conditions

The workflow is provided in Appendix E.

5.5 Commercial Application

Due to the provision of details on all cell parameters, the tool can be used for a variety of purposes, depending on the primary point of interest of the user. However, the main purpose is the ability to judge different BESS systems, different BESS services and the overall feasibility of the BESS. The process for this evaluation is shown in Figure 76. The individual steps are discussed in the following.

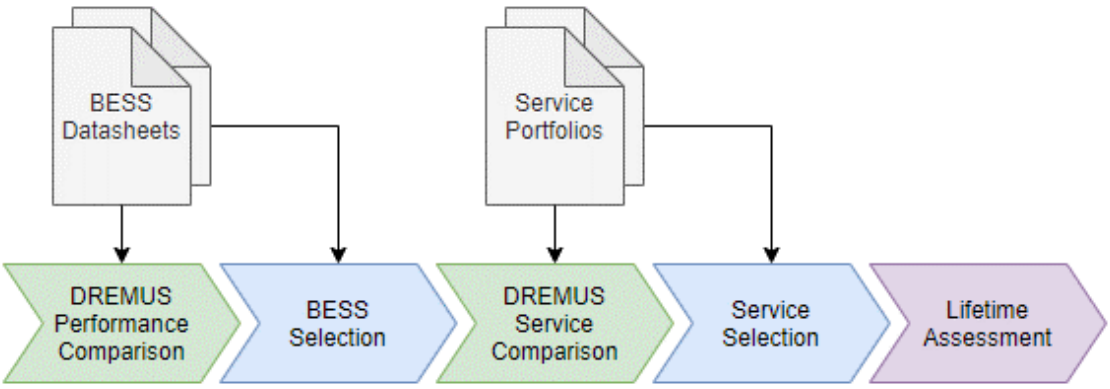

Figure 76: BESS Project Planning and Evaluation Process with DREMUS

BESS Evaluation

To select the best BESS for an application requires a thorough comparison of all options. In most cases, price and long-term performance are the most important factors. Comparing the

long term performance is most difficult, since different systems quote different time frames and utilisation conditions for their degradation.

The factor k_{DS} offers the advantage of comparing these specifications against each other in the context of the specific BESS. A lower value results in a lower degradation speed and thus longer life under the same utilisation. If the remaining capacity has a significant impact on the long term value of the system k_{DS80} can be chosen as reference instead.

Although not compared, k_{DS} has been determined in submission six for two storage systems. In both cases the values were much lower than 1, meaning they outperform the tested cells significantly.

BESS Service Evaluation

Battery services are, as established in 2.2.5, complex to compare due to their differences in utilisation and contract period. For the application of DREMUS a utilisation profile for each service must be predetermined and (due to calendric ageing aspects) must cover the same time period.

The linear degradation is the best indicator to establish the impact of each service. Using additionally the monetary value each service generates in that time period, a more relative term of value generation can be determined:

$$\frac{Value}{Deg_{lin}} = Degradation\ Value \tag{86}$$

The degradation value not only describes how much value the system generates per lost linear health but also provides an indication on the total unadjusted value generated by a BESS dedicated solely to that service.

In the case study the degradation value of the dedicated service would have amounted to approximately five times the capital expenses. However, this does not take into account any of the components and aspects of the BESS that must be included in the lifetime assessment.

Lifetime Assessment

To perform a lifetime assessment of the BESS, which is essential for the overall economic evaluation, it is necessary to put the investment costs against the expected value generation of the system. However, several additional aspects need to be taken into account:

- Prediction reliability: The assessment relies on a stable and/or predictable source of value for the BESS over its lifetime. As pointed out in 2.4, these circumstances can change quickly and are market dependent. An overhead should be considered to include value loss.

- Discount rates: Since the BESS is a long term investment, more stable investment alternatives need to be taken into account for the evaluation. This can be done through the inclusion of discount rates for the determination of the net present value, or alternatively through the comparison of the internal rate of return.
- Surrounding system: Although being the most crucial asset and being the only one majorly affected by the changes in provided services, the battery itself is not the only cost factor to be taken into account. Surrounding electronics such as the converter have a limited lifespan as well. Further additional running costs such as maintenance and operation will have an effect as well.

In the case study the last point in particular had a crucial impact. While the BESS was predicted to have a very long lifespan it was unreasonable to assume that the remaining system would reach similar lifetimes. This overall extended the required amortisation period significantly.

Overall DREMUS provides a tool for the analysis of BESS and the short- and long-term estimation of its value. It should, however, only be used in the context of a realistic and wholistic assessment.

6 Project and Outcome Evaluation

This section serves as overall conclusion for both this report and the project. In the first part the project objectives and targets as well as the overall progression are evaluated. Then an overview on the learning achieved in this project is provided. The third part describes the perspectives for future work, potentially extending the insights and results achieved. Finally the prospects of this project on a macroscopic scale conclude this report.

6.1 Project Conclusion

The outlined project objectives in 1.2 have been addressed in this report as follows:

- Chapter 2.2 investigated the individual perspectives of the primary stakeholders in stationary energy storage systems. From these perspectives power- and energy-oriented value streams for BESS have been identified. Most of these value streams are of partial or full commercial interest to EDF.
- Chapter 2.3 compared the available UK energy storage technologies regarding their ability to provide the outlined value streams based on costs, space, ramping and efficiency requirements. Battery storage, and specifically Li-Ion has been identified as the most capable storage system for this purpose. As operator of existing Li-Ion BESS this technology was of primary interest to EDF as well.
- In chapter 2.5 the physicochemical mechanisms of Li-Ion cells have been discussed as part of the investigation into battery modelling. This investigation provided an overview on the state of the art of BESS modelling and identified that the current modelling approaches lack detail and/or flexibility and adaptability. It further provided the foundation for the development of a BESS model fulfilling those requirements.
- Section 3 and 3.3 in particular described the battery cell tests performed to confirm and identify the in literature displayed battery cell behaviour. Although valuable data has been provided on the electrical and thermal behaviour, no reliable ageing data for the model development could be generated, due to excessive acceleration of ageing processes using elevated temperature.
- Section 4 described the development and reasoning of a universally applicable and adaptable BESS model based on externally and internally generated experimental data, literature and the expected known variables on a BESS.
- In section 5 a Python tool has been developed based on the model. The tool has been designed to be flexibly applied to any storage system and any use case and to fit the requirements and preferences of the EDF Energy R&D UK centre.
- In chapter 5.5 the commercial application of the tool is discussed and the case study performed in submission six is referenced. The analysis of the case study provided an

improvement of the value forecast and statements regarding amortisation and lifetime value of the storage project. The benefit to EDF has been proven by improving value projection accuracy by 4 % and identifying amortisation projection and risk.

With the development of DREMUS, the target of developing a universally applicable BESS model has been accomplished. Using this tool, BESS solutions can be directly compared against each other regarding long term performance. Further, the value streams generated by BESS can be optimised and the overall lifetime assessment can be reliably performed. The key advantage of this tool is that it provides the best possible approximation of the BESS based on the manufacturer data.

It should be pointed out that with the tool provided the initial purpose of assessing the techno-economic feasibility of micro-generation co-located battery storage can still be fulfilled.

6.2 Learning and Contribution

There are several insights gained from this project. The biggest and main insight is the core methodology of abstracting a BESS from the generally available information on the system given by the manufacturer. This was previously not sufficiently investigated and will help both EDF and other third parties to improve the approach of BESS modelling. The modelling approach has been peer-reviewed and accepted by the “Journal of Energy Storage”.

In connection to this, it has been shown that the electrical parameters τ and $\frac{R_1}{R_0}$ may vary over lifetime and between cells, but are generally very stable within a similar range. Although this should ideally be confirmed through more cell tests, this allows for an acceptable approximation of cell properties even without detailed knowledge on the cell.

Experimentally a thermal dissipation model for a pouch cell module has been generated. This is considered an improvement over a single cell thermal model due to the common structure of a BESS. It can be referenced directly or potentially be integrated in a larger thermal model if the data is given.

Another particular contribution to be pointed out is the ageing model, which is unique in the fact that it is:

- Based on the chemical first-principles of SEI formation
- Fitted by experimental data to reflect the sensitivities of real cells
- Split into an absolute and a linear component allowing direct degradation comparison of operation and
- Adjustable to the specific degradation speed of a storage system based on its datasheet.

No existing ageing model has been identified fulfilling all four of these requirements.

Further insight gained is the data on the capacitive utilisation of Li-Ion cells. A new frequency measure, the CDTF, has been introduced that allows to distinguish electrical and chemical utilisation of the battery cell. Although the implications for battery degradation must be investigated further, it has been shown that specifically for power-oriented applications BESS operation may partially be driven by the capacitive, and not the chemical capabilities of the cells. The dependency of those properties on current amplitude, SoC, configuration and degradation has also been shown. The results from this investigation have been peer-reviewed and published in the “Journal of Energy Storage”.

6.3 Limitations and Recommendations for Future Work

There are several aspects of this model that can be improved upon through additional data and research. Firstly, additional data on cell, battery or converter behaviour can improve and validate the presented model. It is designed with future modification in mind and can be improved through any additional data given on the storage system.

A crucial part to mention would be multi-cell modelling. There are technical restrictions in the current modelling approach that make multi-cell modelling impossible. However, parallel computation, e.g. using a graphics card and a different tool could enable this. This would further require a more detailed investigation into cell-to-cell variability regarding electrical, thermal and degradation behaviour.

Further improvements can be made through a more widespread experimental confirmation of the relative parameters determined for the electrical model. Relative parameters are a key method of estimating the behaviour of an arbitrary Li-Ion cell and thus essential for a modelling approach like the one presented.

The impact of the capacitive utilisation of Li-Ion cells on the degradation may potentially play an important role in the ageing estimation, particularly when focussing on SEI formation. This will require several further tests ideally with different cell types and with pulses at adjusted frequencies. This may also affect the necessary resolution of cycling data and thus the computation time of the model.

Overall this model was constructed based on the principles of converter and battery behaviour and data obtained from individual cells. Ideally this model should also be validated for a full BESS by comparing the predicted performance from the datasheet to the actual performance change over time under the exact conditions.

While this is not the primary function of the model, after installation of a BESS it would also be possible to dynamically adapt the model to the use case through comparison between prediction and measured behaviour. This should ideally be compared again to existing models based on this principle.

The current ageing model is based on carbon-based Li-Ion cells. However, as long as the parameters don't change it can be replaced in the tool through any other ageing model and can potentially be extended towards other battery technologies. Associated changes to the electrical and thermal components must then be considered as well.

When trying to improve on the given modelling approach, it is necessary to consider the primary given limitation of data availability. Any degree of precision that is added may increase the assumptions necessary for a reliable approximation and must therefore be confirmed for all considered technologies. The assumptions made in this project were only accepted if they were either necessary or considered reliable based on data from experiments and/or literature.

6.4 Prospects and Outlook

The primary outcome of this project, the Li-Ion DREMUS model and tool, has promising outcomes for a wide variety of stakeholders. Primarily this is of interest to EDF from a commercial perspective. Angeliki Loukatou, research engineer at the EDF Energy R&D UK centre has already confirmed that the tool will be integrated into an existing battery storage optimisation tool for case studies such as optimal valuation of energy storage assets co-located with renewable energy sources. She also confirmed that the tool will be useful to mitigate the frequent lack of available battery data from manufacturers and will support the assessment of storage installations planned within the next 15-20 years.

Outside of EDF the model can be used by any other potential investor in BESS to make the same assessment. This way, BESS can be used more economically. Only using the general behaviour outlined in the degradation formula it would also be possible to optimise the utilisation for an extension of life of BESS. This would make them more sustainable.

Since DREMUS increases the tangibility of BESS this may lead to higher and widespread implementation of battery storage, which in turn also increases the general flexibility of the GB power grid or other regions where increasing investment in renewable energy requires the replacement of large generator inertia.

In a contrary perspective, being able to accurately assess the value of battery storage allows for the determination of the overall most economical solution for the assurance of grid stability. Where battery storage provides a necessity to the grid but has been proven to be financially

disadvantageous to investors, the investment needs to be incentivised or the service remuneration needs to be increased appropriately.

Appendix A

Reference	ID	Types
(164)	Ecker	NMC
(185)	Omar	LFP
(174)	Muenze	N/A
(110)	Abdul	N/A
(166)	Wang	LFP
(167)	Han	LFP, LMO
(168)	Lee	NMC
(169)	Groot	LFP
(170)	Forma	LFP
(171)	Forte	LFP, LCO

Reference	ID	Types
(161)	Groll	LFP
(172)	Su	NMC
(157)	Stroe1	LFP
(158)	Stroe2	LFP
(175)	Li1/2	LFP
(159)	Schma	NMC
(151)	Xu	LMO
(163)	Farzi	N/A
(173)	Hoog	NMC
(133)	Redon	NMC

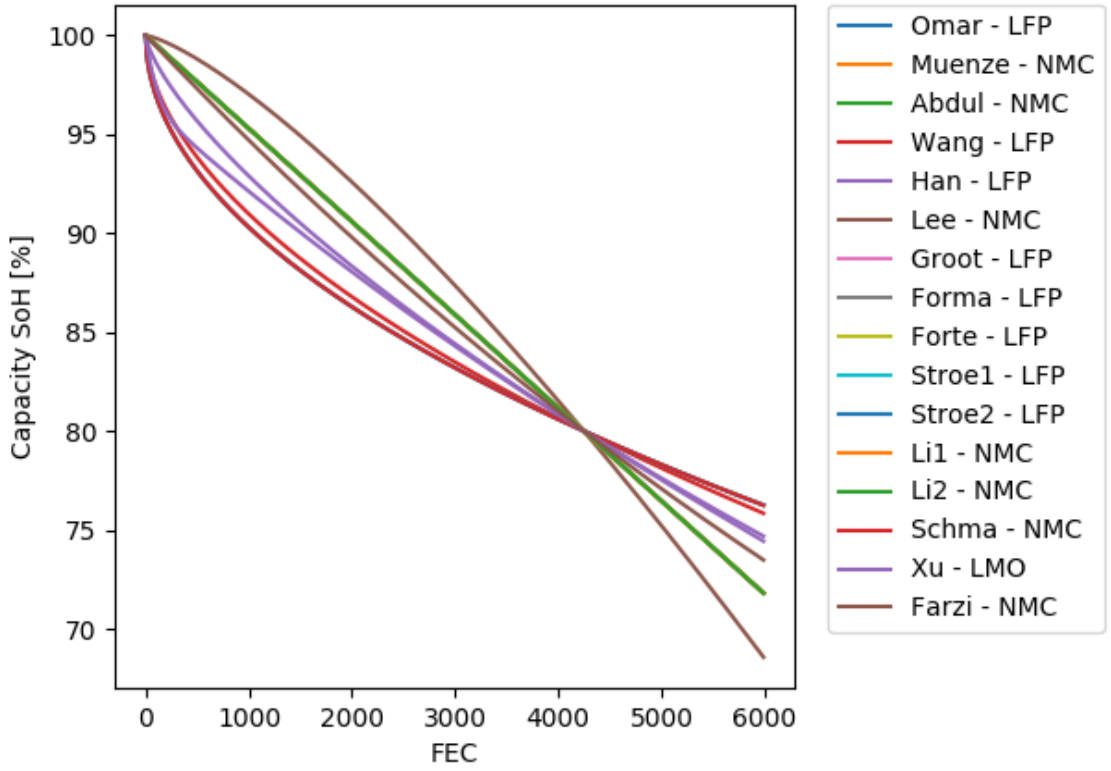

Figure 77: Adjusted FEC dependency of the ageing models

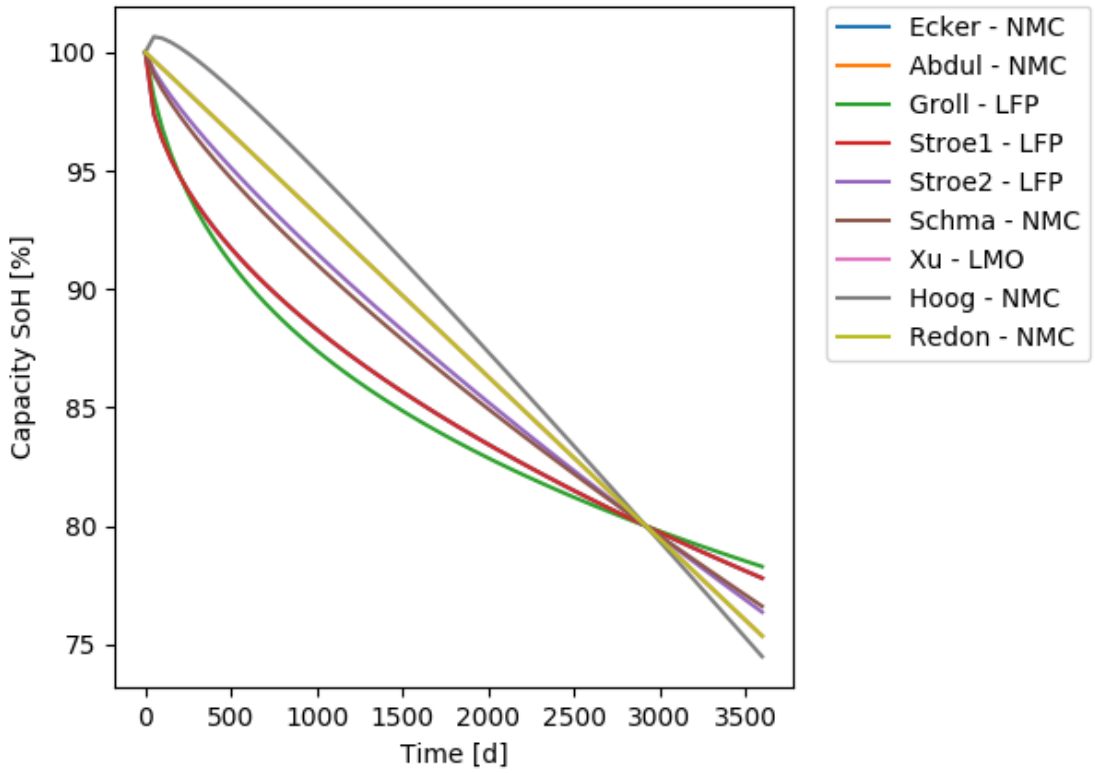

Figure 78: Time dependency of the ageing models

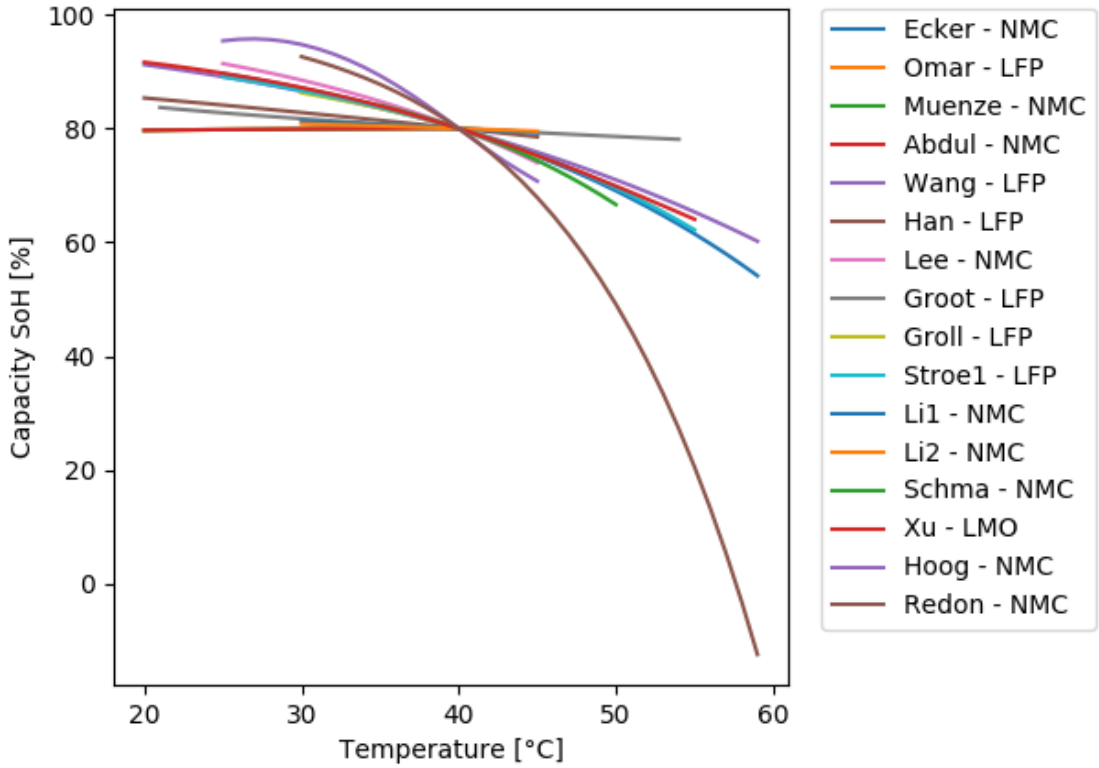

Figure 79: Temperature dependency of the ageing models

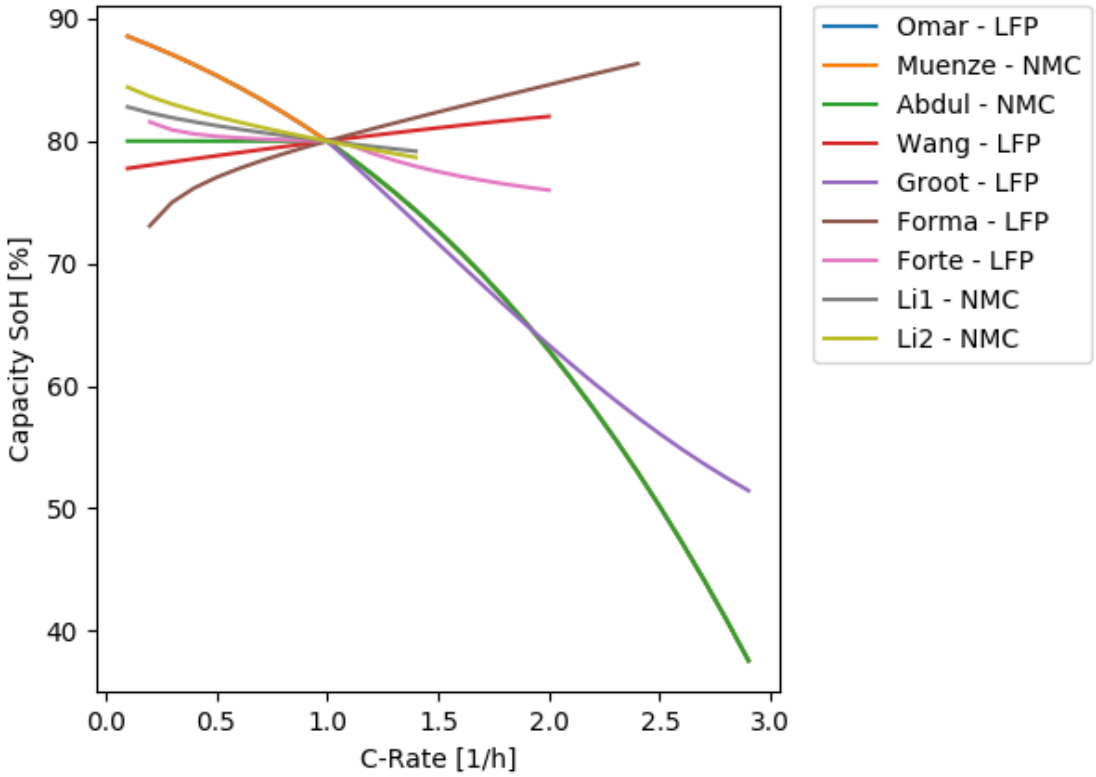

Figure 80: C-Rate dependency of the ageing models

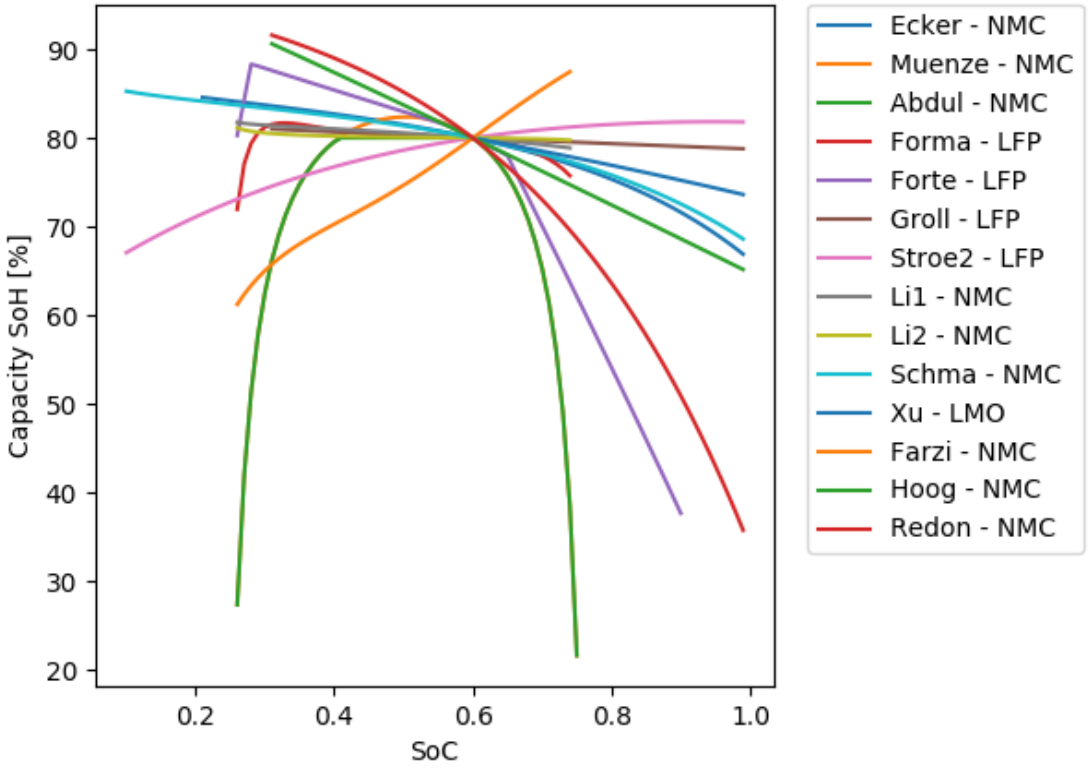

Figure 81: SoC dependency of the ageing models

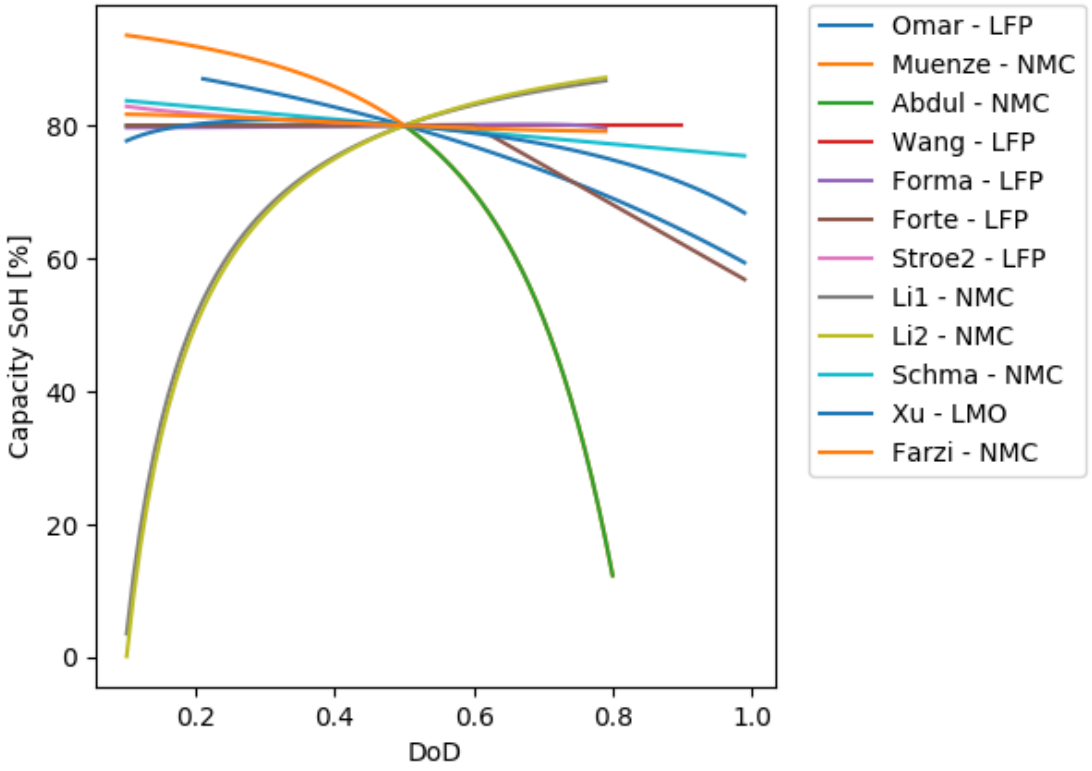

Figure 82: DoD dependency of the ageing models

Appendix B

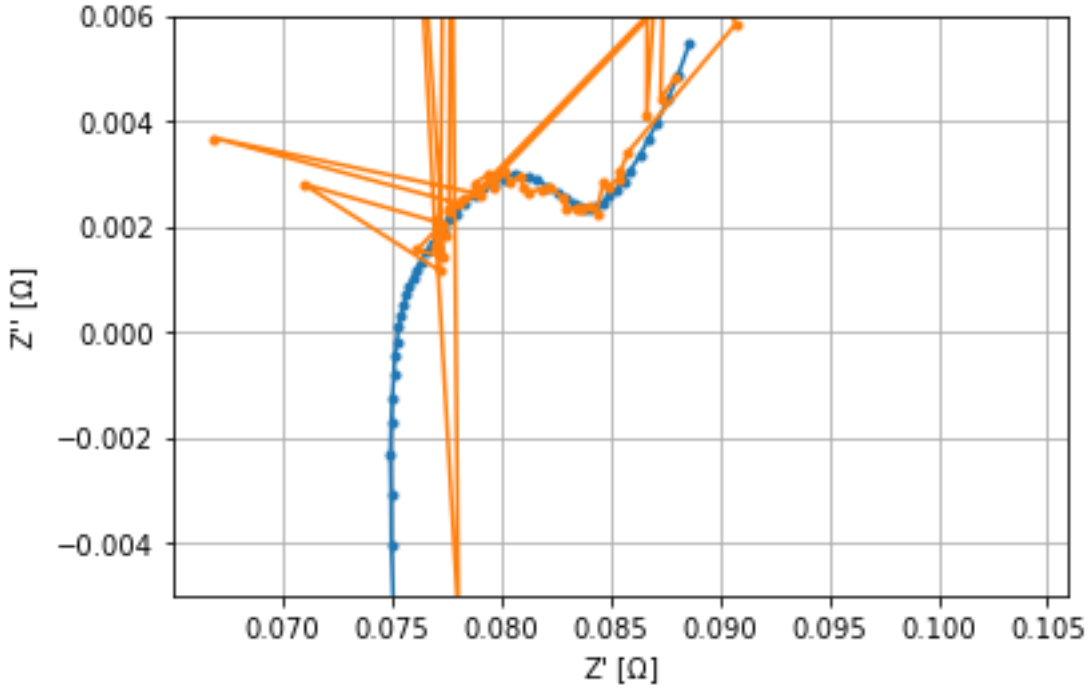

Figure 83: Solartron auto- (blue) vs manual (orange) Lissajous analysis of a Nickel-Metal-Hydride cell

Appendix C

Identified Hazards

Hazard 1:	Short-circuiting of pouch cells during connection or reference electrode insertion.
Existing control measures:	Insulated tools, PPE, safety induction, insertion by experienced staff member, glovebox
Additional control measures required:	Handling with care, marking of contacts, securing environment, second party check, following handling instructions
By whom and when:	Martin Rogall, Tazdin Amietszajew, 01/05/2018

Evaluation of risk:
Severity of injury: Major Likelihood: Possible Risk factor: Moderate

Hazard 2:	Mechanical damaging of cells during transport, dismantling or testing
Existing control measures:	Handling with care, Insulated tools, PPE, following handling instructions, safety induction
Additional control measures required:	Use of trolleys and elevators for transport, second party check, avoidance of instability hazards in the environment
By whom and when:	Martin Rogall, 01/05/2018

Evaluation of risk:
Severity of injury: Major Likelihood: Possible Risk factor: Moderate

Hazard 3:	Spontaneous thermal runaway
Existing control measures:	Protective gear
Additional control measures required:	Respectful handling and storage of cells, thermal monitoring
By whom and when:	Martin Rogall, 01/05/2018

Evaluation of risk:
Severity of injury: Major Likelihood: Unlikely Risk factor: Low

Hazard 4:	Cell stress due to over-charge, over-heating , fast charging, reverse polarity input, false temperature input, malfunction
Existing control measures:	Profile application analysis, setting of limits and stop conditions, following handling instructions
Additional control measures required:	Initial supervision, thermal monitoring, equipment assessment and control
By whom and when:	Martin Rogall, 01/05/2018

Evaluation of risk:
Severity of injury: Serious Likelihood: Unlikely Risk factor: Low

Hazard 7:	Injury due to laboratory conditions
Existing control measures:	PPE in lab, safety induction
Additional control measures required:	Following handling instructions
By whom and when:	Martin Rogall, 01/05/2018

Evaluation of risk:
Severity of injury: Serious Likelihood: Possible Risk factor: Low

Hazard 8:	Chain reaction in-between cells or other objects in vicinity
Existing control measures:	PPE in lab, safety induction
Additional control measures required:	Separation of cells from any potential chain causes
By whom and when:	Martin Rogall, 01/05/2018

Evaluation of risk:
Severity of injury: Major Likelihood: Unlikely Risk factor: Low

Hazard 5:	Slips, trips and falls
Existing control measures:	Inspection and clearing of environment from any hazards, awareness, safety induction
Additional control measures required:	Signage for high risk areas
By whom and when:	Martin Rogall, 01/05/2018

Evaluation of risk:
Severity of injury: Serious Likelihood: Unlikely Risk factor: Low

Hazard 6:	Third party interference with testing process or cell storage
Existing control measures:	Storing and testing of cells only in designated areas, safety induction
Additional control measures required:	Signage
By whom and when:	Martin Rogall, 01/05/2018

Evaluation of risk:
Severity of injury: Serious Likelihood: Possible Risk factor: Low

Hazard 9:	Cell fuming
Existing control measures:	Area ventilation
Additional control measures required:	
By whom and when:	Martin Rogall, 01/05/2018

Evaluation of risk:
Severity of injury: Serious Likelihood: Unlikely Risk factor: Low

Hazard 10:	Electrolyte leakage during reference electrode insertion
Existing control measures:	PPE, safety induction, insertion by experienced staff member, glovebox
Additional control measures required:	
By whom and when:	Tazdin Amietszajew, 01/05/2018

Evaluation of risk:
Severity of injury: Superficial Likelihood: Unlikely Risk factor: Very low

Appendix D

This appendix outlines the 28 day cycling programs used in the experiment outlined in chapter 3.3. They have been applied using a Digatron battery cycler and are processed sequentially. Each step is executed until the limit conditions are met. The relevant operator types are as follows:

- SET: Setting conditions and variables.
- PAU: Time-limited pause step.
- CHA: Charge step.
- DCH: Discharge step.
- TABLE: Execution of profiles provided in text format. The tables themselves can for reasons of confidentiality not be provided.
- BEG: Start of a profile to be cycled.
- CYC: Cycle previous defined profile given number of times.
- STO: Completion of test.

Calculation | Save & End | Save | Save as... | Skip step | Cancel | Show main progr.

Step	Label	Operator	Nominal Value	Limit	Action	Registration
1		SET				STANDARD
2		SET		> 4.7 V < 2 V > 70 C	INT INT INT	
3		TASK	0 SafeTask			
4		TASK	1 OUW			
5		PAU		10 sec		1 sec
6		TABLE	ARB6			10 sec
7		CHA	33 A 4.15 V	< 3.3 A		1 sec
8		PAU		1 h		1 sec
9		DCH	33 A 2.5 V	< 3.3 A		1 sec
10		PAU		1 h		1 sec
11		SET	Ah = 0			
12		CHA	33 A 4.15 V	> 33 Ah		1 sec
13		STO				

Figure 84: Cycling Programme for ARB

Calculation | Save & End | Save | Save as... | Skip step | Cancel | Show main progr.

Step	Label	Operator	Nominal Value	Limit	Action	Registration
1		SET				STANDARD
2		SET		> 4.4 V < 2 V > 70 C	INT INT INT	
3		TASK	0 SafeTask			
4		TASK	1 OUW			
5		PAU		10 sec		1 sec
6		BEG				
7		SET	Timer1 = 24 h			
8		PAU		Timer1		10 sec
9		CYC	19 *			
10		CHA	33 A 4.15 V	< 3.3 A		1 sec
11		PAU		1 h		1 sec
12		DCH	33 A 2.5 V	< 3.3 A		1 sec
13		PAU		1 h		1 sec
14		SET	Ah = 0			
15		CHA	33 A 4.15 V	> 33 Ah		1 sec
16		STO				

Figure 85: Cycling Programme for CAL

Calculation | Save & End | Save | Save as... | Skip step | Cancel | Show main progr.

Step	Label	Operator	Nominal Value	Limit	Action	Registration
1		SET				STANDARD
2		SET		> 4.7 V < 2 V > 70 C	INT INT INT	
3		TASK	0 SafeTask			
4		TASK	1 OUW			
5		PAU		10 sec		1 sec
6		TABLE	EFR61			10 sec
7		TABLE	EFR62			10 sec
8		TABLE	EFR63			10 sec
9		TABLE	EFR64			10 sec
10		TABLE	EFR65			10 sec
11		CHA	33 A 4.15 V	< 3.3 A		1 sec
12		PAU		1 h		1 sec
13		DCH	33 A 2.5 V	< 3.3 A		1 sec
14		PAU		1 h		1 sec
15		SET	Ah = 0			
16		CHA	33 A 4.15 V	> 33 Ah		1 sec
17		STO				

Figure 86: Cycling Programme for EFR

Calculation | Save & End | Save | Save as... | Skip step | Cancel | Show main progr.

	Step	Label	Operator	Nominal Value	Limit	Action	Registration
	1		SET				STANDARD
	2		SET		> 4.4 V < 2 V > 70 C	INT INT INT	
	3		TASK	0 SafeTask			
	4		TASK	1 OUW			
	5		PAU		10 sec		1 sec
	6		BEG	outer			
	7		SET	Timer1 = 24 h			
	8		BEG	inner			
	9		CHA	33 A 4.15 V	 1 sec		10 sec
	10		DCH	33 A 2.5 V	 1 sec		10 sec
	11		CYC	14400 *			
	12		PAU		Timer1		10 sec
	13		CYC	19 *			
	14		CHA	33 A 4.15 V	< 3.3 A		1 sec
	15		PAU		1 h		1 sec
	16		DCH	33 A 2.5 V	< 3.3 A		1 sec
	17		PAU		1 h		1 sec
	18		SET	Ah = 0			
	19		CHA	33 A 4.15 V	> 33 Ah		1 sec
	20		STO				

Figure 87: Cycling Programme for MCY

Calculation | Save & End | Save | Save as... | Skip step | Cancel | Show main progr.

	Step	Label	Operator	Nominal Value	Limit	Action	Registration
	2		SET		> 4.4 V < 2 V > 70 C	INT INT INT	
	3		TASK	0 SafeTask			
	4		TASK	1 OUW			
	5		PAU		10 sec		1 sec
	6		BEG				
	7		SET	Timer1 = 24 h			
	8		CHA	33 A 4.15 V	< 3.3 A		10 sec
	9		PAU		1 h		10 sec
	10		DCH	33 A 2.5 V	< 3.3 A		10 sec
	11		PAU		1 h		10 sec
	12		CHA	33 A 4.15 V	< 3.3 A		10 sec
	13		PAU		1 h		10 sec
	14		DCH	33 A 2.5 V	< 3.3 A		10 sec
	15		PAU		1 h		10 sec
	16		SET	Ah = 0			
	17		CHA	33 A 4.15 V	> 33 Ah		10 sec
	18		PAU		Timer1		10 sec
	19		CYC	19 *			
	20		CHA	33 A 4.15 V	< 3.3 A		1 sec
	21		PAU		1 h		1 sec
	22		DCH	33 A 2.5 V	< 3.3 A		1 sec
	23		PAU		1 h		1 sec
	24		SET	Ah = 0			
	25		CHA	33 A	> 33 Ah		1 sec

Figure 88: Cycling Programme for FCY

Appendix E

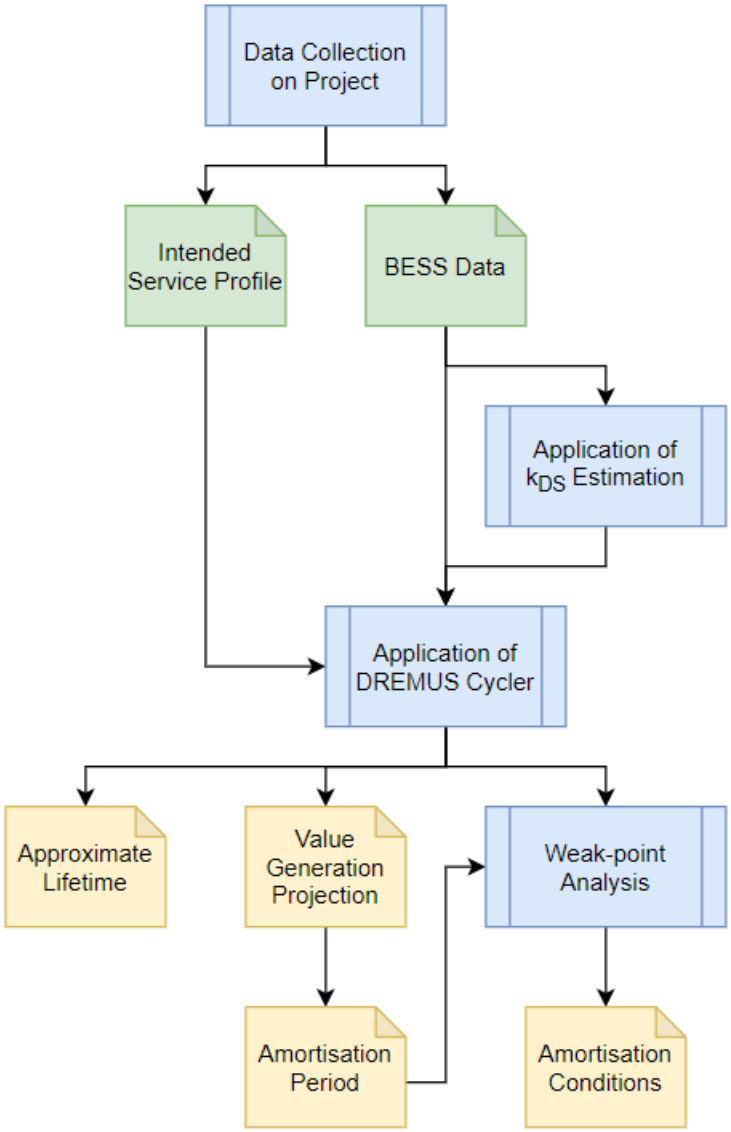

Figure 89: BESS Case Study Workflow (blue: process; green: input files; yellow: outputs)

References

1. ROGALL, Martin, AMIETSZAJEW, Tazdin, BHAGAT, Rohit, BRUCOLI, Maria and GREENWOOD, David. On the utilisation of the pseudo-capacitive capabilities of Li-ion cells for the provision of frequency response services. *Journal of Energy Storage* [online]. 2019. Vol. 22, no. February, p. 311–317. DOI 10.1016/j.est.2019.02.028. Available from: https://doi.org/10.1016/j.est.2019.02.028

2. CERAOLO, M., LUTZEMBERGER, G. and POLI, D. Aging evaluation of high power lithium cells subjected to micro-cycles. *Journal of Energy Storage* [online]. 2016. Vol. 6, p. 116–124. DOI 10.1016/j.est.2016.03.006. Available from: http://dx.doi.org/10.1016/j.est.2016.03.006

3. ROGALL, Martin, BARAI, Anup, BRUCOLI, Maria, LUK, Patrick, BHAGAT, Rohit and GREENWOOD, David. DREMUS : A Data-Restricted Multi-Physics Simulation Model for Lithium-Ion Battery Storage. *Journal of Energy Storage* [online]. DOI 10.1016/j.est.2020.102051. Available from: https://doi.org/10.1016/j.est.2020.102051

4. THE SWITCH. Electricity Distribution Networks. [online]. 2016. [Accessed 7 November 2016]. Available from: http://theswitch.co.uk/electricity-distribution

5. THE SWITCH. Electricity Transmission Networks. [online]. 2016. [Accessed 7 November 2016]. Available from: http://theswitch.co.uk/electricity-transmission

6. BUTLER, Scott. UK Electricity Networks. [online]. 2001. [Accessed 14 May 2021]. Available from: http://www.parliament.uk/documents/post/e5.pdf

7. NATIONAL GRID. Separating the Electricity System Operator (ESO) from Electricity Transmission (ET). [online]. 2019. [Accessed 14 August 2020]. Available from: https://www.nationalgrid.com/uk/electricity-transmission/about-us/we-are-changing/separating-electricity-system-operator-electricity-transmission

8. OFGEM. *Electricity Interconnectors* [online]. 2017. [Accessed 21 March 2017]. Available from: https://www.ofgem.gov.uk/electricity/transmission-networks/electricity-interconnectors

9. LETCHER, Trevor M. *Storing Energy: with Special Reference to Renewable Energy Sources* [online]. Elsevier, 2016. ISBN 9780128034408. Available from: http://store.elsevier.com/Storing-Energy/Trevor-Letcher/isbn-9780128034408/

10. DEPARTMENT FOR BUSINESS ENERGY & INDUSTRIAL STRATEGY. *UK National Energy and Climate Plan (NECP)* [online]. 2019. [Accessed 12 August 2020]. Available from: https://assets.publishing.service.gov.uk/government/uploads/system/uploads/attachment_data/file/774235/national_energy_and_climate_plan.pdf

11. DEPARTMENT FOR BUSINESS ENERGY & INDUSTRIAL STRATEGY. *DIGEST OF UNITED KINGDOM ENERGY STATISTICS 2020* [online]. 2020. [Accessed 13 August 2020]. Available from: www.gov.uk/government/organisations/department-for-business-energy-and-

12. NATIONAL GRID ESO. *Future Energy Scenarios* [online]. 2020. Available from: https://www.nationalgrideso.com/document/173821/download

13. MILLER, N W, CLARK, K and SHAO, M. Frequency responsive wind plant controls: Impacts on grid performance. In : *2011 IEEE Power and Energy Society General Meeting*. IEEE, 2011. p. 1–8.

14. THE FARADAY INSTITUTION. The Faraday Institution announces a further £55 million for energy storage research – The Faraday Institution. [online]. 2019. [Accessed 18 November 2020]. Available from: https://faraday.ac.uk/sept-2019-project-announcement/

15. ENGINEERING AND PHYSICAL SCIENCES RESEARCH COUNCIL. ISCF Faraday Challenge - Batteries for Britain - EPSRC website. [online]. 2017. [Accessed 13 August 2020]. Available from: https://epsrc.ukri.org/funding/calls/iscffaradaychallengebatteries/

16. THE FARADAY INSTITUTION. What is the Faraday Battery Challenge? – The Faraday Institution. [online]. 2020. [Accessed 5 November 2020]. Available from: https://faraday.ac.uk/post-with-video/

17. WORLD NUCLEAR ASSOCIATION. COVID-19 Coronavirus and Nuclear Energy - World Nuclear Association. [online]. 2020. [Accessed 18 August 2020]. Available from: https://www.world-nuclear.org/information-library/current-and-future-generation/covid-19-coronavirus-and-nuclear-energy.aspx

18. NATIONAL GRID. Enhanced Frequency Response. [online]. 2016. [Accessed 14 May 2021]. Available from: http://www2.nationalgrid.com/WorkArea/DownloadAsset.aspx?id=8589935616

19. ELEXON. Trading & Settlement. [online]. 2017. [Accessed 2 May 2017]. Available

from: https://www.elexon.co.uk/reference/technical-operations/trading-settlement/

20. ELEXON. Imbalance Pricing Guidance. [online]. 2013. [Accessed 14 May 2021]. Available from: https://www.elexon.co.uk/wp-content/uploads/2016/10/Imbalance_Pricing_guidance_v11.0.pdf

21. ELEXON. The Electricity Trading Arrangements. *Guidance paper* [online]. 2015. [Accessed 14 May 2021]. Available from: https://www.elexon.co.uk/wp-content/uploads/2015/10/beginners_guide_to_trading_arrangements_v5.0.pdf

22. ELEXON. Balancing Mechanism Units (BM Units). [online]. 2016. [Accessed 14 May 2021]. Available from: https://www.elexon.co.uk/wp-content/uploads/2016/09/bm_units_guidance_v5.0.pdf

23. ELEXON. What are bids and offers? [online]. 2020. [Accessed 17 August 2020]. Available from: https://www.elexon.co.uk/knowledgebase/what-are-bids-and-offers/

24. NATIONAL GRID. *Mandatory Frequency Response* [online]. 2017. [Accessed 30 January 2017]. Available from: http://www2.nationalgrid.com/uk/services/balancing-services/frequency-response/mandatory-frequency-response/

25. NATIONAL GRID. Firm Frequency Response (FFR). [online]. 2017. [Accessed 14 May 2021]. Available from: https://www.nationalgrid.com/sites/default/files/documents/Firm Frequency Response 1.1.pdf

26. NATIONAL GRID. Enhanced Frequency Response: Invitation to tender for pre-qualified parties. [online]. 2016. [Accessed 14 May 2021]. Available from: http://www2.nationalgrid.com/WorkArea/DownloadAsset.aspx?id=8589935616

27. NATIONAL GRID. Short Term Operating Reserve (STOR). [online]. 2013. [Accessed 14 May 2021]. Available from: http://www2.nationalgrid.com/uk/services/balancing-services/reserve-services/short-term-operating-reserve/

28. NATIONAL GRID. Fast Reserve Service Description. [online]. 2013. [Accessed 14 May 2021]. Available from: http://www2.nationalgrid.com/WorkArea/DownloadAsset.aspx?id=11757

29. NATIONAL GRID ESO. List of all balancing services. [online]. [Accessed 17 August 2020]. Available from:

https://www.nationalgrideso.com/balancing-services/list-all-balancing-services

30. ENERGY NETWORKS ASSOCIATION. *Good Practice Guide Active Network Management*. 2015.

31. ENERGY UK. Electricity Market Reform. [online]. 2017. [Accessed 27 March 2017]. Available from: http://www.energy-uk.org.uk/policy/electricity-market-reform.html

32. ENGIE. Understanding the Capacity Market. [online]. 2016. [Accessed 14 May 2021]. Available from: http://business.engie.co.uk/wp-content/uploads/2016/07/capacitymarketguide.pdf

33. NATIONAL GRID. Capacity Market User Support Guide. [online]. 2014. [Accessed 14 May 2021]. Available from: https://www.energy-uk.org.uk/files/docs/Policies/Capacity Market/capacity_market_user_support_guide.pdf

34. JENKINS, Nick, EKANAYAKE, Janaka and STRBAC, Goran. *Distributed Generation*. The Institution of Engineering and Technology, 2010. ISBN 978-1-84919-116-6.

35. NATIONAL GRID ESO. *Response and Reserve Roadmap* [online]. 2019. [Accessed 17 August 2020]. Available from: https://www.nationalgrideso.com/about-us/business-planning-riio/forward-plans-2021

36. NATIONAL GRID ESO. Electricity Ten Year Statement. [online]. 2019. [Accessed 17 August 2020]. Available from: https://www.nationalgrideso.com/document/157451/download

37. OFGEM. Understanding the profits of the large energy suppliers. [online]. 2016. [Accessed 14 February 2017]. Available from: https://www.ofgem.gov.uk/gas/retail-market/retail-market-monitoring/understanding-profits-large-energy-suppliers

38. USWITCH LIMITED. Energy bills explained. [online]. 2017. [Accessed 14 February 2017]. Available from: https://www.uswitch.com/gas-electricity/guides/energy-bills/#step11

39. USWITCH LIMITED. What is Economy 7 meter and how does the tariff work? [online]. 2017. [Accessed 14 February 2017]. Available from: https://www.uswitch.com/gas-electricity/guides/economy-7/

40. DECC and UK DEPARTMENT OF ENERGY AND CLIMATE CHANGE. *Smart Metering Implementation Programme* [online]. 2013. Available from: https://www.gov.uk/government/publications/smart-metering-summary-planFrom

Duplicate 1 (Smart Metering Implementation Programme - UK Department of Energy and Climate Change)NULL

41. OCTOPUS ENERGY. Agile Octopus. [online]. [Accessed 18 August 2020]. Available from: https://octopus.energy/agile/?gclid=EAIaIQobChMIouX4roil6wIVchh9Ch0ueQVpEAAYASAAEgLX2vD_BwE#

42. NATIONAL GRID. Transmission Network Use of System Charges. [online]. 2017. [Accessed 24 February 2017]. Available from: http://www2.nationalgrid.com/UK/Industry-information/System-charges/Electricity-transmission/Transmission-network-use-of-system-charges/

43. NATIONAL GRID. *Connection and Use of System Code* [online]. 2015. [Accessed 9 February 2017]. Available from: http://www2.nationalgrid.com/The-CUSC/The-Connection-and-Use-of-System-Code/Complete-CUSC---14-March-2017/

44. EA TECHNOLOGY. *A Good Practice Guide on Electrical Energy Storage*. EA Technology, 2014. ISBN 9781874290209.

45. AKHIL, Abbas A, HUFF, Georgianne, CURRIER, Aileen B, KAUN, Benjamin C, RASTLER, Dan M, CHEN, Stella Bingqing, COTTER, Andrew L, BRADSHAW, Dale T and GAUNTLETT, William D. DOE / EPRI 2013 Electricity Storage Handbook in Collaboration with NRECA. [online]. 2013. [Accessed 14 May 2021]. Available from: http://www.sandia.gov/ess/publications/SAND2013-5131.pdf

46. ELEXON. Embedded Generation. [online]. 2016. [Accessed 14 May 2021]. Available from: https://www.elexon.co.uk/wp-content/uploads/2016/01/Embedded_Generation_v7.0.pdfNULL

47. DEPARTMENT FOR BUSINESS ENERGY & INDUSTRIAL STRATEGY. *UK Energy Statistics, 2019 & Q4 2019* [online]. 2020. [Accessed 20 August 2020]. Available from: www.gov.uk/government/statistics/provisional-uk-greenhouse-gas-emissions-national-

48. UK DEPARTMENT OF ENERGY AND CLIMATE CHANGE. CFD Auction Guidance. [online]. 2014. [Accessed 14 May 2021]. Available from: https://www.gov.uk/government/uploads/system/uploads/attachment_data/file/358132/Auction_guidance_Final.pdf

49. OFGEM. About the FIT scheme. [online]. 2017. [Accessed 31 January 2017]. Available from: https://www.ofgem.gov.uk/environmental-programmes/fit/about-fit-scheme

50. EPG ENERGY LIMITED. Industry charges. [online]. 2017. [Accessed 24 February 2017]. Available from: http://www.endco.co.uk/market-information/industry-charges/

51. ELEXON. Losses. [online]. 2017. [Accessed 10 March 2017]. Available from: https://www.elexon.co.uk/reference/technical-operations/losses/NULL

52. GOOD ENERGY. Generator glossary. [online]. 2017. [Accessed 14 May 2021]. Available from: https://www.goodenergy.co.uk/media/1403/generatorglossary.pdfNULL

53. ALEXANDER, Jo. Supplier Charges in the Capacity Market. [online]. 2016. [Accessed 14 May 2021]. Available from: https://www.emrsettlement.co.uk/documents/2016/09/emrs-webinar-supplier-charges-in-the-capacity-market.pdf

54. DEPARTMENT FOR BUSINESS, Energy & Industrial Strategy. Contracts for Difference for Low Carbon Electricity Generation Consultation on proposed amendments to the scheme. [online]. 2020. [Accessed 20 August 2020]. Available from: https://assets.publishing.service.gov.uk/government/uploads/system/uploads/attachment_data/file/937634/cfd-proposed-amendments-scheme-2020-ar4-government-response.pdf

55. ELEXON. Profiling. [online]. 2017. [Accessed 14 April 2019]. Available from: https://www.elexon.co.uk/operations-settlement/profiling/From Duplicate 2 (Profiling - Elexon)NULL

56. ELEXON. *Average profiling data per Profile Class (regression data evaluated at 10-year average temperatures)* [online]. 2017. Available from: https://www.elexon.co.uk/wp-content/uploads/2012/01/Average_Profiling_data_201314_evaluated@10yearNET_v1.0.xlsxNULL

57. THE SWITCH. Powers and duties of GEMA. [online]. 2017. [Accessed 3 May 2017]. Available from: https://www.ofgem.gov.uk/publications-and-updates/powers-and-duties-gema

58. UKPOWER. Compare Gas and Electricity Prices per kWh. [online]. 2020. [Accessed 20 August 2020]. Available from: https://www.ukpower.co.uk/home_energy/tariffs-per-unit-kwh

59. WESTERN POWER DISTRIBUTION. *Connecting Microgeneration and other new*

technologies [online]. 2017. Available from: https://www.westernpower.co.uk/docs/connections/Generation/Microgeneration_web.aspx

60. MAREI, M.I., EL-SAADANY, E.F. and SALAMA, M.M.a. Flexible distributed generation. *IEEE Power Engineering Society Summer Meeting,* [online]. 2002. [Accessed 14 May 2021]. Available from: https://www.ukpowernetworks.co.uk/internet/en/our-services/documents/EOI FDG-C Walpole East (EPN) v1.1.pdf

61. SCOTTISH & SOUTHERN ELECTRICITY NETWORKS. Alternative generation connections. [online]. 2017. [Accessed 23 February 2017]. Available from: https://www.ssepd.co.uk/AlternativeGenerationConnections/

62. VEANY, James. A guide to electricity distribution connections policy. [online]. 2014. [Accessed 14 May 2021]. Available from: https://www.ofgem.gov.uk/publications-and-updates/guide-electricity-distribution-connections-policy

63. U.S. DEPARTMENT OF ENERGY. Global Energy Storage Database | Energy Storage Systems. [online]. 2020. [Accessed 24 August 2020]. Available from: https://www.sandia.gov/ess-ssl/global-energy-storage-database-home/

64. LOW-TECH MAGAZINE. Ditch the Batteries: Off-Grid Compressed Air Energy Storage. [online]. 2018. [Accessed 24 August 2020]. Available from: https://www.lowtechmagazine.com/2018/05/ditch-the-batteries-off-the-grid-compressed-air-energy-storage.html

65. YU, Aiping, CHABOT, Victor, ZHANG, Jiujun and AIPING YU, VICTOR CHABOT, Jiujun Zhang. *Electrochemical Supercapacitors for Energy Storage and Delivery*. CRC Press, 2017. ISBN 9781439869901.

66. HUGGINS, Robert A. *Energy storage: Fundamentals, materials and applications, second edition*. Second Edi. Stanford : Springer, 2015. ISBN 9783319212395.

67. DANIEL, Claus and BESENDARD, Jürgen O. *Handbook of Battery Materials*. Second Edi. Wiley-VCH Verlag, 2011. ISBN 9783527637188.

68. LINDEN, David. *Linden's Handbook of Batteries*. The McGraw-Hill Companies, Inc., 2010. ISBN 0-07-135978-8.

69. ARGYROU, Maria C., CHRISTODOULIDES, Paul and KALOGIROU, Soteris A. Energy storage for electricity generation and related processes: Technologies appraisal and

grid scale applications. *Renewable and Sustainable Energy Reviews* [online]. 1 October 2018. Vol. 94, p. 804–821. [Accessed 26 August 2020]. DOI 10.1016/j.rser.2018.06.044. Available from: https://linkinghub.elsevier.com/retrieve/pii/S1364032118304817

70. CARBON TRUST, STRBAC, Goran, AUNEDI, Marko, TENG, Fei and PUDJIANTO, Danny. Can storage help reduce the cost of a future UK electricity system? [online]. 2016. P. 120. Available from: https://www.carbontrust.com/media/672486/energy-storage-report.pdf

71. AKKU-ABC. Akkuvergleich und Energiedichte verschiedener Akkutypen. [online]. 2017. [Accessed 31 March 2017]. Available from: http://www.akku-abc.de/akku-vergleich.php

72. ITWISSEN.INFO. Bleiakku. [online]. 2017. [Accessed 3 April 2017]. Available from: http://www.itwissen.info/Bleiakku-lead-storage-battery.html

73. ITWISSEN.INFO. NiCd-Akku. [online]. 2017. [Accessed 3 April 2017]. Available from: http://www.itwissen.info/NiCd-Akku-nickel-cadmium-NiCd.html

74. ITWISSEN.INFO. Lithium-Mangandioxid-Batterie. [online]. 2017. [Accessed 3 April 2017]. Available from: http://www.itwissen.info/Lithium-Mangandioxid-Batterie-lithium-manganese-dioxide-battery-LiMnO2.html

75. BUCHMANN, Isidor. BU-215: Summary Table of Nickel-based Batteries. [online]. 2017. [Accessed 3 April 2017]. Available from: http://batteryuniversity.com/learn/article/bu_215_summary_table_of_nickel_based_batteries

76. BUCHMANN, Isidor. BU-216: Summary Table of Lithium-based Batteries. [online]. 2017. [Accessed 3 April 2017]. Available from: http://batteryuniversity.com/learn/article/bu_216_summary_table_of_lithium_based_batteries

77. BUCHMANN, Isidor. BU-214: Summary Table of Lead-based Batteries. [online]. 2017. [Accessed 3 April 2017]. Available from: http://batteryuniversity.com/learn/article/bu_214_summary_table_of_lead_based_batteries

78. AUSFELDER, Florian, BEILMANN, Christian, BERTAU, Martin, BRÄUNINGER, Sigmar, HEINZEL, Angelika, HOER, Renate, KOCH, Wolfram, MAHLENDORF, Falko, METZELTHIN, Anja, PEUCKERT, Marcell, PLASS, Ludolf, RÄUCHLE, Konstantin,

REUTER, Martin, SCHAUB, Georg, SCHIEBAHN, Sebastian, SCHWAB, Ekkehard, SCHÜTH, Ferdi, STOLTEN, Detlef, TESSMER, Gisa, WAGEMANN, Kurt and ZIEGAHN, Karl Friedrich. Energiespeicherung als Element einer sicheren Energieversorgung. *Chemie-Ingenieur-Technik* [online]. 2015. Vol. 87, no. 1–2, p. 17–89. DOI 10.1002/cite.201400183. Available from: http://onlinelibrary.wiley.com/doi/10.1002/cite.201400183/epdf

79. XE. XE Currency Converter: EUR to USD. [online]. 2017. [Accessed 3 April 2017]. Available from: http://www.xe.com/currencyconverter/convert/?From=EUR&To=USD

80. MAHNKE, Eva and MÜHLENHOFF, Jörg. Strom speichern. [online]. 2012. [Accessed 14 May 2021]. Available from: http://www.unendlich-viel-energie.de/media/file/160.57_Renews_Spezial_Strom_speichern_mar13_online.pdf

81. THIELMANN, Axel, ISENMANN, Ralf and WIETSCHEL, Martin. *Technologie-Roadmap Lithium-Ionen-Batterien 2030* [online]. June 2010. Available from: http://www.isi.fraunhofer.de/isi-wAssets/docs/t/de/publikationen/TRM-LIB2030.pdf

82. INTERNATIONAL ELECTROTECHNICAL COMMISSION. Electrical Energy Storage. [online]. 2011. [Accessed 14 May 2021]. Available from: http://www.iec.ch/whitepaper/pdf/iecWP-energystorage-LR-en.pdf

83. TAM, K-s S. Energy storage technologies for future electric power systems. *IET Seminar Digest* [online]. 2015. Vol. 2015, no. 8. DOI 10.1049/ic.2015.0238. Available from: http://ieeexplore.ieee.org/stamp/stamp.jsp?arnumber=7832691

84. BUKHARI, Syed Murtaza Ali Shah, MAQSOOD, Junaid, BAIG, Mirza Qutab, ASHRAF, Suhail and KHAN, Tamim Ahmed. Comparison of Characteristics-Lead Acid, Nickel Based, Lead Crystal and Lithium Based Batteries. In : *Proceedings - UKSim-AMSS 17th International Conference on Computer Modelling and Simulation, UKSim 2015* [online]. Institute of Electrical and Electronics Engineers Inc., 23 September 2016. p. 444–450. [Accessed 26 August 2020]. ISBN 9781479987122. Available from: http://ieeexplore.ieee.org/document/7576583/

85. AKKU-ABC. Nickel Metallhydrid Akkus - NiMH Akku. [online]. 2017. [Accessed 31 March 2017]. Available from: http://www.akku-abc.de/nimh-akku.php

86. NITTA, Naoki, WU, Feixiang, LEE, Jung Tae and YUSHIN, Gleb. Li-ion battery materials: Present and future. *Materials Today* [online]. 2015. Vol. 18, no. 5, p. 252–264. DOI 10.1016/j.mattod.2014.10.040. Available from: http://dx.doi.org/10.1016/j.mattod.2014.10.040

87. SCROSATI, Bruno and GARCHE, Jürgen. Lithium batteries: Status, prospects and future. *Journal of Power Sources* [online]. 1 May 2010. Vol. 195, no. 9, p. 2419–2430. [Accessed 3 January 2018]. DOI 10.1016/J.JPOWSOUR.2009.11.048. Available from: http://www.sciencedirect.com/science/article/pii/S0378775309020564?via=ihub

88. YANG, Xiao Guang, LENG, Yongjun, ZHANG, Guangsheng, GE, Shanhai and WANG, Chao Yang. Modeling of lithium plating induced aging of lithium-ion batteries: Transition from linear to nonlinear aging. *Journal of Power Sources* [online]. 2017. Vol. 360, p. 28–40. DOI 10.1016/j.jpowsour.2017.05.110. Available from: http://dx.doi.org/10.1016/j.jpowsour.2017.05.110

89. WU, Hui and CUI, Yi. Designing nanostructured Si anodes for high energy. *Nano Today*. 2012. Vol. 7, p. 414–429. DOI 10.1016/j.nantod.2012.08.004.

90. TANG, Jialiang, DYSART, Arthur D, HEE, Dong, SARASWAT, Ram, SHAVER, Gregory M and POL, Vilas G. Tang et al. - 2017 - Electrochimica Acta Fabrication of Carbon Silicon Composite as Lithium-ion Anode with Enhanced Cycling Stability.pdf. *Electrochimica Acta* [online]. 2017. Vol. 247, p. 626–633. DOI 10.1016/j.electacta.2017.06.178. Available from: http://dx.doi.org/10.1016/j.electacta.2017.06.178

91. ZHANG, Xiaobin, PENG, Huei, WANG, Hewu and OUYANG, Minggao. Hybrid Lithium Iron Phosphate Battery and Lithium Titanate Battery Systems for Electric Buses. *IEEE Transactions on Vehicular Technology*. 2018. Vol. 67, no. 2, p. 956–965. DOI 10.1109/TVT.2017.2749882.

92. STOLDT, C. R. and LEE, S. H. All-solid-state lithium metal batteries for next generation energy storage. In : *2013 Transducers and Eurosensors XXVII: The 17th International Conference on Solid-State Sensors, Actuators and Microsystems, TRANSDUCERS and EUROSENSORS 2013* [online]. IEEE, June 2013. p. 2819–2822. [Accessed 26 August 2020]. ISBN 9781467359818. Available from: http://ieeexplore.ieee.org/document/6627392/

93. NATIONAL GRID ESO. THE GRID CODE ISSUE 5: Revision 45. [online]. 2020. [Accessed 27 August 2020]. Available from: https://www.nationalgrideso.com/industry-information/codes/grid-code/code-documents

94. GISSEY, Giorgio Castagneto, DODDS, Paul E and ENERGY, U C L. Regulatory barriers to energy storage deployment: the UK perspective. [online]. 2016. [Accessed 14 May 2021]. Available from: https://www.birmingham.ac.uk/Documents/college-

eps/energy/Publications/RESTLESS-brief-Regulatory-barriers-to-energy-storage-deployment-July-2016.pdf

95. OFGEM. *Open letter on implications of charging reform on electricity storage* [online]. 2019. [Accessed 27 August 2020]. Available from: https://www.ofgem.gov.uk/system/files/docs/2017/07/upgrading_our_energy_system_-

96. COYNE, Brendan. Battery Storage - A business case for battery storage. [online]. 2017. [Accessed 14 May 2021]. Available from: http://herorenewables.co.uk/batterystorage/

97. LEVER, Andrew, SANDERS, David, LEHMANN, Nils, RAVISHANKAR, Manu, ASHCROFT, Michael, STRBAC, Goran, AUNEDI, Marko, TENG, Fei and PUDIJANTO, Danny. *Can storage help reduce the cost of a future UK electricity system?* [online]. 2016. [Accessed 14 May 2021]. Available from: https://www.researchgate.net/publication/299490476_Can_storage_help_reduce_the_cost_of_a_future_UK_electricity_system

98. LITTLECHILD, Stephen. Competition, regulation and price controls in the GB retail energy market. *Utilities Policy* [online]. 1 June 2018. Vol. 52, p. 59–69. [Accessed 3 September 2020]. DOI 10.1016/j.jup.2018.04.007. Available from: https://linkinghub.elsevier.com/retrieve/pii/S0957178717303375

99. GOV.UK. VAT rates. [online]. 2017. [Accessed 7 March 2017]. Available from: https://www.gov.uk/vat-ratesNULL

100. GOV.UK. VAT Notice 701/19: fuel and power. [online]. 2016. [Accessed 7 March 2017]. Available from: https://www.gov.uk/government/publications/vat-notice-70119-fuel-and-power/vat-notice-70119-fuel-and-powerNULL

101. GOV.UK. VAT rates on different goods and services. [online]. 2014. [Accessed 7 March 2017]. Available from: https://www.gov.uk/guidance/rates-of-vat-on-different-goods-and-servicesNULL

102. OLIVER SCHMIDT, ADAM HAWKES, AJAY GAMBHIR, IAIN STAFFEL, SCHMIDT, Oliver, HAWKES, Adam, GAMBHIR, Ajay, STAFFELL, Iain, OLIVER SCHMIDT, ADAM HAWKES, AJAY GAMBHIR and IAIN STAFFEL. Cost-effective electricity storage: Will it enable us to fully decarbonise power generation. In : *UK Energy Storage Conference* [online]. 2016. p. 2030. [Accessed 3 January 2018]. Available from: http://energysuperstore.org/esrn/wp-content/uploads/2017/01/UKES2016-Poster_Oliver-Schmidt.pdf

103. BLOOMBERGNEF. Battery Pack Prices Cited Below $100/kWh for the First Time in 2020, While Market Average Sits at $137/kWh. [online]. 2020. [Accessed 31 May 2021]. Available from: https://about.bnef.com/blog/battery-pack-prices-cited-below-100-kwh-for-the-first-time-in-2020-while-market-average-sits-at-137-kwh/

104. CORDOBA-ARENAS, Andrea and RIZZONI, Prof Giorgio. *Aging Propagation Modeling and State-of-Health Assessment in Advanced Battery Systems Dissertation* [online]. The Ohio State University, 2013. Available from: https://etd.ohiolink.edu/apexprod/rws_olink/r/1501/10?p10_etd_subid=90928&clear=10#abstract-files

105. DUBARRY, Matthieu, BAURE, George, PASTOR-FERNÁNDEZ, Carlos, WIDANAGE, W. Dhammika and MARCO, James. Battery energy storage system modeling: A combined comprehensive approach. *Journal of Energy Storage* [online]. 2019. Vol. 21, no. August 2018, p. 172–185. DOI 10.1016/j.est.2018.11.012. Available from: https://doi.org/10.1016/j.est.2018.11.012

106. NATIONAL RENEWABLE ENERGY LABORATORY (NREL) and NEUBAUER, Jeremy. *Battery Lifetime Analysis and Simulation Tool (BLAST) Documentation* [online]. 2014. Available from: http://www.nrel.gov/transportation/energystorage/blast.html

107. UDDIN, Kotub, GOUGH, Rebecca, RADCLIFFE, Jonathan, MARCO, James and JENNINGS, Paul. Techno-economic analysis of the viability of residential photovoltaic systems using lithium-ion batteries for energy storage in the United Kingdom. *Applied Energy*. 2017. Vol. 206, no. August, p. 12–21. DOI 10.1016/j.apenergy.2017.08.170.

108. GUI, Qiang, SU, Hao, FENG, Donghan, ZHOU, Yun, XU, Ran, YAN, Zheng and LEI, Ting. A novel linear battery energy storage system (BESS) life loss calculation model for BESS-integrated wind farm in scheduled power tracking. In : *IET Conference Publications* [online]. Institution of Engineering and Technology, 2019. p. 240 (8 pp.)-240 (8 pp.). [Accessed 11 September 2020]. Available from: https://digital-library.theiet.org/content/conferences/10.1049/cp.2019.0495

109. D. PELZER D. CIECHANOWICZ, A Knoll, PELZER, Dominik, CIECHANOWICZ, David, KNOLL, Alois and D. PELZER D. CIECHANOWICZ, A Knoll. Energy arbitrage through smart scheduling of battery energy storage considering battery degradation and electricity price forecasts. *IEEE PES Innovative Smart Grid Technologies Conference Europe*. 2016. P. 472–477. DOI 10.1109/ISGT-Asia.2016.7796431.

110. ABDULLA, Khalid, DE HOOG, Julian, MUENZEL, Valentin, SUITS, Frank, STEER, Kent, WIRTH, Andrew and HALGAMUGE, Saman. Optimal Operation of Energy Storage Systems Considering Forecasts and Battery Degradation. *IEEE Transactions on Smart Grid*. 2016. Vol. PP, no. 99, p. 1–11. DOI 10.1109/TSG.2016.2606490.

111. FOGGO, Brandon and YU, Nanpeng. Improved battery storage valuation through degradation reduction. *IEEE Transactions on Smart Grid* [online]. 2018. Vol. 9, no. 6, p. 5721–5732. DOI 10.1109/TSG.2017.2695196. Available from: http://ieeexplore.ieee.org/document/7917324/

112. HUA, Yin, CORDOBA-ARENAS, Andrea, WARNER, Nicholas and RIZZONI, Giorgio. A multi time-scale state-of-charge and state-of-health estimation framework using nonlinear predictive filter for lithium-ion battery pack with passive balance control. *Journal of Power Sources* [online]. 2015. Vol. 280, p. 293–312. DOI 10.1016/j.jpowsour.2015.01.112. Available from: http://dx.doi.org/10.1016/j.jpowsour.2015.01.112

113. GALLARDO-LOZANO, Javier, ROMERO-CADAVAL, Enrique, MILANES-MONTERO, M. Isabel and GUERRERO-MARTINEZ, Miguel A. Battery equalization active methods. *Journal of Power Sources* [online]. 2014. Vol. 246, p. 934–949. DOI 10.1016/j.jpowsour.2013.08.026. Available from: http://dx.doi.org/10.1016/j.jpowsour.2013.08.026

114. CAMPESTRINI, Christian, KEIL, Peter, SCHUSTER, Simon F. and JOSSEN, Andreas. Ageing of lithium-ion battery modules with dissipative balancing compared with single-cell ageing. *Journal of Energy Storage*. 2016. Vol. 6, p. 142–152. DOI 10.1016/j.est.2016.03.004.

115. VON SRBIK, Marie Therese, MARINESCU, Monica, MARTINEZ-BOTAS, Ricardo F. and OFFER, Gregory J. A physically meaningful equivalent circuit network model of a lithium-ion battery accounting for local electrochemical and thermal behaviour, variable double layer capacitance and degradation. *Journal of Power Sources*. 2016. Vol. 325, p. 171–184. DOI 10.1016/j.jpowsour.2016.05.051.

116. HE, Hongwen, XIONG, Rui and FAN, Jinxin. Evaluation of lithium-ion battery equivalent circuit models for state of charge estimation by an experimental approach. *Energies*. 2011. Vol. 4, no. 4, p. 582–598. DOI 10.3390/en4040582.

117. AHMED, Ryan, GAZZARRI, Javier, ONORI, Simona, HABIBI, Saeid, JACKEY, Robyn, RZEMIEN, Kevin, TJONG, Jimi and LESAGE, Jonathan. Model-Based Parameter Identification of Healthy and Aged Li-ion Batteries for Electric Vehicle Applications. *SAE*

International Journal of Alternative Powertrains [online]. 2015. Vol. 4, no. 2, p. 2015-01–0252. DOI 10.4271/2015-01-0252. Available from: http://papers.sae.org/2015-01-0252/

118. ECKER, Madeleine, GERSCHLER, Jochen B., VOGEL, Jan, K??BITZ, Stefan, HUST, Friedrich, DECHENT, Philipp, SAUER, Dirk Uwe, KÄBITZ, Stefan, HUST, Friedrich, DECHENT, Philipp and SAUER, Dirk Uwe. Development of a lifetime prediction model for lithium-ion batteries based on extended accelerated aging test data. *Journal of Power Sources*. 2012. Vol. 215, p. 248–257. DOI 10.1016/j.jpowsour.2012.05.012.

119. CACCIATO, Mario, NOBILE, Giovanni, SCARCELLA, Giuseppe and SCELBA, Giacomo. Real-Time Model-Based Estimation of SOC and SOH for Energy Storage Systems. *IEEE Transactions on Power Electronics*. 2017. Vol. 32, no. 1, p. 794–803. DOI 10.1109/TPEL.2016.2535321.

120. UDDIN, Kotub, PICARELLI, Alessandro, LYNESS, Christopher, TAYLOR, Nigel and MARCO, James. An Acausal Li-Ion Battery Pack Model for Automotive Applications. *Energies*. 2014. Vol. 7, no. 9, p. 5675–5700. DOI 10.3390/en7095675.

121. BULLER, S., THELE, M., DONCKER, R.W. De and KARDEN, E. Impedance-Based Simulation Models of Supercapacitors and Lithium-ion Batteries for Power Electronic Applications. *IEEE Industry Applications Magazine*. 2005. Vol. 11, no. 2, p. 742–747. DOI 10.1109/MIA.2005.1405828.

122. CHEN, Min and RINCÓN-MORA, Gabriel A. Accurate electrical battery model capable of predicting runtime and I-V performance. *IEEE Transactions on Energy Conversion*. 2006. Vol. 21, no. 2, p. 504–511. DOI 10.1109/TEC.2006.874229.

123. MAMUN, A., NARAYANAN, I., WANG, D., SIVASUBRAMANIAM, A. and FATHY, H.K. Multi-objective optimization of demand response in a datacenter with lithium-ion battery storage. *Journal of Energy Storage* [online]. 2016. Vol. 7, p. 258–269. DOI 10.1016/j.est.2016.08.002. Available from: http://linkinghub.elsevier.com/retrieve/pii/S2352152X16301025

124. PASTOR-FERNANDEZ, Carlos, DHAMMIKA WIDANAGE, W., MARCO, James, GAMA-VALDEZ, Miguel Angel and CHOUCHELAMANE, Gael H. Identification and quantification of ageing mechanisms in Lithium-ion batteries using the EIS technique. *2016 IEEE Transportation Electrification Conference and Expo, ITEC 2016*. 2016. DOI 10.1109/ITEC.2016.7520198.

125. ZHANG, Caiping, JIANG, Jiuchun, ZHANG, Linjing, LIU, Sijia, WANG, Leyi and LOH,

Poh Chiang. A generalized SOC-OCV model for lithium-ion batteries and the SOC estimation for LNMCO battery. *Energies*. 2016. Vol. 9, no. 11. DOI 10.3390/en9110900.

126. BIRKL, Christoph R., ROBERTS, Matthew R., MCTURK, Euan, BRUCE, Peter G. and HOWEY, David A. Degradation diagnostics for lithium ion cells. *Journal of Power Sources* [online]. 2016. Vol. 341, p. 373–386. DOI 10.1016/j.jpowsour.2016.12.011. Available from: http://dx.doi.org/10.1016/j.jpowsour.2016.12.011

127. IRAOLA, U., AIZPURU, I., CANALES, J. M., ETXEBERRIA, A. and GIL, I. Methodology for thermal modelling of lithium-ion batteries. *IECON Proceedings (Industrial Electronics Conference)*. 2013. P. 6752–6757. DOI 10.1109/IECON.2013.6700250.

128. BIRKL, C. R., MCTURK, E., ROBERTS, M. R., BRUCE, P. G. and HOWEY, D. A. A parametric open circuit voltage model for lithium ion batteries. *Journal of the Electrochemical Society*. 2015. Vol. 162, no. 12, p. A2271–A2280. DOI 10.1149/2.0331512jes.

129. SWIERCZYNSKI, Maciej, STROE, Daniel Ioan, STAN, Ana Irina, TEODORESCU, Remus and SAUER, Dirk Uwe. Selection and performance-degradation modeling of limo2/li 4ti5o12 and lifepo4/c battery cells as suitable energy storage systems for grid integration with wind power plants: An example for the primary frequency regulation service. *IEEE Transactions on Sustainable Energy*. 2014. Vol. 5, no. 1, p. 90–101. DOI 10.1109/TSTE.2013.2273989.

130. CHANG, Chin-Yao, TULPULE, Punit, RIZZONI, Giorgio, ZHANG, Wei and DU, Xinyu. A probabilistic approach for prognosis of battery pack aging. *Journal of Power Sources* [online]. 2017. Vol. 347, p. 57–68. DOI 10.1016/j.jpowsour.2017.01.130. Available from: http://linkinghub.elsevier.com/retrieve/pii/S0378775317301404

131. BIRKL, C R and HOWEY, D A. Model identification and parameter estimation for LiFePO 4 batteries. In : *IET Hybrid and Electric Vehicles Conference (HEVC),*. 2013. p. 1–6.

132. DUBARRY, Matthieu, TRUCHOT, Cyril and LIAW, Bor Yann. Synthesize battery degradation modes via a diagnostic and prognostic model. *Journal of Power Sources* [online]. 2012. Vol. 219, p. 204–216. DOI 10.1016/j.jpowsour.2012.07.016. Available from: http://dx.doi.org/10.1016/j.jpowsour.2012.07.016

133. REDONDO-IGLESIAS, Eduardo, VENET, Pascal and PELISSIER, Serge. Global Model for Self-discharge and Capacity Fade in Lithium-ion Batteries Based on the

Generalized Eyring Relationship. *IEEE Transactions on Vehicular Technology*. 2017. Vol. XX, no. XX, p. 1–10. DOI 10.1109/TVT.2017.2751218.

134. CHEN, Haisheng, CONG, Thang Ngoc, YANG, Wei, TAN, Chunqing, LI, Yongliang and DING, Yulong. Progress in electrical energy storage system: A critical review. *Progress in Natural Science* [online]. 2009. Vol. 19, no. 3, p. 291–312. DOI 10.1016/j.pnsc.2008.07.014. Available from: http://dx.doi.org/10.1016/j.pnsc.2008.07.014

135. DTI. Review of electrical energy storage technologies and systems and of their potential for the UK. [online]. 2004. P. 1–34. DOI DG/DTI/00055/00/00, URN NUMBER 04/1876. Available from: http://www.wearemichigan.com/JobsAndEnergy/documents/file15185.pdf

136. HADJIPASCHALIS, Ioannis, POULLIKKAS, Andreas and EFTHIMIOU, Venizelos. Overview of current and future energy storage technologies for electric power applications. *Renewable and Sustainable Energy Reviews*. 2009. Vol. 13, no. 6–7, p. 1513–1522. DOI 10.1016/j.rser.2008.09.028.

137. ZIMMERMAN, Albert H. Self-discharge losses in lithium-ion cells. *IEEE Aerospace and Electronic Systems Magazine*. 2004. Vol. 19, no. 2, p. 19–24. DOI 10.1109/MAES.2004.1269687.

138. SWIERCZYNSKI, Maciej, STROE, Daniel Ioan, STAN, Ana Irina, TEODORESCU, Remus and KAER, Soren Knudsen. Investigation on the Self-discharge of the LiFePO4/C nanophosphate battery chemistry at different conditions. *IEEE Transportation Electrification Conference and Expo, ITEC Asia-Pacific 2014 - Conference Proceedings*. 2014. P. 1–6. DOI 10.1109/ITEC-AP.2014.6940762.

139. RAHMOUN, Ahmad and BIECHL, Helmuth. Modelling of Li-ion batteries using equivalent circuit diagrams. *Przeglad Elektrotechniczny* [online]. 2012. Vol. 88, no. 7 B, p. 152–156. Available from: http://red.pe.org.pl/articles/2012/7b/40.pdf

140. GAILANI, Ahmed, AL-GREER, Maher, SHORT, Michael and CROSBIE, Tracey. Degradation cost analysis of Li-Ion batteries in the capacity market with different degradation models. *Electronics (Switzerland)*. 2020. Vol. 9, no. 1. DOI 10.3390/electronics9010090.

141. BERNARDI, D., PAWLIKOWSKI, E. and NEWMAN, J. A General Energy Balance For Battery Systems. *Journal of the Electrochemical Society*. 1985. Vol. 132, no. 1, p. 5–12. DOI 10.1149/1.2113792.

142. ISMAIL, Nur Hazima Faezaa, TOHA, Siti Fauziah, AZUBIR, Nor Aziah Mohd, MD ISHAK, Nizam Hanis, HASSAN, Mohd Khair and KSM IBRAHIM, Babul Salam. Simplified heat generation model for lithium ion battery used in electric vehicle. *IOP Conference Series: Materials Science and Engineering*. 2013. Vol. 53, no. 1, p. 1–6. DOI 10.1088/1757-899X/53/1/012014.

143. WILLIFORD, Ralph E., VISWANATHAN, Vilayanur V. and ZHANG, Ji-guang Guang. Effects of entropy changes in anodes and cathodes on the thermal behavior of lithium ion batteries. *Journal of Power Sources*. 2009. Vol. 189, no. 1, p. 101–107. DOI 10.1016/j.jpowsour.2008.10.078.

144. REYNIER, Y., YAZAMI, R. and FULTZ, B. The entropy and enthalpy of lithium intercalation into graphite. *Journal of Power Sources*. 2003. Vol. 119–121, p. 850–855. DOI 10.1016/S0378-7753(03)00285-4.

145. SUN, Hongguang, WANG, Xiaohui, TOSSAN, Brian and DIXON, Regan. Three-dimensional thermal modeling of a lithium-ion battery pack. *Journal of Power Sources* [online]. 2012. Vol. 206, p. 349–356. DOI 10.1016/j.jpowsour.2012.01.081. Available from: http://dx.doi.org/10.1016/j.jpowsour.2012.01.081

146. CAPRON, Odile, BRUSSEL, Vrije Universiteit, SAMBA, Ahmadou, BRUSSEL, Vrije Universiteit, OMAR, Noshin, BRUSSEL, Vrije Universiteit, BRUSSEL, Vrije Universiteit, COOSEMANS, Thierry, VAN DEN BOSSCHE, Peter and VAN MIERLO, Joeri. Lithium-ion batteries: Thermal behaviour investigation of unbalanced modules. *Sustainability (Switzerland)*. 2015. Vol. 7, no. July, p. 8374–8398. DOI 10.3390/su7078374.

147. BECKER, Dominic J., WETZEL, Thomas, WERNER, Daniel, LOGES, André, BECKER, Dominic J. and WETZEL, Thomas. Thermal conductivity of Li-ion batteries and their electrode con fi gurations e A novel combination of modelling and experimental approach. *Journal of Power Sources*. 2017. Vol. 364, p. 72–83. DOI 10.1016/j.jpowsour.2017.07.105.

148. KAZIM, Anton Lidbeck and SYED, Raza. *Experimental Characterization of Li-ion Battery cells for Thermal Management in Heavy Duty Hybrid Applications* [online]. Chalmers University of Technology, 2017. [Accessed 18 June 2020]. Available from: https://odr.chalmers.se/bitstream/20.500.12380/252994/1/252994.pdf

149. SPOTNITZ, R. Simulation of capacity fade in lithium-ion batteries. *Journal of Power Sources*. 2003. Vol. 113, no. 1, p. 72–80. DOI 10.1016/S0378-7753(02)00490-1.

150. SCHUSTER, Simon F., BRAND, Martin J., CAMPESTRINI, Christian,

GLEISSENBERGER, Markus and JOSSEN, Andreas. Correlation between capacity and impedance of lithium-ion cells during calendar and cycle life. *Journal of Power Sources* [online]. 2016. Vol. 305, p. 191–199. DOI 10.1016/j.jpowsour.2015.11.096. Available from: http://dx.doi.org/10.1016/j.jpowsour.2015.11.096

151. XU, Bolun, OUDALOV, Alexandre, ULBIG, Andreas, ANDERSSON, Göran Goran and KIRSCHEN, Daniel S. Modeling of Lithium-Ion Battery Degradation for Cell Life Assessment. *IEEE Transactions on Smart Grid* [online]. 2016. Vol. 3053, no. c, p. 1–1. DOI 10.1109/TSG.2016.2578950. Available from: http://ieeexplore.ieee.org/lpdocs/epic03/wrapper.htm?arnumber=7488267%5Cnhttp://ieeexplore.ieee.org/document/7488267/

152. GAO, Yang, JIANG, Jiuchun, ZHANG, Caiping, ZHANG, Weige, MA, Zeyu and JIANG, Yan. Lithium-ion battery aging mechanisms and life model under different charging stresses. *Journal of Power Sources* [online]. 2017. Vol. 356, p. 103–114. DOI 10.1016/j.jpowsour.2017.04.084. Available from: http://dx.doi.org/10.1016/j.jpowsour.2017.04.084

153. TANIM, Tanvir R. and RAHN, Christopher D. Aging formula for lithium ion batteries with solid electrolyte interphase layer growth. *Journal of Power Sources* [online]. 2015. Vol. 294, p. 239–247. DOI 10.1016/j.jpowsour.2015.06.014. Available from: http://dx.doi.org/10.1016/j.jpowsour.2015.06.014

154. SCHUSTER, Simon F., BACH, Tobias, FLEDER, Elena, MÜLLER, Jana, BRAND, Martin, SEXTL, Gerhard and JOSSEN, Andreas. Nonlinear aging characteristics of lithium-ion cells under different operational conditions. *Journal of Energy Storage* [online]. 2015. Vol. 1, no. 1, p. 44–53. DOI 10.1016/j.est.2015.05.003. Available from: http://dx.doi.org/10.1016/j.est.2015.05.003

155. MARTINEZ-LASERNA, E., SARASKETA-ZABALA, E., STROE, D. I., SWIERCZYNSKI, M., WARNECKE, A., TIMMERMANS, J. M., GOUTAM, S. and RODRIGUEZ, P. Evaluation of lithium-ion battery second life performance and degradation. *ECCE 2016 - IEEE Energy Conversion Congress and Exposition, Proceedings*. 2016. DOI 10.1109/ECCE.2016.7855090.

156. BAUER, Marius, GUENTHER, Clemens, KASPER, Michael, PETZL, Mathias and DANZER, Michael A. Discrimination of degradation processes in lithium-ion cells based on the sensitivity of aging indicators towards capacity loss. *Journal of Power Sources* [online]. 2015. Vol. 283, p. 494–504. DOI 10.1016/j.jpowsour.2015.02.130. Available from: http://dx.doi.org/10.1016/j.jpowsour.2015.02.130

157. STROE, Daniel, SWIERCZYNSKI, Maciej, STAN, Ana-irina and TEODORESCU, Remus. Accelerated Lifetime Testing Methodology for Lifetime Estimation of Lithium-ion Batteries used in Augmented Wind Power Plants Accelerat Methodol ogy for n of Lithium- behave in used. *IEEE TRANSACTIONS ON INDUSTRY APPLICATIONS*. 2013. Vol. 50, no. 6, p. 690–698. DOI 10.1109/TIA.2014.2321028.

158. STROE, Daniel Ioan, SWIERCZYNSKI, Maciej, STROE, Ana Irina, LAERKE, Rasmus, KJAER, Philip Carne and TEODORESCU, Remus. Degradation Behavior of Lithium-Ion Batteries Based on Lifetime Models and Field Measured Frequency Regulation Mission Profile. *IEEE Transactions on Industry Applications*. 2016. Vol. 52, no. 6, p. 5009–5018. DOI 10.1109/TIA.2016.2597120.

159. SCHMALSTIEG, Johannes, KÄBITZ, Stefan, ECKER, Madeleine and SAUER, Dirk Uwe. A holistic aging model for Li(NiMnCo)O2 based 18650 lithium-ion batteries. *Journal of Power Sources* [online]. 2014. Vol. 257, p. 325–334. DOI 10.1016/j.jpowsour.2014.02.012. Available from: http://dx.doi.org/10.1016/j.jpowsour.2014.02.012

160. SCHMALSTIEG, Johannes, KÄBITZ, Stefan, ECKER, Madeleine and SAUER, Dirk Uwe. From accelerated aging tests to a lifetime prediction model: Analyzing lithium-ion batteries. In : *2013 World Electric Vehicle Symposium and Exhibition, EVS 2014*. 2014. p. 1–12. ISBN 9781479938322.

161. GROLLEAU, Sébastien, DELAILLE, Arnaud, GUALOUS, Hamid, GYAN, Philippe, REVEL, Renaud, BERNARD, Julien, REDONDO-IGLESIAS, Eduardo and PETER, Jérémy. Calendar aging of commercial graphite/LiFePO4 cell - Predicting capacity fade under time dependent storage conditions. *Journal of Power Sources* [online]. 2014. Vol. 255, p. 450–458. DOI 10.1016/j.jpowsour.2013.11.098. Available from: http://dx.doi.org/10.1016/j.jpowsour.2013.11.098

162. PASTOR-FERNÁNDEZ, C, WIDANAGE, W D, CHOUCHELAMANE, G H and MARCO, J. A SoH Diagnosis and Prognosis Method to Identify and Quantify Degradation Modes in Li-ion Batteries using the IC / DV technique. In : *6th Hybrid and Electric Vehicles Conference (HEVC 2016)* [online]. 2016. p. 1–6. Available from: https://ieeexplore.ieee.org/document/7884018

163. FARZIN, Hossein, FOTUHI-FIRUZABAD, Mahmud and MOEINI-AGHTAIE, Moein. A Practical Scheme to Involve Degradation Cost of Lithium-Ion Batteries in Vehicle-to-Grid Applications. *IEEE Transactions on Sustainable Energy*. 2016. Vol. 7, no. 4, p. 1730–1738. DOI 10.1109/TSTE.2016.2558500.

164. ECKER, M., GERSCHLER, J.B. B., VOGEL, J., KÄBITZ, S., HUST, F., DECHENT, P. and SAUER, D.U. U. Analyzing calendar aging data towards a lifetime prediction model for lithium-ion batteries. In : *26th Electric Vehicle Symposium 2012*. 2012. p. 47–58. ISBN 9781622764211.

165. OMAR, N., FIROUZ, Y., TIMMERMANS, J. M., MONEM, M. Abdel, GUALOUS, H., COOSEMANS, Th, VAN DEN BOSSCHE, P. and VAN MIERLO, J. Lithium iron phosphate - Assessment of calendar life and change of battery parameters. *2014 IEEE Vehicle Power and Propulsion Conference, VPPC 2014*. 2014. DOI 10.1109/VPPC.2014.7007095.

166. WANG, John, LIU, Ping, HICKS-GARNER, Jocelyn, SHERMAN, Elena, SOUKIAZIAN, Souren, VERBRUGGE, Mark, TATARIA, Harshad, MUSSER, James and FINAMORE, Peter. Cycle-life model for graphite-LiFePO4 cells. *Journal of Power Sources* [online]. 2011. Vol. 196, no. 8, p. 3942–3948. DOI 10.1016/j.jpowsour.2010.11.134. Available from: http://dx.doi.org/10.1016/j.jpowsour.2010.11.134

167. HAN, Xuebing, OUYANG, Minggao, LU, Languang and LI, Jianqiu. A comparative study of commercial lithium ion battery cycle life in electric vehicle: Capacity loss estimation. *Journal of Power Sources* [online]. 2014. Vol. 268, p. 658–669. DOI 10.1016/j.jpowsour.2014.06.111. Available from: http://dx.doi.org/10.1016/j.jpowsour.2014.06.111

168. LEE, You Jin, CHOI, Hae Young, HA, Chung Wan, YU, Ji Hyun, HWANG, Min Ji, DOH, Chil Hoon and CHOI, Jeong Hee. Cycle life modeling and the capacity fading mechanisms in a graphite/LiNi0.6Co0.2Mn0.2O2 cell. *Journal of Applied Electrochemistry*. 2015. Vol. 45, no. 5, p. 419–426. DOI 10.1007/s10800-015-0811-6.

169. GROOT, Jens, SWIERCZYNSKI, Maciej, STAN, Ana Irina and KÆR, Søren Knudsen. On the complex ageing characteristics of high-power LiFePO4/graphite battery cells cycled with high charge and discharge currents. *Journal of Power Sources* [online]. 2015. Vol. 286, p. 475–487. DOI 10.1016/j.jpowsour.2015.04.001. Available from: http://dx.doi.org/10.1016/j.jpowsour.2015.04.001

170. FORMAN, Joel C., MOURA, Scott J., STEIN, Jeffrey L. and FATHY, Hosam K. Optimal Experimental Design for Modeling Battery Degradation. *ASME 2012 5th Annual Dynamic Systems and Control Conference Joint with the JSME 2012 11th Motion and Vibration Conference, DSCC 2012-MOVIC 2012*. 2012. Vol. 1, p. 309–318. DOI 10.1115/DSCC2012-MOVIC2012-8751.

171. FORTENBACHER, Philipp and ANDERSSON, Göran Goran. Battery Degradation

Maps for Power System Optimization and as a Benchmark Reference. *2017 IEEE Manchester PowerTech, Powertech 2017* [online]. 2017. DOI 10.1109/PTC.2017.7980977. Available from: http://arxiv.org/abs/1703.03690

172. SU, Laisuo, ZHANG, Jianbo, HUANG, Jun, GE, Hao, LI, Zhe, XIE, Fengchao and LIAW, Bor Yann. Path dependence of lithium ion cells aging under storage conditions. *Journal of Power Sources* [online]. 2016. Vol. 315, no. 2012, p. 35–46. DOI 10.1016/j.jpowsour.2016.03.043. Available from: http://dx.doi.org/10.1016/j.jpowsour.2016.03.043

173. DE HOOG, Joris, TIMMERMANS, Jean Marc, IOAN-STROE, Daniel, SWIERCZYNSKI, Maciej, JAGUEMONT, Joris, GOUTAM, Shovon, OMAR, Noshin, VAN MIERLO, Joeri and VAN DEN BOSSCHE, Peter. Combined cycling and calendar capacity fade modeling of a Nickel-Manganese-Cobalt Oxide Cell with real-life profile validation. *Applied Energy* [online]. 2017. Vol. 200, p. 47–61. DOI 10.1016/j.apenergy.2017.05.018. Available from: http://dx.doi.org/10.1016/j.apenergy.2017.05.018

174. MUENZEL, Valentin, DE HOOG, Julian, BRAZIL, Marcus, VISHWANATH, Arun and KALYANARAMAN, Shiv. A multi-factor battery cycle life prediction methodology for optimal battery management. *e-Energy 2015 - Proceedings of the 2015 ACM 6th International Conference on Future Energy Systems*. 2015. No. January, p. 57–66. DOI 10.1145/2768510.2768532.

175. LI, Zhe, LU, Languang, OUYANG, Minggao and XIAO, Yuankun. Modeling the capacity degradation of LiFePO4/graphite batteries based on stress coupling analysis. *Journal of Power Sources* [online]. 2011. Vol. 196, no. 22, p. 9757–9766. DOI 10.1016/j.jpowsour.2011.07.080. Available from: http://dx.doi.org/10.1016/j.jpowsour.2011.07.080

176. RAMADASS, P., HARAN, Bala, GOMADAM, Parthasarathy M., WHITE, Ralph and POPOV, Branko N. Development of First Principles Capacity Fade Model for Li-Ion Cells. *Journal of the Electrochemical Society*. 2004. Vol. 151, no. 2, p. 196–203. DOI 10.1149/1.1634273.

177. SAFARI, M, MORCRETTE, M, TEYSSOT, A and DELACOURT, C. Life-Prediction Methods for Lithium-Ion Batteries Derived from a Fatigue Approach. *Journal of The Electrochemical Society* [online]. 2010. Vol. 157, no. 6, p. A713. DOI 10.1149/1.3374634. Available from: http://jes.ecsdl.org/content/157/6/A713.abstract%5Cnhttp://jes.ecsdl.org/cgi/doi/10.11

49/1.3374634

178. SMITH, Kandler, SAXON, Aron, KEYSER, Matthew, LUNDSTROM, Blake, CAO, Ziwei, ROC, Albert and CORP, Sunpower. Life prediction model for grid-connected Li-ion battery energy storage system. *Proceedings of the American Control Conference*. 2017. P. 4062–4068. DOI 10.23919/ACC.2017.7963578.

179. FORMAN, Joel C., BASHASH, Saeid, STEIN, Jeffrey L. and FATHY, Hosam K. Forman et al. - 2011 - Reduction of an Electrochemistry-Based Li-Ion Battery Model via Quasi-Linearization and Padé Approximation.pdf. *Journal of The Electrochemical Society* [online]. 2011. Vol. 158, no. 2, p. A93. DOI 10.1149/1.3519059. Available from: http://jes.ecsdl.org/cgi/doi/10.1149/1.3519059

180. OPTIMUM BATTERY CO., Ltd. 12v 100ah Lithium Ion Batteries Lifepo4 Battery - Product on Alibaba.com. [online]. 2018. [Accessed 16 January 2018]. Available from: https://www.alibaba.com/product-detail/12V-100Ah-lithium-ion-batteries-LiFePO4_728913459.html

181. KÄBITZ, Stefan, GERSCHLER, Jochen Bernhard, ECKER, Madeleine, YURDAGEL, Yusuf, EMMERMACHER, Brita, ANDRÉ, Dave, MITSCH, Tim and SAUER, Dirk Uwe. Cycle and calendar life study of a graphite|LiNi1/3Mn 1/3Co1/3O2 Li-ion high energy system. Part A: Full cell characterization. *Journal of Power Sources* [online]. 2013. Vol. 239, p. 572–583. DOI 10.1016/j.jpowsour.2013.03.045. Available from: http://dx.doi.org/10.1016/j.jpowsour.2013.03.045

182. BROUSSELY, M., HERREYRE, S., BIENSAN, P., KASZTEJNA, P., NECHEV, K. and STANIEWICZ, R. J. Aging mechanism in Li ion cells and calendar life predictions. *Journal of Power Sources*. 2001. Vol. 97–98, p. 13–21. DOI 10.1016/S0378-7753(01)00722-4.

183. SARASKETA-ZABALA, E., GANDIAGA, I., MARTINEZ-LASERNA, E., RODRIGUEZ-MARTINEZ, L. M. and VILLARREAL, I. Cycle ageing analysis of a LiFePO4/graphite cell with dynamic model validations: Towards realistic lifetime predictions. *Journal of Power Sources* [online]. 2015. Vol. 275, p. 573–587. DOI 10.1016/j.jpowsour.2014.10.153. Available from: http://dx.doi.org/10.1016/j.jpowsour.2014.10.153

184. NAMOR, Emil, TORREGROSSA, Dimitri, SOSSAN, Fabrizio, CHERKAOUI, Rachid and PAOLONE, Mario. Assessment of battery ageing and implementation of an ageing aware control strategy for a load leveling application of a lithium titanate battery energy storage system. *2016 IEEE 17th Workshop on Control and Modeling for Power*

Electronics, COMPEL 2016. 2016. DOI 10.1109/COMPEL.2016.7556779.

185. OMAR, Noshin, MONEM, Mohamed Abdel, FIROUZ, Yousef, SALMINEN, Justin, SMEKENS, Jelle, HEGAZY, Omar, GAULOUS, Hamid, MULDER, Grietus, VAN DEN BOSSCHE, Peter, COOSEMANS, Thierry and VAN MIERLO, Joeri. Lithium iron phosphate based battery - Assessment of the aging parameters and development of cycle life model. *Applied Energy* [online]. 2014. Vol. 113, p. 1575–1585. DOI 10.1016/j.apenergy.2013.09.003. Available from: http://dx.doi.org/10.1016/j.apenergy.2013.09.003

186. BARAI, Anup, UDDIN, Kotub, WIDANALAGE, W. D., MCGORDON, Andrew and JENNINGS, Paul. The effect of average cycling current on total energy of lithium-ion batteries for electric vehicles. *Journal of Power Sources* [online]. 2016. Vol. 303, p. 81–85. DOI 10.1016/j.jpowsour.2015.10.095. Available from: http://dx.doi.org/10.1016/j.jpowsour.2015.10.095

187. LEWERENZ, Meinert, MÜNNIX, Jens, SCHMALSTIEG, Johannes, KÄBITZ, Stefan, KNIPS, Marcus and SAUER, Dirk Uwe. Systematic aging of commercial LiFePO4|Graphite cylindrical cells including a theory explaining rise of capacity during aging. *Journal of Power Sources*. 2017. Vol. 345, p. 254–263. DOI 10.1016/j.jpowsour.2017.01.133.

188. MATHIEU, Romain, BAGHDADI, Issam, BRIAT, Olivier, GYAN, Philippe and VINASSA, Jean Michel. D-optimal design of experiments applied to lithium battery for ageing model calibration. *Energy* [online]. 2017. Vol. 141, p. 2108–2119. DOI 10.1016/j.energy.2017.11.130. Available from: https://doi.org/10.1016/j.energy.2017.11.130

189. PETIT, Martin, PRADA, Eric and SAUVANT-MOYNOT, Valérie. Development of an empirical aging model for Li-ion batteries and application to assess the impact of Vehicle-to-Grid strategies on battery lifetime. *Applied Energy* [online]. 2016. Vol. 172, p. 398–407. DOI 10.1016/j.apenergy.2016.03.119. Available from: http://dx.doi.org/10.1016/j.apenergy.2016.03.119

190. EBERT, Fabian, SEXTL, Gerhard and LIENKAMP, Markus. Effect of a flexible battery module bracing on cell aging. In : *2017 12th International Conference on Ecological Vehicles and Renewable Energies, EVER 2017*. 2017. ISBN 9781538616925.

191. CANNARELLA, John and ARNOLD, Craig B. Stress evolution and capacity fade in constrained lithium-ion pouch cells. *Journal of Power Sources* [online]. 2014. Vol. 245, p. 745–751. DOI 10.1016/j.jpowsour.2013.06.165. Available from:

http://dx.doi.org/10.1016/j.jpowsour.2013.06.165

192. BARAI, Anup, UDDIN, Kotub, DUBARRY, Matthieu, SOMERVILLE, Limhi, MCGORDON, Andrew, JENNINGS, Paul and BLOOM, Ira. A comparison of methodologies for the non-invasive characterisation of commercial Li-ion cells. *Progress in Energy and Combustion Science* [online]. 2019. Vol. 72, p. 1–31. DOI 10.1016/j.pecs.2019.01.001. Available from: https://doi.org/10.1016/j.pecs.2019.01.001

193. OFGEM. *Energy Demand Research Project* [online]. 2011. [Accessed 22 May 2018]. Available from: https://www.ofgem.gov.uk/gas/retail-market/metering/transition-smart-meters/energy-demand-research-project

194. UK DATA SERVICE. Smart Meter Energy Demand Research Project : Data Release. [online]. 2014. [Accessed 14 May 2021]. Available from: http://doc.ukdataservice.ac.uk/doc/7591/mrdoc/pdf/7591_edrp_accompanying_documentation.pdf

195. CACI. Acorn User Guide. [online]. 2007. [Accessed 14 May 2021]. Available from: https://manualzilla.com/doc/6892872/acorn-user-guide?page=2

196. ENVIRONMENTAL CHANGE NETWORK. Site Information: Drayton. [online]. 2017. [Accessed 23 August 2017]. Available from: http://data.ecn.ac.uk/sites/ecnsites.asp?site=T01

197. SOLARWORLD. Sunmodule Plus SW 270 MONO (33mm frame). [online]. 2015. [Accessed 14 May 2021]. Available from: http://www.rexelenergysolutions.co.uk/media/pdfs/2500820079_DataSheet.pdf

198. TRINA SOLAR. Trinasmart: The Optimized Solution. [online]. 2014. [Accessed 14 May 2021]. Available from: http://www.rexelenergysolutions.co.uk/media/pdfs/EN_TSM_DC05A.052_DC05A.082_datasheet_FEB_2014_web.pdf

199. LG ELECTRONICS. LG NeON 2Black. [online]. 2015. [Accessed 14 May 2021]. Available from: https://www.rexelenergysolutions.co.uk/media/pdfs/2500796997_DataSheet.pdf

200. SMA and BOY, Sunny. Sunny Boy 1.5 / 2.5. [online]. 2015. [Accessed 14 May 2021]. Available from: http://www.sma-uk.com/fileadmin/content/global/Products/Documents/Wechselrichter_ohne_Trafo/Data_Sheet_SB_1.5_2.5.pdf

201. SMA. SUNNY BOY 3000TL / 3600TL / 4000TL / 5000TL. [online]. 2017. [Accessed 14 May 2021]. Available from: http://shop.solar-pur.de/s/pdf/SB4000TL-21.pdf

202. SOLAREDGE. SolarEdge Single Phase Inverters SE2200 - SE6000. [online]. 2014. [Accessed 14 May 2021]. Available from: http://shop.solar-pur.de/s/pdf/solaredge/se2200_se6000.pdf

203. GIBSON, Peter, SONG, China Nanhao, SANTIAGO, Germany, INDIA, Senn, KUMAR, Prashant, HIDEKI, Japan, AUSTRALIA, Morita, ALLEN, Jamie, 7C, Otto-Volger-Str and PLANT, Holland. CHANGE YOUR ENERGY CHARGE YOUR LIFE. [online]. 2016. [Accessed 14 May 2021]. Available from: http://m.lgchem.com/upload/file/product/ESS_LGChem_ENG.pdf

204. BLOOM, Ira, WALKER, Lee K., BASCO, John K., ABRAHAM, Daniel P., CHRISTOPHERSEN, Jon P. and HO, Chinh D. Differential voltage analyses of high-power lithium-ion cells. 4. Cells containing NMC. *Journal of Power Sources*. 2010. Vol. 195, no. 3, p. 877–882. DOI 10.1016/j.jpowsour.2009.08.019.

205. SCHMITT, Julius, MAHESHWARI, Arpit, HECK, Michael, LUX, Stephan and VETTER, Matthias. Impedance change and capacity fade of lithium nickel manganese cobalt oxide-based batteries during calendar aging. *Journal of Power Sources* [online]. 2017. Vol. 353, p. 183–194. DOI 10.1016/j.jpowsour.2017.03.090. Available from: http://linkinghub.elsevier.com/retrieve/pii/S037877531730397X

206. BARSOUKOV, Evgenij and MACDONALD, J. Ross. *Impedance Spectroscopy: Theory, Experiment, and Applications* [online]. Wiley-Interscience, 2010. ISBN 9786468600. Available from: http://books.google.com/books?hl=en&lr=&id=StDjdRnT72AC&oi=fnd&pg=PR9&dq=Supersymmetry:+Theory,+Experiment,+and+Cosmology&ots=VfJ4xl4eAq&sig=sh9EfE3rqkdk6iEl0Jxpbqt9oFg

207. ZHUANG, Quan-chao, QIU, Xiang-yun and XU, Shou-dong. Diagnosis of Electrochemical Impedance Spectroscopy in Lithium-Ion Batteries. *InTech* [online]. 2012. P. 189–226. DOI 10.5772/26749. Available from: http://www.intechopen.com/books/lithium-ion-batteries-new-developments/diagnosis-of-electrochemical- impedance-spectroscopy-in-lithium-ion-batteries

208. NATIONAL GRID. Firm Frequency Response. [online]. 2016. [Accessed 14 May 2021]. Available from: http://www2.nationalgrid.com/uk/services/balancing-services/frequency-response/firm-frequency-response/

209. NATIONAL GRID. Firm Frequency Response Tender Rules and Standard Contract Terms. [online]. 2016. [Accessed 14 May 2021]. Available from: https://www.nationalgrid.com/sites/default/files/documents/FFR SCTs - Issue 8 Feb 1st 2017_0.pdf

210. NATIONAL GRID. Firm Frequency Response: Tender Assessment Principles. [online]. 2005. No. August, p. 1–3. Available from: https://www.nationalgrideso.com/sites/eso/files/documents/Tender Assessment Principles.pdf

211. UDDIN, Kotub, MOORE, Andrew D., BARAI, Anup and MARCO, James. The effects of high frequency current ripple on electric vehicle battery performance. *Applied Energy* [online]. 2016. Vol. 178, p. 142–154. DOI 10.1016/j.apenergy.2016.06.033. Available from: http://dx.doi.org/10.1016/j.apenergy.2016.06.033

212. UDDIN, Kotub, SOMERVILLE, Limhi, BARAI, Anup, LAIN, Michael, ASHWIN, T. R., JENNINGS, Paul and MARCO, James. The impact of high-frequency-high-current perturbations on film formation at the negative electrode-electrolyte interface. *Electrochimica Acta* [online]. 2017. Vol. 233, p. 1–12. DOI 10.1016/j.electacta.2017.03.020. Available from: http://dx.doi.org/10.1016/j.electacta.2017.03.020

213. BESSMAN, Alexander, SOARES, Rudi, WALLMARK, Oskar, SVENS, Pontus and LINDBERGH, Göran. Aging effects of AC harmonics on lithium-ion cells. *Journal of Energy Storage*. 2019. Vol. 21, no. October 2018, p. 741–749. DOI 10.1016/j.est.2018.12.016.

214. UNO, Masatoshi and TANAKA, Koji. Influence of high-frequency charge-discharge cycling induced by cell voltage equalizers on the life performance of lithium-ion cells. *IEEE Transactions on Vehicular Technology*. 2011. Vol. 60, no. 4, p. 1505–1515. DOI 10.1109/TVT.2011.2127500.

215. PASTOR-FERNÁNDEZ, Carlos, UDDIN, Kotub, CHOUCHELAMANE, Gael H., WIDANAGE, W. Dhammika and MARCO, James. A Comparison between Electrochemical Impedance Spectroscopy and Incremental Capacity-Differential Voltage as Li-ion Diagnostic Techniques to Identify and Quantify the Effects of Degradation Modes within Battery Management Systems. *Journal of Power Sources*. 2017. Vol. 360, p. 301–318. DOI 10.1016/j.jpowsour.2017.03.042.

216. FIROUZ, Y, RELAN, R, TIMMERMANS, J M, OMAR, N, BOSSCHE, P Van Den and MIERLO, J Van. Advanced lithium ion battery modeling and nonlinear analysis based

on robust method in frequency domain : Nonlinear characterization and non-parametric modeling. *Energy* [online]. 2016. Vol. 106, p. 602–617. DOI 10.1016/j.energy.2016.03.028. Available from: http://dx.doi.org/10.1016/j.energy.2016.03.028

217. FLEMING, Joe, AMIETSZAJEW, Tazdin, CHARMET, Jerome, ROBERTS, Alexander John, GREENWOOD, David and BHAGAT, Rohit. The design and impact of in-situ and operando thermal sensing for smart energy storage. *Journal of Energy Storage* [online]. 2019. Vol. 22, no. January, p. 36–43. DOI 10.1016/j.est.2019.01.026. Available from: https://doi.org/10.1016/j.est.2019.01.026

218. AMETEK SCIENTIFIC INSTRUMENTS. ModuLab XM ECS | Potentiostat | Solartron Analytical. [online]. 2018. [Accessed 17 September 2018]. Available from: https://www.ameteksi.com/products/potentiostats/single-channel/modulab-xm-series/modulab-xm-ecs

219. NATIONAL GRID ESO. Historic frequency data. [online]. 2021. [Accessed 27 April 2021]. Available from: https://www.nationalgrideso.com/balancing-services/frequency-response-services/historic-frequency-data

220. BLOOM, I., COLE, B. W., SOHN, J. J., JONES, S. A., POLZIN, E. G., BATTAGLIA, V. S., HENRIKSEN, G. L., MOTLOCH, C., RICHARDSON, R., UNKELHAEUSER, T., INGERSOLL, D. and CASE, H. L. An accelerated calendar and cycle life study of Li-ion cells. *Journal of Power Sources*. 2001. Vol. 101, no. 2, p. 238–247. DOI 10.1016/S0378-7753(01)00783-2.

221. BETZIN, Christopher, WOLFSCHMIDT, Holger and LUTHER, Matthias. Electrical operation behavior and energy efficiency of battery systems in a virtual storage power plant for primary control reserve. *International Journal of Electrical Power and Energy Systems* [online]. 2018. Vol. 97, no. October 2017, p. 138–145. DOI 10.1016/j.ijepes.2017.10.038. Available from: https://doi.org/10.1016/j.ijepes.2017.10.038

222. SMA SOLAR TECHNOLOGY AG. *Sunny Island 3.0M/ 4.4M*. 2018.

223. SMA SOLAR TECHNOLOGY AG. *Sunny Boy Storage 2.5*. 2014.

224. SMA SOLAR TECHNOLOGY AG. *SUNNY CENTRAL Storage*. 2018.

225. SMA SOLAR TECHNOLOGY AG. *Sunny Island 6.0H/8.0H*. 2018.

226. SOLAX POWER. *Solax Inverter*. 2018.

227. ABB. *ABB central inverters*. 2013.

228. SOLAREDGE. *SolarEdge StorEdge Solution with Backup Installation Guide*. 2018.

229. MULTIPLUS, The, AC, Two, THE, Outputs, MULTI, V a, PANEL, Multi Control, CHARGER, Phoenix, INFORMATION, Technical, CONFIGURE, Bus Quick and VICTRON ENERGY. *MultiPlus inverter / charger*. 2000.

230. SOLAREDGE. *SolarEdge Installation Guide*. 2018.

231. KACO NEW ENERGY. *blueplanet gridsave 250 TL3*. 2018.

232. KACO NEW ENERGY. blueplanet gridsave 1 000 TL3. . 2018. P. 3–4.

233. KACO NEW ENERGY. *blueplanet gridsave 50.0 TL3-S*. 2018.

234. SMITH, Kandler A., RAHN, Christopher D. and WANG, Chao-yang Yang. Control oriented 1D electrochemical model of lithium ion battery. *Energy Conversion and Management*. 2007. Vol. 48, no. 9, p. 2565–2578. DOI 10.1016/j.enconman.2007.03.015.

235. COGSWELL, Daniel A. and BAZANT, Martin Z. Coherency strain and the kinetics of phase separation in LiFePO 4 nanoparticles. *ACS Nano*. 2012. Vol. 6, no. 3, p. 2215–2225. DOI 10.1021/nn204177u.

236. SAW, L. H., YE, Yonghuang and TAY, A. A.O. Electrochemical-thermal analysis of 18650 Lithium Iron Phosphate cell. *Energy Conversion and Management* [online]. 2013. Vol. 75, p. 162–174. DOI 10.1016/j.enconman.2013.05.040. Available from: http://dx.doi.org/10.1016/j.enconman.2013.05.040

237. XIA, L., NAJAFI, E., LI, Z., BERGVELD, H. J. and DONKERS, M. C.F. A computationally efficient implementation of a full and reduced-order electrochemistry-based model for Li-ion batteries. *Applied Energy*. 2017. Vol. 208, no. August, p. 1285–1296. DOI 10.1016/j.apenergy.2017.09.025.

238. SMITH, Kandler, SAXON, Aron, KEYSER, Matthew, LUNDSTROM, Blake, CAO, Ziwei and ROC, Albert. Life Prediction Model for Grid - Connected Li - ion Battery Energy Storage System. In : *2017 American Control Conference*. 2017. p. 4062–4068. ISBN 9781509059928.

239. HE, Zhichao, GUO, Dongxu, LIU, Xu and YANG, Geng. An Evaluation Method of Battery DC Resistance Consistency Caused by Temperature Variation. *IEEE 2017 20th International Conference on Electrical Machines and Systems (ICEMS)*. 2017. DOI 10.1109/ICEMS.2017.8056426.

240. SHADMAN RAD, M., DANILOV, D. L., BAGHALHA, M., KAZEMEINI, M. and NOTTEN, P. H.L. Adaptive thermal modeling of Li-ion batteries. *Electrochimica Acta* [online]. 2013. Vol. 102, p. 183–195. DOI 10.1016/j.electacta.2013.03.167. Available from: http://dx.doi.org/10.1016/j.electacta.2013.03.167

241. ZHENG, Linfeng, ZHU, Jianguo, WANG, Guoxiu, LU, Dylan Dah Chuan, MCLEAN, Peter and HE, Tingting. Experimental analysis and modeling of temperature dependence of lithium-ion battery direct current resistance for power capability prediction. *2017 20th International Conference on Electrical Machines and Systems, ICEMS 2017*. 2017. P. 0–3. DOI 10.1109/ICEMS.2017.8056426.

242. GONG, Xianzhi. *Modeling of Lithium-ion Battery Considering Temperature and Aging Uncertainties* [online]. 2016. [Accessed 24 August 2018]. Available from: https://deepblue.lib.umich.edu/bitstream/handle/2027.42/134041/Gong Dissertation Final.pdf?sequence=1&isAllowed=y

243. HANIFF MAHMUD, Amirul, HILMI CHE DAUD, Zul and ASUS, Zainab. the Impact of Battery Operating Temperature and State of Charge on the Lithium-Ion Battery Internal Resistance. *Jurnal Mekanikal* [online]. 2017. Vol. 40, no. June, p. 1–8. Available from: https://mech.utm.my/wp-content/uploads/2017/12/1-THE-IMPACT-OF-BATTERY-OPERATING-TEMPERATURE-AND-STATE-OF-CHARGE-ON-THE-LITHIUM-ION-BATTERY-INTERNAL-RESISTANCE.pdf

244. WANG, Dian, BAO, Yun and SHI, Jianjun. Online lithium-ion battery internal resistance measurement application in state-of-charge estimation using the extended kalman filter. *Energies*. 2017. Vol. 10, no. 9. DOI 10.3390/en10091284.

245. GIORDANO, Giuseppe, KLASS, Verena, BEHM, Marten, LINDBERGH, Goran and SJOBERG, Jonas. Model-based lithium-ion battery resistance estimation from electric vehicle operating data. *IEEE Transactions on Vehicular Technology*. 2018. Vol. 67, no. 5, p. 3720–3728. DOI 10.1109/TVT.2018.2796723.

246. NIKOLIAN, Alexandros, JAGUEMONT, Joris, DE HOOG, Joris, GOUTAM, Shovon, OMAR, Noshin, VAN DEN BOSSCHE, Peter and VAN MIERLO, Joeri. Complete cell-level lithium-ion electrical ECM model for different chemistries (NMC, LFP, LTO) and temperatures (−5 °C to 45 °C) – Optimized modelling techniques. *International Journal of Electrical Power and Energy Systems* [online]. 2018. Vol. 98, no. November 2017, p. 133–146. DOI 10.1016/j.ijepes.2017.11.031. Available from: https://doi.org/10.1016/j.ijepes.2017.11.031

247. ABU-SHARKH, Suleiman and DOERFFEL, Dennis. Rapid test and non-linear model

characterisation of solid-state lithium-ion batteries. *Journal of Power Sources*. 2004. Vol. 130, p. 266–274. DOI 10.1016/j.jpowsour.2003.12.001.

248. PEI, Lei, WANG, Tiansi, LU, Rengui and ZHU, Chunbo. Development of a voltage relaxation model for rapid open-circuit voltage prediction in lithium-ion batteries. *Journal of Power Sources* [online]. 2014. Vol. 253, p. 412–418. DOI 10.1016/j.jpowsour.2013.12.083. Available from: http://dx.doi.org/10.1016/j.jpowsour.2013.12.083

249. GOLUBKOV, Andrey W., SCHEIKL, Sebastian, PLANTEU, René, VOITIC, Gernot, WILTSCHE, Helmar, STANGL, Christoph, FAULER, Gisela, THALER, Alexander and HACKER, Viktor. Thermal runaway of commercial 18650 Li-ion batteries with LFP and NCA cathodes - Impact of state of charge and overcharge. *RSC Advances*. 2015. Vol. 5, no. 70, p. 57171–57186. DOI 10.1039/c5ra05897j.

250. HUA, Yin, XU, Min, LI, Mian, MA, Chengbin and ZHAO, Chen. Estimation of state of charge for two types of lithium-ion batteries by nonlinear predictive filter for electric vehicles. *Energies*. 2015. Vol. 8, no. 5, p. 3556–3577. DOI 10.3390/en8053556.

251. SRINIVASAN, Rengaswamy, BAISDEN, A Carson, CARKHUFF, Bliss G. and BUTLER, Michael H. The five modes of heat generation in a Li-ion cell under discharge. *Journal of Power Sources* [online]. 2014. Vol. 262, p. 93–103. DOI 10.1016/j.jpowsour.2014.03.062. Available from: http://dx.doi.org/10.1016/j.jpowsour.2014.03.062

252. AGUBRA, Victor and FERGUS, Jeffrey. Lithium ion battery anode aging mechanisms. *Materials*. 2013. Vol. 6, no. 4, p. 1310–1325. DOI 10.3390/ma6041310.

253. KUBIAK, P, EDSTRÖM, K and MORCRETTE, M. Review on ageing mechanisms of different Li-ion batteries for automotive applications. *Journal of Power Sources*. 2013. Vol. 12, p. 03691. DOI 10.1016/j.jpowsour.2013.05.040.

254. ECKER, Madeleine, NIETO, Nerea, KÄBITZ, Stefan, SCHMALSTIEG, Johannes, BLANKE, Holger, WARNECKE, Alexander and SAUER, Dirk Uwe. Calendar and cycle life study of Li(NiMnCo)O2-based 18650 lithium-ion batteries. *Journal of Power Sources* [online]. 2014. Vol. 248, p. 839–851. DOI 10.1016/j.jpowsour.2013.09.143. Available from: http://dx.doi.org/10.1016/j.jpowsour.2013.09.143

255. TIPPMANN, Simon, WALPER, Daniel, BALBOA, Luis, SPIER, Bernd and BESSLER, Wolfgang G. Low-temperature charging of lithium-ion cells part I: Electrochemical modeling and experimental investigation of degradation behavior. *Journal of Power*

Sources [online]. 2014. Vol. 252, p. 305–316. DOI 10.1016/j.jpowsour.2013.12.022. Available from: http://dx.doi.org/10.1016/j.jpowsour.2013.12.022

256. BARAI, Anup, GUO, Yue, MCGORDON, Andrew and JENNINGS, Paul. A Study of the Effects of External Pressure on the Electrical Performance of a Lithium-ion Pouch Cell. In : *2013 International Conference on Connected Vehicles and Expo (ICCVE)* [online]. 2013. p. 2–6. ISBN 9781479924912. Available from: http://ieeexplore.ieee.org/articleDetails.jsp?arnumber=6799809%5Cnhttp://ieeexplore.ieee.org/iel7/6784566/6799751/06799809.pdf?arnumber=6799809

257. SAFARI, M., MORCRETTE, M., TEYSSOT, A. and DELACOURT, C. Multimodal physics-based aging model for life prediction of Li-Ion batteries. *Journal of the Electrochemical Society*. 2009. Vol. 156, no. 3. DOI 10.1149/1.3043429.

258. WALDMANN, Thomas, WILKA, Marcel, KASPER, Michael, FLEISCHHAMMER, Meike and WOHLFAHRT-MEHRENS, Margret. Temperature dependent ageing mechanisms in Lithium-ion batteries - A Post-Mortem study. *Journal of Power Sources* [online]. 2014. Vol. 262, p. 129–135. DOI 10.1016/j.jpowsour.2014.03.112. Available from: http://dx.doi.org/10.1016/j.jpowsour.2014.03.112

259. LEGRAND, N., KNOSP, B., DESPREZ, P., LAPICQUE, F. and RAËL, S. Physical characterization of the charging process of a Li-ion battery and prediction of Li plating by electrochemical modelling. *Journal of Power Sources* [online]. 2014. Vol. 245, p. 208–216. DOI 10.1016/j.jpowsour.2013.06.130. Available from: http://dx.doi.org/10.1016/j.jpowsour.2013.06.130

260. LG CHEM. LG Chem Lithium-ion Battery Limited Warranty. [online]. 2017. [Accessed 30 May 2021]. Available from: https://www.sharp.co.uk/cps/rde/xbcr/documents/documents/Service_Information/Warranty/RESU3.3-6.5-10-Limited-Warranty-EU-Standard-EN-v1.1-191030.pdf

261. SMA SOLAR TECHNOLOGY AG. Operating manual: Sunny Island 4.4M/6.0H/8.0H. [online]. 2016. [Accessed 30 May 2021]. Available from: https://files.sma.de/downloads/SI44M-80H-12-BE-en-13.pdf

262. LG CHEM. PRODUCT BOOK : Essential Information for RESU LV/HV. [online]. 2019. [Accessed 30 May 2021]. Available from: https://www.sharp.co.uk/cps/rde/xbcr/documents/documents/Marketing/Datasheet/RESU-Product-Book_EN_V1.5_191125.pdf

263. RENUGEN. LG Chem RESU 6.5kWh Lithium Battery. [online]. 2021.

[Accessed 31 May 2021]. Available from: https://www.renugen.co.uk/lg-chem-resu-6-5kwh-lithium-battery/

264. WIND & SUN LTD. SMA Sunny Island Off Grid Inverters. [online]. 2021. [Accessed 31 May 2021]. Available from: http://www.windandsun.co.uk/products/Inverters/SMA-Inverters/SMA-Sunny-Island-Off-Grid-Inverters#9794

265. GOCOMPARE.COM. Energy – KWh explained. [online]. 2021. [Accessed 31 May 2021]. Available from: https://www.gocompare.com/gas-and-electricity/guide/energy-per-kwh/#:~:text=According to the Department for,p%2FkWh for their electricity.

266. SCOTTISH FRIENDLY. Scottish Bond | 10 Year Tax-Free Investment. [online]. 2020. [Accessed 4 October 2020]. Available from: https://www.scottishfriendly.co.uk/tax-free-investments/scottish-bond